Skin Penetration from Non-Lethal Munitions

Final Technical Report

September 2021

Joshua Etu, MBA

AMERICAN SYSTEMS
Engineering, Strategy & Analysis Directorate

Daniel F Shedd
Parker R Berthelson
Jared A Rifkin
J Sebastian Giudice
Jason L Forman
Matthew B Panzer

University of Virginia Center for Applied Biomechanics

This work was conducted by AMERICAN SYSTEMS under #N000174-17-D-0031, Task Order #10 "Skin Penetration Risk from Non-Lethal Projectiles" for the Joint Intermediate Force Capabilities Office. The views opinions and finding should not be construed as representing the official position of either the Department of Defense or the Sponsoring organization.

Distribution Statement A: Unlimited Distribution (September 2021).

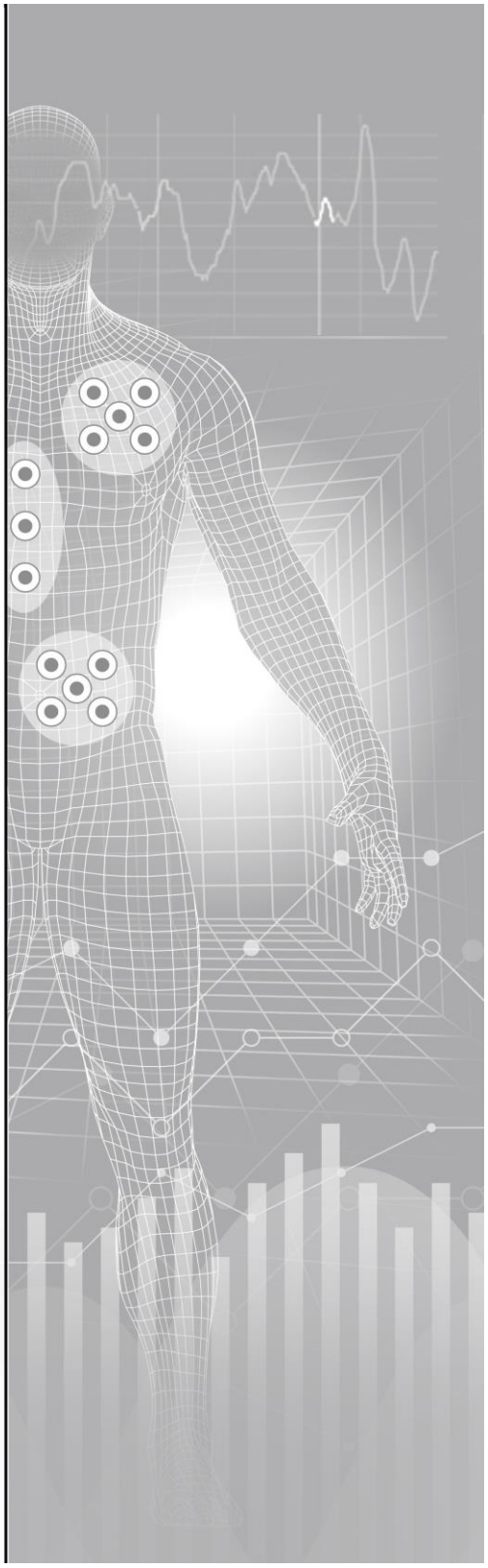


Table of Contents

List of Tables 6
List of Figures 8
Table of Acronyms 12
Executive Summary 14
Introduction 14
Research Aims 14
Aim 1 14
Methods 14
Results 15
Aim 2 15
Methods 15
Results 15
Aim 3 15
Methods 15
Results 16
Conclusion 16
Introduction 18
Background 18
Aims 20
Aim 1: High-Rate Blunt Impact in Human Cadaveric Tissue 21
Overview 21
Methods 21
Test Setup and Equipment 21
High-Rate Linear Impactor and Configurable Barrels 21
Impactors 21
Enclosure and Chair Assembly 22
High-Speed Cameras 23
Shear Wave Elastography System 24
PMHS Testing Procedure 24
PMHS Procurement 24
Subject Preparation and Pre-Test Imaging 25
Impactor Testing 27

Post-Test Imaging and Autopsy 29
Data Analysis 31
Impact Velocity Measurement 31
Tissue Thickness Measurement 31
Shear Wave Elastography 32
Statistical Analysis 32
Injury Risk Curve Development 32
Results 33
Anthropometry 33
Tissue Temperature 34
Impact Velocity Calculations 34
Tissue Thickness Measurements 35
Shear Wave Velocity Measurements 39
PMHS IRF Covariate Assessment 43
PMHS IRF Model Development 44
PMHS Model 1 (Covariates: Skin Thickness, Impactor Shape, and Impactor Diameter) 44
PMHS Model 2 (Covariates: Skin Thickness and Impactor Shape) 45
PMHS Model 3 (Covariate: Skin Thickness) 46
PMHS IRF Response Comparisons 47
Conclusions 54
Aim 2: High-Rate Blunt Impact in Ovine Cadaveric Tissue 57
Overview 57
Methods 57
Test Setup and Equipment 57
Suspension Harness 57
Modifications to Enclosure and Test Area 57
Ovine Testing Procedure 57
Procurement of Ovine Subjects and Pre-Test Imaging 57
Tissue Storage and Temperature Conditions 58
Subject Preparation and Pre-Test Imaging 59
Impactor Testing 60
Necropsy 61
Data Analysis 62

Impact Velocity, Tissue Thickness, and SWE Measurements 62
Injury Risk Curve Development 62
Ovine IRF Comparisons 62
Statistical Analysis 62
Results 62
Anthropometry 62
Tissue Temperature Measurements 63
Impact Velocity 65
Tissue Thickness Measurements 66
SWE Measurements 70
Ovine IRF Covariate Assessment 74
Ovine IRF Development 76
Ovine Model 1 (Covariate: Body Region, Dataset: All Data) 76
Ovine Model 2 (Covariate: No Covariates, Dataset: All Data) 77
Ovine Model 3 (Covariate: No Covariates, Dataset: Fresh/Lab Temp.) 78
Ovine Model 4 (Covariate: No Covariates, Dataset: Thawed/Lab Temp.) 79
Ovine Model 5 (Covariate: No Covariates, Dataset: Fresh/Warmed) 79
Ovine Model 6 (Covariate: Body Region, Dataset: Fresh/Lab Temp.) 80
Ovine Model 7 (Covariate: Body Region, Dataset: Thawed/Lab Temp.) 81
Ovine Model 8 (Covariate: Body Region, Dataset: Fresh/Warmed) 82
Ovine IRF Response Comparisons 83
Comparison Between PMHS and Ovine Body Regions 93
Conclusions 100
Aim 3: Model Development and Validation 104
Overview 104
Methods 104
Model Overview 104
Software and Unit System 105
Torso Model Updates 105
Skin Material Updates 105
Adipose Tissue Material Updates 106
Muscle Material Updates 107
Mesh Refinement 109

Boundary Conditions 110
Impactor Models 110
Impact Conditions 111
Impact Velocities 112
Parametric Study and Simulation Matrix 112
Parametric Study of Skin and Adipose Tissue Stiffness 112
Baseline (or Mean) Material Properties 113
Simulation Post-Processing 114
Statistical Meta-Modeling 115
Injury Risk Function Development 115
Results 118
Effect of Mesh Refinement 118
Effect of Impactor and Impact Velocity 119
Effect of Skin and Adipose Material Properties 125
Statistical Meta-Modeling 129
Injury Risk Function 131
Conclusions 136
References 140
Appendices 145
Appendix 1: PMHS Anthropometry Instructions 145
Appendix 2: PMHS Impact Descriptions 148
Appendix 3: PMHS Autopsy Results 160
Appendix 4: PMHS Injury Risk Function Covariate Assessment 173
Appendix 5: PMHS Tissue Thickness 178
Appendix 6: PMHS Model 1 Covariate Comparisons 181
Appendix 7: PMHS Model 2 Covariate Comparisons 195
Appendix 8: PMHS Model 3 Covariate Comparisons 198
Appendix 9: Ovine Anthropometry Instructions 199
Appendix 10: Ovine Impact Descriptions 201
Appendix 11: Ovine Autopsy Results 217
Appendix 12: Ovine Tissue Thickness 234
Appendix 13: Ovine Injury Risk Function Covariate Assessment 237
Appendix 14: Ovine Model 2 Plotting 242

List of Tables

Table I: Specifications for the six free-flight impactors 22
Table II: General anthropometric details for each PMHS 25
Table III: Anatomical axis landmarks 26
Table IV: Impact location exclusion zone sizes 26
Table V: Test matrix for the PMHS impactor testing* 28
Table VI: Autopsy assessments 31
Table VII: PMHS anthropometry results 33
Table VIII: PMHS Surface Tissue Temperature 34
Table IX: PMHS Tissue Thickness per Tissue Layer 36
Table X: PMHS Shear Wave Velocity per Tissue Layer 39
Table XI: PMHS Covariate Assessment 43
Table XII: Covariate Details for PMHS IRFs 44
Table XIII: Coefficient Values for PMHS Model 1 44
Table XIV: Weibull IRF Statistics for PMHS Model 1 45
Table XV: Coefficient Values for PMHS Model 2 45
Table XVI: Weibull IRF Statistics for PMHS Model 2 46
Table XVII: Coefficient Values for PMHS Model 3 46
Table XVIII: Weibull IRF Statistics for PMHS Model 3 47
Table XIX: Predicted PMHS Injury Risk For Varied Skin Thickness (Mean ± 1 SD) 49
Table XX: Predicted PMHS Injury Risk For Varied Body Region 50
Table XXI: Predicted PMHS Injury Risk For Impactor Shape 52
Table XXII: Predicted PMHS Injury Risk for Varied Impactor Diameter 53
Table XXIII: Test matrix for Ovine impactor testing 58
Table XXIV: Ovine anthropometry results 62
Table XXV: Ovine tissue temperature results 65
Table XXVI: Ovine Tissue Thickness per Tissue Layer 66
Table XXVII: Ovine Shear Wave Velocity per Tissue Layer 70
Table XXVIII: Ovine Covariate Assessment 76
Table XXIX: Covariate Details for Ovine IRFs 76
Table XXX: Coefficient Values for Ovine Model 1 77
Table XXXI: Weibull IRF Statistics for Ovine Model 1 77
Table XXXII: Coefficient Values for Ovine Model 2 78
Table XXXIII: Weibull IRF Statistics for Ovine Model 2 78
Table XXXIV: Coefficient Values for Ovine Model 3 78
Table XXXV: Weibull IRF Statistics for Ovine Model 3 79
Table XXXVI: Coefficient Values for Ovine Model 4 79
Table XXXVII: Weibull IRF Statistics for Ovine Model 4 79
Table XXXVIII: Coefficient Values for Ovine Model 5 80
Table XXXIX: Weibull IRF Statistics for Ovine Model 5 80
Table XL: Coefficient Values for Ovine Model 6 80
Table XLI: Weibull IRF Statistics for Ovine Model 6 81

Table XLII: Coefficient Values for Ovine Model 7 81
Table XLIII: Weibull IRF Statistics for Ovine Model 7 82
Table XLIV: Coefficient Values for Ovine Model 8 82
Table XLV: Weibull IRF Statistics for Ovine Model 8 83
Table XLVI: Predicted Ovine Injury Risk for Varied Body Region 83
Table XLVII: Predicted Injury Risk for the Univariate Storage/Temp. Condition Comparison 85
Table XLVIII: Squared Error For the Univariate Storage/Temp. Condition Comparison 85
Table XLIX: Squared Error For the Shoulder Region Storage/Temp. Condition Comparison 87
Table L: Squared Error For the Ribs Region Storage/Temp. Condition Comparison 89
Table LI: Squared Error for the Stomach Region Storage/Temp. Condition Comparison 90
Table LII: Squared Error For the Rump Region Storage/Temp. Condition Comparison 92
Table LIII: Predicted Injury Risk for PMHS Upper Chest vs Ovine Body Region Comparison 93
Table LIV: Squared Error Comparisons Between Ovine Regions and PMHS Upper Chest 94
Table LV: Predicted Injury Risk for PMHS Abdomen vs Ovine Body Region Comparison 95
Table LVI: Squared Error Comparisons Between Ovine Regions and PMHS Abdomen 96
Table LVII: Predicted Injury Risk for PMHS Upper Back vs Ovine Body Region Comparison 97
Table LVIII: Squared Error Comparisons Between Ovine Regions and PMHS Upper Back 98
Table LIX: Predicted Injury Risk for PMHS Lower Back vs Ovine Body Region Comparison 99
Table LX: Squared Error Comparisons Between Ovine Regions and PMHS Lower Back 99
Table LXI. Overview of the modified ATBM v0.86 model flesh (skin, muscle, adipose layer) parts. 104
Table LXII. Model unit system. 105
Table LXIII. Impact locations, corresponding node ID in the unrefined ATBM v0.86 model, and the locations abbreviations. 111
Table LXIV: MPS-95 results from the four impact locations using the 0.75 in. spherical impactor. 121
Table LXV: MPS-95 for the seven impact velocities simulated at the AB-R impact location. 123
Table LXVI: MPS-95 results for the six impactor form factors striking. 124
Table LXVII: Weibull injury risk function parameters for UC-R location 133
Table LXVIII: Injury risk values for UC-R location 133
Table LXIX: Weibull injury risk function parameters for AB-R location 134
Table LXX: Injury risk values for AB-R location 134
Table LXXI: Weibull injury risk function parameters for UB-R location 134
Table LXXII: Injury risk values for UB-R location 134
Table LXXIII: Weibull injury risk function parameters for LB-R location 135
Table LXXIV: Injury risk values for LB-R location 135
Table A2-LXIX: PMHS 1 Impact Descriptions 148
Table A2-LXX: PMHS 2 Impact Descriptions 150
Table A2-LXXI: PMHS 3 Impact Descriptions 152
Table A2-LXXII: PMHS 4 Impact Descriptions 154
Table A2-LXXIII: PMHS 5 Impact Descriptions 156
Table A2-LXXIV: PMHS 6 Impact Descriptions 158
Table A3-LXXV: PMHS 1 Autopsy Results 161
Table ALXXVI: PMHS 2 Autopsy Results 163
Table A3-LXXVII: PMHS 3 Autopsy Results 165
Table A3-LXXVIII: PMHS 4 Autopsy Results 167

Table A3-LXXIX: PMHS 5 Autopsy Results 169
Table A3-LXXX: PMHS 6 Autopsy Results 171
Table A4-LXXXI: Full PMHS Covariate Assessment (In Increasing Order of p-Value) 173
Table A10-LXXXII: Ovine 1 (Fresh/Lab Temp Flank) Impact Descriptions 201
Table A10-LXXXIII: Ovine 1 (Thawed/Lab Temp Flank) Impact Descriptions 202
Table A10-LXXXIV: Ovine 2 (Fresh/Lab Temp Flank) Impact Descriptions 203
Table A10-LXXXV: Ovine 2 (Thawed/Lab Temp Flank) Impact Descriptions 204
Table A10-LXXXVI: Ovine 3 (Fresh/Lab Temp Flank) Impact Descriptions 205
Table A10-LXXXVII: Ovine 3 (Thawed/Lab Temp Flank) Impact Descriptions 206
Table A10-LXXXVIII: Ovine 4 (Fresh/Lab Temp Flank) Impact Descriptions 207
Table A10-LXXXIX: Ovine 4 (Fresh/Warmed Flank) Impact Descriptions 208
Table A10-XC: Ovine 5 (Fresh/Lab Temp Flank) Impact Descriptions 209
Table A10-XCI: Ovine 5 (Fresh/Warmed Flank) Impact Descriptions 210
Table A10-XCII: Ovine 6 (Fresh/Lab Temp Flank) Impact Descriptions 211
Table A10-XCIII: Ovine 6 (Fresh/Warmed Flank) Impact Descriptions 212
Table A10-XCIV: Ovine 7 (Fresh/Lab Temp Flank) Impact Descriptions 213
Table A10-XCV: Ovine 7 (Thawed/Lab Temp Flank) Impact Descriptions 214
Table A10-XCVI: Ovine 8 (Thawed/Lab Temp, Left Flank) Impact Descriptions 215
Table A10-XCVII: Ovine 8 (Thawed/Lab Temp, Right Flank) Impact Descriptions 216
Table A11-XCVIII: Ovine 1 (Fresh/Lab Temp Flank) Autopsy Results 218
Table A11-XCIX: Ovine 1 (Thawed/Lab Temp Flank) Autopsy Results 219
Table A11-C: Ovine 2 (Fresh/Lab Temp Flank) Autopsy Results 220
Table A11-CI: Ovine 2 (Thawed/Lab Temp Flank) Autopsy Results 221
Table A11-CII: Ovine 3 (Fresh/Lab Temp Flank) Autopsy Results 222
Table A11-CIII: Ovine 3 (Thawed/Lab Temp Flank) Autopsy Results 223
Table A11-CIV: Ovine 4 (Fresh/Lab Temp Flank) Autopsy Results 224
Table A11-CV: Ovine 4 (Fresh/Warmed) Autopsy Results 225
Table A11-CVI: Ovine 5 (Fresh/Lab Temp Flank) Autopsy Results 226
Table A11-CVII: Ovine 5 (Fresh/Warmed) Autopsy Results 227
Table A11-CVIII: Ovine 6 (Fresh/Lab Temp Flank) Autopsy Results 228
Table A11-CIX: Ovine 6 (Fresh/Warmed) Autopsy Results 229
Table A11-CX: Ovine 7 (Fresh/Lab Temperature) Autopsy Results 230
Table A11-CXI: Ovine 7 (Thawed/Lab Temperature) Autopsy Results 231
Table A11-CXII: Ovine 8 (Thawed/Lab Temperature, Left Flank) Autopsy Results 232
Table A11-CXIII: Ovine 8 (Thawed/Lab Temperature, Right Flank) Autopsy Results 233
Table A13-CXIV: All Possible Ovine Covariates (In Increasing Order of p-Value) 237
Table A14-CXV: Predicted Injury Risk for Ovine Model 2 242

List of Figures

Figure 1: High-rate linear impactor system. 21
Figure 2: The six free-flight impactors. 22
Figure 3: Enclosure and chair setup for PMHS positioning. 23
Figure 4: High-speed camera and lighting configuration. 24

Figure 5: Anatomical axis definitions. 26
Figure 6: Impact site and exclusion zone criteria for each impactor size. 27
Figure 7: PMHS anatomical impact regions. 28
Figure 8: Impactor velocity as a function of impactor pressure for all tested PMHS impact cases. 35
Figure 9: Tissue thickness measurements for each PMHS specimen. 37
Figure 10: Tissue thickness measurements for each PMHS body region. 39
Figure 11: Tissue shear wave velocity measurements for each PMHS specimen. 41
Figure 12: Tissue shear wave velocity measurements for each PMHS body region. 42
Figure 13: The effects of overall skin thickness variations on the PMHS IRF response. 49
Figure 14: The effects of regional skin thickness variations on the PMHS IRF response 51
Figure 15: The effects of impactor shape variations on the PMHS IRF response. 52
Figure 16: The effects of impactor diameter variations on the PMHS IRF response. 54
Figure 17: Ovine test setup and anatomical impact regions. 60
Figure 18: Impactor velocity as a function of impactor pressure for all tested Ovine impact cases. 66
Figure 19: Tissue thickness measurements for each ovine specimen. 68
Figure 20: Tissue thickness measurements for each ovine body region. 70
Figure 21: Tissue shear wave velocity measurements for each ovine specimen. 72
Figure 22: Tissue shear wave velocity measurements for each ovine body region. 74
Figure 23: The effects of the impacted body region on the ovine injury response. 84
Figure 24: The effects of tissue storage/temperature using univariate models. 86
Figure 25: The effects of tissue storage/temperature using regional models (Shoulder region). 88
Figure 26: The effects of tissue storage/temperature using regional models (Ribs region). 89
Figure 27: The effects of tissue storage/temperature using regional models (Stomach region). 91
Figure 28: The effects of tissue storage/temperature using regional models (Rump region). 92
Figure 29: Comparison of the PMHS' Upper Chest region response to each ovine body region. 94
Figure 30: Comparison of the PMHS' Abdomen region response to each ovine body region. 96
Figure 31: Comparison of the PMHS' Upper Back region response to each ovine body region. 98
Figure 32: Comparison of the PMHS' Lower Back region response to each ovine body region. 100
Figure 33. Skin material card and parameters. 105
Figure 34. Constitutive model verification from experimental data. 106
Figure 35. Adipose tissue material card and parameters. 106
Figure 36. Muscle material card in Skin Penetration Model 1.0 107
Figure 37. Stress relaxation results from underlying tissue (muscle) calibration. 108
Figure 38. Flesh model verification. 108
Figure 39. Comparison of flesh part responses between the ATBM and modified torso model. 109
Figure 40. Overview of the parametric mesh refinement. 110
Figure 41. Impactor form factors. 111
Figure 42. Locally refined flesh meshes for impact locations defined in Table LXIII. 112
Figure 43. Material variation for the skin constitutive model. 113
Figure 44. Material variation for the adipose tissue constitutive model (from Sun et al., 2020) [26].45.
Material variation for the adipose tissue constitutive model (from Sun et al., 2020) [26]. 113
Figure 46. Impact area for computing the MPS for an impact simulation. 114
Figure 47: Process of calculating MPS-95 for an impact simulation. 115
Figure 48: Predictor distributions (N = 100,000) for generation of injury risk function. 116

Figure 49: Calculation of 5th, 50th, and 95th percentile MPS-95 for each injury risk. 117
Figure 50: Characteristic length of the solid adipose layer elements in the locally-refined mesh for the AB-R impact location. 118
Figure 51: MPS prediction of the locally refined (top) and unrefined/coarse (bottom) models. 119
Figure 52: Effect of impact velocity and impactor geometry. 120
Figure 53: MPS distributions at each impact site. 121
Figure 54: MPS of skin and rib using different impactor diameters. 122
Figure 55: Effect of impact velocity on MPS distributions. 123
Figure 56: MPS distributions for the six impactor form factors. 124
Figure 57: Effect of static coefficient of friction on MPS distribution and MPS-95. 125
Figure 58: Effect of skin and adipose tissue stiffness for 156.6 m/s impacts using the 1.00 in. cylinder. 126
Figure 59: Effect of skin and adipose tissue stiffness for the 119.9 m/s impacts using the 0.75 in. sphere. 127
Figure 60: Effect of skin and adipose tissue stiffness on MPS distribution for the 156.6 m/s impacts using the 1.00 in. cylinder. 128
Figure 61: Effect of skin and adipose tissue stiffness on MPS distribution for the 119.9 m/s impacts using the 0.75 in. sphere. 128
Figure 62: Assessment of meta-model fit. 129
Figure 63: Slice plot of the fit meta-model. 130
Figure 64: Lower bound, median, and upper bound injury risk function for the UC-R impact location. The bounds represent the variance in the predictor variables used to construct the meta-model. 131
Figure 65: Lower bound, median, and upper bound injury risk function for the AB-R impact location. The bounds represent the variance in the predictor variables used to construct the meta-model. 132
Figure 66: Lower bound, median, and upper bound injury risk function for the UB-R impact location. The bounds represent the variance in the predictor variables used to construct the meta-model. 132
Figure 67: Lower bound, median, and upper bound injury risk function for the LB-R impact location. The bounds represent the variance in the predictor variables used to construct the meta-model. 133
Figure 65: Injury risk variation when considering variation in both tissue mechanical properties and impactor design (blue) and considering variation in only impactor design (orange). 136
Figure A4-65: PMHS covariate assessment for the impact location variables. 174
Figure A4-66: PMHS covariate assessment for the impact condition variables. 175
Figure A4-67: PMHS covariate assessment for the tissue thickness variables. 176
Figure A4-68: PMHS covariate assessment for the tissue shear wave velocity variables. 177
Figure A5-69: Intra-subject comparison of mean tissue thickness per PMHS body region. 179
Figure A5-70: Comparison of variations in subject-level tissue thickness at each PMHS body region. ... 180
Figure A6-71: Comparison of Local Skin Thickness effects (PMHS Model 1). 182
Figure A6-72: Comparison of Body Region effects (PMHS Model 1). 183
Figure A6-73: Comparison of Impactor Shape effects (PMHS Model 1, mean skin thickness). 184
Figure A6-74: Comparison of Impactor Shape effects (PMHS Model 1, -1 SD skin thickness). 185
Figure A6-75: Comparison of Impactor Shape effects (PMHS Model 1, +1 SD skin thickness). 186
Figure A6-76: Comparison of Impactor Shape effects (PMHS Model 1, Upper Chest skin thickness). 187
Figure A6-77: Comparison of Impactor Shape effects (PMHS Model 1, Abdomen skin thickness). 188
Figure A6-78: Comparison of Impactor Shape effects (PMHS Model 1, Upper Back skin thickness). 189
Figure A6-79: Comparison of Impactor Shape effects (PMHS Model 1, Lower Back skin thickness). 190

Figure A6-80: Comparison of Impactor Diameter effects (PMHS Model 1, mean skin thickness). 191
Figure A6-81: Comparison of Impactor Diameter effects (PMHS Model 1, -1 SD skin thickness). 191
Figure A6-82: Comparison of Impactor Diameter effects (PMHS Model 1, +1 SD skin thickness). 192
Figure A6-83: Comparison of Impactor Diameter effects (PMHS Model 1, Upper Chest skin thickness). 192
Figure A6-84: Comparison of Impactor Diameter effects (PMHS Model 1, Abdomen skin thickness). ... 193
Figure A6-85: Comparison of Impactor Diameter effects (PMHS Model 1, Upper Back skin thickness).. 193
Figure A6-86: Comparison of Impactor Diameter effects (PMHS Model 1, Lower Back skin thickness).. 194
Figure A7-87: Comparison of Skin Thickness effects (PMHS Model 2). 195
Figure A7-88: Comparison of Body Region effects (PMHS Model 2). 195
Figure A7-89: Comparison of Impactor Shape effects (PMHS Model 2, mean skin thickness). 196
Figure A7-90: Comparison of Impactor Shape effects (PMHS Model 2, regional skin thickness). 197
Figure A8-91: Comparison of Skin Thickness effects (PMHS Model 3). 198
Figure A8-92: Comparison of Body Region effects (PMHS Model 3). 198
Figure A12-93: Intra-subject comparison of mean tissue thickness per Ovine body region. 236
Figure A12-94: Comparison of variations in subject-level tissue thickness at each ovine body region. .. 236
Figure A13-95: Ovine covariate assessment for the impact location variables. 238
Figure A13-96: Ovine covariate assessment for the tissue temperature variables. 239
Figure A13-97: Ovine covariate assessment for the tissue thickness variables. 240
Figure A13-98: Ovine covariate assessment for the tissue shear wave velocity variables. 241
Figure A14-99: Univariate ovine model with 95% confidence interval. 242

Table of Acronyms

Acronym	Definition
Ab	Abdomen
AB-R	Right Abdomen
ANOVA	Analysis of Variance
ATBM	Advanced Total Body Model
BMI	Body Mass Index
BUMED	US Department of the Navy Bureau of Medicine and Surgery
CAD	Computer Aided Design
CT	Computed Tomography
ELFORM	Element Formulation
FE	Finite Element
IACUC	Institutional Animal Care and Use Committee
IDA	Institutes for Defense Analyses
IRB-HSU	Institutional Review Board for Human Surrogate Use
IRF	Injury Risk Function
JIFCO	Joint Intermediate Force Capabilities Office
L1	First Lumber Vertebra
LB	Lower Back
LB-R	Right Lower Back
MPS	Maximum Principal Strain
MPS-95	95th Percentile Maximum Principal Strain
MRI	Magnetic Resonance Imaging
MSE	Mean Squared Error
NSD	No Significant Difference
PID	Part ID
PMHS	Post-Mortem Human Surrogates
PSI	Pounds per Square Inch
RSI	Risk of Significant Injury

SD	Standard Deviation
SE	Standard Error
SWE	Shear Wave Elastography
T1	First Thoracic Vertebra
UB	Upper Back
UB-R	Right Upper Back
UC	Upper Chest
UC-R	Right Upper Chest
UVA	University of Virginia
UVA-CAB	University of Virginia Center for Applied Biomechanics
VIBE	Volumetric Interpolated Breath-Hold Examination

Executive Summary

Introduction

The US Government has developed finite element models of the human torso for the calculation of Risk of Significant Injury (RSI) due to blunt impact trauma. These models are equipped with existing skin penetration capabilities; however, these features are nascent compared to those found in models that contain deeper tissue layers. As such, AMERICAN SYSTEMS and the University of Virginia Center for Applied Biomechanics (UVA-CAB) investigated the interactions between free-flight blunt impactors and post-mortem human skin to inform and improve these penetration models. During this study, AMERICAN SYSTEMS and UVA-CAB developed an experimental testing and analysis methodology to support the model development and integration through an iterative approach.

In collaboration with the Joint Intermediate Force Capabilities Office (JIFCO), the Institutes for Defense Analyses (IDA) and the Johns Hopkins University's Applied Physics Lab, our team developed 3 primary research aims.

Research Aims

1. Assess the tolerance of post-mortem human skin to localized blunt trauma *in-situ*.
2. Assess the tolerance of post-mortem ovine tissue to localized blunt trauma *in-situ* and evaluate the suitability of ovine as a surrogate for human tissue, and the effects of temperature and storage conditions.
3. Develop a new finite element model of the human flesh to better calculate the risk of significant skin penetration from blunt trauma indenters.

Aim 1

Methods

PMHS testing was conducted using a pneumatically driven, high-rate, linear impactor system, capable of propelling impactors of multiple diameters (0.50 in., 0.75 in., and 1.00 in.) at velocities greater than 180 m/s. Further, six free-flight impactors were designed and fabricated: two (beveled-cylinder and spherical) at each diameter, controlling their masses so that the induced pressure upon impact was independent of the impactor geometry.

After approval by the University of Virginia's postmortem tissue Institutional Review Board, six thawed, approximately 50th percentile male (height: 66-73 in., weight: 142-212 lb., age: 32-63 yr., BMI: 19-29 kg/m^2) post-mortem human surrogates (PMHS) were impacted in 4 primary areas on the human torso. Each area was impacted 4-5 times, for a total of 221 impacts. In addition to the location of impact, the impactor geometry and velocity were varied throughout testing. Overall, numerous data collection methodologies were applied, including pre and post-test MRI, ultrasound imaging for tissue thickness, high-speed video, autopsy, and photography.

A variety of data analysis techniques were employed following testing. Notably, tissue thickness measurements from ultrasound imaging were compared between specimens and body regions using Analysis of Variance (ANOVA) testing. Further, injury risk functions (IRFs), using Weibull survival distributions, were developed to relate the risk of significant skin injury to the impactor velocity and any additional covariates that were determined to be significant. Comparisons were made between the IRFs to assess the effects of each model covariate on the injury risk response.

Results

In total, 84 of the 221 impacts resulted in significant skin penetration, 71 of the 221 impacts were located over bone, and 6 of those 71 over-bone impacts resulted in a bony fracture. From this data, three injury risk functions (IRFs) were developed, each with varying degrees of specificity. The best-fit PMHS IRF (PMHS Model 1) related this risk to the skin thickness, impactor shape, and impactor diameter by incorporating each variable as a model covariate. Overall, the skin thickness, which differed between specimens and body regions, demonstrated the strongest influence on penetration risk, with the risk decreasing at regions of increased skin thickness. The impactor geometry (shape and diameter) also affected the injury response, with the spherical impactors with larger diameters producing the greatest risk.

Aim 2

Methods

High-rate blunt impact testing was conducted on eight whole-body, cadaveric ovine specimens to assess the tolerance of ovine skin to localized blunt impacts *in situ*. These tests were performed using different storage conditions (fresh and frozen-thawed) and tissue temperatures (laboratory and body temperature). Test day palpation, as well as post-test necropsy, was performed at each test site to assess the level of tissue failure. Pre-test imaging via MRI and shear wave elastography were utilized to determine the tissue thickness and shear wave velocity (an analogue of tissue stiffness) at each test location. Finally, injury risk functions were developed to assess the effects of impact velocity on the injury response, as well as to compare the cadaveric ovine tissue injury thresholds to those of the PMHS.

The specimens were impacted with the 0.75 in. beveled-cylindrical impactor in four locations on the body: the shoulder, ribs, stomach, and rump on each side of the animal. In addition to the location on the animal, the velocity and tissue storage/temperature conditions were varied throughout testing.

Results

In total, 80 of the 313 impact cases resulted in skin penetration, 155 of the 313 tests were conducted over bony backing materials, and 2 of the 155 bony impacts resulted in fractures. No model covariates associated with the tissue storage or temperature conditions were found to significantly affect the model fit. Similarly, univariate IRF comparisons showed that the Thawed/Lab Temperature injury response was nearly identical to that of the Fresh/Lab Temperature condition, with a mean squared error (MSE) of only 2.34. While the Fresh/Warmed response remained within the confidence intervals of the other conditions at most injury risk levels, there was disagreement between the risk curves at the lower tails, suggesting that the tissue temperature may affect the risk of skin penetration.

Additionally, the response of the PMHS Upper Chest fell within the ovine shoulder confidence interval, and the PMHS Abdomen curve stayed within the ovine stomach and rump confidence intervals. This indicates that ovine tissue may be an appropriate surrogate for PMHS tissue in these locations. Further similarities were noted between the ovine ribs, stomach, and rump responses and those of the PMHS upper chest at conditional velocity/injury risk levels.

Aim 3

Methods

This project utilized a 50th percentile male torso model and a set of nonlethal, free-flight impactor models, corresponding to the impactor geometries used in Aims 1 and 2. The torso model, modified from the

Advanced Total Body Model (ATBM) v0.86, was updated with new material models for the flesh (skin, adipose, and muscle) parts, as well as an algorithm that locally refined the mesh within these regions. These additions improved the skin deformation prediction and increased the spatial resolution in the simulated strain field in the flesh. This approach was chosen, as opposed to remeshing the entire flesh, to minimize the computational cost required to run the simulations.

Impact simulations were conducted at the anatomical impact locations used and described in Aim 1. These were defined relative to the anatomical coordinate system and averaged across all six subjects. The same anatomical coordinate system was then defined in the ATBM v0.86 model, and the nodes corresponding to the average impact locations were selected as test locations. For each simulation, skin deformation was quantified using maximum principal strain (MPS-95; across elements and time) within each pre-defined impact area.

Simulations were conducted to assess the effects of various predictor variables on the MPS-95 results. Further, a large-scale parametric study was conducted involving 1,433 impact simulations to inform the development of a meta-model, capable of predicting MPS-95 based on impact velocity, skin stiffness, adipose stiffness, impactor diameter, and impactor shape.

Results

In this study, a new finite element model of the human flesh was developed and validated for its ability to predict the likelihood of significantly injuring the skin using a rigid, blunt impactor. From this model, increasing impactor velocity resulted in greater MPS-95. This relationship between impact velocity and MPS-95 was determined to be linear at intermediate velocities (102.1-156.6 m/s), with some nonlinearity at the upper and lower bounds. Additionally, the MPS-95 response patterns were often dependent on the impactor shape, with the spherical impactors typically resulting in MPS concentrations at the location of first contact and cylindrical impactors producing increased MPS around the periphery. Skin stiffness, and adipose tissue to a lesser extent, also showed stronger correlations with MPS-95. With these variable effects quantified, a large-scale parametric study was developed to inform a meta-model capable of predicting MPS-95 from impact velocity, skin stiffness, adipose stiffness, impactor diameter, and impactor shape. The model fit was then compared to simulation data, producing an R^2 value of 0.99, slope of 0.99, and intercept of 0.004. From this meta-model, an injury risk function, based on a Weibull distribution, was developed to describe the risk of significant skin injury in terms of MPS-95.

Conclusion

Overall, the impact experiments conducted by AMERICAN SYSTEMS and the UVA-CAB consisted of over two hundred post-mortem human impact tests and over three hundred post-mortem ovine impact tests. From this experimentation, skin thickness (impact location), impactor shape, and impactor diameter were determined to be the most significant covariates for modeling the risk of PMHS skin penetration in response to impactor velocity. Similarly, the ovine risk model included the impact location; however, no anatomical correlates for this variable (tissue thickness or stiffness) could be determined. Additionally, the ovine assessment did not demonstrate a significant difference in skin penetration risk between tissue storage conditions (fresh or frozen-thawed). The tissue temperature conditions (lab temperature and warmed), contrarily, showed some minor distinction, suggesting that additional experimentation may be necessary to fully quantify these effects. Comparing the two species models, the ovine tissue showed promise as a surrogate for anterior human torso tissue, specifically at the upper chest and abdomen, under rigid blunt impacts. Further, a finite element model of the human flesh, including separate layers for skin, adipose, and muscle tissues, was developed and validated with the experimental data. A large-

scale parametric study of 1,433 simulations was designed to inform a meta-model capable of quickly predicting MPS-95 based on several test parameters. From this, an injury risk function was developed to relate MPS-95 to risk of skin penetration. In addition to the models, themselves, a user guide (including an analyst guide) has been provided to describe the methodology for utilizing each model. Future studies should expand experimental testing to include additional impactor geometries, tissue temperature conditions, and clothed specimens.

Introduction

Background

Less lethal weapons (LLWs), sometimes referred to as non-lethal weapons, are frequently observed in interactions between civilians and the military or law enforcement. These devices typically rely on blunt impacts from impactors, such as beanbag munitions or rubber bullets, as a form of crowd control [1]. These munitions are designed to minimize the risk of injury while maintaining utility as a deterrent with effective stopping power. Despite LLW munitions typically being blunt and designed to minimize injury risk, penetrative injuries are not uncommon and may become more likely depending on the location of the impact [2]. In fact, during protests in the United States during June 2020, over 50% of the hospitalizations caused by LLWs were due to blunt impacts [3]. Given their increased prevalence, there is a need to further explore the mechanisms of injury and the impact factors that drive the thresholds of injury to guide future LLW design and regulation toward human safety.

Several previous studies have experimentally modeled the general, isolated skin response to various types of perturbations. For instance, Kong et al. (2020) examined skin failure under dynamic indentations [4]. Other studies investigated the mechanical response of skin via torsional, tensile, and suction tests [5–8]. Considering the use-cases of LLWs, the injuries seen from indentations are likely the most relevant. However, while these studies succeed at isolating the skin response, they are unable to fully capture the collective behavior of skin, subcutaneous fat, and muscle.

Studying the response of the collective flesh (skin and underlying tissue layers) has been notably important when investigating the injury response across a diverse population. For instance, skin thickness and elasticity have been linked to population factors such as age, gender, and other demographical features [9, 10]. Adipose tissue, a crucial factor in automotive skin deformation, has also become an increasingly diverse component in body composition with obesity rates nearly tripling in the past 50 years [11, 12]. The fascia and muscle may also warrant consideration as backing materials that influence the boundary conditions throughout an impact. The thickness and material properties of each of these flesh layers are diverse across different anatomical locations even within the same individual [13]. Including the underlying tissue backing materials for *in situ* skin penetration testing may allow for the identification of higher-risk populations and an improved understanding of the factors driving penetration risk.

These risks are typically quantified through the development of injury risk functions (IRFs), which relate injury risk as a function of some experimental predictor [14]. Survival analyses, which take the form of Weibull, log-normal, or log-logistic distributions, are typically fit to the injury data, in place of the traditional logistic regression. This provides added relevance within the model by incorporating assumptions from proper data censoring [14, 15]. Previous studies classified potential penetrative injuries from LLWs using a risk of significant injury (RSI) framework, where an open wound to the thorax would be deemed significant if the depth exceeded the thickness of the dermis [1]. Others defined penetrative skin injury risk using metrics like the blunt criterion (BC), which described blunt skin injury risk as a factor of impactor kinematic energy, impactor size, and target size [16]. Bir et al. later refined this definition through post-mortem human surrogate (PMHS) testing by describing the injury risk as a factor of impactor energy density [17]. Additionally, the sectional density, which relates the mass of a impactor to its cross-sectional area, has been recently been used as a design criterion due to its strong correlation with penetrative injuries [18]. While previous studies incorporated test variables into the injury risk assessment, survival analysis will allow for the development of multivariate IRFs that include

compounding factors, such as impactor geometry variables (shape and size), as well as anatomical factors (such as local tissue properties).

While previous studies investigated the risk of inducing penetrative skin injuries within post-mortem human surrogates (PMHS), these techniques are accompanied by a slew of limitations. Namely, studies that utilize PMHS often include limited sample sizes (N < 10 specimens) due to difficulties in procurement and availability [19]. This scarcity also often requires the freezing and thawing of PMHS over extended periods of time to preserve the tissue between procurement and testing [20]. Unfortunately, the effects of this prolonged storage on tissue mechanics are poorly understood and require further assessment. Additionally, while PMHS are the closest avenue for testing human tissue at high-rate or injurious scenarios, they are incapable of capturing any effects associated with living tissue, such as active musculature, which may be relevant for impact cases [13].

To combat these limitations, previous studies have identified and utilized animal surrogates that closely represented the response seen in humans. These animal studies have been conducted to assess the likelihood of skin penetration under impacts using a wide variety of animal species, including porcine, ovine, bovine, equine, and hircine models [18]. While no animal model is perfectly representative of the human skin response, porcine specimens are considered most similar in cases of ballistics studies; however, the anatomical structure of porcine skin is much tougher than that of humans despite the relative similarities in skin thickness [18, 21, 22]. Alternatively, the thigh regions of ovine and hircine specimens are often used in studies of human skin penetration due to their similar penetration thresholds compared to that of PMHS [18, 23]. The remaining body regions of these animals are understudied, and a comprehensive comparison between these animals and human skin has not been conducted. As such, this study presents an assessment of ovine skin tissue as a potential surrogate for human skin tissue under high-rate impacts from rigid, blunt impactors.

One advantage of using animal surrogates is their ability to be testing under fresh, or near-fresh, tissue conditions quickly following euthanasia, obviating any potential confounders associated with prolonged tissue storage. Subsequently, by leveraging these surrogate models, the near-fresh response may be compared to that of frozen-thawed specimens or to tissue under varied temperature conditions. Previously, these concepts have been preliminarily explored using porcine or PMHS tissue samples. The effects of the freeze-thaw cycle on cadaveric porcine skin tissue were investigated by Breeze et al. (2015) and James (2020), with both concluding that there was no significant difference in the skin penetration response of the fresh and frozen-thawed tissue [18, 24]. These studies, however, were limited by sample size or the inability to test both conditions within the same specimen [18]. Similarly, while not ballistic-in-nature, Sun (2021) also found no initial significant differences in the response of fresh and frozen-thawed excised PMHS adipose tissue samples under high-rate impacts [25]. Despite these initial findings, James (2020) noted that prolonged refrigeration produced increased response variability, suggesting that tissue storage may have some influence on the skin penetration risk [18]. Further, to assess the influence of tissue temperature, Humphrey (2017) and Sun (2021) impacted excised PMHS organ tissue and adipose tissue samples, respectively, reheated to approximately the core temperature of live humans (37 °C, 98.6 °F). While the organ tissue demonstrated significant differences in the response, compared to that of non-heated tissue, the adipose tissue did not [25, 26]. To fully quantify the effects of these factors, a comprehensive study is needed that compares the injury response of intra-specimen tissue storage and temperature differences. By using animal surrogates in place of PMHS, this study may investigate the

response of fresh tissue and cover a wider range of ambient temperatures to fully assess these effects on tissue perforation risk.

In addition to cadaveric and animal surrogates for investigating flesh penetration risk, computational models provide a flexible and efficient approach for investigating injury risk and biomechanical responses of soft tissue [27]. In many cases, experimental datasets are constrained, or limited, by the specific boundary conditions used in the testing protocols. As a result, many of the derived injury risk functions are limited to those conditions. By linking experimental work with computational modeling, more flexible computational metrics for injury risk may be utilized to adapt injury risk functions to a wider range of applications or boundary conditions. For example, an experimental injury risk function developed to assess injury risk using impact velocity may only be applicable for the specific impactor used to compute that injury risk function. If a suitable model is developed to assess deformation metrics for injury, such as maximum principal strain, that injury risk function can be converted to assess injury risk as a function of maximum principal strain, which could be assessed using similar models under other loading conditions (e.g., from a different projectile shape). In this study, a torso computational model will be developed and used to develop injury risk functions to relate skin deformation (maximum principal strain) to injury risk, informed by injury risk functions developed from experimental data.

Aims

The goals of this study are to quantify the relationships between impact velocity, maximum principal strain (MPS), and the risk of penetrative skin injury in PMHS, and to investigate the effects of various testing variables, such as impactor geometry, impact location, and tissue storage and temperature conditions, on the response. Further, this study aims to determine the effectiveness of ovine skin tissue as a surrogate for post-mortem human tissue.

The specific aims of this research include:

1. Assess the tolerance of post-mortem human skin to localized blunt trauma *in-situ*.
2. Assess the tolerance of post-mortem ovine tissue to localized blunt trauma *in-situ* and evaluate the suitability of ovine as a surrogate for human tissue, and the effects of temperature and storage conditions.
3. Develop a new finite element model of the human flesh to better calculate the risk of significant skin penetration from blunt trauma indenters.

Aim 1: High-Rate Blunt Impact in Human Cadaveric Tissue

Overview

High-rate blunt impact testing was conducted on six Post-Mortem Human Surrogates (PMHS) to assess the tolerance of human skin to localized blunt impacts *in situ*. Test day palpation, as well as post-test autopsy, were performed at each test site to assess the level of tissue failure. Pre- and post-test imaging via magnetic resonance imaging (MRI) and shear wave elastography (SWE) were utilized to determine the tissue thickness and stiffness at each test location. Finally, injury risk curves were developed to compare the effects of impactor shape, size, and anatomical region on the injury risk under increasing impact velocity.

Methods

Test Setup and Equipment

High-Rate Linear Impactor and Configurable Barrels

All PMHS tests were conducted using a pneumatically driven, high-rate, linear impactor system that was designed and fabricated by the UVA-CAB, shown in Figure 1 (a). This system was capable of propelling a <20 g free-flight impactor at greater than 180 m/s. To minimize the risk of impactors undergoing deformation during the propulsion phase, this device was designed with an acceleration distance of 2 m to reduce the peak propulsive force. Further, to account for varied impactor shapes and sizes, the system was equipped with three easily configured barrels of different internal diameters: 0.50 in., 0.75 in., and 1.00 in. The system was designed to operate at pressures between 0-200 PSI. The anterior end of the barrel was fitted with a laser sight to support alignment of impact sites. impactor

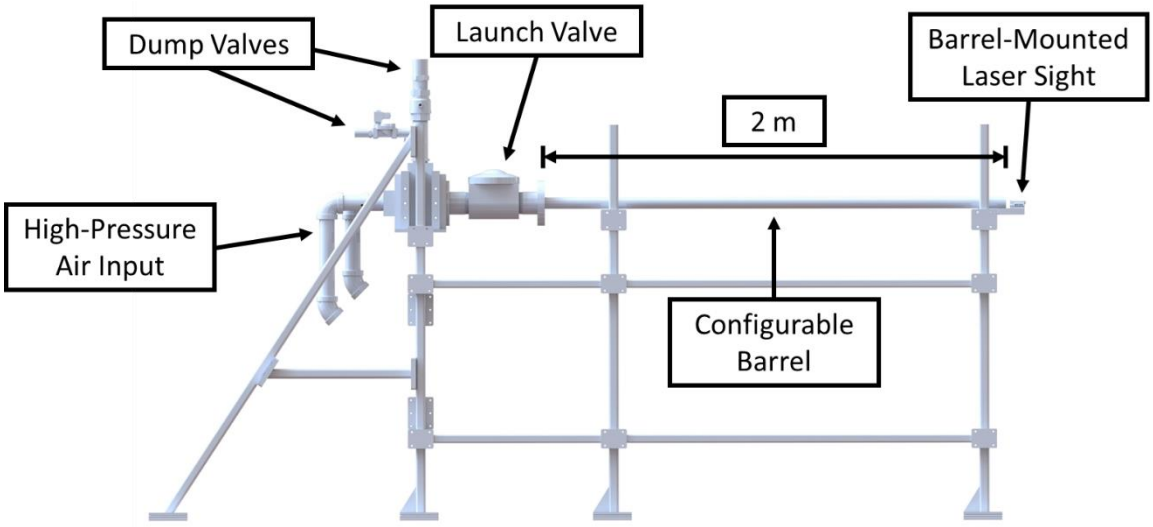


Figure 1: High-rate linear impactor system.

The high-rate linear impactor system was equipped with three configurable barrels of varying internal diameter (0.50 in., 0.75 in., and 1.00 in.).

Impactors

In total, six free-flight impactors were designed and fabricated to assess the effects of varied shapes and sizes. These included a spherical and cylindrical impactor at each of three diameters: 0.50 in., 0.75 in., and

1.00 in. The cylindrical impactors had a 1/16 in. fillet on the edge of the anterior contact surface. The mass of each impactor was selected to ensure that the mass per cross-sectional area (also known as sectional density) was a constant 2.3 g/cm^2 for each geometry. These impactors are detailed in Table I and Figure 2. Each impactor was initially characterized using speed runs sweeping from 5-50 PSI.

Table I: Specifications for the six free-flight impactors

Diameter (in.)	Shape	Mass (g)	Material
0.50	Sphere	2.9	Aluminum
0.50	Cylinder	2.9	Aluminum
0.75	Sphere	6.5	Aluminum
0.75	Cylinder	6.5	Aluminum
1.00	Sphere	11.6	Delrin
1.00	Cylinder	11.6	Aluminum

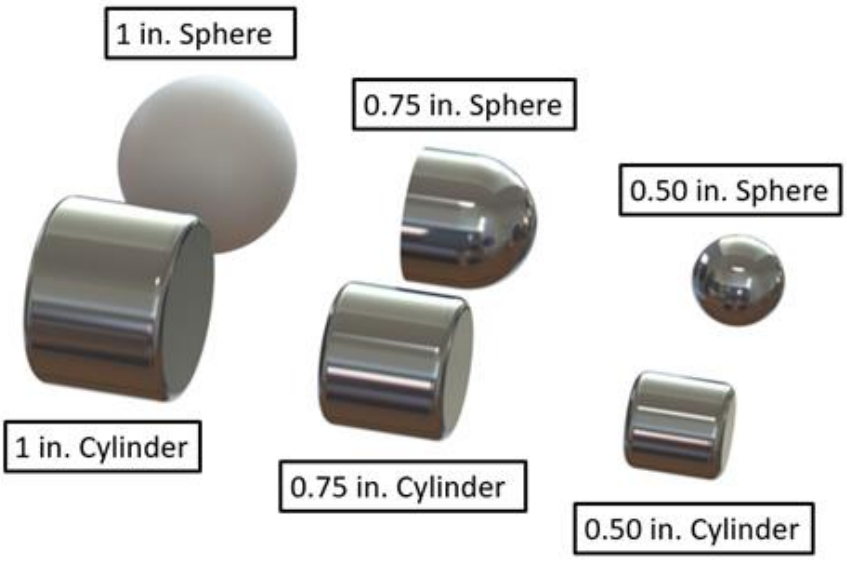


Figure 2: The six free-flight impactors.

Six free-flight impactors were used throughout testing: 0.50 in. Sphere, 0.75 in. Sphere, 1.00 in. Sphere, 0.50 in. Cylinder, 0.75 in. Cylinder, and 1.00 in. Cylinder.

Enclosure and Chair Assembly

A large (91 in. x 58 in. x 52 in.) enclosure was designed and fabricated to prevent the impactor from exiting the test area following impact with the PMHS. This both ensured the safety of the researchers throughout testing, as well as keeping potential biological contaminants within the test area. The skeleton of the enclosure was constructed using 80/20 beams. The front and (subject) left walls utilized clear polycarbonate (to allow for high-speed video), with the front wall including a 2 in. diameter cutout through which the impactor could enter the enclosure during free-flight. The remaining walls and roof

were constructed from white-painted, wooden boards and were removable throughout testing for subject positioning. Additionally, a chair, made from aluminum sheets and 80/20 beams, was centered within the enclosure to support the PMHS throughout testing. A CAD depiction of the final enclosure, chair, and PMHS setup is provided in Figure 3. The roof of the enclosure was designed with an open area to allow the subject to be supported from a gantry above the system.



Figure 3: Enclosure and chair setup for PMHS positioning.

An enclosure was built to contain any post-impact ricochet and prevent external contamination throughout testing. This structure was manufactured using 80/20 beams and polycarbonate walls. An additional wooden wall and roof were included but not pictured.

High-Speed Cameras

Three nac Memrecam GX-1 (nac Image Technology, Salem, MA) high-speed cameras were setup around the enclosure to record each impact test. One was affixed above the impactor barrel to capture the front view of the impact, another was placed normal to the (subject's left) side of the enclosure to record the full free-flight of the impactor for velocity measurement, and the final camera was for an oblique of each test. Further, three additional camera lights were placed around the enclosure to ensure that there was sufficient lighting for these high-speed cameras. This setup is shown in Figure 4.

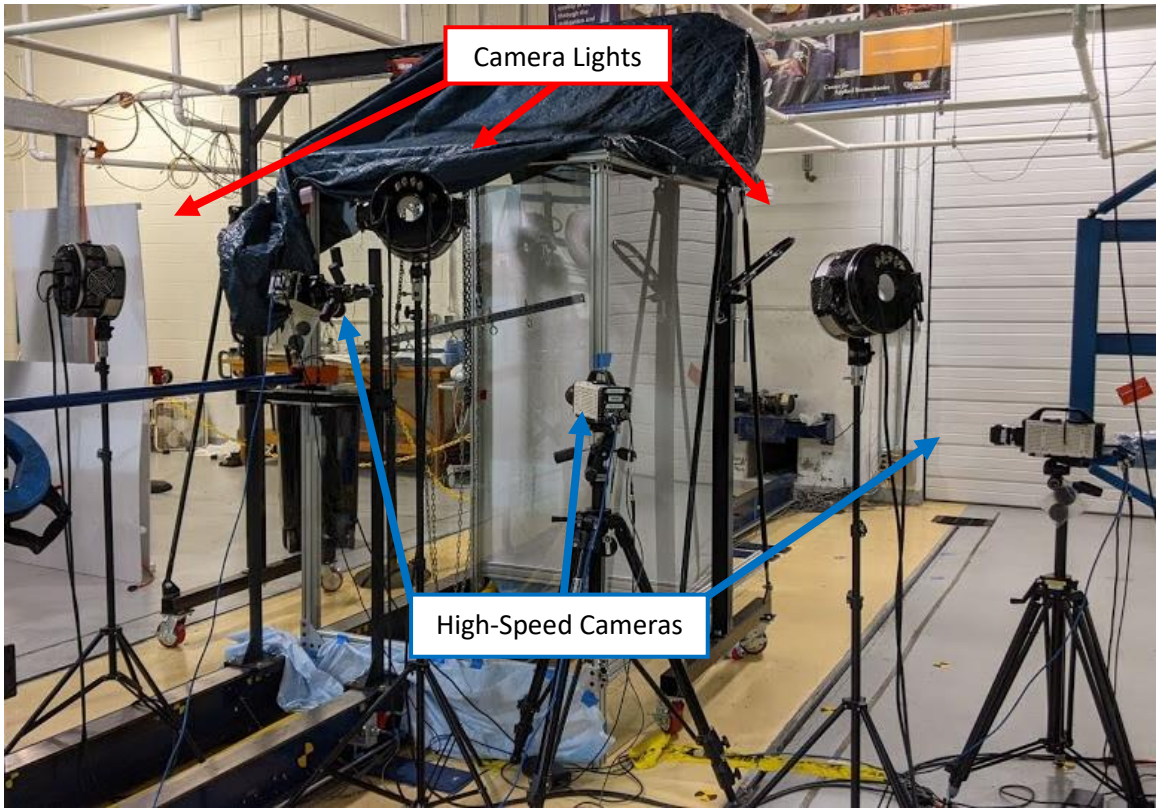


Figure 4: High-speed camera and lighting configuration.

Three high-speed nac cameras were setup to capture each impact test from various angles. Three camera lights were also interspaced throughout the testing environment to ensure proper lighting for the nac cameras. Also pictured, a gantry was constructed around the testing enclosure to suspend the specimens throughout testing.

Shear Wave Elastography System

An Aixplorer Multiwave ultrasound machine (SuperSonic imagine, Aix-en-Provence, France) with a SuperLinear SL15-4 probe was used for SWE and B-mode imaging. All SWE measurements were taken in units of m/s using the "Penetration" SWE Optimization setting, which is optimized for high-velocity shear waves for imaging of deeper, stiffer tissue [28].

PMHS Testing Procedure

PMHS Procurement

The PMHS study was approved by both the UVA Center for Applied Biomechanics cadaver protocol committee and the University of Virginia Institutional Review Board for Human Surrogate Use (IRB-HSU). Six male PMHS were procured for this study, based on an inclusion-criteria of: height 66-73 in., weight 140-195 lb., age 18-60 yr., BMI of 20-30 kg/m^2, and no previous thoracic injury or surgery. Upon procurement, all PMHS were imaged using Computed Tomography (CT) to screen for any pre-mortem injuries or anatomical irregularities. These findings, as well as general anthropometric details, for each

PMHS are provided in Table II. Based on specimen availability, some inclusion criteria were relaxed to include specimens near the original range.

Table II: General anthropometric details for each PMHS

Specimen	Age (yr.)	Height (in.)	Weight (lb.)	BMI (kg/m^2)	Notes
PMHS 1	36	69	195	28.8	Acute bilateral anterior rib fractures on the left 4th, 5th, and 6th ribs and the right 6th rib.
PMHS 2	35	72	212	28.7	
PMHS 3	63	68	185	28.1	
PMHS 4	60	66	147	23.7	Healed chronic bilateral upper rib fractures (ribs 1-5).
PMHS 5	32	73	142	18.7	
PMHS 6	49	71	186	25.9	

Subject Preparation and Pre-Test Imaging

Before impactor testing, each frozen PMHS was removed from the freezer and was thawed for approximately five days in the lab or until the tissue reached lab temperature (~65°F). Once thawed, each PMHS completed a pre-testing MRI scan. The MRI protocol included a large field of view axial T1-turbo spin echo, and a coronal and axial Dixon volumetric interpolated breath-hold examination (VIBE) with in/out phase, water, and fat sequences.

Following MRI, anthropometry measurements were collected using body calipers and measuring tape. Measurements were taken with the PMHS in a supine posture. Details on each measurement are provided in Appendix 1.

Subjects were positioned in the seated posture with support from the head/neck via the gantry system such that the spine was oriented vertically. With the PMHS in a seated posture, midlines were drawn on each torso to standardize the measurement of impact locations across the six PMHS. This included the anterior midline (defined from the sternal notch to the navel), the posterior midline (defined from the T1 spinous process to the L1 spinous process), and the transverse axis (defined radially from the xyphoid process). These axes are detailed in Figure 5 and Table III.

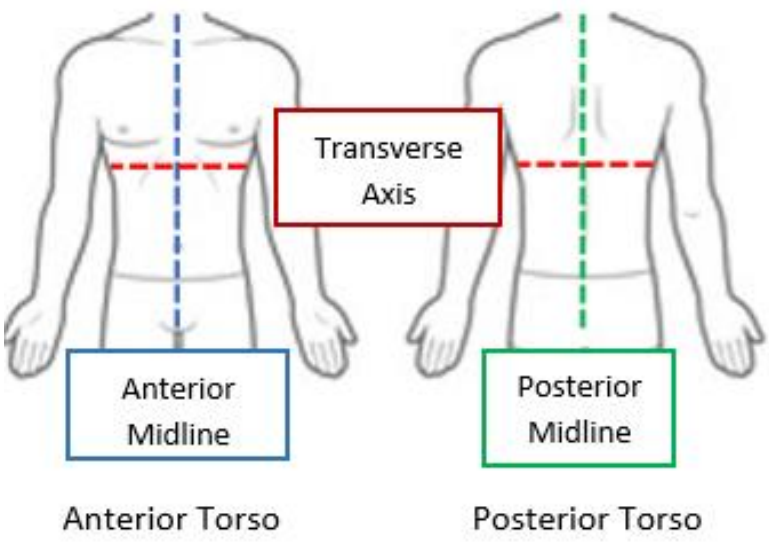


Figure 5: Anatomical axis definitions.

Three anatomical axes were defined on each PMHS. The anterior midline was defined from the sternal notch to the navel, the posterior midline was defined from the T1 spinous process to the L1 spinous process, and the transverse axis was defined radially from the xyphoid process.

Table III: Anatomical axis landmarks

Axis	Landmark 1	Landmark 2
Anterior Midline	Sternal Notch	Navel
Posterior Midline	T1 Spinous Process	L1 Spinous Process
Transverse	Xyphoid Process	

Each impact location was marked on the PMHS to designate the location of pre-test ultrasound imaging. First, a 5 in. diameter circle was marked at each body region (bilateral abdomen, upper chest, lower back, and upper back). Within this large circle, 4-5 individual impact locations were defined, along with exclusion zones (at which no impacts would overlap). These exclusion zones were established as 2.5 times the diameter of the impactor. Due to the size of these exclusion zones, the tests involving the 1.00 in. impactors only included four impacts per region, as opposed to the five impacts per 0.50 in. and 0.75 in. test region. These marking patterns are described in Table IV and Figure 6.

Table IV: Impact location exclusion zone sizes

Impactor Diameter	Impacts per Body Region	Exclusion Zone Diameter
1.00 in.	4	2.50 in.
0.75 in.	5	1.88 in.
0.50 in.	5	1.25 in.

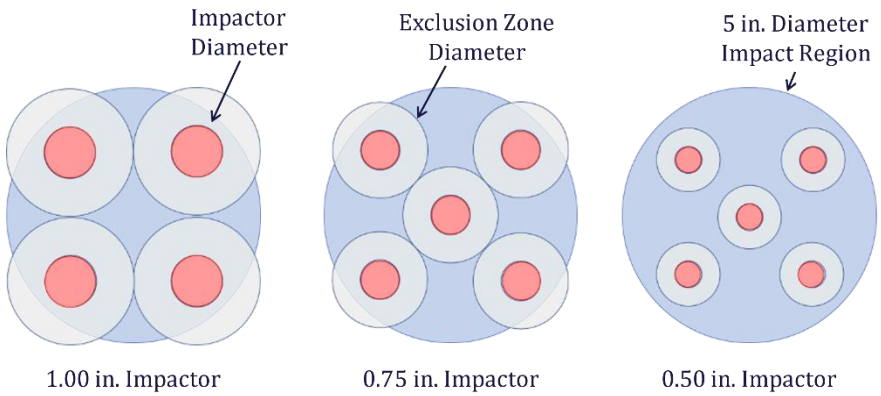


Figure 6: Impact site and exclusion zone criteria for each impactor size.

A 5 in. diameter zone was defined for each anatomical impact region. Within these, five impact sites were defined per region for the 0.50 in. and 0.75 in. impactors, while four impact sites were defined for the 1.00 in. impactors. Each impact site included an exclusion zone that was 2.5 times the diameter of the impactor size.

Once defined, each impact location was imaged using the Aixplorer Multiwave ultrasound machine with the SL15-4 probe with the PMHS in a seated posture. Five SWE images were taken at each test site using an image depth of 3.5 cm, and one B-mode image was captured at a depth of 5 cm.

Impactor Testing

Ahead of impact testing, the suspended PMHS was relocated into the testing enclosure and positioned in a seated posture on the seat. In addition to the gantry, which supported the PMHS' head and neck, foam blocks and ratchet straps were used to support the torso in the upright position.

Four primary body regions were selected for impactor testing (upper chest, abdomen, upper back, and lower back), as shown in Figure 7 (a). The upper chest was defined as the region inferior to the clavicle, lateral to the sternum, and medial to the axilla. The abdomen was defined as the region inferior to the ribcage, superior to the pelvis, and lateral to the navel. The upper back was defined as inferior to the scapula, superior to the transverse midline, and lateral to the transverse processes. The lower back was defined as inferior to the transverse midline, superior to the pelvis, and lateral to the transverse processes.

Each region was impacted bilaterally, with the left and right sides of any given PMHS being impacted with the two different shape (sphere and cylinder) impactors of the same size (0.50 in., 0.75 in., or 1.00 in.). For example, the right upper chest of PMHS 1 was impacted by the 0.50 in. sphere, while the left upper chest was impacted by the 0.50 in. cylinder. The full test matrix is provided in Table V.

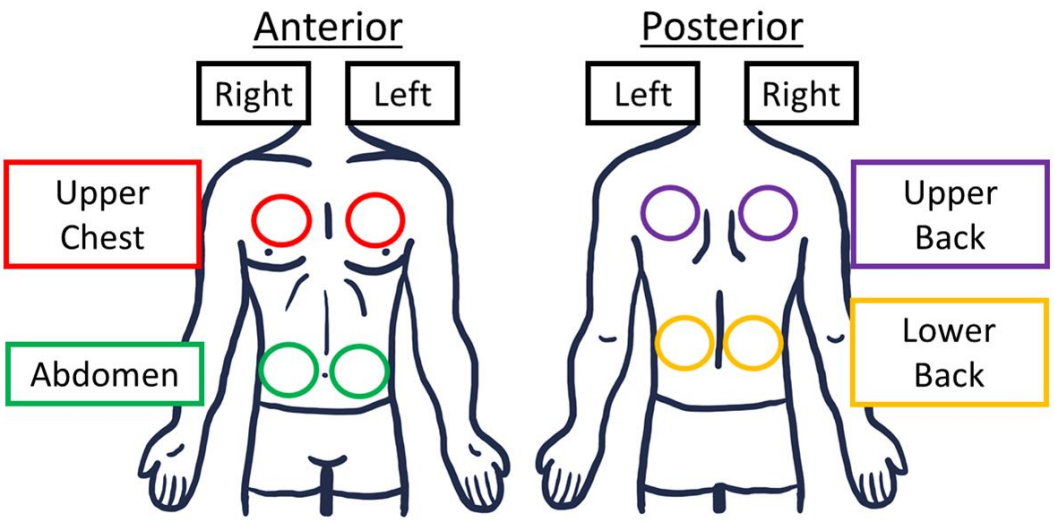


Figure 7: PMHS anatomical impact regions.

Four anatomical impact regions were defined for each PMHS. These included the Upper Chest, Abdomen, Upper Back, and Lower Back. Each region was defined for both the left and right sides of each PMHS.

*Table V: Test matrix for the PMHS impactor testing**

Region	Side	PMHS 1	PMHS 2	PMHS 3	PMHS 4	PMHS 5	PMHS 6
Upper Chest	Right	0.50 in. Sphere	1.00 in. Sphere	0.75 in. Sphere	0.50 in. Cylinder	1.00 in. Cylinder	0.75 in. Cylinder
	Left	0.50 in. Cylinder	1.00 in. Cylinder	0.75 in. Cylinder	0.50 in. Sphere	1.00 in. Sphere	0.75 in. Sphere
Abdomen	Right	0.75 in. Sphere	0.50 in. Sphere	1.00 in. Sphere	0.75 in. Cylinder	0.50 in. Cylinder	1.00 in. Cylinder
	Left	0.75 in. Cylinder	0.50 in. Cylinder	1.00 in. Cylinder	0.75 in. Sphere	0.50 in. Sphere	1.00 in. Sphere
Upper Back	Right	0.75 in. Sphere	0.50 in. Sphere	1.00 in. Sphere	0.75 in. Cylinder	0.50 in. Cylinder	1.00 in. Cylinder
	Left	0.75 in. Cylinder	0.50 in. Cylinder	1.00 in. Cylinder	0.75 in. Sphere	0.50 in. Sphere	1.00 in. Sphere
Lower Back	Right	0.50 in. Sphere	1.00 in. Sphere	0.75 in. Sphere	0.50 in. Cylinder	1.00 in. Cylinder	0.75 in. Cylinder
	Left	0.50 in. Cylinder	1.00 in. Cylinder	0.75 in. Cylinder	0.50 in. Sphere	1.00 in. Sphere	0.75 in. Sphere
Number of Impacts**		40	36	36	40	36	36

** Orange cells indicate a 0.50 in. diameter, blue cells indicate a 0.75 in. diameter, and green cells indicate a 1.00 in. diameter. Lighter colored cells indicate spherical impactor shape, and darker colored cells indicate cylindrical impactor shape.*

*** Of the 224 planned impact cases, 221 total impacts were conducted.*

For each test, the gantry and supporting foam blocks were used to reposition the PMHS to ensure that the high-rate linear impactor was aligned with the desired test location. Before each impact, the surface temperature of the local tissue at the impact site was measured using a handheld Etekcity infrared thermometer (Vesync Co., Anaheim, CA, USA).

The impact velocity for each test was selected to bound the 50% injury risk threshold for each PMHS. Within each body region, the first impact (of 4-5) utilized the 50% injury risk velocity, determined by previous experiments. In subsequent tests within the same body region, the impact velocity was increased or decreased based on the "injury" or "non-injury" result, respectively, from previous tests. Full descriptions of each impact test, as well as the binary injury result are provided in Appendix 2.

Each impact was captured using the three high-speed cameras at 10,000 frames per second with a resolution of 512 pixels x 384 pixels. After each impact, the test site was photographed, inspected visually, and palpated. If the impactor penetrated into or through the skin, the diameter and depth of injury were measured, the diameter and depth of penetration were measured. Additionally, the distance of each impact from the anatomical (midline and transverse) axes were measured.

Post-Test Imaging and Autopsy

Following the completion of testing, each PMHS was imaged again using MRI, following the same MRI protocol from pre-test imaging.

Each PMHS was autopsied to fully assess the severity of each impact test and to retrieve any impactors that were left within the tissue. Using a binary "injury" or "no injury" assessment criteria, each impact was investigated at various levels, as described in

Table VI. Full results from each autopsy are provided in Appendix 3.

Table VI: Autopsy assessments

Binary Assessment Level	Description
Minor Skin Damage	Any permanent deformation or damage to the skin that did not result in any full thickness skin failure
Skin Failure	An injury that penetrated through the skin tissue significantly enough that fat was visible but was not > 5 mm deep
Penetration (> 5 mm)	An injury that penetrated > 5 mm into the tissue, often entering the subcutaneous fat layer [1]
Full Fat Disruption	An injury that penetrated fully through the subcutaneous fat but did not penetrate into the fascia layer
Partial Muscle Disruption	An injury that penetrated through the fascia and into the muscle but not fully through the muscle
Full Muscle Disruption	An injury that penetrated all the way through the muscle layers; often, these impacts stopped against the peritoneum or pleural membrane
Full Penetration	An injury that penetrated through all available tissue; often, these impacts entered the peritoneum, pleural membrane, or stopped against bone
Presence of Bone	The presence of bone as a backing material
Fracture	Any induced fractures of present bone

Data Analysis

Impact Velocity Measurement

High speed video files were converted from .mcf to .avi for use with Matlab (MathWorks Inc., Natick, MA, USA) scripts to calculate the free-flight velocity of each impact. To calibrate the script, a visible reference of known size was used to convert pixel values to measurable units. The centroid of the impactor, once in frame, was tracked to impact. Instantaneous velocity was computed as change in position per frame. This was converted to m/s using the camera's frame rate. Low velocities computed from frames at impact and outliers were removed to compute the mean velocity of an impactor flight.

Tissue Thickness Measurement

Matlab scripts were developed to measure the thickness of each tissue layer (skin, fat, fascia, and muscle) from the SWE and B-mode ultrasound images at each impact location. The Matlab script allowed the users to manually select the bounds of each tissue layer at three separate locations per ultrasound image. The three regions were then averaged per tissue layer to determine the thickness at each impact location. These location-based thickness were also averaged per body region (with left and right separated) and per subject (with left and right combined).

Shear Wave Elastography

Because shear stiffness was related to the square of shear wave velocity, the output from the SWE machine was set to wave speed. The average shear wave velocities for each tissue from the thickness measurements in each SWE image were calculated using a custom Matlab script. This script involved selecting the tissue of interest within the image, calculating the shear wave velocity of each pixel in this region using the associated color bar values, and averaging the velocity at each pixel within the selected boundaries. The previous thickness measurements were used as guidelines in determining regions of interest for corresponding images.

Statistical Analysis

To understand how our tissue thickness and shear wave velocity measurements varied by region and by specimen, we performed several analysis of variance (ANOVA) tests. We considered one-way analyses, using either specimen or region as our grouping factor. The multcompare function in Matlab was used to perform Tukey-Kramer corrections for multiple comparisons.

Injury Risk Curve Development

PMHS injury risk functions (IRFs) were developed using custom R scripts. Each IRF was fit to the experimental data using interval censored Weibull distributions through the survreg() function with the RStudio (RStudio PBC, Boston, MA, USA) package Survival [29]. All models used the impactor's free-flight velocity (m/s) as the primary predictor and the binary ("yes" or "no") injury (> 5 mm of penetration) designation as the outcome [1]. The general equations for the Weibull IRFs are provided in Equation 1-Equation 3 [30]:

$$Injury\ Risk = 1 - e^{-x^{\alpha}}$$

Equation 1: The survival function for the Weibull distribution.

$$\alpha = \frac{1}{e^{logscale}}$$

Equation 2: The shape parameter for the Weibull distribution.

$$x = Velocity * e^{-[\beta_0 + (\beta_1 * X_1) + \cdots + (\beta_n * X_n)]}$$

Equation 3: Covariate survival time for the Weibull distribution.

where *logscale* is a constant output given by the survreg() function, β_0 is the intercept of the model fit, β_n is the coefficient for each model covariate X_n.

The model covariates were determined by independently adding each test variable to the survreg() call. The overall p-value for each model was collected and compared to other potential covariates. This analysis is shown in Appendix 4. The covariates that produced the lowest log-likelihood p-values were then implemented, one-at-a-time, into the model to determine the best combination. Further, a *cluster* term was added to the models to identify specimen-based groupings within the dataset for robust variance calculation [29]. This term counteracted cross-subject variance and reduced the standard errors of the models.

The IRFs were used to compare the effects of each selected on the injury response. The predict.survreg() function within RStudio was used to determine the predicted response under each set of test conditions. Each predicted fit and 95% confidence interval were then plotted and compared to other test parameters.

Results

Anthropometry

Anthropometry measurements (Mean ± 1 SD) are provided in Table VII. Details on each measurement are provided in Appendix 1.

Table VII: PMHS anthropometry results

Body Region	Measurement	Mean ± 1 SD
	Age (yr)	45.8 ± 12.3
	Height (in.)	69.8 ± 2.41
	Weight (lb)	177.8 ± 25.2
	BMI (kg/m^2)	25.7 ± 3.6
Shoulder	Biacromial Breadth (cm)	37.8 ± 2.6
	Interscye Distance (cm)	32.7 ± 4.0
Chest	Chest Breadth, 4th Rib (cm)	34.2 ± 4.4
	Chest Breadth, 8th Rib (cm)	34.7 ± 4.2
	Chest Depth, 4th Rib (cm)	22.1 ± 2.6
	Chest Depth, 8th Rib (cm)	22.7 ± 2.4
	Chest Circumference, 4th Rib (cm)	102.1 ± 9.8
	Chest Circumference, 8th Rib (cm)	102.4 ± 10.0
Waist	Waist Breadth, 8cm Above Umbilicus (cm)	35.6 ± 4.4
	Waist Breadth, at Umbilicus (cm)	36.2 ± 4.0
	Waist Breadth, 8cm Below Umbilicus (cm)	34.5 ± 3.5
	Waist Depth, 8cm Above Umbilicus (cm)	20.1 ± 2.9
	Waist Depth, at Umbilicus (cm)	19.5 ± 2.9
	Waist Depth, 8cm Below Umbilicus (cm)	19.0 ± 2.3
	Waist Circumference, 8cm Above Umbilicus (cm)	98.7 ± 11.3
	Waist Circumference, at Umbilicus (cm)	98.1 ± 12.7
	Waist Circumference, 8cm Below Umbilicus (cm)	93.6 ± 11.2

Hip	Hip Breadth (cm)	34.9 ± 2.2
	Hip Depth (cm)	18.2 ± 1.1
	Hip Circumference (cm)	93.9 ± 8.2
Buttock	Buttock Breadth (cm)	36.4 ± 3.1
	Buttock Depth (cm)	17.0 ± 3.2
	Buttock Circumference (cm)	97.9 ± 5.3

Tissue Temperature

The surface tissue temperature was collected at each impact location ahead of testing. The mean (±1 SD) tissue temperature values for each PMHS are provided in Table VIII.

Table VIII: PMHS Surface Tissue Temperature

Specimen	Surface Tissue Temperature (°F) (Mean ± 1 SD)
All PMHS (N = 6)	64.8 ± 2.3
PMHS 1	66.7 ± 2.1
PMHS 2	66.7 ± 2.3
PMHS 3	62.9 ± 1.8
PMHS 4	64.8 ± 2.1
PMHS 5	64.5 ± 0.7
PMHS 6	63.1 ± 1.1

Impact Velocity Calculations

Impactor velocity was calculated for each test case using high-speed video. These values are provided in Figure 8.

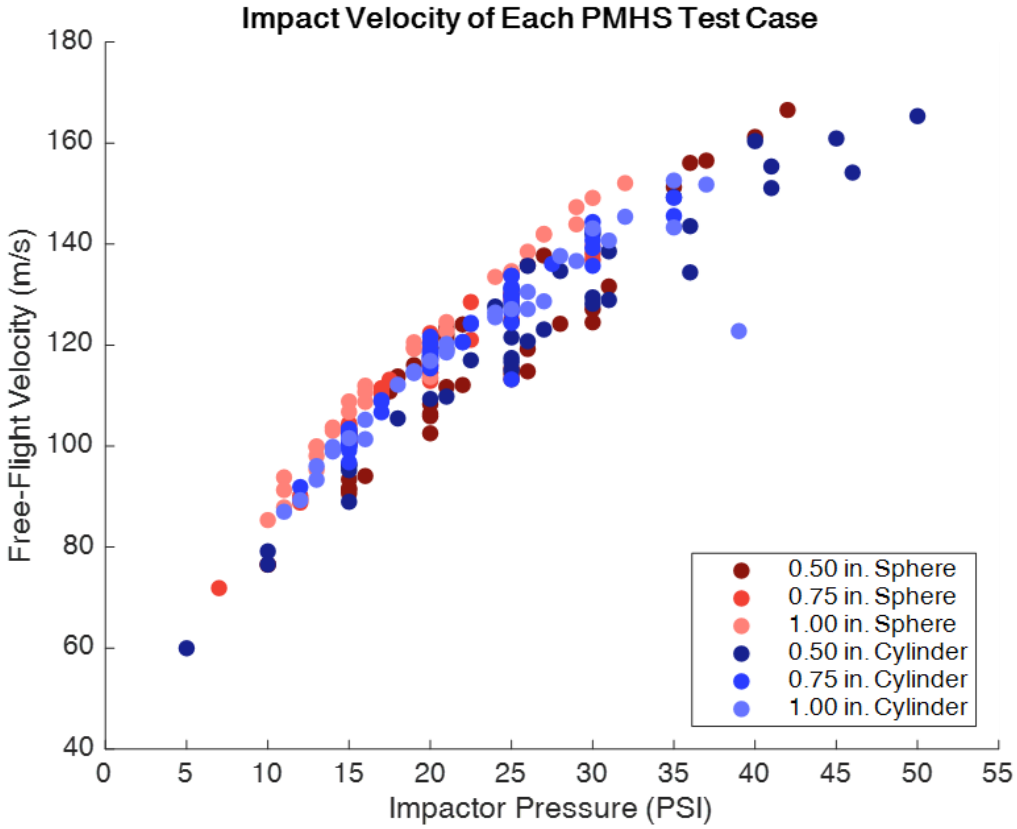


Figure 8: Impactor velocity as a function of impactor pressure for all tested PMHS impact cases. Free-flight velocity (m/s) was calculated for each impact case from high-speed video. These values were plotted against the test-day impactor pressure (PSI).

The thickness of each tissue layer (skin, subcutaneous fat, fascia, and muscle) was measured at each impact location using ultrasound imaging. As no ultrasound imaging was collected for PMHS 1, no tissue thickness data was available for that specimen. Further, some tissue layer measurements were limited by the depth of the ultrasound imaging, which showed a maximum depth of 5 cm per impact location. The mean (± 1 SD) tissue thickness for each layer (across PMHS 2-6) are provided in Table IX.

Tissue Thickness Measurements

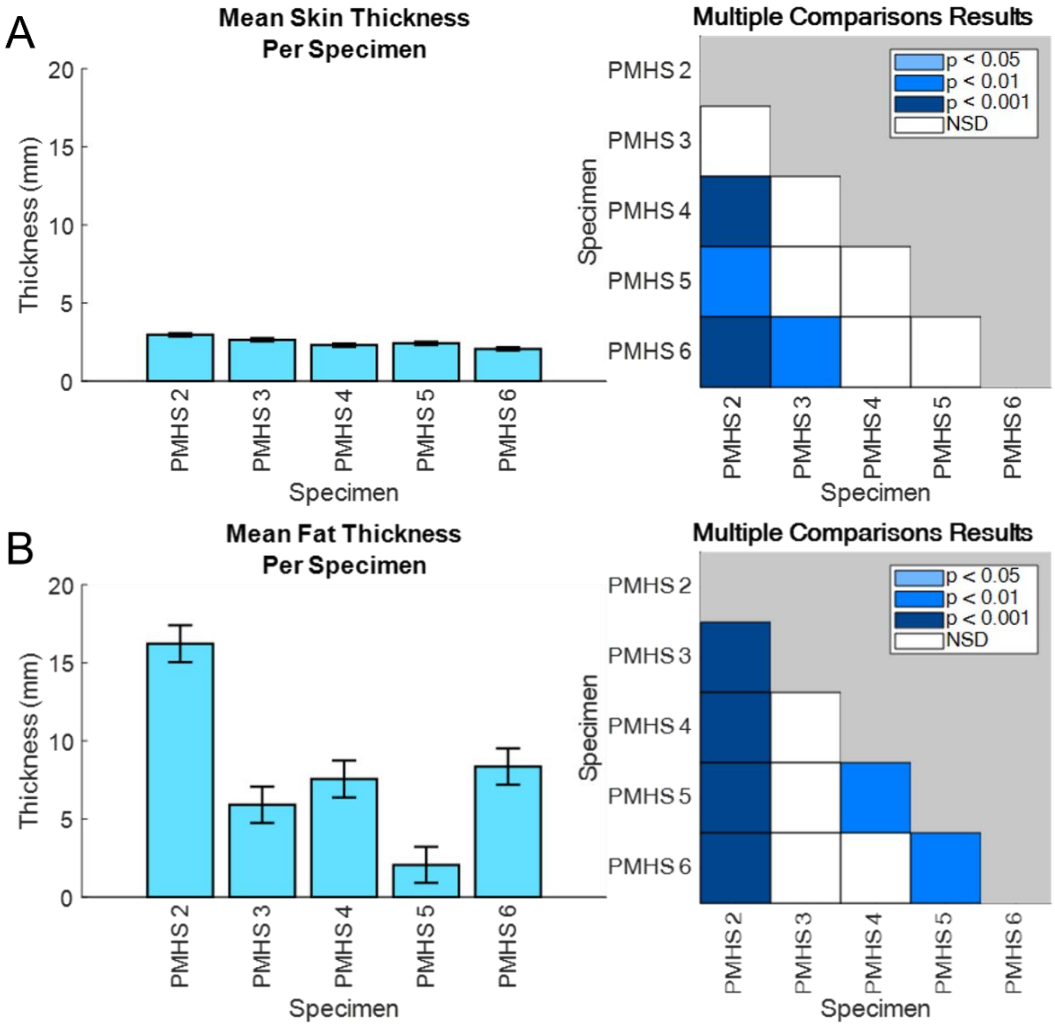
The thickness of each tissue layer (skin, subcutaneous fat, fascia, and muscle) was measured at each impact location using ultrasound imaging. As no ultrasound imaging was collected for PMHS 1, no tissue thickness data was available for that specimen. Further, some tissue layer measurements were limited by the depth of the ultrasound imaging, which showed a maximum depth of 5 cm per impact location. The mean (± 1 SD) tissue thickness for each layer (across PMHS 2-6) are provided in Table IX.

Table IX: PMHS Tissue Thickness per Tissue Layer

Tissue Layer	Tissue Thickness (mm) (Mean ± 1 SD)
Skin	2.48 ± 0.71
Subcutaneous Fat	7.95 ± 8.24
Fascia	1.70 ± 0.70
Muscle	12.2 ± 7.78

Overall, the muscle layer was the thickest (12.2 mm), followed by the subcutaneous fat (7.95 mm), the skin (2.48 mm), and then the fascia (1.70 mm). Further, the subcutaneous fat layers had the greatest variance across the PMHS with a standard deviation of 8.24 mm.

The mean thickness of each tissue layer is presented per specimen in Figure 9. Here, the specimen-specific tissue thickness is compared at each layer using one factor ANOVA.



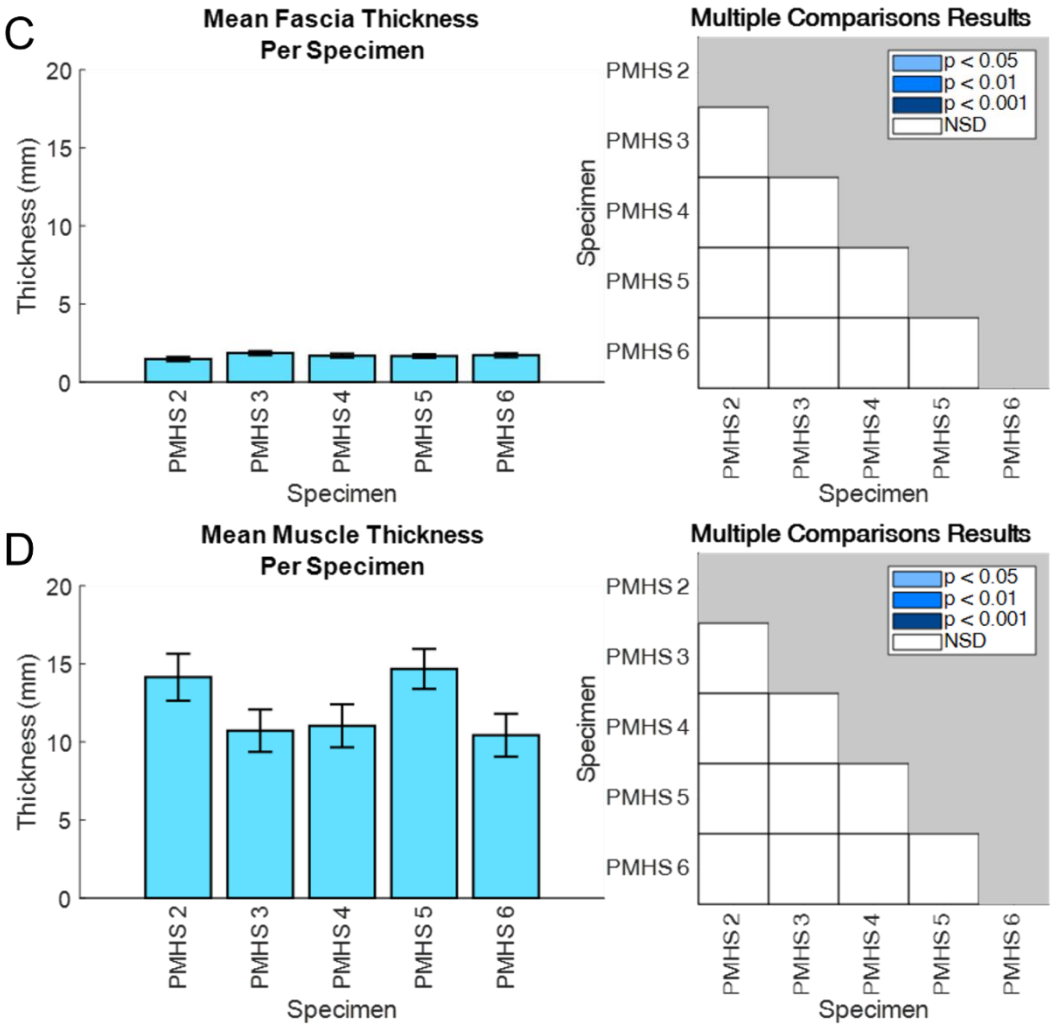
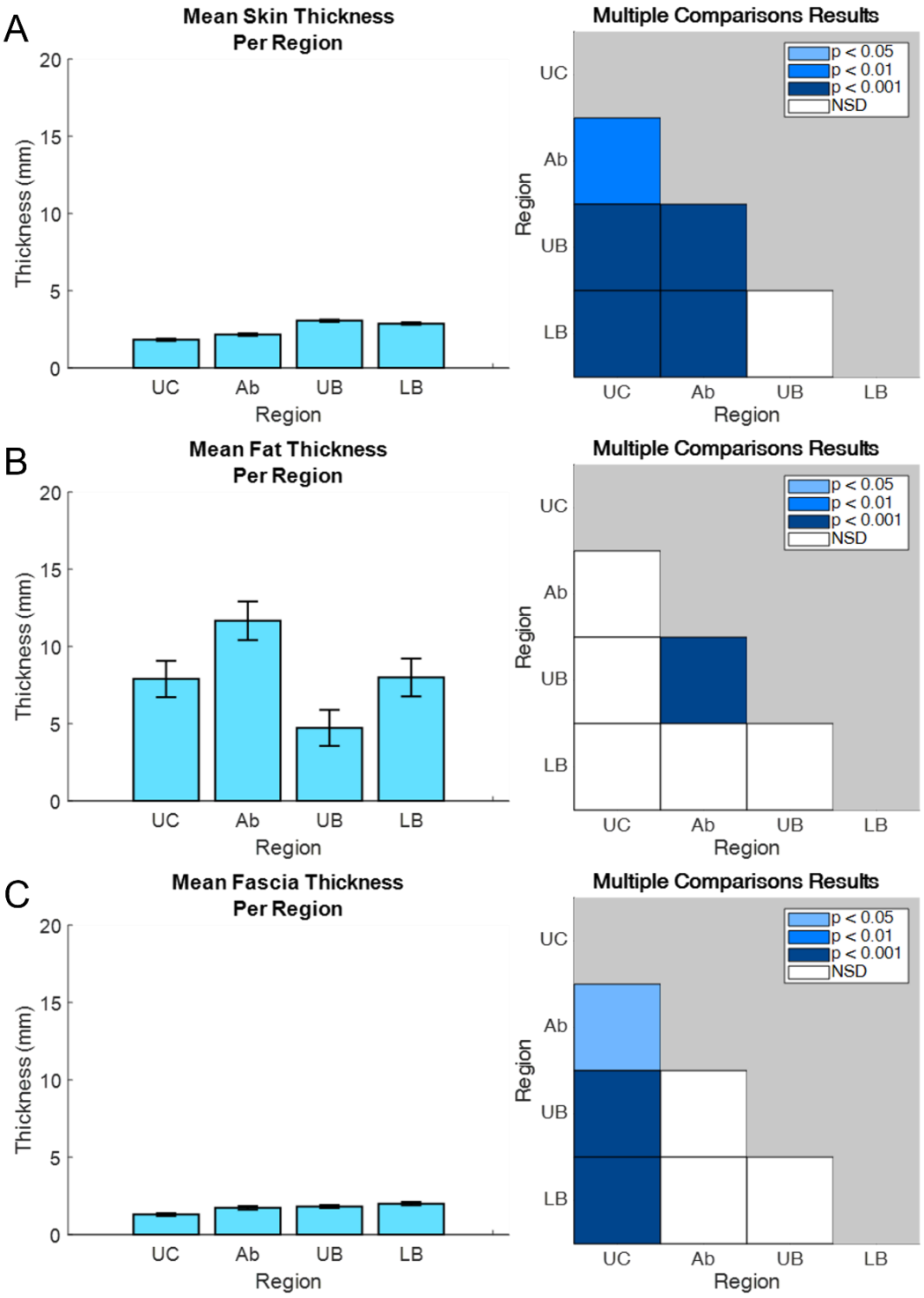


Figure 9: Tissue thickness measurements for each PMHS specimen.

This figure presents bar charts of mean tissue thickness (±1 SE) (left) and multiple comparisons significance analysis (right) for the each PMHS at every tissue layer: (a) skin, (b) fat, (c) fascia, and (d) muscle. NSD = no significant difference.

Figure 9 (a) showed that PMHS 2 contained a significantly thicker skin layer than PMHS 4-6 ($p < 0.01$), while PMHS 3 had significantly thicker skin than PMHS 6 ($p < 0.01$). Figure 9 (b) showed that PMHS 2 had a significantly thicker fat layer than all other specimens ($p < 0.001$), and PMHS 5 was had significantly thinner fat than PMHS 4 and PMHS 6 ($p < 0.01$). Figure 9 (c-d) showed that there were not significant differences between specimens at the deeper tissue layers (fascia or muscle).

Additional comparisons were made between body regions (Upper Chest, Abdomen, Upper Back, and Lower Back) by averaging the thickness of each like-region tissue layer across specimens. This comparison is presented in Figure 10.


A
Mean Skin Thickness
Per Region
Thickness (mm)
0
5
10
15
20
UC
Ab
UB
LB
Region
Multiple Comparisons Results
p < 0.05
p < 0.01
p < 0.001
NSD
UC
Ab
UB
LB
Region
B
Mean Fat Thickness
Per Region
Thickness (mm)
0
5
10
15
20
UC
Ab
UB
LB
Region
Multiple Comparisons Results
p < 0.05
p < 0.01
p < 0.001
NSD
UC
Ab
UB
LB
Region
C
Mean Fascia Thickness
Per Region
Thickness (mm)
0
5
10
15
20
UC
Ab
UB
LB
Region
Multiple Comparisons Results
p < 0.05
p < 0.01
p < 0.001
NSD
UC
Ab
UB
LB
Region

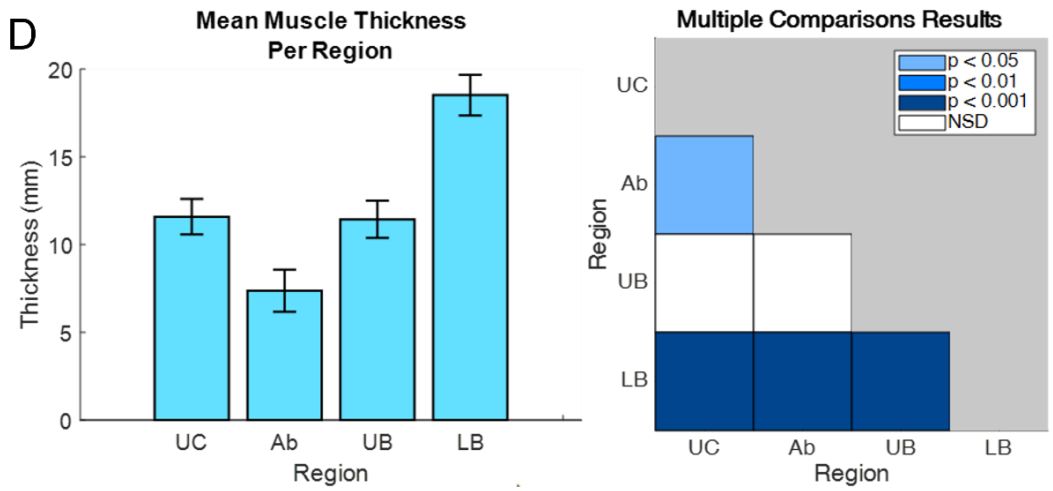


Figure 10: Tissue thickness measurements for each PMHS body region.

This figure presents bar charts of mean tissue thickness (±1 SE) (left) and multiple comparisons significance analysis (right) for each body region at every tissue layer: (a) skin, (b) fat, (c) fascia, and (d) muscle. UC = Upper Chest, Ab = Abdomen, UB = Upper Back, and LB = Lower Back. NSD = no significant difference.

Figure 10 (a) showed that the posterior body regions (Upper Back and Lower Back) were the only regions with similar skin thickness ($p > 0.05$), with the posterior regions being significantly thicker ($p < 0.001$) than the anterior regions (Upper Chest and Abdomen). Further, the Abdomen had significantly thicker skin than the Upper Chest ($p < 0.01$). Figure 10 (b) showed that the only significant difference at the fat layer was between the Abdomen and the Lower Back ($p < 0.001$), with the Abdomen containing much thicker fat than the Lower Back. Figure 10 (c) showed that the Upper Chest contained a significantly thinner fascia layer than the posterior regions ($p < 0.001$) and the Abdomen ($p < 0.05$). Finally, Figure 10 (d) showed that the Lower Back contained significantly thicker muscle layers than all other regions ($p < 0.001$), and the Upper Chest contained thicker muscles than the Abdomen ($p < 0.05$). Additional tissue thickness results are provided in Appendix 5.

Shear Wave Velocity Measurements

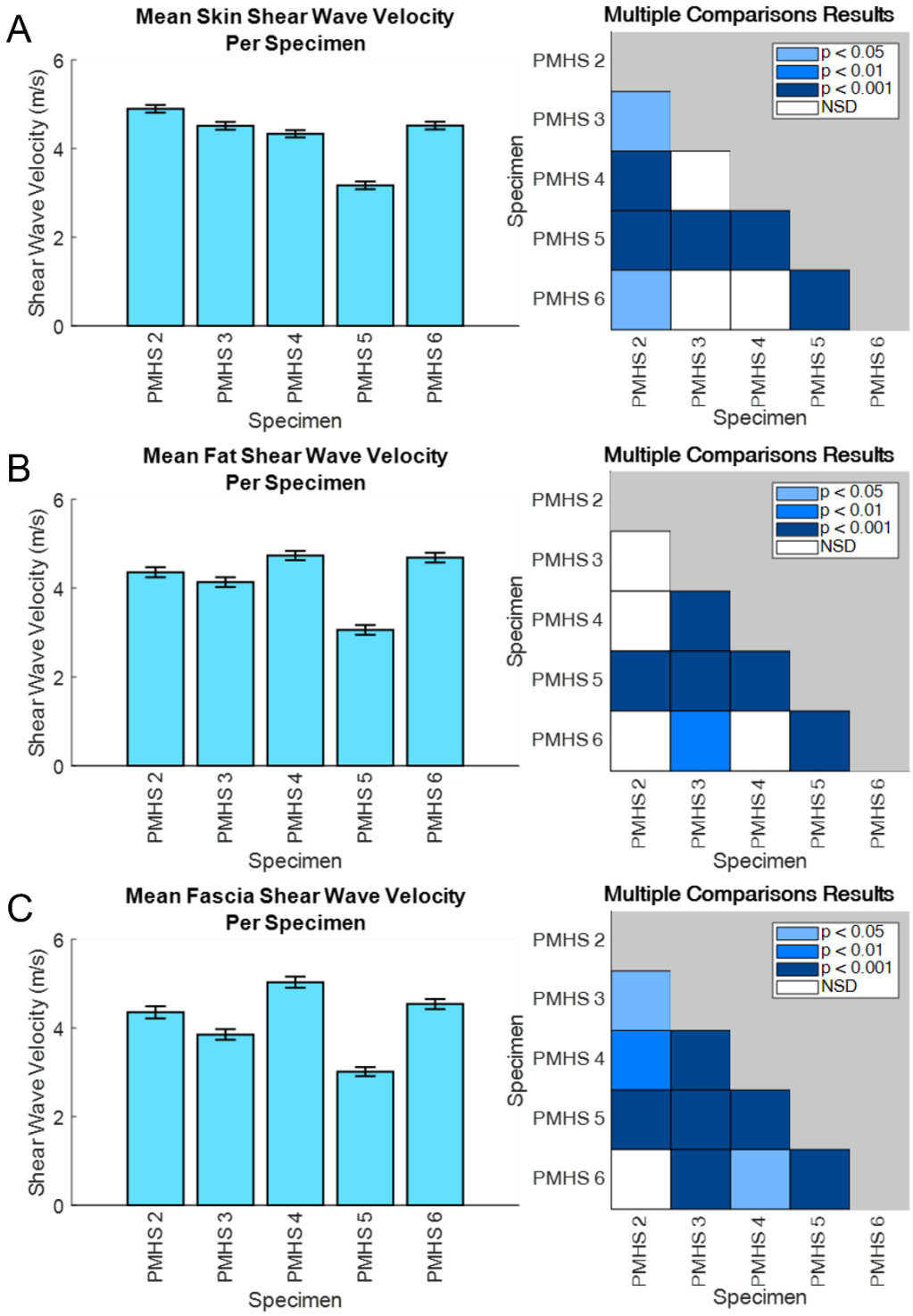
The shear wave velocity of each tissue layer (skin, subcutaneous fat, fascia, and muscle) was measured at each impact location using ultrasound imaging, as it was directly proportional to tissue stiffness. As no ultrasound imaging was collected for PMHS 1, no SWE data was available for that specimen. The mean (± 1 SD) shear wave velocity for each layer (across PMHS 2-6) are provided in Table X.

Table X: PMHS Shear Wave Velocity per Tissue Layer

Tissue Layer	Shear Wave Velocity (m/s) (Mean ± 1 SD)
Skin	4.27 ± 1.12
Subcutaneous Fat	4.20 ± 1.56
Fascia	4.07 ± 1.50
Muscle	3.33 ± 1.34

Overall, the stiffest tissue layer was the skin (shear wave velocity = 4.27 m/s), followed by the subcutaneous fat (4.20 m/s), the fascia (4.07 m/s), and then the muscle (3.33 m/s).

The mean shear wave velocity for each specimen is depicted in Figure 11. Here, the specimen-specific shear wave velocity is compared at each layer using one factor ANOVA.



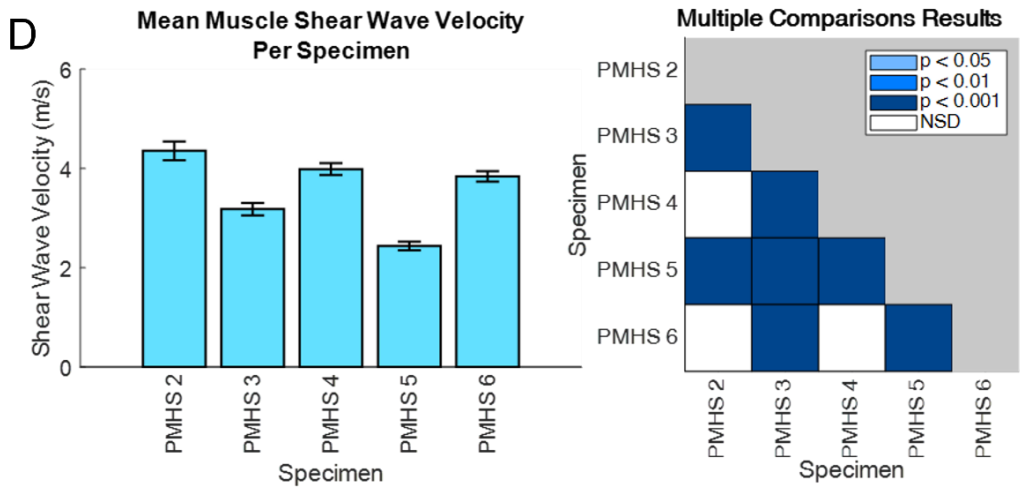
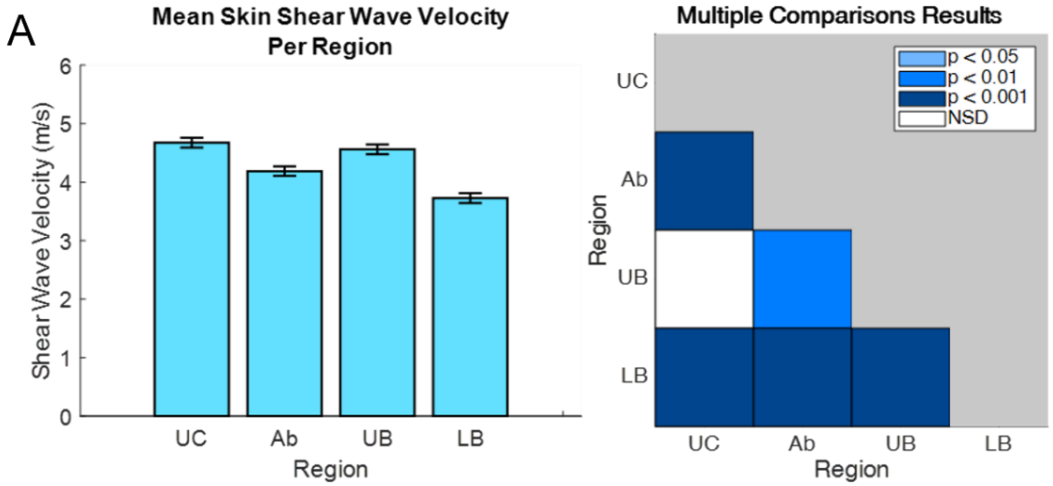


Figure 11: Tissue shear wave velocity measurements for each PMHS specimen.

This figure presents bar charts of mean tissue shear wave velocity (±1 SE) (left) and multiple comparisons significance analysis (right) for the each PMHS at every tissue layer: (a) skin, (b) fat, (c) fascia, and (d) muscle. NSD = no significant difference.

Overall, PMHS 5 had consistently lower tissue stiffness than the other specimens ($p < 0.001$). In Figure 11 (a), PMHS 2 had the stiffest skin; in Figure 11 (b), PMHS 4 and 6 had the stiffest fat, but not significantly more than PMHS 2; in Figure 11 (c), every specimen besides PMHS 2 and 6 had unique fascia stiffnesses; in Figure 11 (d), PMHS 2, 4, and 6 had the stiffest muscle ($p < 0.001$).

Additional comparisons were made between body regions (Upper Chest, Abdomen, Upper Back, and Lower Back) by averaging the stiffness of each like-region tissue layer across specimens. This comparison is presented in Figure 12.



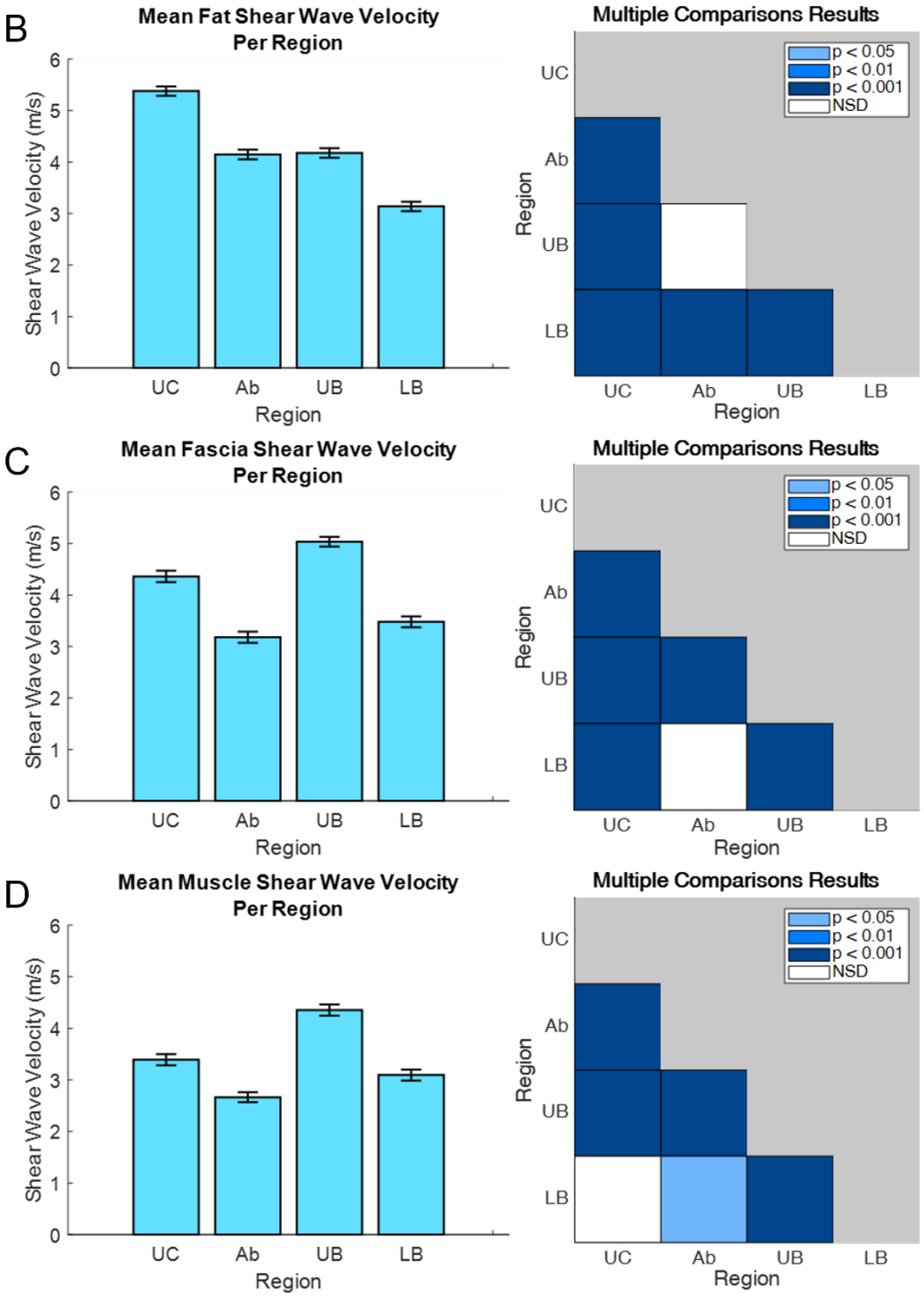


Figure 12: Tissue shear wave velocity measurements for each PMHS body region.

This figure presents bar charts of mean tissue shear wave velocity (±1 SE) (left) and multiple comparisons significance analysis (right) for each body region at every tissue layer: (a) skin, (b) fat, (c) fascia, and (d) muscle. UC = Upper Chest, Ab = Abdomen, UB = Upper Back, and LB = Lower Back. NSD = no significant difference.

In Figure 12 (a), the superior regions of all PMHS had stiffer skin than the inferior regions. Figure 12 (b) showed that Upper Chest fat tissue was significantly stiffer ($p < 0.001$) than that of all other regions; Abdomen and Upper Back were significantly stiffer ($p < 0.001$) than Lower Back. Figure 12 (c) revealed that the fascia in the Upper Back was significantly stiffer ($p < 0.001$) than Upper Chest which was also significantly ($p < 0.001$) stiffer than both inferior regions. Again, in Figure 12 (d), Upper Back had the stiffest muscle tissue ($p < 0.001$), while Abdomen had the least stiff tissue ($p < 0.001$ vs. Upper Chest; $p < 0.05$ vs. Lower Back).

PMHS IRF Covariate Assessment

Following the independent covariate analysis, the eight most significant covariates for the PMHS IRF model are provided in Table XI. The full list of assessed covariates, and their associated p-values, are provided in Appendix 4.

Table XI: PMHS Covariate Assessment
(Covariates Shown in Order of Increasing p-Value)

Covariate	p-Value
Skin Thickness (mm)	4.0e-07
Body Region	2.0e-06
Impactor Shape	4.6e-03
Specimen ID	1.3e-02
Fascia Shear Wave Velocity (m/s)	1.4e-02
Muscle Thickness (mm)	5.8e-02
Fat Shear Wave Velocity (m/s)	1.5e-01
Muscle Shear Wave Velocity (m/s)	2.6e-01

The following covariates were determined to be significant for the PMHS IRF: skin thickness, body region, impactor shape, specimen ID, and fascia shear wave velocity. Specimen ID, while significant, was deemed too specific for a useful analysis and was excluded. Further, the Specimen term was included in each model within the cluster(Specimen) function as a means of grouping variance. Additionally, it was determined that the Skin Thickness covariate essentially included the same information as the Body Region covariate, due to the significant differences in skin thickness between regions. Therefore, the more significant and less specific covariate (Skin Thickness) was determined to be the more useful.

While not significant on its own, the Impactor Diameter was determined to be significant when added with the Impactor Shape covariate. In total, the most significant combination of covariates included Skin Thickness, Impactor Shape, and Impactor Diameter.

PMHS IRF Model Development

In total, three PMHS IRFs were developed. The most specific, and best-fit, of which (PMHS Model 1) utilized the specimen's local skin thickness (*mm*), the impactor shape (sphere or cylinder), and the impactor diameter (in.) as covariates. Two less specific models were also developed for applications outside of the specific conditions of this test series. The first of which (PMHS Model 2) excluded the impactor diameter covariate, leaving skin thickness and impactor shape. Finally, the most general model (PMHS Model 3) incorporated skin thickness as the sole covariate. Additional details on these covariates are provided in Table XII.

Table XII: Covariate Details for PMHS IRFs

Covariate	Type	Bounds/Categories
Skin Thickness (mm)	Continuous	1.39 – 4.39
Impactor Shape	Categorical	Sphere, Cylinder
Impactor Diameter (in.)	Continuous	0.50 – 1.00

As all models used skin thickness as a covariate, data from PMHS 1 was excluded from the model fit, since no ultrasound images were taken for PMHS 1.

PMHS Model 1 (Covariates: Skin Thickness, Impactor Shape, and Impactor Diameter)

The fit for PMHS Model 1 was calculated by substituting Equation 4 into Equation 1 & Equation 2:

$$x = Velocity * e^{-[\beta_0+(\beta_1*SkinThickness)+(\beta_2*Shape{:}Sphere)+(\beta_3*Diameter)]}$$

Equation 4: The Weibull survival function for PMHS Model 1

where *Velocity* is the free-flight impactor velocity (*m/s*), *Skin Thickness* is the local skin thickness of the specimen (*mm*), *Diameter* is the diameter of the impactor (*in.*), and *Shape:Sphere* is a binary value (1 or 0) depending on whether the impactor shape is a sphere. The values for the coefficients (*logscale*, β_0, β_1, β_2, and β_3) are provided in Table XIII.

Table XIII: Coefficient Values for PMHS Model 1 (Covariates: Skin Thickness, Shape, & Diameter)

Coefficient	Covariate	Magnitude	Standard Error	p-Value
β_0	Intercept	4.60413	0.13494	< 2.0e-16
β_1	Skin Thickness (mm)	0.21151	0.04884	1.5e-05
β_2	Impactor Shape (Sphere)	-0.14410	0.00637	< 2.0e-16
β_3	Impactor Diameter (in.)	-0.16440	0.08651	3.5e-02
	Logscale	-2.01484	0.18497	< 2.0e-16

Additional statistics for this model fit are provided in Table XIV.

Table XIV: Weibull IRF Statistics for PMHS Model 1
(Covariates: Skin Thickness, Shape, & Diameter)

Statistic	Value
Scale	0.133
Loglikelihood (Model)	-94.10
Loglikelihood (Intercept Only)	-116.0
Chi Squared	43.84
Degrees of Freedom	3.000
p-Value	1.6e-09
Number of Newton-Raphson Iterations	16.00
n	182.0

As Model 1 requires detailed specifications of the impactor, two less-specific IRFs were developed for cases in which these values are not known. The first of which (PMHS Model 2) utilized the specimen's local skin thickness (mm) and the impactor shape as covariates. Additional details on these covariates are provided in Table XII.

PMHS Model 2 (Covariates: Skin Thickness and Impactor Shape)

The fit for PMHS Model 2 is calculated by substituting Equation 5 into Equation 1 & Equation 2:

$$x = Velocity * e^{-[\beta_0 + (\beta_1 * SkinThickness) + (\beta_2 * Shape{:}Sphere)]}$$

Equation 5: The Weibull survival function for PMHS Model 2

where *Velocity* is the free-flight impactor velocity (*m/s*), *Skin Thickness* is the local skin thickness of the specimen (*mm*), and *Shape:Sphere* is a binary value (1 or 0) depending on whether the impactor shape is a sphere. The values for the coefficients (*logscale*, β_0, β_1, and β_2) are provided in Table XV.

Table XV: Coefficient Values for PMHS Model 2
(Covariates: Skin Thickness & Shape)

Coefficient	Covariate	Magnitude	Standard Error	p-Value
β_0	Intercept	4.45798	0.12936	< 2.0e-16
β_1	Skin Thickness (mm)	0.22309	0.05722	9.7e-05
β_2	Impactor Shape (Sphere)	-0.14782	0.00723	< 2.0e-16
	Logscale	-1.95975	0.17095	< 2.0e-16

Additional statistics for this model fit are provided in Table XVI.

Table XVI: Weibull IRF Statistics for PMHS Model 2 (Covariates: Skin Thickness & Shape)

Statistic	Value
Scale	0.141
Loglikelihood (Model)	-95.90
Loglikelihood (Intercept Only)	-116.0
Chi Squared	40.16
Degrees of Freedom	2.000
p-Value	1.9e-09
Number of Newton-Raphson Iterations	17.00
n	182.0

PMHS Model 3 (Covariate: Skin Thickness)

For the most general model (PMHS Model 3), all impactor-based parameters were removed from the model fit. The remaining model only utilized the specimen's local skin thickness (*mm*) as its sole covariate. The skin thickness covariate details are, again, provided in Table XII. Additionally, the equation for the new model is provided in Equation 6 and can be substituted into Equation 1 & Equation 2 to calculate the model fit for any given skin thickness value.

$$x = Velocity * e^{-[\beta_0 + (\beta_1 * Skin\ Thickness)]}$$

Equation 6: The Weibull distribution formula using skin thickness as a covariate

where *Velocity* is the free-flight impactor velocity (*m/s*) and *Skin Thickness* is the local skin thickness of the specimen (*mm*). The values for the coefficients (*logscale*, β_0, and β_1) are provided in Table XVII.

Table XVII: Coefficient Values for PMHS Model 3 (Covariate: Skin Thickness)

Coefficient	Covariate	Magnitude	Standard Error	p-Value
β_0	Intercept	4.3808	0.1611	< 2.0e-16
β_1	Skin Thickness (mm)	0.2363	0.0719	1.0e-03
	Logscale	-1.7011	0.1393	< 2.0e-16

Additional statistics for this model fit are provided in Table XVIII.

Table XVIII: Weibull IRF Statistics for PMHS Model 3
(Covariate: Skin Thickness)

Statistic	Value
Scale	0.182
Loglikelihood (Model)	-103.0
Loglikelihood (Intercept Only)	-116.0
Chi Squared	25.95
Degrees of Freedom	1.000
p-Value	3.5e-07
Number of Newton-Raphson Iterations	10.00
n	182.0

PMHS IRF Response Comparisons

To assess the effects of each covariate on the PMHS injury response, the following comparisons were made using the most specific model (PMHS Model 1), which accounted for the specimen's local skin thickness, the impactor shape, and the impactor diameter as covariates. For simplicity, these comparisons were made by predicting the model response for a standardized set of impact scenarios. Unless specified, the predictions were made using a fixed skin thickness of 2.48 mm (the average across all six PMHS), a cylindrical impactor shape, and an impactor diameter of 0.75 in. Additional PMHS Model 1 prediction comparisons, using other covariate values, are presented in Appendix 6. Further, IRF comparisons using PMHS Model 2 and PMHS Model 3 are presented in Appendices 7 and 8, respectively.

First, the effects of variations in the skin thickness covariate were assessed predicting the IRF response for the 0.75 in. cylinder impactor at the mean (± 1 SD) skin thickness. A few key injury risk levels are highlighted in

Table XIX and the full predicted response with 95% confidence intervals are plotted in Figure 13.

Table XIX: Predicted PMHS Injury Risk For Varied Skin Thickness (Mean ± 1 SD)
(Impactor Shape = Cylinder, Impactor Diameter = 0.75 in.)

	Impactor Velocity (m/s)		
Injury Risk (%)	**-1 SD Skin Thickness (1.77 mm)**	**Mean Skin Thickness (2.48 mm)**	**+1 SD Skin Thickness (3.20 mm)**
5	86.4	100.4	116.9
10	95.1	110.5	128.7
15	100.8	117.1	136.4
25	108.8	126.4	147.2
50	122.3	142.1	165.5
75	134.1	155.9	181.5

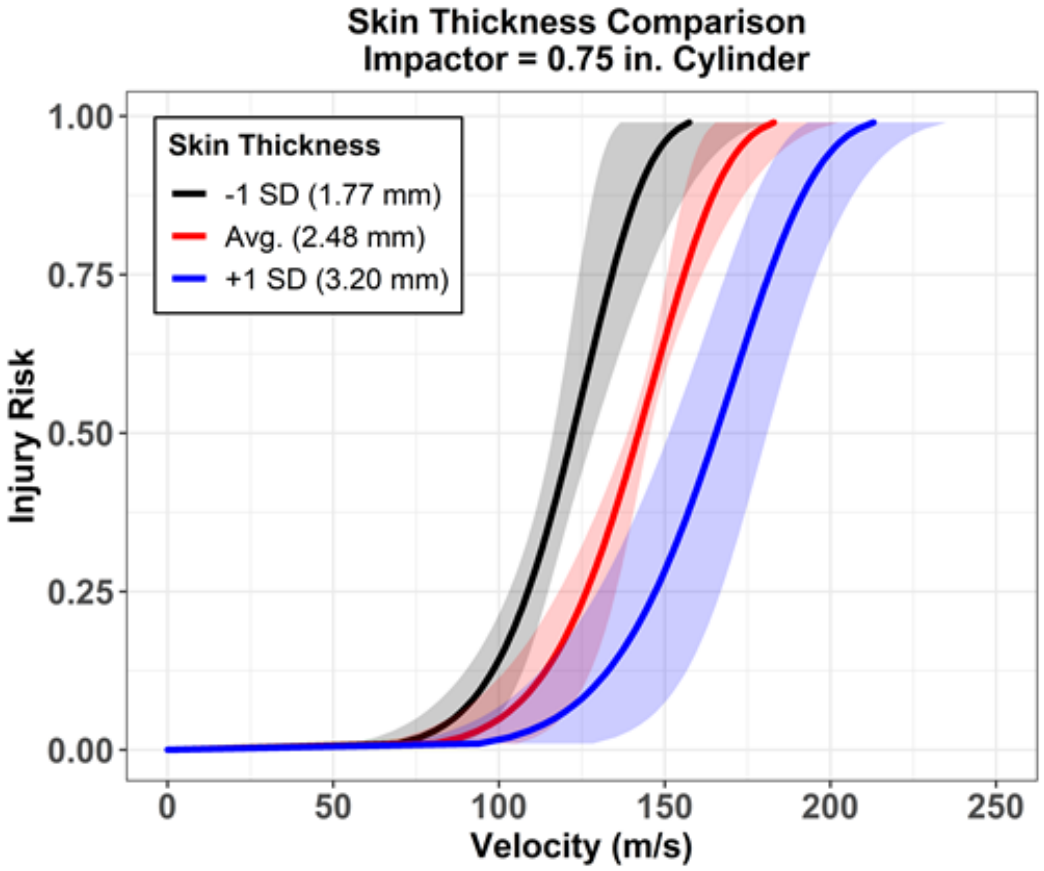


Figure 13: The effects of overall skin thickness variations on the PMHS IRF response.
The IRF response was predicted for the 0.75 in. cylinder impactor at three skin thickness levels (1.77 mm, 2.48 mm, and 3.20 mm) representing the mean thickness (± 1 SD) for the six PMHS. The corridors represent the 95% confidence intervals for each predicted response.

Figure 13 shows that, within the range of tested specimens, variations in skin thickness resulted in significant shifts of the predicted response, with the thinner skin resulting in a greater injury risk at a lower velocity. Additionally, the model with the greatest skin thickness produced the widest confidence interval, likely indicating a gap in the dataset and the additional variability of response at the extreme skin thickness.

Next, the effects of regional skin thickness were assessed by predicting the IRF response for the 0.75 in. cylinder impactor at the average skin thickness of each body region. These included 1.83 mm for the Upper Chest, 2.16 mm for the Abdomen, 3.06 mm for the Upper Back, and 2.87 mm for the Lower Back. A few key injury risk levels are highlighted in Table XXIII and the full predicted response with 95% confidence intervals are plotted in Figure 14.

Table XX: Predicted PMHS Injury Risk For Varied Body Region
(Impactor Shape = Cylinder, Impactor Diameter = 0.75 in.)

	Impactor Velocity (m/s)			
Injury Risk (%)	**Upper Chest (Skin Thickness = 1.83 mm)**	**Abdomen (Skin Thickness = 2.16 mm)**	**Upper Back (Skin Thickness = 3.06 mm)**	**Lower Back (Skin Thickness = 2.87 mm)**
5	87.5	93.8	113.5	109.1
10	96.3	103.3	125.0	120.0
15	102.1	109.4	132.4	127.2
25	110.1	118.1	142.9	137.2
50	123.8	132.8	160.6	154.3
75	135.8	145.7	176.2	169.3

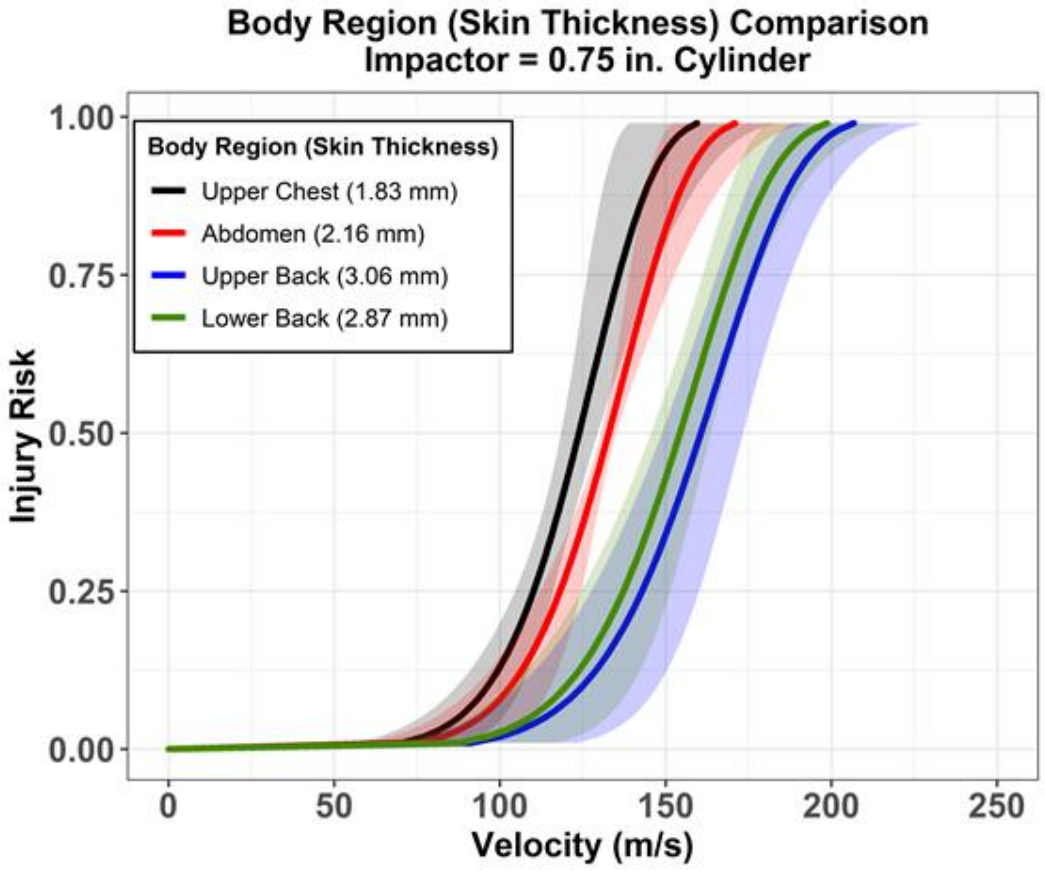


Figure 14: The effects of regional skin thickness variations on the PMHS IRF response.

The IRF response was predicted for the 0.75 in. cylinder impactor at four skin thickness levels (1.83 mm, 2.16 mm, 3.06 mm, and 2.87 mm) representing the mean thickness for the Upper Chest, Abdomen, Upper Back, and Lower Back, respectively. The corridors represent the 95% confidence intervals for each predicted response.

Figure 14 shows that the response across body regions was grouped by which side of the body was being impacted (anterior or posterior). Generally, the anterior regions (Upper Chest and Abdomen) contained thinner skin, which resulted in a greater injury risk at lower velocities. Conversely, the posterior regions (Upper Back and Lower Back) had thicker skin, requiring higher impact velocities to produce increased injury risk. Like in Figure 13, the 95% confidence intervals were much wider under elevated skin thickness (posterior regions), likely due to increased variance of response and lower sampling under these conditions.

Further, the effects of impactor shape were assessed by predicting the IRF response for a 0.75 in. diameter impactor at the average PMHS skin thickness (2.48 mm) for both the spherical and cylindrical impactor shapes. A few key injury risk levels are highlighted in Table XXIV and the full predicted response with 95% confidence intervals are plotted in Figure 15.

Table XXI: Predicted PMHS Injury Risk For Impactor Shape
(Skin Thickness = 2.48 mm, Impactor Diameter = 0.75 in.)

	Impactor Velocity (m/s)	
Injury Risk (%)	**Shape = Sphere**	**Shape = Cylinder**
5	86.9	100.4
10	95.7	110.5
15	101.4	117.1
25	109.4	126.4
50	123.0	142.1
75	134.9	155.9

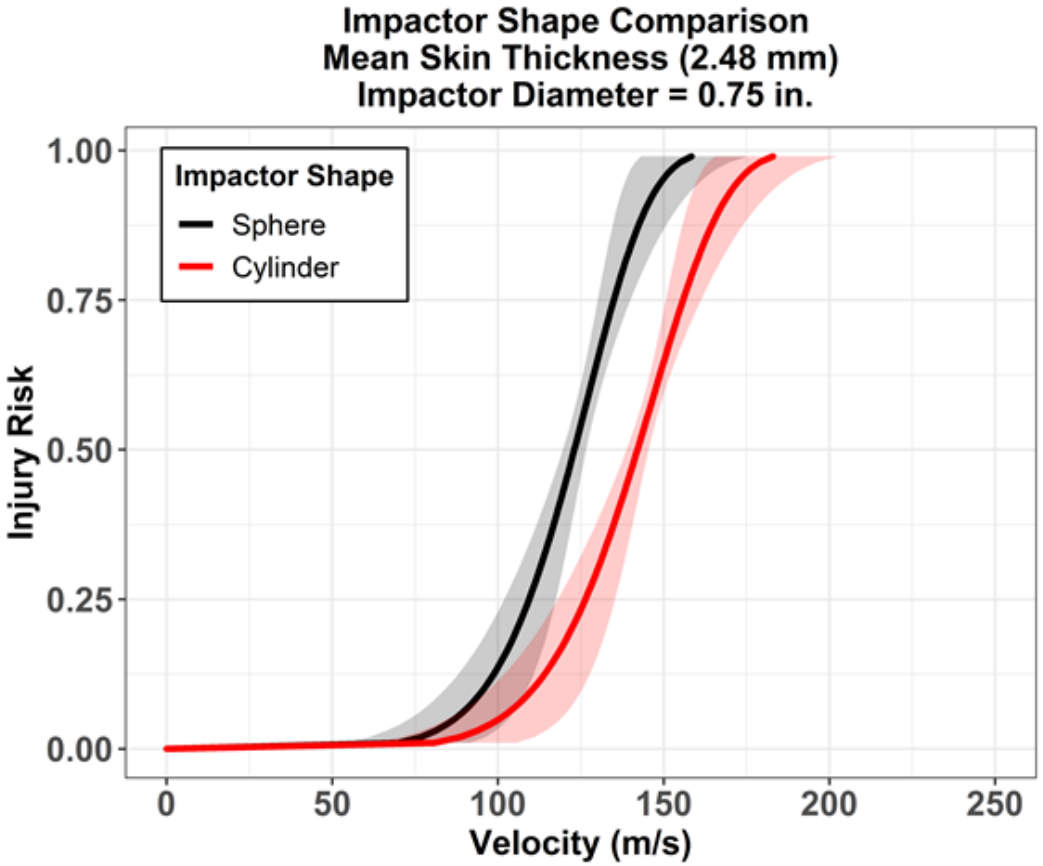


Figure 15: The effects of impactor shape variations on the PMHS IRF response.
The IRF response was predicted for the 0.75 in. impactor at the average PMHS skin thickness (2.48 mm) for the spherical and cylindrical impactor shapes. The corridors represent the 95% confidence intervals for each predicted response.

Figure 15 shows that, generally, the spherical impactor shape produced a greater injury risk than the cylindrical impactor shape under lower velocities. Further, the 50% injury risk range has an extremely thin 95% confidence interval, due to the increased sampling at this injury level throughout testing, as compared to the tails of the curve.

The effects of impactor diameter were then assessed by predicting the IRF response for the cylindrical impactor at the average PMHS skin thickness (2.48 mm) for each of the tested impactor diameters (0.50 in., 0.75 in., and 1.00 in.). A few key injury risk levels are highlighted in Table XXII and the full predicted response with 95% confidence intervals are plotted in Figure 16.

Table XXII: Predicted PMHS Injury Risk for Varied Impactor Diameter
(Skin Thickness = 2.48 mm, Impactor Shape = Cylinder)

	Impactor Velocity (m/s)		
Injury Risk (%)	**Diameter = 0.50 in.**	**Diameter = 0.75 in.**	**Diameter = 1.00 in.**
5	104.6	100.4	96.4
10	115.2	110.5	106.1
15	122.0	117.1	112.4
25	131.7	126.4	121.3
50	148.1	142.1	136.4
75	162.4	155.9	149.6

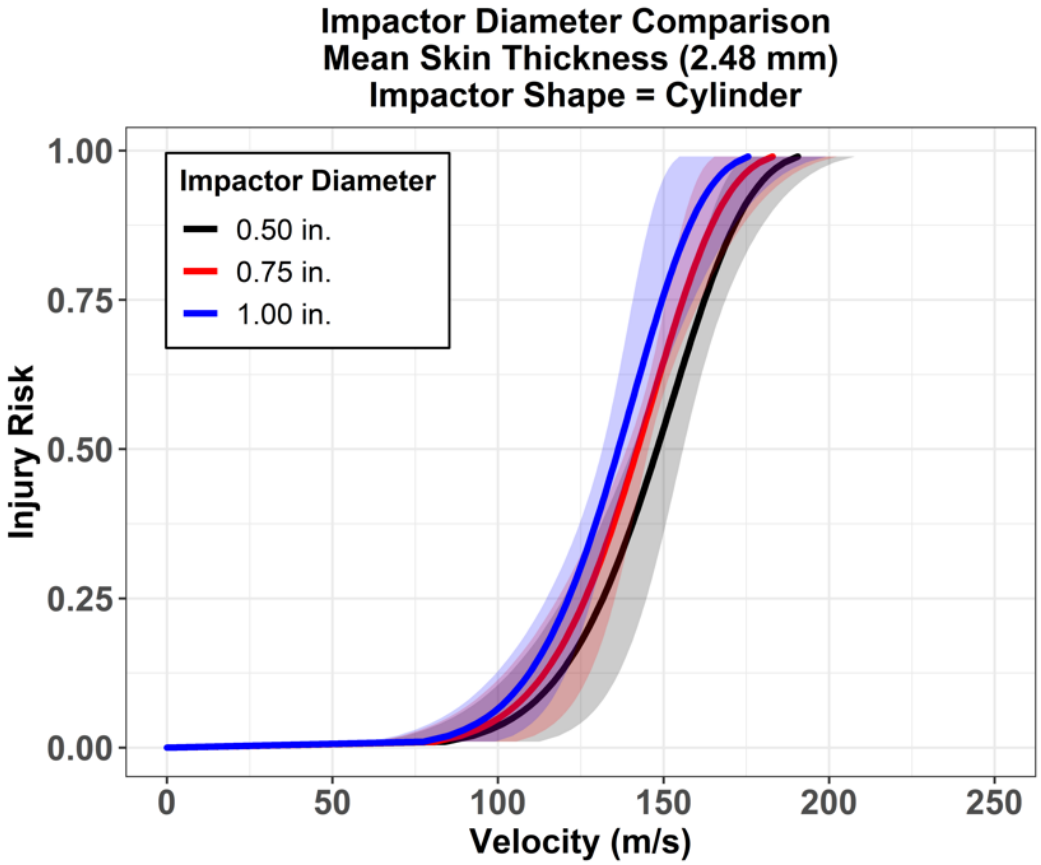


Figure 16: The effects of impactor diameter variations on the PMHS IRF response.

The IRF response was predicted for the cylindrical impactor at the average PMHS skin thickness (2.48 mm) for each tested impactor diameter (0.50 in., 0.75 in., and 1.00 in.). The corridors represent the 95% confidence intervals for each predicted response.

Figure 16 shows that the larger impact diameters produced increased injury risk under lower velocity. While this shows a general trend, it is important to acknowledge that this covariate was implemented as a continuous value, and therefore, must maintain a numerical ordering (1.00 in. > 0.75 in. > 0.50 in.). Overall, while there were slight differences in the injury risk per impact diameter, the effects of this covariate were much less than those of the skin thickness or impactor shape covariates.

Conclusions

Impactor testing was conducted on six approximately 50% percentile male PMHS (height: 66-73 in., weight: 142-212 lb, age: 32-63 years, BMI: 19-29 kg/m^2) to quantify the tolerance of human skin to high-rate blunt impacts. A total of 221 impacts were conducted to assess velocities from 60-167 m/s using three impactor diameters (0.50 in., 0.75 in., and 1.00 in.) across two impactor shapes (sphere and cylinder). Autopsies were conducted on each PMHS to document the presence of penetration into the skin, as well as the severity of injury. Additionally, each impact site was palpated to determine whether the impact was conducted over a bony region. In total, 84 of the 221 impacts resulted in skin penetration

(> 5 mm), 71 of the 221 impacts were located over bone, and 6 of those 71 over-bone impacts resulted in a bony fracture.

Ultrasound images were collected at each impact site ahead of testing, and these images were analyzed to assess the anatomical thickness and shear wave velocity (an analogue to stiffness) of each tissue layer (skin, fat, fascia, and muscle). There was one PMHS (PMHS 2) that contained notably thicker skin and fat layers than the other specimens and one PMHS (PMHS 5) that was significantly less fatty than most other specimens. Similarly, PMHS 2 produced the greatest shear wave velocity at the skin layer, and PMHS 5 produced the lowest shear wave velocity (stiffness) at every tissue layer. Further, the posterior body regions (Upper Back and Lower Back) had the thickest skin layers, followed by the Abdomen and Upper Chest. Interestingly, the fat layers were not significantly different across regions, except for the Abdomen having thicker fat than the Upper Back. Additionally, the superior regions (Upper Chest and Upper Back) produced the greatest shear wave velocity (higher stiffness) at the skin layer, with the Upper Chest containing the stiffest fat layer, as well.

Before developing a final IRF, fifteen possible covariates were analyzed to determine which were significant to the injury response. These included impact location and testing environment variables (specimen ID, side of the body, body region, surface tissue temperature, and the presence of bone), impactor geometry variables (diameter and shape), and the tissue thickness and shear wave velocity (stiffness) at each tissue layer (skin, fat, fascia, and muscle). Of these, the following variables were determined to have a significant effect on the injury response (in order of most to least significant): skin thickness, body region, impactor shape, specimen ID, and fascia shear wave velocity (stiffness). Further, the impactor diameter variable, while not significant in isolation, became significant when added alongside the impactor shape covariate. When combined, the best-fit PMHS IRF (PMHS Model 1) used skin thickness, impactor shape, and impactor diameter as covariates. This model was fit using a Weibull survival distribution with velocity (m/s) as the primary predictor to predict the likelihood of injury (>5 mm penetration) [1]. Additional less-specific IRFs were developed for application outside the bounds of this study's test conditions. These included a model that used skin thickness and impactor shape as covariates (PMHS Model 2), as well as a general model that only used skin thickness as a covariate (PMHS Model 3).

The most-specific model (PMHS Model 1) was used to make comparisons between the covariates and their effect on the injury response. Generally, increased skin thickness resulted in a lower risk of penetration, with the tested population variability (± 1 SD) resulting in significant shifts of the IRF curves. Similarly, the body regions with thicker skin resulted in a lower injury risk than those with thin skin; therefore, the posterior regions (Upper Back and Lower Back) produced lower risk than the anterior regions (Upper Chest and Abdomen). Further, the spherical impactors had a higher injury risk than the cylindrical impactors, with increased impactor diameter also producing greater injury risk (1.00 in. > 0.75 in. > 0.50 in.).

Overall, the risk of injury at a given velocity was primarily dependent on the location of impact and its anatomical makeup, with the impactor variables (shape and diameter) also contributing [17]. For these impactors, with a uniform sectional density of 2.3 g/mm^2, the mean (± 1 SD) velocity that produced a penetrative injury was 122.5 ± 16.5 m/s. The influence of the skin thickness on the injury risk points to a level of subject-specificity that may benefit from additional anatomical diversity in future testing. Interestingly, while tissue thickness was very influential on the response, the shear wave velocity (an analogue of stiffness) had very little effect. Further, the impactor shape was fairly significant to the

response, which indicates that other geometries and materials may warrant further investigation in the future. The impactor diameter also had an effect, although much less significant, on the response. The decreased influence of the diameter may be due to the purposeful matching of the sectional density of each impactor design, as impactor sectional density has previously been shown to have a significant influence on the risk of skin penetration [18]. Lastly, the presence of bone within the backing material of each impact site was tested as a potential categorical covariate and was determined to be insignificant within our testing population.

The IRFs developed within this study are applicable for determining the risk of penetrating human skin (> 5 mm of penetration) for 50th percentile males using blunt, rigid impactors [1]. The most specific IRF (PMHS Model 1) can be used so long as the skin thickness is known and the impactor is spherical or cylindrical, with a diameter between 0.50 in. and 1.00 in and a sectional density of 2.3 g/cm^2. If the diameter is outside of these bounds, but the other two variables are known, PMHS Model 2 may be used. Similarly, if only the skin thickness is known or if the impactor is a shape or diameter not tested, then PMHS Model 3 may be used. These models may have limited applicability for impact conditions significantly different that those performed in this report.

Future studies should expand the impactor types to non-rigid and non-blunt impactors, such as piercing impactors. Further, the impact cases in this study were all roughly perpendicular to the skin. Additional testing may be necessary to investigate the mechanics and thresholds of skin failure under oblique impact cases. Lastly, this study was conducted with only six PMHS, one of which was not imaged using ultrasound and therefore was excluded from the skin thickness-based IRF development. The low sample size, combined with the targeted 50% injury risk throughout testing, produced low certainty at the tails of the IRF. Future studies should increase the sample size, target the upper and lower bounds of the injury risk, and expand the pool of subject anthropometry to include specimens with more diverse size/BMI, as well as to investigate female injury. An additional limitation of this study is that all testing was performed on post-mortem tissue that had been previously frozen and thawed. The difference in penetration risk between this tissue and living tissue is unknown at the present, although there has been some data suggesting this difference may not be large [24]. The effect of freezing and thawing cadaveric tissue is one of the focuses of Aim 2 later in this report. Further, the effects of clothing on the penetrative risk are not addressed by this work and should be investigated in a future study, as the presence of clothing create a protective effect that may decrease the injury risk. Therefore, the injury risk results presented in this study are likely conservative due to the direct impacts on the nude skin.

Aim 2: High-Rate Blunt Impact in Ovine Cadaveric Tissue

Overview

High-rate blunt impact testing was conducted on eight whole-body, cadaveric ovine specimens to assess the tolerance of ovine skin to localized blunt impacts *in situ*. These tests were performed after different storage conditions (fresh and frozen-thawed) and different tissue temperatures (laboratory and body temperature). Test day palpation, as well as post-test necropsy, were performed at each test site to assess the level of tissue failure. Pre-test imaging via MRI and shear wave elastography were utilized to determine the tissue thickness and shear wave velocity (stiffness) at each test location. Finally, injury risk functions were developed to assess the effects of impact velocity on the injury response, as well as to compare the cadaveric ovine tissue injury thresholds to that of the PMHS.

Methods

Test Setup and Equipment

Generally, the test setup and methodology was designed to mimic the experiments performed on PMHS in Aim 1. Modifications to the testing procedure from that previously described are listed below.

Suspension Harness

A harness was designed to suspend each ovine specimen within the testing enclosure in a typical standing posture. It consisted of a long metal beam with holes periodically along the entire length. Eyebolts were attached at four locations along the beam to suspend support straps. These straps held the ovine specimens near the neck, shoulder, stomach, and rump.

Modifications to Enclosure and Test Area

To accommodate the length of the sheep, as compared to the width of the PMHS, minor adjustments were made to the enclosure and test area. Namely, the enclosure was widened by removing the wooden side-wall and roof. In their place, a plastic tarp was draped over the entire enclosure to ensure that the impactors would not leave the test area following impacts. Additionally, the chair assembly was removed from the enclosure, as the ovine specimens were fully supported by the suspension harness.

Ovine Testing Procedure

Procurement of Ovine Subjects and Pre-Test Imaging

The ovine study was approved by the UVA Institutional Animal Care and Use Committee (IACUC). The UVA-approved protocol was additionally reviewed and approved by the US Department of the Navy Bureau of Medicine and Surgery (BUMED). Eight male ovine specimens were procured for this study, based on an inclusion criterion of 140-200 lb, to roughly match the size of the PMHS. The ovine specimens were exclusively male to avoid potential exposure of Query fever (Q-fever) that is sometimes found in female sheep [31]. All specimens were procured from Mary C Baugher (Ruckersville, VA), shorn, and transported to Fontaine Research Park at the University of Virginia. The ovine specimens were allowed to acclimate for at least 3 days and were euthanized via intravenous Euthasol at 1 mL/10 lb of body weight. Immediately following euthanasia, each ovine specimen was imaged using MRI under a similar protocol used for the PMHS, as described in Aim 1. Following MRI, all specimens were transported back to UVA-

CAB and re-shorn. Additional shearing was performed first with electric sheep shears, and then a closer shearing with a standard electric razor.

Tissue Storage and Temperature Conditions

The ovine testing sought to investigate the influence of tissue temperature and storage conditions on the tissue response to localized blunt impacts. As such, three storage conditions/temperature skews were selected (fresh/lab temperature, frozen-thawed/lab temperature, and fresh/warmed), each with their own subject preparation methodologies. For the initial six ovine specimens, the left flank was reserved for the fresh/lab temperature conditions, while half of the right flanks were designated for frozen-thawed/lab temperature testing and half were used in the fresh/warmed tests. Two additional specimens were added to the supplement areas of lower confidence within the injury risk function. As such, the left flank of Ovine 7 was tested under fresh/lab temperature conditions, while the right flank of Ovine 7 and both flanks of Ovine 8 were tested under frozen-thawed/lab temperature conditions. The test matrix is provided Table XXIII.

Table XXIII: Test matrix for Ovine impactor testing

Specimen	Flank	Storage Condition*	Temperature*	Number of Impacts**
Ovine 1	Left	Fresh	Lab Temperature	20
	Right	Frozen-Thawed	Lab Temperature	20
Ovine 2	Left	Fresh	Lab Temperature	20
	Right	Frozen-Thawed	Lab Temperature	20
Ovine 3	Left	Fresh	Lab Temperature	20
	Right	Frozen-Thawed	Lab Temperature	20
Ovine 4	Left	Fresh	Lab Temperature	20
	Right	Fresh	Warmed	20
Ovine 5	Left	Fresh	Lab Temperature	20
	Right	Fresh	Warmed	20
Ovine 6	Left	Fresh	Lab Temperature	20
	Right	Fresh	Warmed	20
Ovine 7	Left	Fresh	Lab Temperature	20
	Right	Frozen-Thawed	Lab Temperature	20
Ovine 8	Left	Frozen-Thawed	Lab Temperature	20
	Right	Frozen-Thawed	Lab Temperature	20

**Green cells indicate that the tissue was tested under the Fresh/Lab Temperature condition, blue cells indicate that the tissue was tested under the Frozen-Thawed/Lab Temperature condition, and orange cells indicate that the tissue was tested under the Fresh/Warmed condition.*

*** Of the 320 planned impact tests, 313 impact tests were conducted.*

Following euthanasia and MRI, most ovine specimens (Ovine 1-7) were first tested under the fresh/lab temperature condition. Before testing, each specimen was stored in a cooler at 40-45°F overnight (12-18 hours). This allowed for the specimen's internal and surface tissue temperatures to stabilize to approximately lab temperature (~65°F).

Following the fresh/lab temperature flank testing, ovine specimens 1-3 and 7-8 were prepared for frozen-thawed/lab temperature testing and stored in a freezer at -5°F for at least one week until fully frozen. Before testing, these specimens were removed from the freezer and allowed to thaw at lab temperature (~65°F) for approximately five days.

The remaining ovine specimens (Ovine 4-6) were prepared for fresh/warmed testing and allowed to remain within the test area overnight (~12-15 hours). During this time, the temperature within the lab was increased to ~75-80°F. Six hours before testing, an electric blanket and space heater were applied to the appropriate flank of the ovine specimen, with temperatures regulated to not overheat the surface tissue. This process continued for ~6-8 hours, with the ovine specimen rotated every thirty minutes to allow for even heating. Testing began once the internal temperature of the specimen reached ~85-90°F. Throughout testing, the lab temperature was controlled at 80°F, and the electric blanket and space heater were reapplied whenever necessary to maintain the ovine specimen's warmed internal temperature.

Subject Preparation and Pre-Test Imaging

Once the desired tissue temperature was reached, the ovine specimen was suspended via the gantry and harness system within the enclosure with the desired testing flank facing the high-rate linear impactor barrel. An electric meat thermometer was inserted into the rump of each specimen, approximately 2 inches beneath the skin, to track the internal temperature of the tissue.

Various anthropometry measurements were then collected using body calipers and measuring tape. Details on each measurement are provided in Appendix 9.

Each impact location was marked on the test flank to designate the location of pre-test ultrasound imaging. This procedure was largely the same as with the PMHS. First, a 5 in. diameter circle was marked at each body region (shoulder, ribs, stomach, and rump). The shoulder was defined as the region posterior to the shoulder blade and anterior to the axilla. The ribs were defined as the region posterior to the axilla and anterior to the most posterior rib. The stomach was defined as the region posterior to the ribcage and anterior to the pelvis. The rump was defined as the region posterior to the stomach. All regions were defined at approximately the same vertical height.

Since the ovine testing only used the 0.75 in. cylindrical impactor, five impact locations were defined at each body region, along with the 1.88 in. diameter exclusion zones, spread within the 5 in. target area such that no impacts would overlap. This test setup and each body region are depicted in Figure 17.

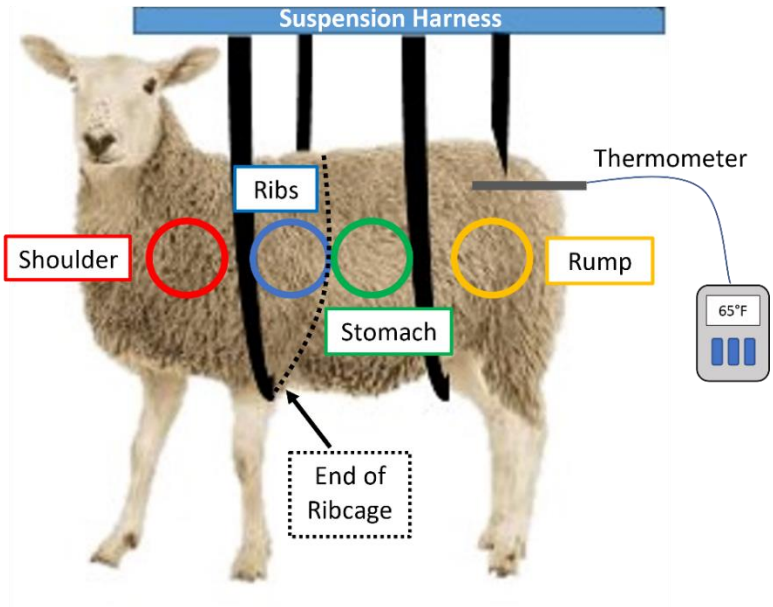


Figure 17: Ovine test setup and anatomical impact regions.

Once defined, each impact location was sheared as close to the skin as possible to improve the ultrasound and shear wave elastography images. Each location was then imaged using the Aixplorer Multiwave ultrasound machine with the SL15-4 probe. Five SWE images were taken at each test site using an image depth of 3.5 cm, and one B-mode image was captured at a depth of 5 cm.

Impactor Testing

For each test, the gantry system was used to reposition the ovine specimen to ensure that the high-rate linear impactor was aligned with the desired test location. Before each impact, the surface and internal tissue temperatures were measured using the Etekcity handheld infrared thermometer and the meat thermometer, respectively.

Unlike the PMHS testing, which centered impacts around the 50% threshold velocity, the ovine impacts targeted 1-2 definite penetration impacts and then incrementally decreased the impact velocity to better assess the low-velocity impact cases. Typically, these impacts ranged from 60.5 m/s to 162.2 m/s. Detailed descriptions of each impact test are provided in Appendix 10.

Two additional ovine specimens were added after the initial data analysis to supplement gaps in the dataset and improve confidence at the upper and lower tails of the injury risk function. As such, four impacts within each body region targeted the 5% injury risk velocity of 81.5 m/s and one impact targeted the 90% injury risk velocity of 153.8 m/s.

Each impact was captured using the three high-speed cameras at 10,000 frames per second with a resolution of 512x384. After each test, the impact site was photographed, inspected visually, and palpated. If there was penetration of the skin, the diameter and depth of penetration were measured.

Necropsy

Each ovine specimen was necropsied to fully assess the severity of each impact test and to retrieve any impactors that were left within the tissue. Using a binary “injury” or “no injury” assessment criteria, each impact was investigated at various levels, as described in Aim 1 (

Table VI). Full autopsy results for each impact test are provided in Appendix 11.

Data Analysis

Impact Velocity, Tissue Thickness, and SWE Measurements

Impact velocity, tissue thickness, and SWE measurements were made using similar custom Matlab scripts and procedures as described in Aim 1.

Injury Risk Curve Development

Ovine IRFs were developed using the same procedure and custom R scripts as described in Aim 1.

Ovine IRF Comparisons

Model predictions and confidence intervals were calculated and plotted in the manner described in Aim 1. Further, the PMHS and ovine body regions were compared to determine which ovine regions responded similarly to the PMHS and, therefore, may be appropriate surrogates for PMHS tissue. The PMHS predictions were calculated using PMHS Model 1, which included skin thickness, impactor shape, and impactor diameter as covariates. Each comparison was made using the average skin thickness of each region, as described previously in Aim 1. Additionally, the impactor shape was fixed at the Cylinder option, and the impactor diameter was fixed at 0.75 in., as these were the only impactor conditions tested in the ovine specimens. The ovine predictions were calculated using Ovine Model 1.

Statistical Analysis

The thickness and shear wave velocity measurements for each tissue layer were compared by body region and specimen using the same analyses described in Aim 1. Notably, however, the shear wave velocity assessments were only conducted on the fresh/lab temperature flanks of each ovine specimen, as preliminary findings determined that the storage/temperature conditions may have affected the shear wave velocity of some of the tissue layers. Additional comparisons were made between the PMHS and Ovine IRF results by calculating the squared error (SE) at several key injury risk levels, as well as by calculating the mean squared error (MSE) for each curve.

Results

Anthropometry

Mean (± 1 SD) anthropometry measurements, taken from each ovine specimen before impact testing, are presented in Table XXIV. Each measurement is detailed in Appendix 9.

Table XXIV: Ovine anthropometry results

Body Region	Measurement	Mean ± 1 SD n = 6
	Weight (lb)	167.2 ± 23.3
	Length (cm)	86.2 ± 7.2

Shoulder	Shoulder Breadth (cm)	26.3 ± 4.0
Chest	Chest Breadth, Mid Rib (cm)	26.0 ± 2.2
	Chest Breadth, Last Rib (cm)	35.8 ± 3.6
	Chest Depth, Mid Rib (cm)	35.1 ± 2.3
	Chest Depth, Last Rib (cm)	39.8 ± 2.3
	Chest Circumference, Mid Rib (cm)	100.4 ± 5.1
	Chest Circumference, Last Rib (cm)	119.9 ± 9.1
Stomach	Stomach Breadth (cm)	37.6 ± 2.8
	Stomach Depth (cm)	41.1 ± 2.4
	Stomach Circumference (cm)	126.6 ± 8.8
Rump	Rump Breadth (cm)	28.6 ± 2.9

Tissue Temperature Measurements

The mean (± 1 SD) surface and internal tissue temperature measurements, taken before each impact test, are provided in

Table XXV for each storage/temperature condition.

Table XXV: Ovine tissue temperature results

Specimen	Storage Condition	Temp. Condition	Surface Temp. (°F) (Mean ± 1 SD)	Internal Temp. (°F) (Mean ± 1 SD)
Ovine 1-6	**Fresh**	**Lab Temperature**	**68.5 ± 4.7**	**64.5 ± 5.6**
Ovine 1	Fresh	Lab Temperature	75.4 ± 1.9	Not Recorded
Ovine 2	Fresh	Lab Temperature	68.9 ± 1.4	70.8 ± 0.5
Ovine 3	Fresh	Lab Temperature	60.0 ± 2.7	53.8 ± 1.8
Ovine 4	Fresh	Lab Temperature	67.7 ± 1.9	61.5 ± 1.1
Ovine 5	Fresh	Lab Temperature	68.9 ± 2.5	67.5 ± 0.5
Ovine 6	Fresh	Lab Temperature	68.6 ± 2.4	66.1 ± 0.8
Ovine 7	Fresh	Lab Temperature	69.8 ± 1.1	67.1 ± 0.2
Ovine 1-3, 7-8	**Frozen/Thawed**	**Lab Temperature**	**67.3 ± 2.7**	**63.5 ± 2.0**
Ovine 1	Frozen/Thawed	Lab Temperature	68.6 ± 1.8	65.5 ± 0.5
Ovine 2	Frozen/Thawed	Lab Temperature	67.0 ± 2.8	61.0 ± 0.0
Ovine 3	Frozen/Thawed	Lab Temperature	64.1 ± 2.9	61.4 ± 0.6
Ovine 7	Frozen/Thawed	Lab Temperature	67.3 ± 2.3	62.5 ± 0.5
Ovine 8 (Left)	Frozen/Thawed	Lab Temperature	69.1 ± 2.0	65.9 ± 0.3
Ovine 8 (Right)	Frozen/Thawed	Lab Temperature	67.5 ± 1.5	65.0 ± 0.0
Ovine 4-6	**Fresh**	**Warmed**	**88.9 ± 6.6**	**86.7 ± 3.5**
Ovine 4	Fresh	Warmed	89.4 ± 5.6	81.9 ± 0.7
Ovine 5	Fresh	Warmed	96.8 ± 6.3	89.9 ± 0.4
Ovine 6	Fresh	Warmed	83.3 ± 3.4	88.7 ± 0.5
PMHS	**Frozen/Thawed**	**Lab Temperature**	**64.8 ± 2.3**	Not Recorded

Impact Velocity

The impactor velocity for each impact was calculated using high-speed video. Each impact case is represented in Figure 18 in terms of both free-flight velocity and impactor pressure.

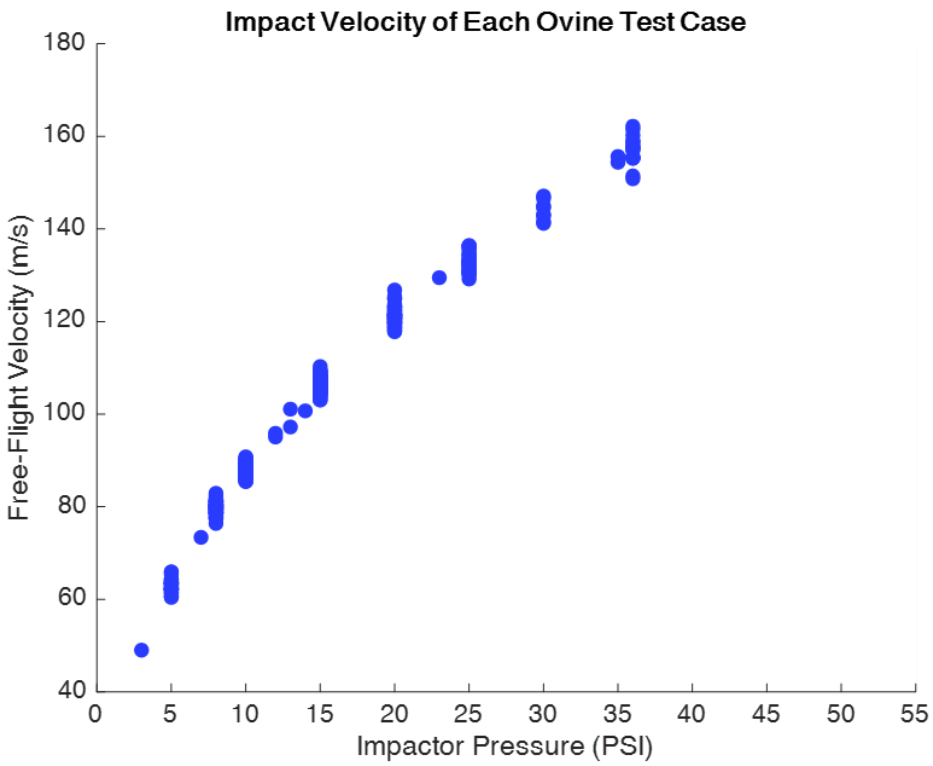


Figure 18: Impactor velocity as a function of impactor pressure for all tested Ovine impact cases. Free-flight velocity (m/s) was calculated for each impact case from high-speed video. These values were plotted against the test-day impactor pressure (PSI).

Tissue Thickness Measurements

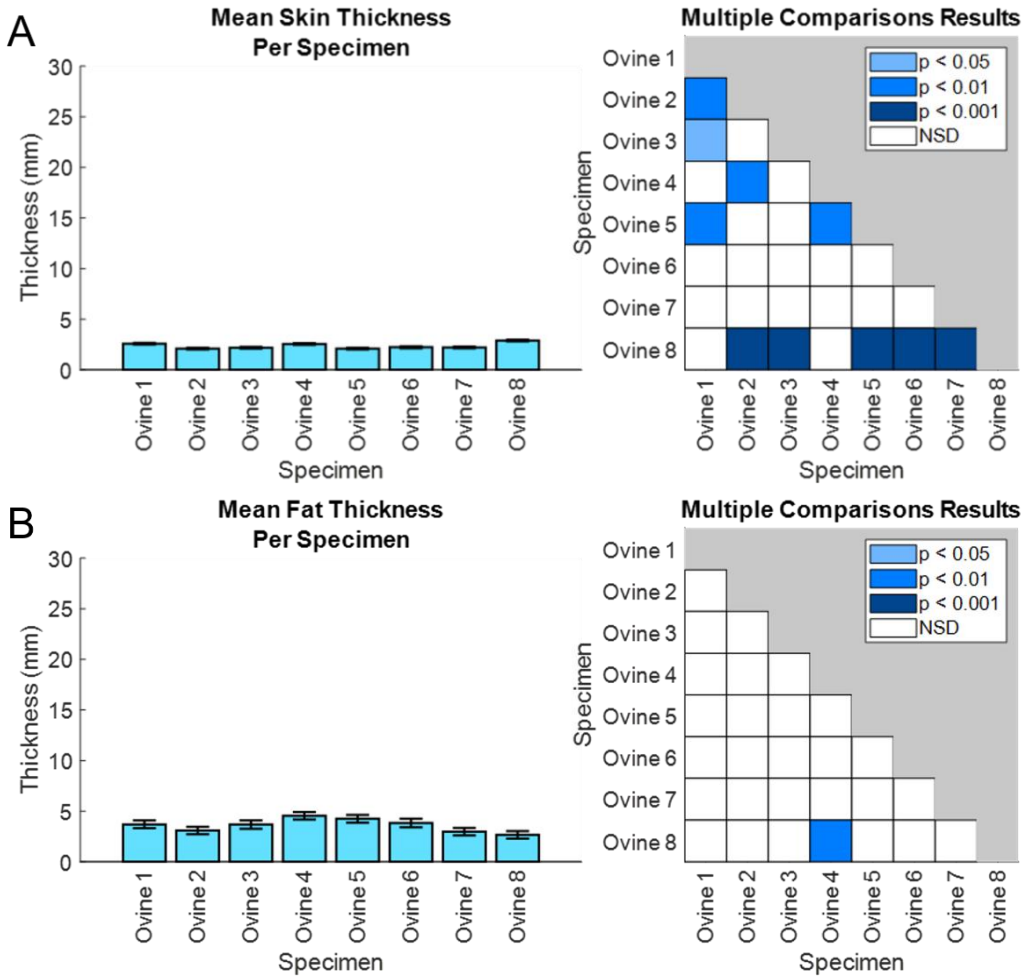
The thickness of each tissue layer (skin, subcutaneous fat, fascia, and muscle) was measured at each impact location using ultrasound imaging. Some tissue layer measurements, namely the muscle layers, were limited by the depth of the ultrasound imaging, which displayed a maximum depth of 5 cm per impact location. The mean (± 1 SD) tissue thickness for each layer (across all ovine specimens) are provided in Table XXVI.

Table XXVI: Ovine Tissue Thickness per Tissue Layer

Tissue Layer	Tissue Thickness (mm) (Mean ± 1 SD)
Skin	2.37 ± 0.61
Subcutaneous Fat	3.61 ± 2.44
Fascia	1.08 ± 0.27
Muscle	19.0 ± 14.1

Much like the PMHS, the muscle layer was the thickest (19.0 mm). This was, again, followed by the subcutaneous fat (3.61 mm), skin (2.37), and fascia (1.08 mm). Muscle was the most variable tissue layer with a standard deviation of 14.1 mm.

The mean thickness of each tissue layer per ovine specimen is depicted in Figure 19. As with the PMHS, the distributions of each tissue's thickness measurements were compared using one-factor ANOVA.



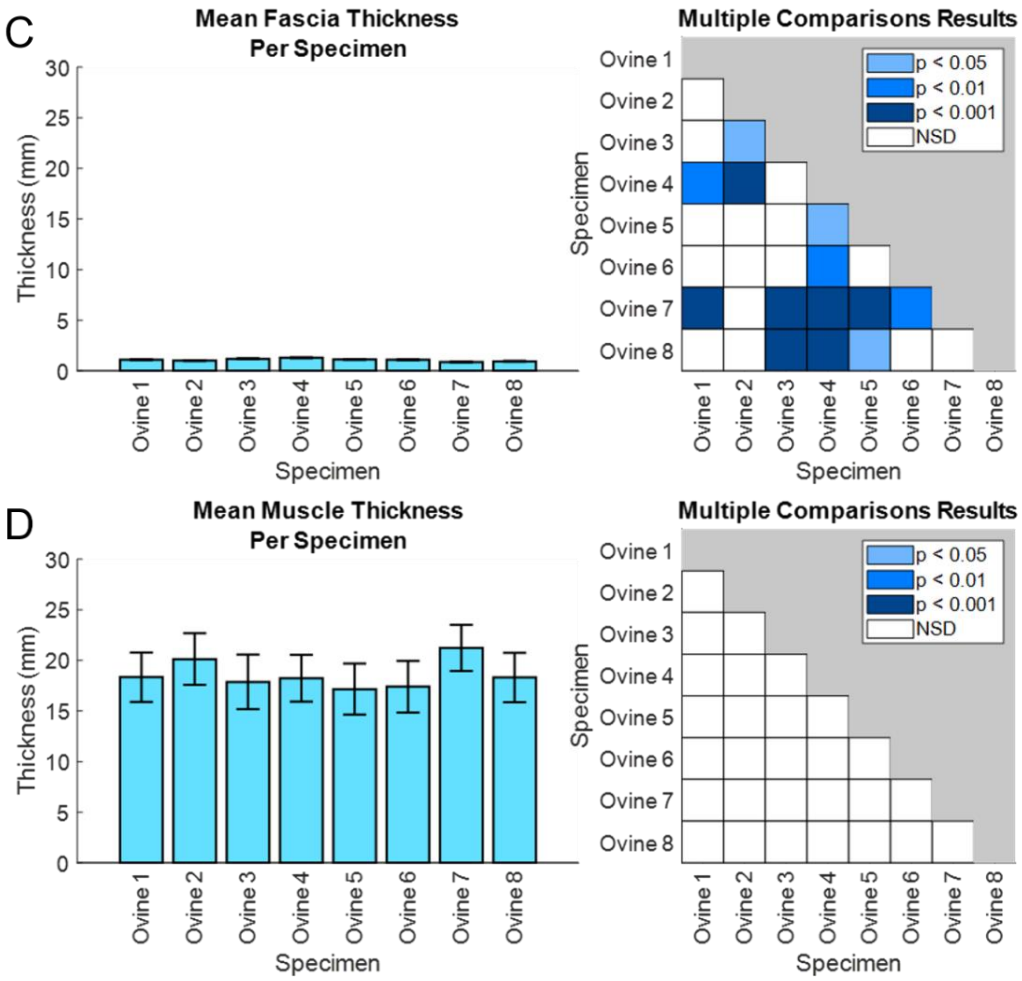
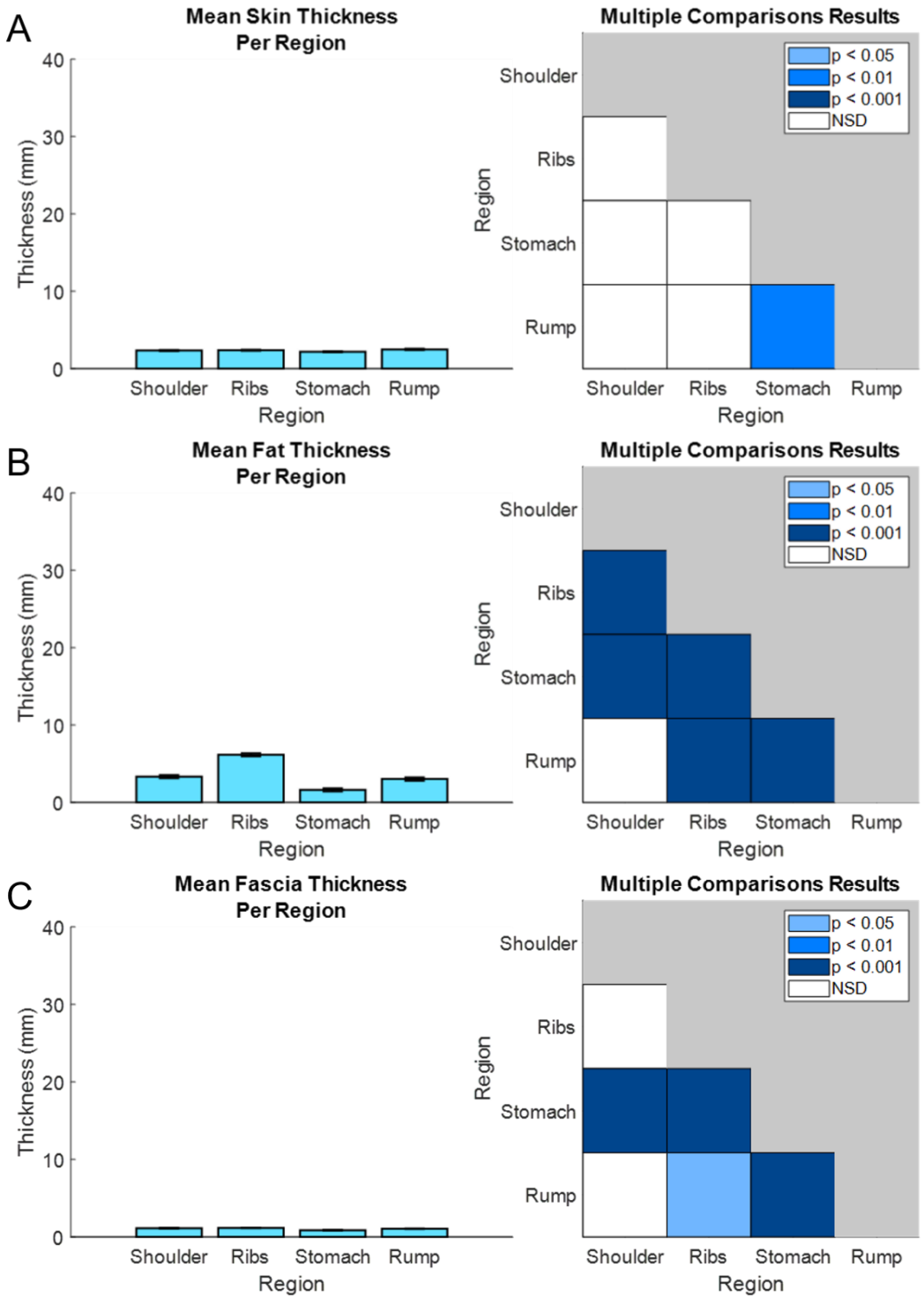


Figure 19: Tissue thickness measurements for each ovine specimen.

This figure presents bar charts of mean tissue thickness (±1 SE) (left) and multiple comparisons significance analysis (right) for the each ovine at every tissue layer: (a) skin, (b) fat, (c) fascia, and (d) muscle. NSD = no significant difference.

Figure 19 showed that tissue thickness was largely homogenous across all ovine specimens. Figure 19 (a) showed that Ovine 5 had significantly thinner skin than Ovines 1, 4, and 8 ($p < 0.01$), while Ovine 8 had significantly thicker skin than all other ovine specimen besides Ovine 1 and 4 ($p < 0.001$). Figure 19 (b) showed that Ovine 4 had significantly thicker fat than Ovine 8 ($p < 0.05$). Figure 19 (c) showed that Ovine 7's fascia layer was significantly thinner than those of all specimens except Ovine 2 and 8 ($p < 0.01$), and Ovine 4's fascia was significantly thicker than those of all specimens except Ovine 3 ($p < 0.05$). Figure 19 (d) showed that there were no significant differences between specimens at the muscle tissue layer.

Additional comparisons were made between body regions (Shoulder, Ribs, Stomach, and Rump) by averaging the thickness of each like-region tissue layer across ovine specimens. This comparison is presented in Figure 20.


A
Mean Skin Thickness
Per Region
Thickness (mm)
0
10
20
30
40
Shoulder
Ribs
Stomach
Rump
Region
Multiple Comparisons Results
p < 0.05
p < 0.01
p < 0.001
NSD
Shoulder
Ribs
Stomach
Rump
Region
B
Mean Fat Thickness
Per Region
Thickness (mm)
0
10
20
30
40
Shoulder
Ribs
Stomach
Rump
Region
Multiple Comparisons Results
p < 0.05
p < 0.01
p < 0.001
NSD
Shoulder
Ribs
Stomach
Rump
Region
C
Mean Fascia Thickness
Per Region
Thickness (mm)
0
10
20
30
40
Shoulder
Ribs
Stomach
Rump
Region
Multiple Comparisons Results
p < 0.05
p < 0.01
p < 0.001
NSD
Shoulder
Ribs
Stomach
Rump
Region

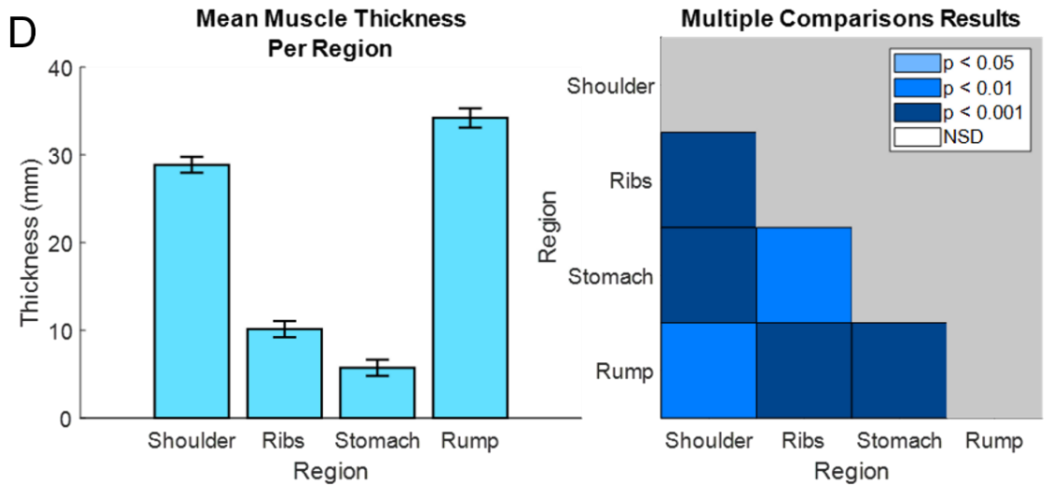


Figure 20: Tissue thickness measurements for each ovine body region.

This figure presents bar charts of mean tissue thickness (±1 SE) (left) and multiple comparisons significance analysis (right) for each body region at every tissue layer: (a) skin, (b) fat, (c) fascia, and (d) muscle. NSD = no significant difference.

Figure 20 (a) showed that the only significant difference in regional skin thickness was that Rump was thicker than Stomach ($p < 0.01$). Figure 20 (b) showed that the fat layer in the Ribs region was significantly thicker than all other regions ($p < 0.001$), while the fat in the Stomach region was significantly thinner than all other regions ($p < 0.001$). Figure 20 (c) showed that the Stomach contained the thinnest fascia layer of all regions ($p < 0.001$), and the Ribs' fascia layer was thicker than those of the Rump. Finally, Figure 20 (d) showed that the Shoulder and Rump contained significantly thicker muscle layers than the Ribs and Stomach ($p < 0.001$). Further tissue thickness results are provided in Appendix 12.

SWE Measurements

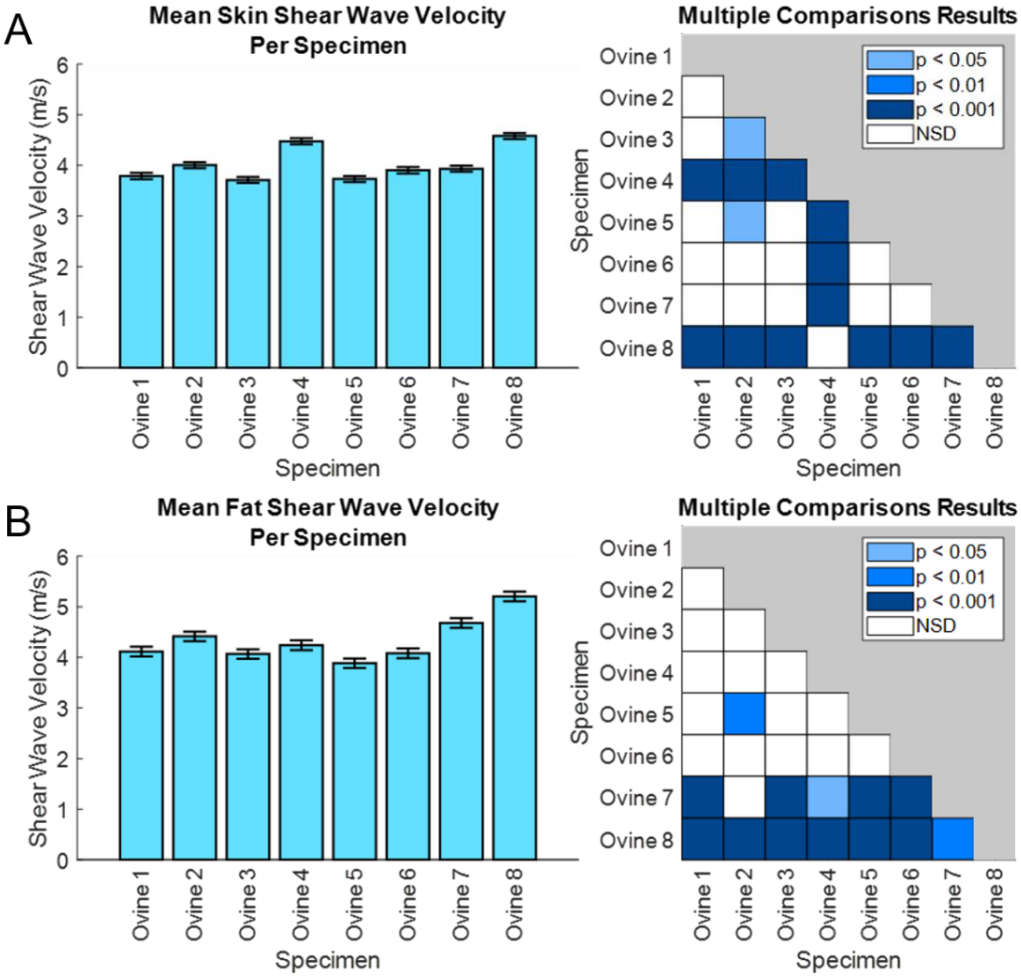
Shear wave velocity was measured at each impact location to approximate the stiffness of each tissue layer (skin, fat, fascia, and muscle). Like with the thickness measures, some shear wave velocity measurements were limited by the depth of the ultrasound imaging, which showed a maximum depth of 5 cm per impact location. The mean (± 1 SD) shear wave velocity for each tissue layer (across all ovine specimens) are provided in Table XXVII.

Table XXVII: Ovine Shear Wave Velocity per Tissue Layer

Tissue Layer	Shear Wave Velocity (m/s) (Mean ± 1 SD)
Skin	4.07 ± 0.59
Subcutaneous Fat	4.61 ± 1.04
Fascia	4.77 ± 1.20
Muscle	4.50 ± 1.09

The stiffest tissue layer was the fascia (shear wave velocity = 4.77 m/s), followed by the subcutaneous fat (4.61 m/s), the muscle (4.50 m/s), and then the skin (4.07 m/s). Notably, all layers but the skin produced greater shear wave velocity than their PMHS counterparts.

The mean shear wave velocity of each tissue layer per ovine specimen is presented in Figure 21 with the associated one-factor ANOVA comparison.



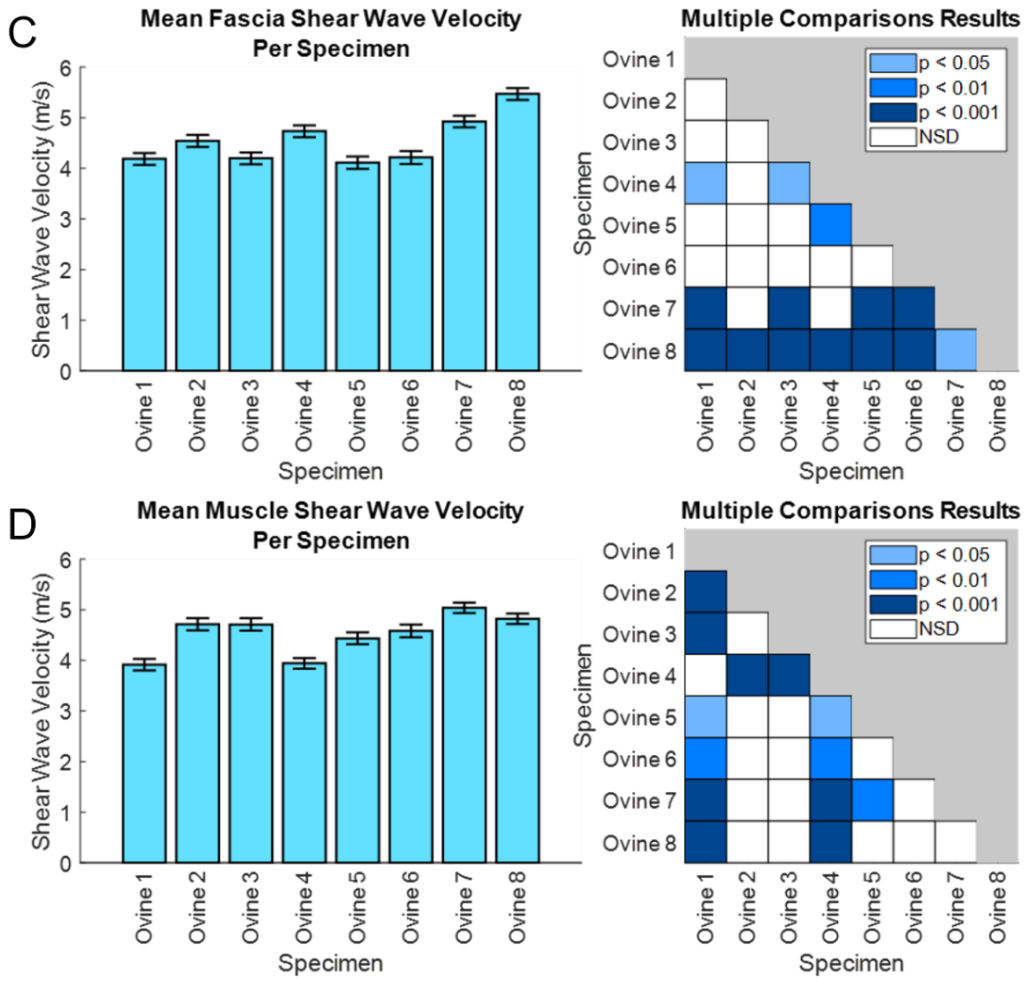
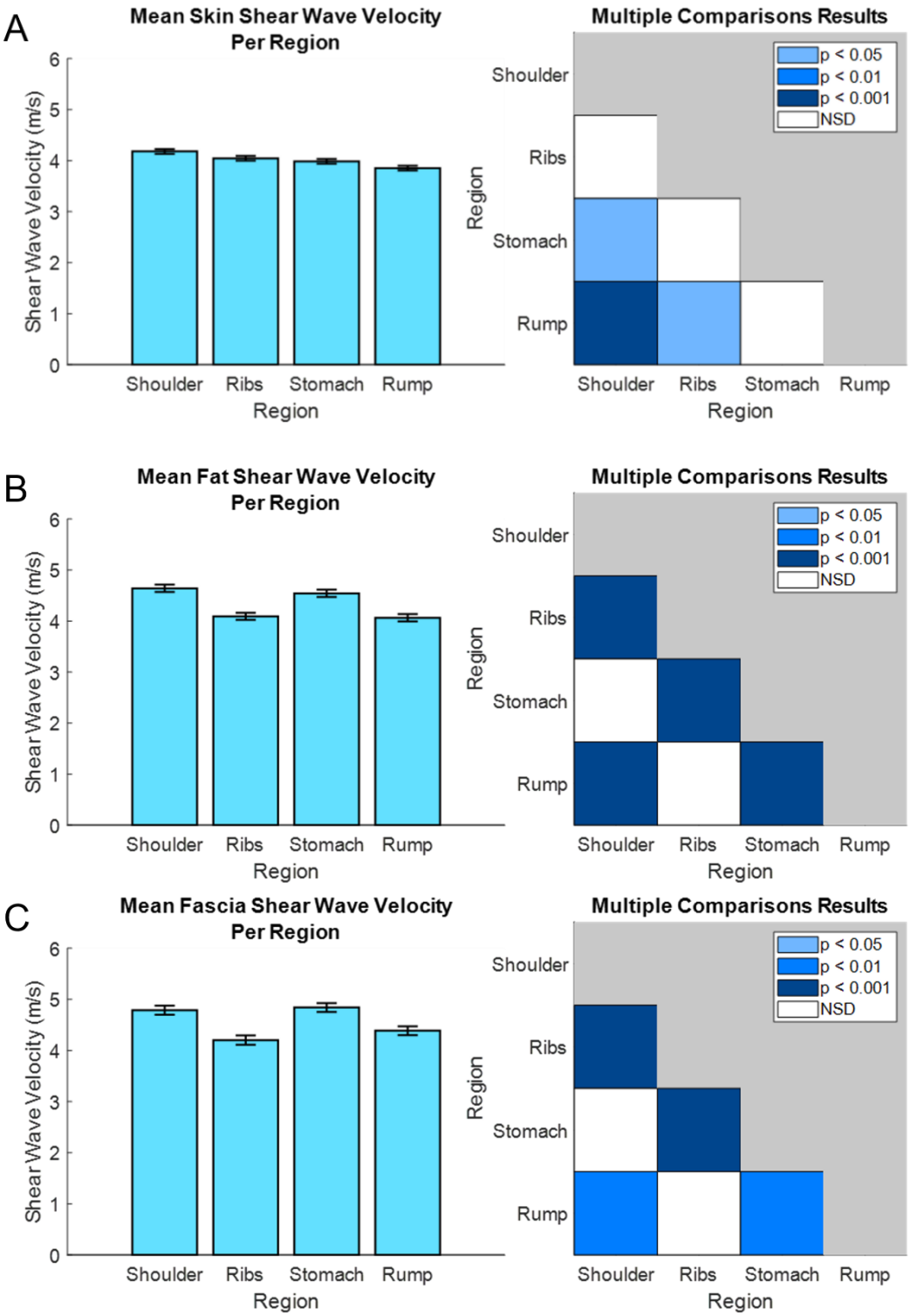


Figure 21: Tissue shear wave velocity measurements for each ovine specimen.

This figure presents bar charts of mean tissue shear wave velocity (±1 SE) (left) and multiple comparisons significance analysis (right) for the each ovine at every tissue layer: (a) skin, (b) fat, (c) fascia, and (d) muscle. NSD = no significant difference.

Figure 21 showed many tissue-dependent trends in stiffness across specimens. Figure 21 (a) showed that Ovines 4 and 8 had significantly stiffer skin than the other ovine specimens ($p < 001$), and Ovine 2's skin was stiffer than that of Ovines 3 and 5 ($p < 0.05$). Figure 21 (b) showed that the fat layers of Ovines 2-6 were mostly consistent in terms of stiffness, with the only significant difference between Ovines 2 and 5. Further, Ovine 8's fat layer was significantly stiffer than all other ovine specimens ($p < 0.01$). Figure 21 (c) showed that fascia layers followed a similar trend, with Ovine 4's fascia being significantly stiffer than that of Ovines 1, 3, and 5 ($p < 0.05$). Again, Ovine 8 contained the stiffest fascia tissue ($p < 0.05$). Figure 21 (d) showed that Ovine 1's muscle tissue was significantly less stiff than all other Ovines, besides that of Ovine 4 ($p < 0.05$). Lastly, Ovine 7's muscle layers were significantly stiffer than those of Ovines 1, 4, and 5.

Additional comparisons were made between body regions (Shoulder, Ribs, Stomach, and Rump) by averaging the shear wave velocity of each like-region tissue layer across ovine specimens. This comparison is presented in Figure 22.


A
Mean Skin Shear Wave Velocity Per Region
Shear Wave Velocity (m/s)
0
1
2
3
4
5
6
Shoulder
Ribs
Stomach
Rump
Region
Multiple Comparisons Results
p < 0.05
p < 0.01
p < 0.001
NSD
Shoulder
Ribs
Stomach
Rump
Region
B
Mean Fat Shear Wave Velocity Per Region
Shear Wave Velocity (m/s)
0
1
2
3
4
5
6
Shoulder
Ribs
Stomach
Rump
Region
Multiple Comparisons Results
p < 0.05
p < 0.01
p < 0.001
NSD
Shoulder
Ribs
Stomach
Rump
Region
C
Mean Fascia Shear Wave Velocity Per Region
Shear Wave Velocity (m/s)
0
1
2
3
4
5
6
Shoulder
Ribs
Stomach
Rump
Region
Multiple Comparisons Results
p < 0.05
p < 0.01
p < 0.001
NSD
Shoulder
Ribs
Stomach
Rump
Region

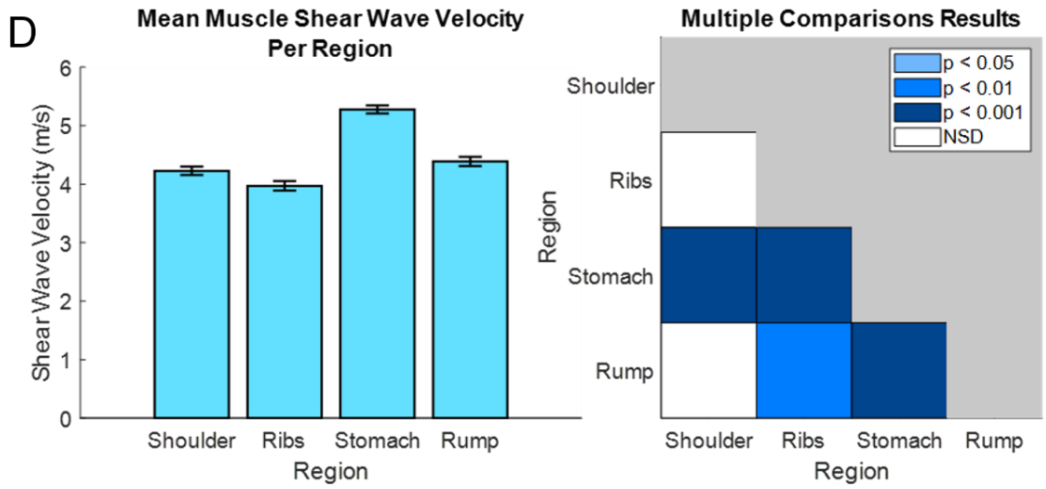


Figure 22: Tissue shear wave velocity measurements for each ovine body region.

This figure presents bar charts of mean tissue shear wave velocity (±1 SE) (left) and multiple comparisons significance analysis (right) for each body region at every tissue layer: (a) skin, (b) fat, (c) fascia, and (d) muscle. NSD = no significant difference.

Figure 22 (a) showed that the Shoulder had significantly stiffer skin than the Stomach and Rump ($p < 0.05$), while Rump had significantly less stiff skin than the Ribs ($p < 0.05$). Figure 22 (b) showed that the Shoulder and Stomach had significantly stiffer fat than the Ribs and Rump ($p < 0.001$). Figure 22 (c) showed that the same trend appeared in the fascia layer ($p < 0.01$). Figure 22 (d) showed that the muscle layer was the significantly stiffer at the Stomach than at any other body region ($p < 0.001$). Further, the Ribs' muscle was significantly less stiff than the Rump's ($p < 0.01$).

Ovine IRF Covariate Assessment

Each test variable was assessed as described in Aim 1 to determine the best covariates for the ovine IRF. The eight most significant covariates for the ovine IRF model are provided in

Table XXVIII. The full list of assessed covariates, and their associated p-values, are provided in Appendix 13.

Table XXVIII: Ovine Covariate Assessment
(Covariates Shown in Order of Increasing p-Value)

Covariate	p-Value
Specimen ID	1.1e-04
Body Region	5.2-03
Fascia Stiffness/Shear Wave Velocity (m/s)	1.3e-01
Fat Stiffness/Shear Wave Velocity (m/s)	1.4e-01
Internal Temperature (°F)	2.9e-01
Fat Thickness (mm)	3.5e-01
Presence of Bone	4.2e-01
Surface Temperature (°F)	4.9e-01

The Specimen ID and Body Region variables were the only covariates that produced significant p-values ($p < 0.05$). Specimen ID, while significant, was deemed too specific for a useful analysis and was excluded as a covariate. Further, the Specimen term was included in each model within the Cluster(Specimen) function as a means of grouping variance.

Ovine IRF Development

Ovine Model 1 (Covariate: Body Region, Dataset: All Data)

Through the covariate analysis, the body region variable was determined to have the greatest influence on the injury response and was selected as the sole covariate for the primary ovine model (Ovine Model 1). Details on this covariate are provided in Table XXIX.

Table XXIX: Covariate Details for Ovine IRFs

Covariate	Type	Bounds/Categories
Body Region	Categorical	Shoulder, Ribs, Stomach, Rump

The formula for Ovine Model 1 is provided in Equation 7 and can be substituted into Equation 1 & Equation 2 to calculate the model fit for any given body region.

$$x = Velocity * e^{-[\beta_0+(\beta_1*Region:Shoulder)+(\beta_2*Region:Stomach)+(\beta_3*Region:Rump)]}$$

Equation 7: The Weibull function for Ovine Model 1, which uses body region as the sole covariate.

where *Velocity* is the free-flight impactor velocity (*m/s*) and *Region:Shoulder, Region:Stomach,* and *Region:Rump* are binary (1 or 0) values depending on which body region is being assessed. The values for the coefficients (*logscale*, β_0, β_1, β_2, and β_3) are provided in Table XXX.

Table XXX: Coefficient Values for Ovine Model 1

Coefficient	Covariate	Magnitude	Standard Error	p-Value
β_0	Intercept	4.8112	0.0339	< 2.0e-16
β_1	Region (Shoulder)	0.0146	0.0695	8.3e-01
β_2	Region (Stomach)	0.1373	0.0392	4.7e-04
β_3	Region (Rump)	0.1384	0.0291	1.9e-06
	Logscale	-1.9370	0.21741	< 2.0e-16

Additional statistics for this model fit are provided in Table XXXI.

Table XXXI: Weibull IRF Statistics for Ovine Model 1

Statistic	Value
Scale	0.144
Loglikelihood (Model)	-108.7
Loglikelihood (Intercept Only)	-115.1
Chi Squared	12.77
Degrees of Freedom	3.000
p-Value	5.2e-03
Number of Newton-Raphson Iterations	7.000
n	313.0

Ovine Model 2 (Covariate: No Covariates, Dataset: All Data)

For instances in which the impact body region is unknown, another model was fit to the data without any covariates. The formula for this univariate ovine model (Ovine Model 2) is provided in Equation 8 and can be substituted into Equation 1 & Equation 2 to calculate the model fit.

$$x = Velocity * e^{-\beta_0}$$

Equation 8: The Weibull distribution formula for Ovine Model 2, which does not include any covariates.

where *Velocity* is the free-flight impactor velocity (*m/s*). The values for the coefficients (*logscale* and β_0) are provided in Table XXXII.

Table XXXII: Coefficient Values for Ovine Model 2

Coefficient	Covariate	Magnitude	Standard Error	p-Value
β_0	Intercept	4.896	0.021	< 2.0e-16
	Logscale	-1.843	0.109	< 2.0e-16

Additional statistics for this model fit are provided in Table XXXIII.

Table XXXIII: Weibull IRF Statistics for Ovine Model 2

Statistic	Value
Scale	0.158
Loglikelihood (Model)	-115.1
Loglikelihood (Intercept Only)	-115.1
Number of Newton-Raphson Iterations	8.00
n	313.0

Details on the key injury risk levels and plotting for Ovine Model 2 are provided in Appendix 14.

Ovine Model 3 (Covariate: No Covariates, Dataset: Fresh/Lab Temp.)

As the tissue storage/temperature condition covariate was determined to be insignificant to the model development, six additional models were developed to assess the effects of each condition on the injury response. First, separate univariate models were fit to each data-subset (Fresh/Lab Temperature, Thawed/Lab Temperature, and Fresh/Warmed) to compare the broad effects of these conditions on the injury response. These are presented in Ovine Models 3-5. Like Ovine Model 2, each of these univariate models utilize Equation 8 and can be substituted into Equation 1 & Equation 2 to calculate the model fit.

Ovine Model 3 was fit using the data from the Fresh/Lab Temperature condition impact cases. The values for the model coefficients (*logscale* and β_0) are provided in Table XXXIV.

Table XXXIV: Coefficient Values for Ovine Model 3

Coefficient	Covariate	Magnitude	Standard Error	p-Value
β_0	Intercept	4.9001	0.0331	< 2.0e-16
	Logscale	-1.8905	0.1640	< 2.0e-16

Additional statistics for this model fit are provided in Table XXXV.

Table XXXV: Weibull IRF Statistics for Ovine Model 3

Statistic	Value
Scale	0.151
Loglikelihood (Model)	-48.8
Loglikelihood (Intercept Only)	-48.8
Number of Newton-Raphson Iterations	8.00
n	140

Ovine Model 4 (Covariate: No Covariates, Dataset: Thawed/Lab Temp.)

Similarly, Ovine Model 4 was fit using the data from the Thawed/Lab Temperature condition impact cases. The values for the model coefficients (*logscale* and β_0) are provided in Table XXXVI.

Table XXXVI: Coefficient Values for Ovine Model 4

Coefficient	Covariate	Magnitude	Standard Error	p-Value
β_0	Intercept	4.8891	0.0318	< 2.0e-16
	Logscale	-1.8681	0.1667	< 2.0e-16

Additional statistics for this model fit are provided in Table XXXVII.

Table XXXVII: Weibull IRF Statistics for Ovine Model 4

Statistic	Value
Scale	0.154
Loglikelihood (Model)	-38.8
Loglikelihood (Intercept Only)	-38.8
Number of Newton-Raphson Iterations	9.00
n	119

Ovine Model 5 (Covariate: No Covariates, Dataset: Fresh/Warmed)

Finally, Ovine Model 5 was fit using the data from the Fresh/Warmed condition impact cases. The values for the model coefficients (*logscale* and β_0) are provided in Table XXXVIII.

Table XXXVIII: Coefficient Values for Ovine Model 5

Coefficient	Covariate	Magnitude	Standard Error	p-Value
β_0	Intercept	4.9100	0.0642	< 2.0e-16
	Logscale	-1.6015	0.3272	9.9e-07

Additional statistics for this model fit are provided in Table XXXIX.

Table XXXIX: Weibull IRF Statistics for Ovine Model 5

Statistic	Value
Scale	0.202
Loglikelihood (Model)	-27.1
Loglikelihood (Intercept Only)	-27.1
Number of Newton-Raphson Iterations	5.00
n	54.0

Ovine Model 6 (Covariate: Body Region, Dataset: Fresh/Lab Temp.)

In addition to the univariate models, separate region-based models (with Body Region as the sole covariate) were fit to each data-subset (Fresh/Lab Temperature, Thawed/Lab Temperature, and Fresh/Warmed) to assess regional differences in storage condition effects. These are presented in Ovine Models 6-8. Like Ovine Model 1, these models utilized Equation 7 and can be substituted into Equation 1 & Equation 2 to calculate the model fit for any given body region.

Ovine Model 6 was fit using the data from the Fresh/Lab Temperature condition impact cases, with the Body Region covariate. The values for the coefficients (*logscale*, β_0, β_1, β_2, and β_3) are provided in Table XL.

Table XL: Coefficient Values for Ovine Model 6

Coefficient	Covariate	Magnitude	Standard Error	p-Value
β_0	Intercept	4.7639	0.0479	< 2.0e-16
β_1	Region (Shoulder)	0.1035	0.0642	8.0e-02
β_2	Region (Stomach)	0.2098	0.0686	1.5e-03
β_3	Region (Rump)	0.1187	0.0416	4.3e-03
	Logscale	-2.0873	0.1773	< 2.0e-16

Additional statistics for this model fit are provided in Table XLI.

Table XLI: Weibull IRF Statistics for Ovine Model 6

Statistic	Value
Scale	0.124
Loglikelihood (Model)	-44.9
Loglikelihood (Intercept Only)	-48.8
Chi Squared	7.72
Degrees of Freedom	3.00
p-Value	5.2e-02
Number of Newton-Raphson Iterations	7.00
n	140

Ovine Model 7 (Covariate: Body Region, Dataset: Thawed/Lab Temp.)

Ovine Model 7 was fit using the data from the Thawed/Lab Temperature condition impact cases, with the Body Region covariate. The values for the coefficients (*logscale*, β_0, β_1, β_2, and β_3) are provided in Table XLII.

Table XLII: Coefficient Values for Ovine Model 7

Coefficient	Covariate	Magnitude	Standard Error	p-Value
β_0	Intercept	4.8552	0.0607	< 2.0e-16
β_1	Region (Shoulder)	-0.1118	0.1271	3.8e-01
β_2	Region (Stomach)	0.0939	0.0592	1.1e-01
β_3	Region (Rump)	0.0815	0.0548	1.4e-01
	Logscale	-1.9876	0.1871	< 2.0e-16

Additional statistics for this model fit are provided in Table XLIII.

Table XLIII: Weibull IRF Statistics for Ovine Model 7

Statistic	Value
Scale	0.137
Loglikelihood (Model)	-35.4
Loglikelihood (Intercept Only)	-38.8
Chi Squared	6.78
Degrees of Freedom	3.00
p-Value	7.9e-02
Number of Newton-Raphson Iterations	7.00
n	119

Ovine Model 8 (Covariate: Body Region, Dataset: Fresh/Warmed)

Ovine Model 8 was fit using the data from the Fresh/Warmed condition impact cases, with the Body Region covariate. The values for the coefficients (*logscale*, β_0, β_1, β_2, and β_3) are provided in Table XLIV.

Table XLIV: Coefficient Values for Ovine Model 8

Coefficient	Covariate	Magnitude	Standard Error	p-Value
β_0	Intercept	4.7830	0.0607	< 2.0e-16
β_1	Region (Shoulder)	0.0236	0.0418	5.7e-01
β_2	Region (Stomach)	-0.0008	0.0902	9.9e-01
β_3	Region (Rump)	0.2228	0.0433	2.7e-07
	Logscale	-1.9949	0.1099	< 2.0e-16

Additional statistics for this model fit are provided in Table XLV.

Table XLV: Weibull IRF Statistics for Ovine Model 8

Statistic	Value
Scale	0.136
Loglikelihood (Model)	-23.9
Loglikelihood (Intercept Only)	-27.1
Chi Squared	6.42
Degrees of Freedom	3.00
p-Value	9.3e-02
Number of Newton-Raphson Iterations	8.00
n	54.0

Ovine IRF Response Comparisons

The following comparison was made using Ovine Model 1 to assess the effects of the categorical body region on the injury response. The model response was predicted for each body region category: Shoulder, Ribs, Stomach, and Rump. A few key injury risk levels are highlighted in Table XLVI, and the full predicted response with 95% confidence intervals are plotted in Figure 23.

Table XLVI: Predicted Ovine Injury Risk for Varied Body Region

	Impactor Velocity (m/s)			
Injury Risk (%)	**Shoulder**	**Ribs**	**Stomach**	**Rump**
5	81.3	80.1	91.9	91.9
10	90.1	88.8	101.9	102.0
15	96.0	94.6	108.5	108.6
25	104.2	102.7	117.8	117.9
50	118.3	116.6	133.7	133.9
75	130.7	128.8	147.8	147.9

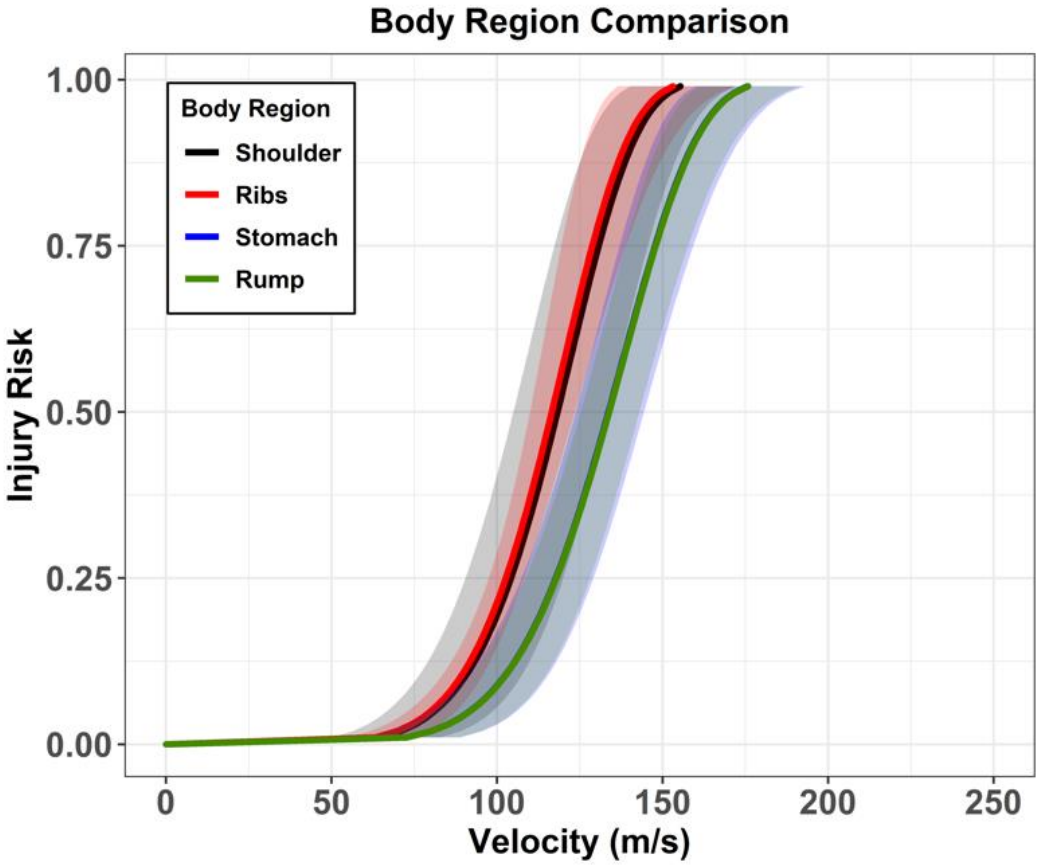


Figure 23: The effects of the impacted body region on the ovine injury response.

The model fit was predicted for each of the four body regions (Shoulder, Ribs, Stomach, and Rump). Corridors represent the 95% confidence interval for each predicted IRF.

Figure 23 shows that, within the range of the tested specimens, variations in the impacted body region resulted in significant shifts in the predicted response. Here, two distinct groups formed based on whether the body region was more anterior (Shoulder and Ribs) or posterior (Stomach and Rump) along the ovine anatomy, with the anterior regions producing greater injury risk from lower impactor velocity. Notably, there was very little difference in the response within each grouping (anterior or posterior).

Further, to assess the effects of tissue storage/temperature on the injury response, separate univariate models were fit to each data-subset (Ovine Models 3-5). The squared error (SE) was calculated at each key injury risk level to quantify the difference between the Ovine Model 3 response and that of Ovine Models 4-5. Additionally, the mean squared error (MSE) was calculated for each full IRF curve. The key injury risk levels are highlighted in Table XLVII, the SE and MSE comparisons are presented in

Table XLVIII, and the full predicted response with 95% confidence intervals are plotted in Figure 24.

Table XLVII: Predicted Injury Risk for the Univariate Storage/Temp. Condition Comparison

	Velocity (m/s)		
Injury Risk (%)	**Fresh/Lab Temp. Ovine Model 3**	**Thawed/Lab Temp. Ovine Model 4**	**Fresh/Warmed Ovine Model 5**
5	85.8	84.0	74.5
10	95.6	93.8	86.2
15	102.1	100.3	94.04
25	111.3	109.6	105.5
50	127.1	125.5	126.0
75	141.1	139.7	133.9

Table XLVIII: Squared Error For the Univariate Storage/Temp. Condition Comparison
SE and MSE values represent difference from the Ovine Model 3 response.

	Squared Error (SE)	
Injury Risk (%)	**Thawed/Lab Temp. Ovine Model 4**	**Fresh/Warmed Ovine Model 5**
5	3.23	89.0
10	3.14	58.8
15	3.04	39.6
25	2.85	16.5
50	2.40	0.21
75	1.93	26.8
MSE	2.34	39.5

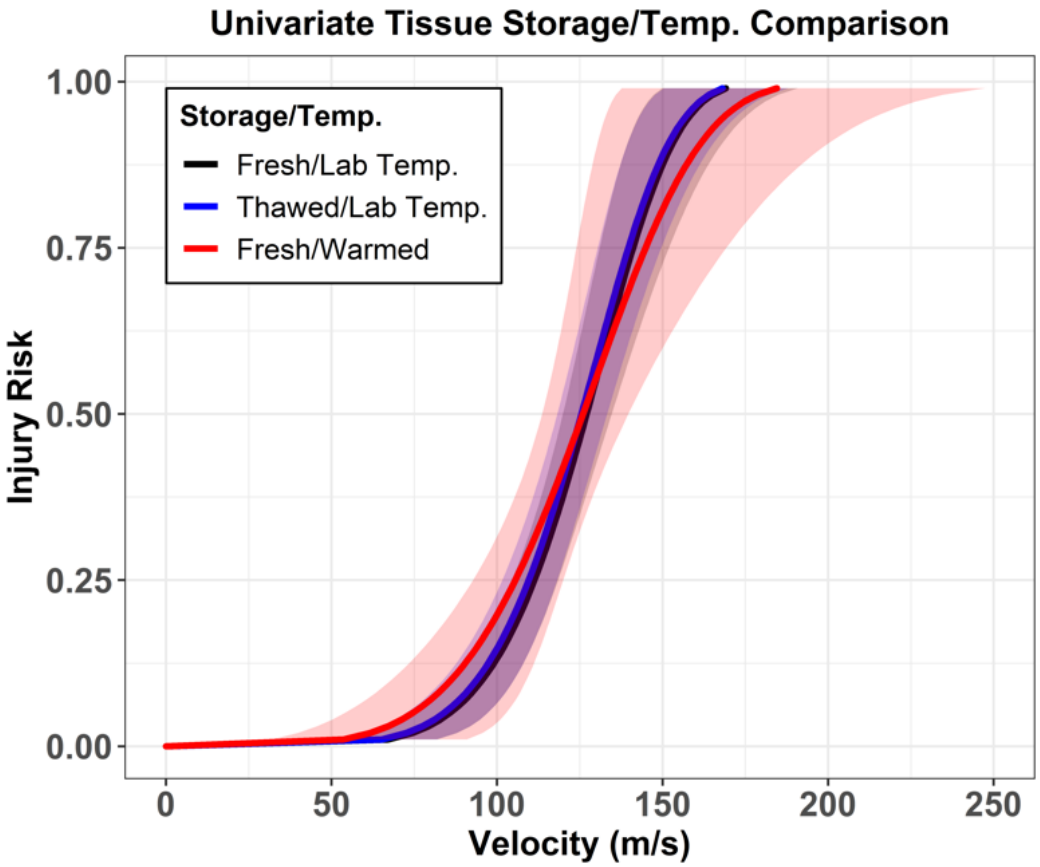


Figure 24: The effects of tissue storage/temperature using univariate models.

Ovine Models 3-5 (univariate models using individual data-subsets) were used to compare the overall effects of tissue storage/temperature conditions on the injury risk response.

Table XLVIII and Figure 24 show that, overall, the tissue storage/temperature conditions had minimal effect on the injury risk response. The Thawed/Lab Temperature subset only had an MSE of 2.34 when compared to the Fresh/Lab Temperature response, while the Fresh/Warmed subset was slightly more different with an MSE of 39.5. However, the Fresh/Warmed response curve stayed within the 95% CI of the other two curves at all injury risk levels, producing greater injury risk at low velocities, intersecting with the Fresh/Lab Temperature curve at approximately the 50% injury risk level, and producing a lower injury risk at high velocities. Notably, the Fresh/Warmed CI was very wide, especially at the tails, likely due to the lesser number of impact cases for this storage/temperature condition (n = 54). Additional data may be necessary to fully quantify the effects of tissue storage/temperature on the injury response.

A second set of models were then fit to each storage/temperature condition data-subset with the categorical body region as the sole covariate (Ovine Models 6-8) to determine the effects of each storage condition on the regional injury response. IRF comparisons were again quantified by calculating the squared error (SE) at a few key injury risk levels and the mean squared error (MSE) for the complete predicted models.

For the comparison of the Shoulder region-based tissue storage/temperature conditions, the SE and MSE comparisons are presented in Table XLIX, and the full predicted response with 95% confidence intervals are plotted in Figure 25.

Table XLIX: Squared Error For the Shoulder Region Storage/Temp. Condition Comparison
SE and MSE values represent difference from the Ovine Model 3 response.

	Squared Error (SE)	
Injury Risk (%)	**Thawed/Lab Temp. Ovine Model 4**	**Fresh/Warmed Ovine Model 5**
5	182.3	68.50
10	195.3	68.47
15	202.9	67.84
25	212.4	66.19
50	225.3	61.64
75	233.5	56.20
MSE	218.3	59.95

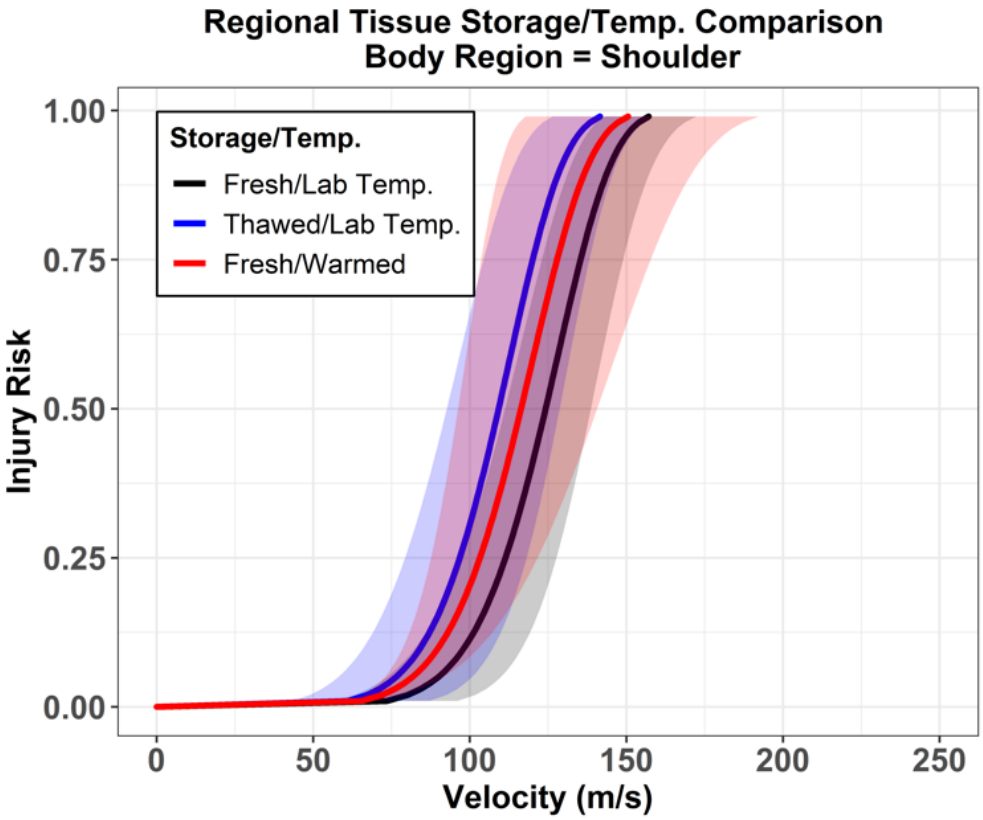


Figure 25: The effects of tissue storage/temperature using regional models (Shoulder region).

Ovine Models 6-8 (regional models using individual data-subsets) were used to compare the regional effects of tissue storage/temperature conditions on the injury risk response. For this comparison, the Shoulder region was assessed.

Table XLIX and Figure 25 show that neither the Thawed/Lab Temperature nor Fresh/Warmed conditions performed very similarly to the Fresh/Lab Temperature condition at the Shoulder region (MSE = 218.3 and 59.95, respectively). Both tissue storage conditions had greater injury risk under lower velocities, with the Thawed/Lab Temperature condition producing the greatest risk.

For the comparison of the Ribs region-based tissue storage/temperature conditions, the SE and MSE comparisons are presented in Table L, and the full predicted response with 95% confidence intervals are plotted in Figure 26.

Table L: Squared Error For the Ribs Region Storage/Temp. Condition Comparison
SE and MSE values represent difference from the Ovine Model 3 response.

	Squared Error (SE)	
Injury Risk (%)	**Thawed/Lab Temp. Ovine Model 4**	**Fresh/Warmed Ovine Model 5**
5	19.20	1.776
10	32.15	0.491
15	42.85	0.065
25	61.28	0.172
50	102.4	2.741
75	149.6	8.059
MSE	107.7	5.364

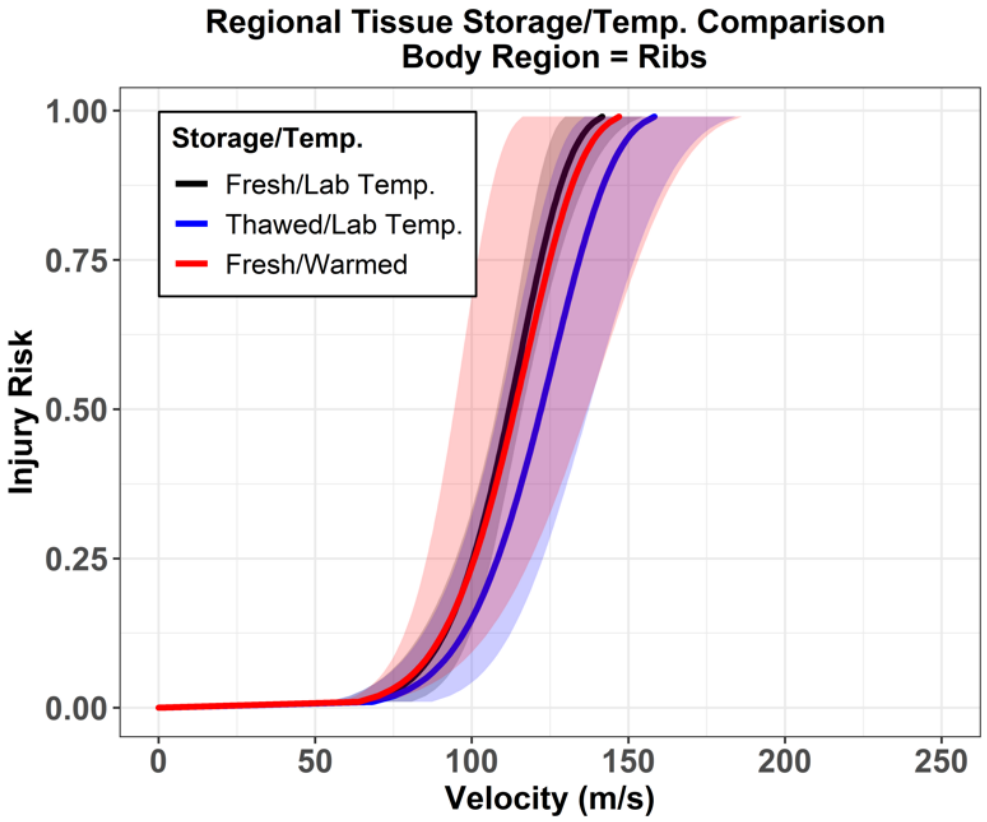


Figure 26: The effects of tissue storage/temperature using regional models (Ribs region).
Ovine Models 6-8 (regional models using individual data-subsets) were used to compare the regional effects of tissue storage/temperature conditions on the injury risk response. For this comparison, the Ribs region was assessed.

Table L and Figure 26 show that the Fresh/Warmed condition responded very similarly to the Fresh/Lab Temperature condition at the Ribs region (MSE = 5.364), with the SE increasing at higher injury risk levels (75%, SE = 8.059). The Thawed/Lab Temperature condition, conversely, was fairly dissimilar to the Fresh/Lab Temperature condition (MSE = 107.7), again, separating at the upper tail (75%, SE = 149.6). Both conditions, however, skewed toward lower risk at all velocity levels.

For the comparison of the Stomach region-based tissue storage/temperature conditions, the SE and MSE comparisons are presented in Table LI, and the full predicted response with 95% confidence intervals are plotted in Figure 27.

Table LI: Squared Error for the Stomach Region Storage/Temp. Condition Comparison
SE and MSE values represent difference from the Ovine Model 3 response.

	Squared Error (SE)	
Injury Risk (%)	**Thawed/Lab Temp. Ovine Model 4**	**Fresh/Warmed Ovine Model 5**
5	37.57	412.9
10	32.90	460.6
15	29.54	491.2
25	24.54	533.7
50	15.99	603.7
75	9.200	662.7
MSE	17.30	587.0

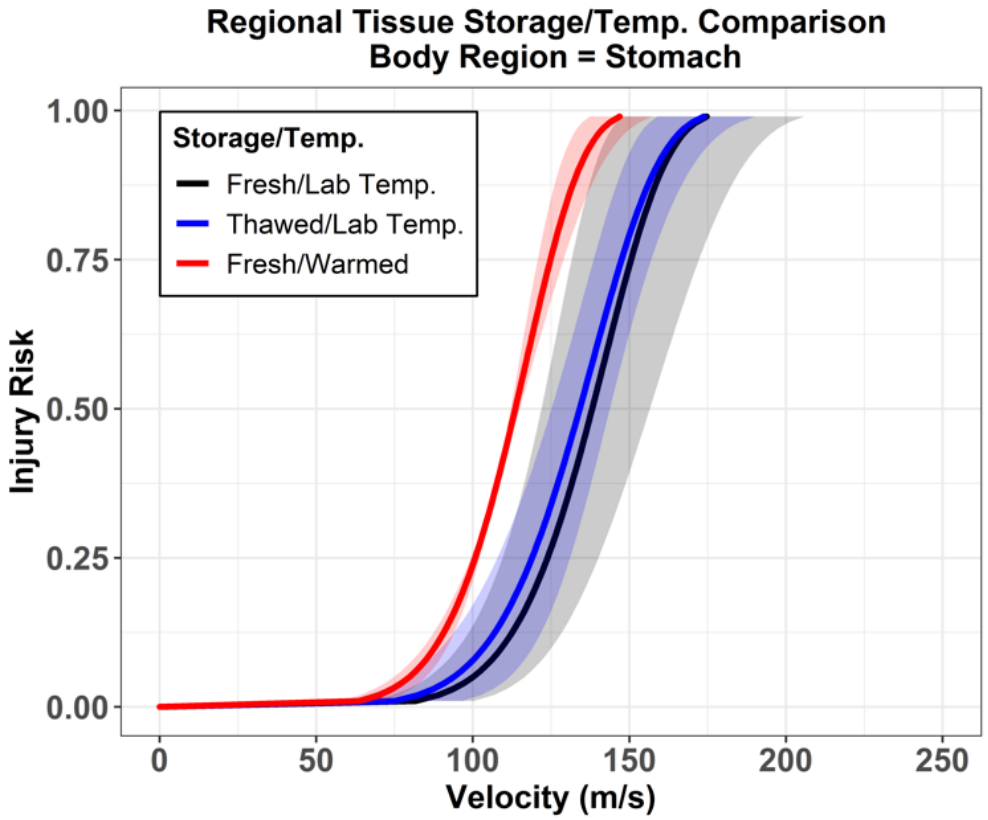


Figure 27: The effects of tissue storage/temperature using regional models (Stomach region).

Ovine Models 6-8 (regional models using individual data-subsets) were used to compare the regional effects of tissue storage/temperature conditions on the injury risk response. For this comparison, the Stomach region was assessed.

Table LI and Figure 27 show that the Thawed/Lab Temperature condition responded similarly to the Fresh/Lab Temperature condition at the Stomach region (MSE = 17.30), with the largest separation in the curves produced under low injury risk (5%, SE = 37.57). The Fresh/Warmed condition, however, was very dissimilar to the Fresh/Lab Temperature curve (MSE = 587.0). Both conditions produced greater injury risk at all velocities than the Fresh/Lab Temperature skew.

For the comparison of the Rump region-based tissue storage/temperature conditions, the SE and MSE comparisons are presented in Table LII, and the full predicted response with 95% confidence intervals are plotted in Figure 28.

Table LII: Squared Error For the Rump Region Storage/Temp. Condition Comparison
SE and MSE values represent difference from the Ovine Model 3 response.

	Squared Error (SE)	
Injury Risk (%)	**Thawed/Lab Temp. Ovine Model 4**	**Fresh/Warmed Ovine Model 5**
5	2.014	69.81
10	6.278	101.6
15	10.59	126.4
25	19.03	167.1
50	40.61	253.1
75	68.10	347.1
MSE	46.12	259.2

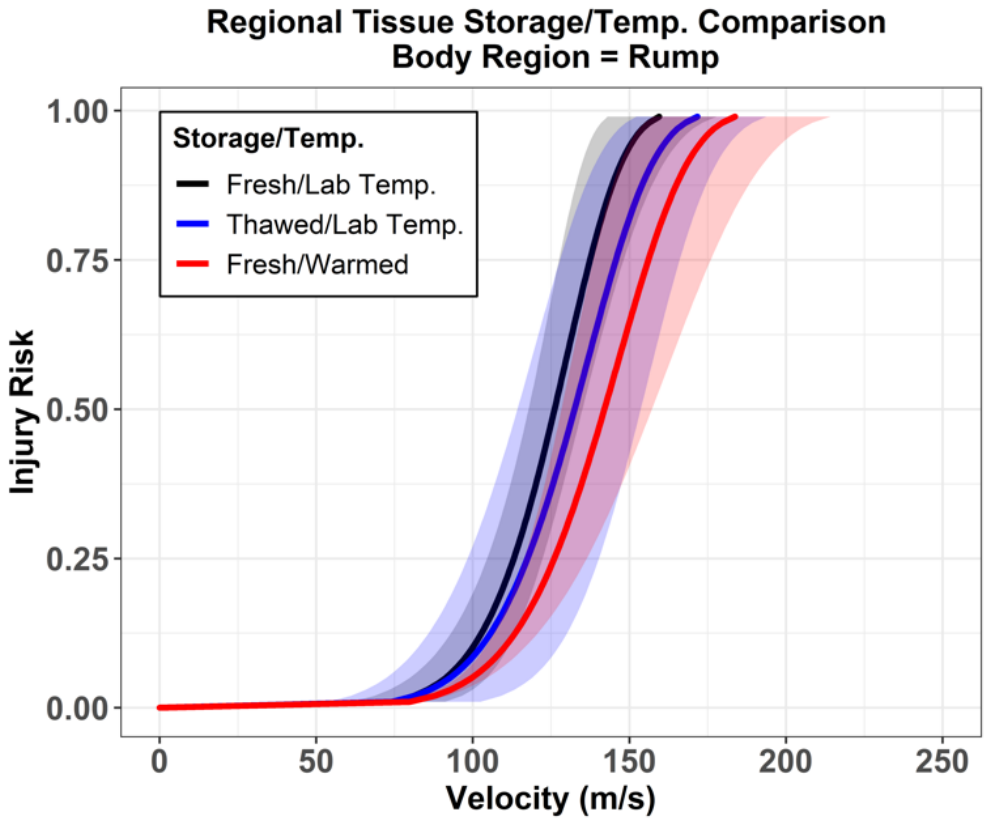


Figure 28: The effects of tissue storage/temperature using regional models (Rump region).
Ovine Models 6-8 (regional models using individual data-subsets) were used to compare the regional effects of tissue storage/temperature conditions on the injury risk response. For this comparison, the Rump region was assessed.

Table LII and Figure 28 show that neither condition produced a similar response to the Fresh/Lab Temperature skew at the Rump region. The Thawed/Lab Temperature condition was the most similar and produced a nearly identical lower tail before separating (MSE = 46.12). The Fresh/Warmed condition was very different, producing a MSE of 259.2. Both conditions had a lower injury risk than the Fresh/Lab Temperature model under all velocities.

Comparison Between PMHS and Ovine Body Regions

To assess the validity of the ovine tissue as a surrogate for human tissue, the predicted IRF response was compared for each body region using PMHS Model 1 and Ovine Model 1. For each comparison, the PMHS response was predicted for the 0.75 in. Cylinder impactor to match the ovine test conditions and the average skin thickness of each body region, and the ovine response was predicted for each categorical body region (Shoulder, Ribs, Stomach, and Rump). IRF comparisons were quantified by calculating the squared error (SE) at a few key injury risk levels and the mean squared error (MSE) for the complete predicted model.

First, comparisons were made between the PMHS Upper Chest body region and each of the ovine body regions. PMHS Model 1 was used to predict the response for the 0.75 in. Cylinder impactor and the average skin thickness of the Upper Chest region (1.83 mm). A few key injury risk levels for each curve are highlighted in Table LIII, the SE and MSE comparisons are presented in Table LIV, and the full predicted response with 95% confidence intervals are plotted in Figure 29.

Table LIII: Predicted Injury Risk for PMHS Upper Chest vs Ovine Body Region Comparison (PMHS Model 1: Impactor Shape = Cylinder, Impactor Diameter = 0.75 in.)

	Velocity (m/s)				
Injury Risk (%)	**PMHS Upper Chest**	**Ovine Shoulder**	**Ovine Ribs**	**Ovine Stomach**	**Ovine Rump**
5	87.5	81.3	80.1	91.9	91.9
10	96.3	90.1	88.8	101.9	102.0
15	102.1	96.0	94.6	108.5	108.6
25	110.1	104.2	102.7	117.8	117.9
50	123.8	118.3	116.6	133.7	133.9
75	135.8	130.7	128.8	147.8	147.9

Table LIV: Squared Error Comparisons Between Ovine Regions and PMHS Upper Chest (PMHS Model 1: Impactor Shape = Cylinder, Impactor Diameter = 0.75 in.)

	Squared Error (SE)			
Injury Risk (%)	**Ovine Shoulder**	**Ovine Ribs**	**Ovine Stomach**	**Ovine Rump**
5	39.1	55.3	18.9	19.8
10	38.3	56.2	31.1	32.4
15	37.3	56.3	41.1	42.8
25	35.4	55.7	58.4	60.5
50	31.1	53.1	97.2	100.3
75	26.4	49.5	142.0	146.1
MSE	**30.3**	**51.4**	**102.4**	**105.5**

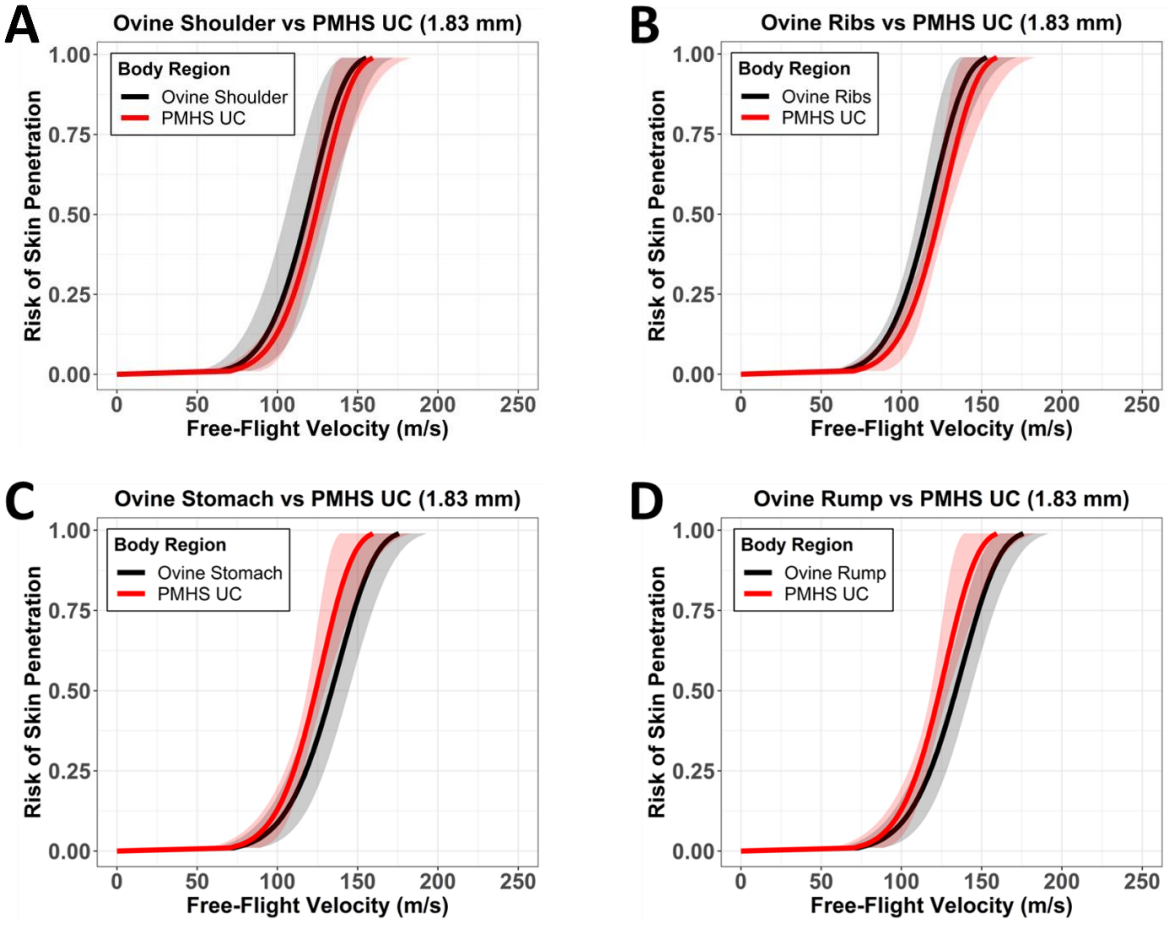


Figure 29: Comparison of the PMHS' Upper Chest region response to each ovine body region. The PMHS Upper Chest (UC) body region was compared to the ovine (a) Shoulder, (b) Ribs, (c) Stomach, and (d) Rump. Corridors represent the 95% confidence interval for each predicted IRF.

Table LIV and Figure 29 show that, generally, the anterior ovine body regions (Shoulder and Ribs) produced the most similar injury response to the PMHS Upper Chest region, with the Shoulder being the greatest surrogate. Figure 29 (a) shows that the ovine Shoulder responded very similarly to the PMHS Upper Chest, producing an MSE of 30.3. Notably, the SE was greatest under low injury risk (5%, MSE = 39.1) and lowest under high injury risk (75%, MSE = 26.4). Figure 29 (b) shows that the ovine Ribs also responded similarly to the PMHS Upper Chest, with an MSE of 51.4. Again, the greatest SE was calculated at the lowest injury risk (5%, MSE = 55.3), and the lowest SE was produced at high injury risk (75%, MSE = 49.5). However, the Upper Chest IRF exited the Ribs CI near the low-to-moderate injury risk levels (6-53%). Figure 29 (c-d) show that the ovine Stomach and Rump responded dissimilarly to the PMHS Upper Chest, with MSE of 102.4 and 105.5, respectively. Both regions were most similar to the Upper Chest under low injury risk, producing SE values less than 61 for injury risk levels below 25%. Interestingly, despite the overall difference in curve shape, the Upper Chest IRF fell within the CIs of both the Stomach and Rump IRFs under low injury risk levels (< 51% for Stomach, < 36% for Rump).

Next, comparisons were made between the PMHS Abdomen body region and each of the ovine body regions. PMHS Model 1 was used to predict the response for the 0.75 in. Cylinder impactor and the average skin thickness of the Abdomen region (2.16 mm). A few key injury risk levels for each curve are highlighted in Table LV, the SE and MSE comparisons are presented in Table LVI, and the full predicted response with 95% confidence intervals are plotted in Figure 30.

Table LV: Predicted Injury Risk for PMHS Abdomen vs Ovine Body Region Comparison (PMHS Model 1: Impactor Shape = Cylinder, Impactor Diameter = 0.75 in.)

	Velocity (m/s)				
Injury Risk (%)	**PMHS Abdomen**	**Ovine Shoulder**	**Ovine Ribs**	**Ovine Stomach**	**Ovine Rump**
5	93.8	81.3	80.1	91.9	91.9
10	103.3	90.1	88.8	101.9	102.0
15	109.4	96.0	94.6	108.5	108.6
25	118.1	104.2	102.7	117.8	117.9
50	132.8	118.3	116.6	133.7	133.9
75	145.7	130.7	128.8	147.8	147.9

Table LVI: Squared Error Comparisons Between Ovine Regions and PMHS Abdomen
(PMHS Model 1: Impactor Shape = Cylinder, Impactor Diameter = 0.75 in.)

	Squared Error (SE)			
Injury Risk (%)	**Ovine Shoulder**	**Ovine Ribs**	**Ovine Stomach**	**Ovine Rump**
5	158.3	189.4	3.921	3.508
10	173.0	209.1	1.934	1.617
15	181.9	221.4	0.935	0.706
25	193.6	237.9	0.102	0.033
50	211.0	263.8	0.819	1.126
75	223.7	284.1	4.386	5.139
MSE	**204.2**	**255.7**	**3.511**	**3.887**

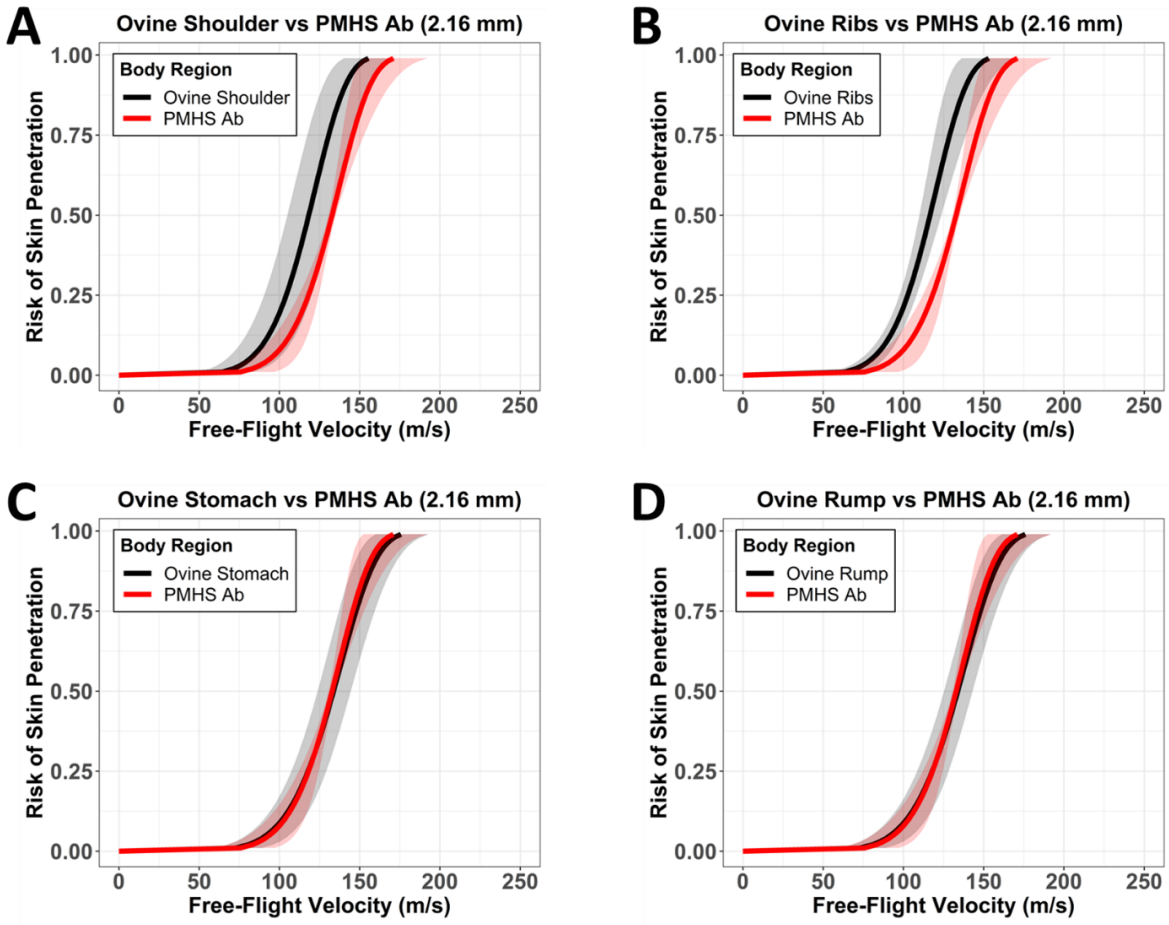


Figure 30: Comparison of the PMHS' Abdomen region response to each ovine body region.
The PMHS Abdomen (Ab) body region was compared to the ovine (a) Shoulder, (b) Ribs, (c) Stomach, and (d) Rump. Corridors represent the 95% confidence interval for each predicted IRF.

Table LVI and Figure 30 show that, overall, the posterior ovine body regions (Stomach and Rump) produced the most similar injury response to the PMHS Abdomen region. Figure 30 (a-b) show that the ovine Shoulder and Ribs responded very dissimilarly to the PMHS Abdomen, with MSE of 204.2 and 255.7, respectively. While both regions were most similar to the Abdomen under low injury risk, no observed risk level produced an SE value less than 158.3. Figure 30 (c-d) show that the Stomach and Rump both produced response curves almost identical to the PMHS Abdomen, with MSE of 3.511 and 3.887, respectively. Both regions had the lowest SE (0.102 and 0.033, respectively) at the 25% injury risk level, at which point the ovine curve and PMHS curve overlapped.

Comparisons were then made between the PMHS Upper Back body region and each of the ovine body regions. PMHS Model 1 was used to predict the response for the 0.75 in. Cylinder impactor and the average skin thickness of the Upper Back region (3.06 mm). A few key injury risk levels for each curve are highlighted in Table LVII, the SE and MSE comparisons are presented in Table LVIII, and the full predicted response with 95% confidence intervals are plotted in Figure 31.

Table LVII: Predicted Injury Risk for PMHS Upper Back vs Ovine Body Region Comparison (PMHS Model 1: Impactor Shape = Cylinder, Impactor Diameter = 0.75 in.)

	Velocity (m/s)				
Injury Risk (%)	**PMHS Abdomen**	**Ovine Shoulder**	**Ovine Ribs**	**Ovine Stomach**	**Ovine Rump**
5	113.5	81.3	80.1	91.9	91.9
10	125.0	90.1	88.8	101.9	102.0
15	132.4	96.0	94.6	108.5	108.6
25	142.9	104.2	102.7	117.8	117.9
50	160.6	118.3	116.6	133.7	133.9
75	176.2	130.7	128.8	147.8	147.9

Table LVIII: Squared Error Comparisons Between Ovine Regions and PMHS Upper Back (PMHS Model 1: Impactor Shape = Cylinder, Impactor Diameter = 0.75 in.)

	Squared Error (SE)			
Injury Risk (%)	**Ovine Shoulder**	**Ovine Ribs**	**Ovine Stomach**	**Ovine Rump**
5	1041	1118	469.1	464.4
10	1212	1305	531.4	525.9
15	1328	1431	572.0	565.9
25	1496	1615	629.2	622.3
50	1795	1944	725.8	717.4
75	2070	2246	809.3	799.5
MSE	**1755**	**1901**	**706.1**	**697.9**

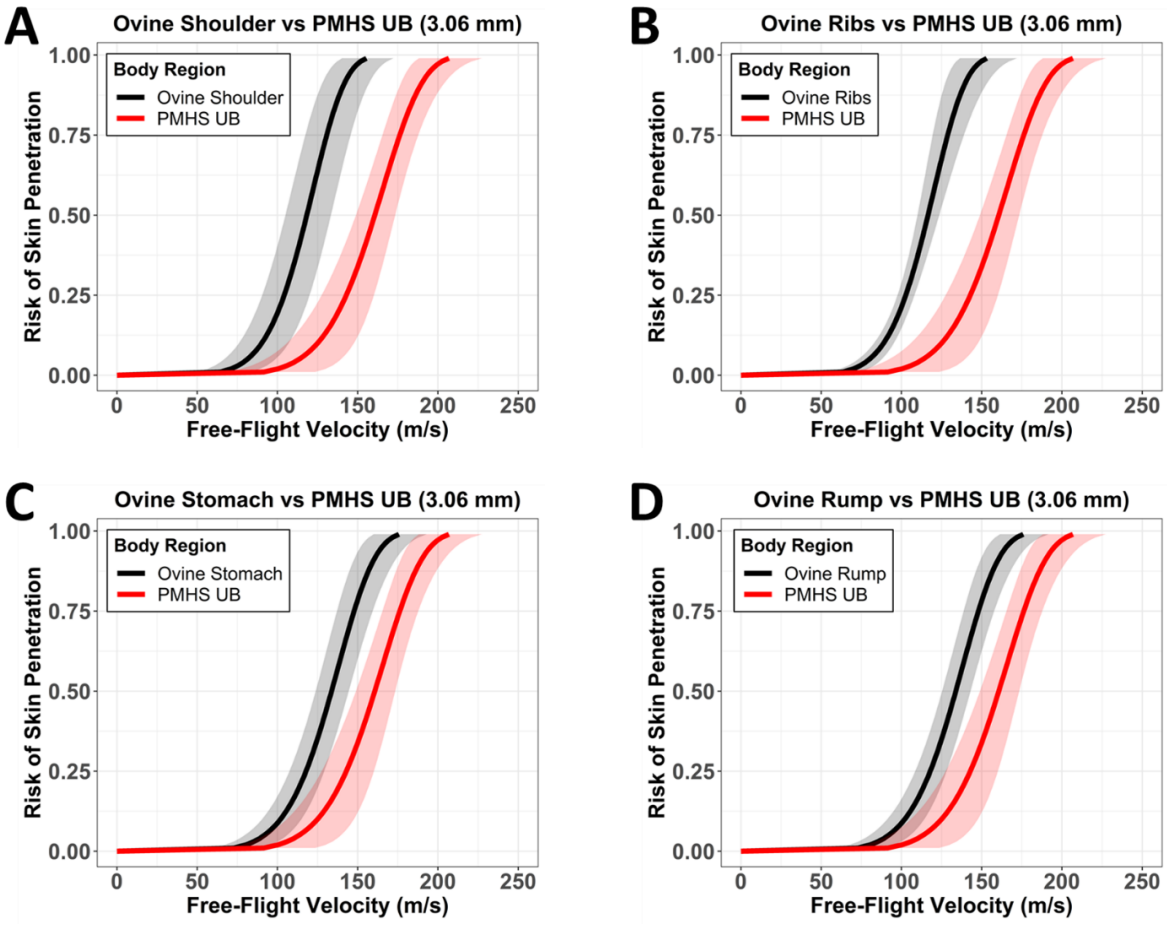


Figure 31: Comparison of the PMHS' Upper Back region response to each ovine body region. The PMHS Upper Back (UB) body region was compared to the ovine (a) Shoulder, (b) Ribs, (c) Stomach, and (d) Rump. Corridors represent the 95% confidence interval for each predicted IRF.

Table LVIII and Figure 31 show that no ovine body regions responded similarly to the PMHS Upper Back region. In generally, the closest match was the Rump (MSE = 697.9), followed by the Stomach (MSE = 706.1), Shoulder (MSE = 1755), and Ribs (MSE = 1901). All four ovine body regions produced their most similar response under the lowest injury risk level (5%) and their most dissimilar response at the highest injury risk level (75%). No observed risk level produced an SE value of less than 464.4.

Finally, comparisons were made between the PMHS Lower Back body region and each of the ovine body regions. PMHS Model 1 was used to predict the response for the 0.75 in. Cylinder impactor and the average skin thickness of the Lower Back region (2.87 mm). A few key injury risk levels for each curve are highlighted in Table LIX, the SE and MSE comparisons are presented in Table LX, and the full predicted response with 95% confidence intervals are plotted in Figure 32.

Table LIX: Predicted Injury Risk for PMHS Lower Back vs Ovine Body Region Comparison (PMHS Model 1: Impactor Shape = Cylinder, Impactor Diameter = 0.75 in.)

	Velocity (m/s)				
Injury Risk (%)	**PMHS Abdomen**	**Ovine Shoulder**	**Ovine Ribs**	**Ovine Stomach**	**Ovine Rump**
5	109.1	79.6	79.1	88.2	91.8
10	120.0	88.6	88.2	98.3	102.3
15	127.2	94.6	94.1	104.9	109.1
25	137.2	103.1	102.5	114.3	118.9
50	154.3	117.6	117.0	130.4	135.7
75	169.3	130.6	129.9	144.7	150.6

Table LX: Squared Error Comparisons Between Ovine Regions and PMHS Lower Back (PMHS Model 1: Impactor Shape = Cylinder, Impactor Diameter = 0.75 in.)

	Squared Error (SE)			
Injury Risk (%)	**Ovine Shoulder**	**Ovine Ribs**	**Ovine Stomach**	**Ovine Rump**
5	772.2	893.1	295.4	291.7
10	893.4	973.3	328.7	324.4
15	974.7	1063	349.7	345.0
25	1092	1195	378.6	373.2
50	1299	1426	424.9	418.5
75	1487	1637	462.6	455.2
MSE	**1269**	**1393**	**412.2**	**406.0**

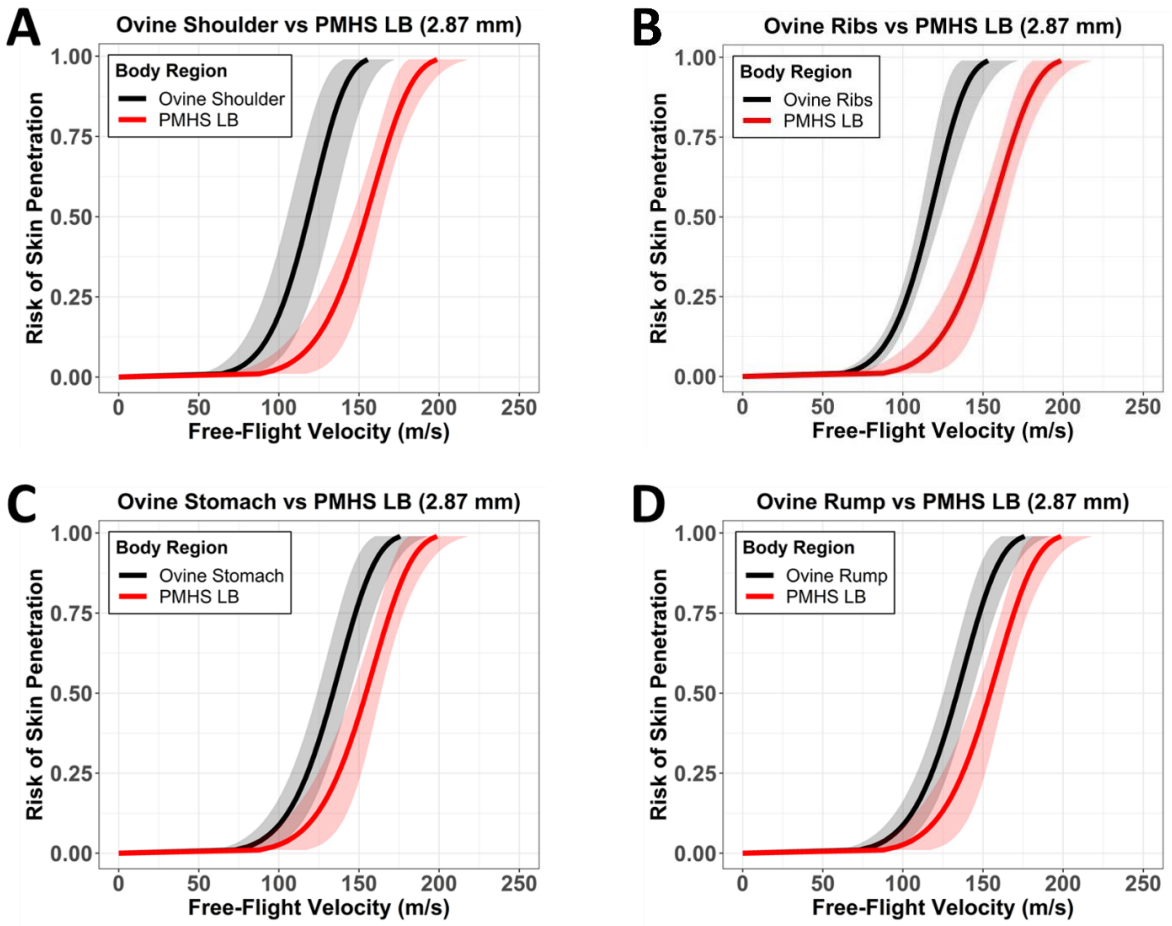


Figure 32: Comparison of the PMHS' Lower Back region response to each ovine body region.
The PMHS Lower Back (LB) body region was compared to the ovine (a) Shoulder, (b) Ribs, (c) Stomach, and (d) Rump. Corridors represent the 95% confidence interval for each predicted IRF.

Table LX and Figure 32 show that no ovine body regions responded similarly to the PMHS Lower Back region. Again, the closest match was the Rump (MSE = 406.0), followed by the Stomach (MSE = 412.2), Shoulder (MSE = 1269), and Ribs (MSE = 1393). All four ovine body regions produced their most similar response under the lowest injury risk level (5%) and their most dissimilar response at the highest injury risk level (75%). No observed risk level produced an SE value of less than 291.7.

Conclusions

Impactor testing was conducted on eight male, cadaveric ovine specimens (weight: 134.5 - 197.8 lb, length: 77 – 92 cm) to quantify the tolerance of ovine skin to high-rate blunt impacts and to compare the response to that of the PMHS to determine whether ovine skin was a comparable surrogate for human skin. A total of 313 impacts were conducted at impact velocities from 60-162 m/s using a 0.75 in.-diameter cylindrical impactor. Tests were conducted across three tissue storage/temperature conditions. These included Fresh/Lab Temperature (surface temp. = 68.5 ± 4.7, internal temp. = 64.5 ± 5.6), Thawed/Lab Temperature (surface temp. = 67.3 ± 2.7, internal temp. = 63.5 ± 2.0), and Fresh/Warmed (surface temp.

= 88.9 ± 6.6, internal temp. 86.7 ± 3.5). Necropsies were conducted on each specimen to document the presence of penetration into the skin, as well as the severity of injury. Each impact site was also palpated to determine whether an impact was conducted over a bony region. In total, 80 of the 313 impacts resulted in skin penetration, 155 of the 313 impacts were located over bone, and 2 of the 155 bony impacts resulted in fractures.

Ultrasound images were collected at each impact site ahead of testing, and these images were analyzed to assess the anatomical thickness and shear wave velocity (an analogue to stiffness) of each tissue layer (skin, fat, fascia, and muscle). Generally, there was little difference in the tissue thickness across specimens, with only minor variations within specific tissue layers. There were, however, specimen-specific differences in the shear wave velocity, with Ovine 8 producing the greatest velocities in the skin (alongside Ovine 4), fat, and fascia layers. Regionally, the Ribs contained the thickest fat layer, the Stomach contained very thin fat and fascia layers, and the Shoulder and Rump contained the thickest muscle compared to the other regions. Additionally, the Shoulder region generally produced greater shear wave velocities within the skin, fat, and fascia layers, while the Stomach produced the greatest shear wave velocity in the muscle layer.

Before developing the final IRF, fifteen possible covariates were analyzed to determine which were significant to the injury response. These included impact location and testing environment variables (specimen ID, side of the body, body region, and the presence of bone), tissue temperature variables (surface tissue temperature, internal tissue temperature, and tissue storage conditions), and the tissue thickness and shear wave velocity (stiffness) at each tissue layer (skin, fat, fascia, and muscle). Of these, the following variables were determined to have a significant effect on the injury response (in order of most to least significant): specimen ID and body region. While the specimen ID was significant to the IRF development, it was implemented into the model within a cluster term rather than as a covariate. Overall, the best-fit ovine IRF (Ovine Model 1) used body region as the sole covariate. This model was fit using a Weibull survival distribution with velocity (m/s) as the primary predictor to predict the likelihood of injury (>5 mm penetration) [1]. An additional, less-specific univariate IRF (Ovine Model 2) was also developed for application outside the bounds of this study's test conditions. As a means of comparing the tissue storage/temperature conditions, six more IRFs were developed using subsets of the data. These included three univariate models (Ovine Models 3-5), as well as three models that utilized the body region covariate (Ovine Models 6-8). From the univariate model (Oven Model 2), the 50% penetration risk level was achieved at 126.2 m/s.

The best-fit model (Ovine Model 1) was used to make compare the effects of the body regions on the injury response. This assessment showed two distinct IRF response groups based on whether the impact occurred on the anterior or posterior end of the specimen. Generally, the anterior body regions (Shoulder and Ribs) predicted a greater injury risk under lower velocities than the posterior body regions (Stomach and Rump). Additionally, the broad effects of the tissue storage/temperature conditions were first assessed using the univariate data-subset models (Ovine Models 3-5). Generally, there was very little difference in the response of the three conditions, with the Fresh/Lab Temperature and Thawed/Lab Temperature skews aligning nearly identically. While the Fresh/Warmed response was slightly different, the full curve stayed within the 95% CI of the other two curves. When assessing the regional differences in the tissue storage/temperature conditions (using Ovine Models 6-8), no distinct or significant trends were apparent, potentially due to the limited sample sizes of each tissue condition.

Further comparisons were made between the ovine injury response and the PMHS injury response from Aim 1. These comparisons utilized Ovine Model 1 and PMHS Model 1, respectively, to compare individual body regions between the two species. Here, the IRF for the PMHS Upper Chest fell within the confidence interval for the ovine Shoulder region at all injury risk levels. Each of the remaining ovine regions coincided with the PMHS Upper Chest region at certain injury risk levels, with the Upper Chest staying within the Ribs CI for risk levels < 6% or > 51%, within the Stomach CI for risk levels < 51%, and within the Rump CI for risk levels < 36%. Similarly, the IRFs for the posterior ovine body regions (Stomach and Rump) produced nearly identical responses to the PMHS Abdomen region, with the Abdomen IRF remaining within the Stomach and Rump CIs. While the ovine specimens responded similarly to the anterior PMHS regions (Upper Chest and Abdomen), no ovine body regions approximated the response of the PMHS posterior (Upper Back and Lower Back). Overall, the data supports the use of the ovine Shoulder as a surrogate for PMHS Upper Chest, as well as the use of the posterior ovine regions (Stomach and Rump) as surrogates for PMHS Abdomen. Additionally, the ovine Ribs, Stomach, and Rump showed promise as conditional surrogates for the PMHS Upper Chest, with the Ribs aligning under high velocity/injury risk, and the Stomach and Rump aligning under low velocity/injury risk.

Overall, the risk of injury was primarily dependent on the regional location of impact, despite both the tissue thickness and shear wave velocity variables showing insignificant influences on the injury risk response. While the fat, fascia, and muscle layers showed significant differences across the various body regions, the skin thickness, one of the predominant injury predictors for the PMHS in Aim 1, was relatively homogenous in both the ovine specimen population for this study and across the ovine body regions. This uniformity likely resulted in the insignificance of the skin thickness covariate seen throughout the IRF development. Further, three types of tissue storage/temperature conditions were tested within the ovine specimens. By comparing the univariate data-subset models (Ovine Model 3-5), it was confirmed that the Fresh/Lab Temperature and Thawed/Lab Temperature tissue storage conditions performed equivalently. This indicates that by freezing and thawing the ovine tissue, no major changes were observed in the injury response, which is similar to what has been documented previously for porcine specimens [24]. Additionally, while there were anecdotal differences noted between the Fresh/Lab Temperature and Fresh/Warmed tissue temperature skews, the analyses could not conclude whether there was or was not a significant difference between these conditions, likely due to the decreased number of Fresh/Warmed test cases (producing a very large confidence interval). These tissue storage phenomena should be investigated further to confirm their influence on the injury risk. Again, the presence of bone within the backing material of each impact site was tested as a potential categorical covariate and was determined to be insignificant within our testing population. Lastly, from the comparison between the regional ovine and PMHS injury risk responses, it was determined that the anterior ovine regions (Shoulder and Ribs) may be viable as surrogates for the PMHS Upper Chest region, and the posterior ovine regions (Stomach and Rump) may be able to approximate the response of the PMHS Abdomen region.

The IRFs developed within this study are applicable for determining the risk of penetrating ovine skin (> 5 mm of penetration) using a rigid, 0.75 in. cylindrical impactor [1]. As Aim 1 showed that the impactor diameter did not have a large effect on the injury risk, these models may be applicable outside of the testing conditions for rigid, cylindrical impactors with diameters between 0.50 in. and 1.00 in. so long as the sectional density is held constant (2.3 g/cm^2). The most specific IRF (Ovine Model 1) can be used as long as the ovine body region is known and falls within the tested regions (Shoulder, Ribs, Stomach, or Rump); otherwise, the univariate model (Ovine Model 2) may be used for general

assessments of injury risk. Further, by determining that the ovine tissue responded similarly to the anterior regions of a PMHS and by confirming that there was no functional difference in the response between the fresh and frozen-thawed ovine tissue response, cadaveric ovine skin (fresh or frozen-thawed) may be used as surrogates for PMHS skin in high-rate blunt impact testing.

Aim 2 of this study was limited in many of the same ways as Aim 1. As previously mentioned, the impactors were limited to rigid, blunt geometries of uniform sectional density. Aim 2, however, was also limited to a single impactor shape and diameter, the 0.75 in. cylinder. Future studies should expand this assessment to non-rigid and non-blunt geometries, as well as to the other impactors tested in Aim 1 to confirm that ovine specimens are an appropriate surrogate under all impactor types. Once again, the impact cases in this study were all roughly perpendicular to the skin. Aim 2 also specifically focused impacts to the flanks of the sheep rather than the underbelly. Additional testing may be necessary to investigate the mechanics and thresholds of skin failure under oblique impact cases, as well as to other regions not on the flanks of the specimens. Several other limitations were logistic-in-nature for testing with freshly sacrificed ovine specimens. Primarily, internal gastrointestinal gasses built up in the hours following euthanasia. This resulted in the stomach region pressurizing and inflating. This was combatted by venting the stomach region throughout testing; however, some inflation remained, potentially creating an artificially taught surface. The suspension harness also contributed to this extraneous skin taughtness by applying pressure to sensitive regions along the sheep's underbelly. Further, the ovine specimens were much more uniform than the PMHS, providing much less cross-subject differentiation in anatomical makeup. This resulted in fewer significant covariates and much less specific IRFs. Finally, the tissue storage/temperature condition preparation provided additional limitations, namely a small sample size per skew. Additionally, the Fresh/Warmed condition was applied significantly after the time of euthanasia; future studies should warm the specimens immediately following the sacrifice to maintain as much nascent body heat as possible to avoid potentially damaging the tissue throughout heating.

Aim 3: Model Development and Validation

Overview

Simulations of the high-rate blunt impact tests described in Aim 1 were conducted using a set of Finite Element (FE) models adapted to this loading environment. The torso model, derived from the Advanced Total Body Model (ATBM) v0.86 developed by L3 Communications (San Diego, CA), was primarily updated through modifications to the flesh material implementations. Impactor models corresponding to those used in the Post-Mortem Human Surrogate (PMHS) experiments were developed and used to simulate impacts at locations corresponding to the impact locations used in the experiments. Finally, maximum principal strain was assessed at the impact site and used to develop a meta-model to investigate the effects of various parameters relating to the boundary conditions (impact location, free-flight velocity, impactor shape, and impactor size) and material variations (skin and adipose layer stiffness) on the predicted skin deformation. Using this meta-model, an injury risk function relating maximum principal strain to penetration risk was derived from PMHS Model 1 developed in Aim 1.

Methods

Model Overview

The models used in this project consisted of a 50th percentile male torso model and a set of nonlethal, free-flight impactor models, corresponding to the impactor geometries used in Aims 1 and 2. The torso FE model consists of a modified ATBM v0.86 model that was updated to improve the model's ability to predict skin deformation under dynamic blunt impact. Modifications primarily focused on updates to the skin, adipose, and muscle (collectively, the flesh) parts of the ATBM v0.86 model (Table LXI). The different model components will be described in detail in the following sections. Further details regarding the development, setup, and results processing, including detailed examples, are provided in the Analyst Guide.

Table LXI. Overview of the modified ATBM v0.86 model flesh (skin, muscle, adipose layer) parts.

	Skin (PID 9000)	**Adipose (PID 8001)**	**Muscle (PID 8000)**
Part Overview[c]			
Elements	N = 5544 Quadrilateral shells ELFORM = 25[a,d]	N = 11088 Hexahedral solids ELFORM = 1[b]	N = 11088 Hexahedral solids ELFORM = 1[b]
Material	Ogden rubber with quasi-linear viscoelasticity[d]	Ogden rubber with quasi-linear viscoelasticity[d]	Ogden rubber with quasi-linear viscoelasticity[d]

[a]Belytschko-Tsay shell with thickness stretch
[b]Constant stress solid element
[c]Oblique images of flesh parts. The surface facing left of the image is anterior.
[d]Updated with respect to ATBM v0.86

Software and Unit System

Consistent with the ATBM v0.86 model, all models used in this study were developed and evaluated using a double precision solver of LS-Dyna (Ansys, Canonsburg, PA) version MPP R12.0.0 (64 bit). The unit system, consistent with the ATBM v0.86 model, is shown in Table LXII. All model inputs and outputs adhere to this unit convention.

Table LXII. Model unit system.

Mass	Length	Time	Force	Stress	Energy	Density
kg	*m*	*s*	*N*	*Pa*	*J*	*kg/m3*

Torso Model Updates

Compared to the ATBM v0.86, the updated torso model includes significant updates to the flesh (skin, adipose, and muscle) parts that were implemented to improve the skin deformation response prediction. Most notably, all three flesh parts were assigned updated Ogden Quasilinear Viscoelastic constitutive models through the *MAT_OGDEN_RUBBER Ls-Dyna material card. In addition, an algorithm for locally refining the flesh mesh at a prescribed impact location was developed to improve the skin deformation prediction, as well as to increase the spatial resolution in the simulated strain field. These updates will be discussed in the following sections.

Skin Material Updates

The updated skin material card is shown in Figure 33. The material parameters were fit to experimental tensile tests of cadaveric skin dog bone specimens and verified by simulating a series of dynamic skin indentation experiments. Details regarding these experiments and the fitting approach are reported in Kong et al., 2020 [4]. Results from the tensile and indentation simulations are shown in Figure 34. In this implementation, the skin quadrilateral elements were updated to utilize a Belytschko-Tsay shell with thickness stretch element formulation (ELFORM = 25 in LS-Dyna).

```
*MAT_OGDEN_RUBBER
$#     mid        ro        pr         n        nv         g      sigf       ref
      9000      1000   0.49999         0         6       0.0       0.0       0.0
$#     mul       mu2       mu3       mu4       mu5       mu6       mu7       mu8
   0.054e6       0.0       0.0       0.0       0.0       0.0       0.0       0.0
$#  alpha1    alpha2    alpha3    alpha4    alpha5    alpha6    alpha7    alpha8
      10.7       0.0       0.0       0.0       0.0       0.0       0.0       0.0
$#      gi     betai     vflag
    0.0430      1E-1         1
$#      gi     betai
    0.3140      1E+0
$#      gi     betai
    0.2400      1E+1
$#      gi     betai
    0.2770      1E+2
$#      gi     betai
    0.0001      1E+3
```

Figure 33. Skin material card and parameters.

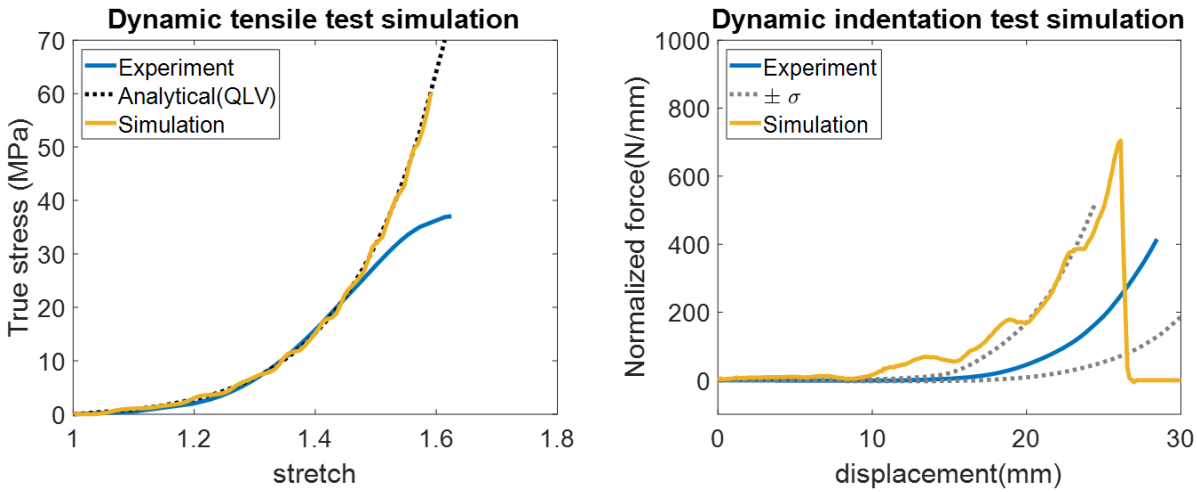


Figure 34. Constitutive model verification from experimental data.

Results from the dynamic tensile simulations used to fit the constitutive model (left) and dynamic indentation simulations used to verify the model response (right). σ represents the experimental standard deviation. Note that stretch is unitless.

Adipose Tissue Material Updates

The updated adipose tissue material card is shown in Figure 35. These materials were fit to dynamic indentation testing of cadaveric adipose tissue. Details regarding these experimental tests and the fitting of this constitutive model are reported in Sun et al., 2020 [25].

```
*MAT_OGDEN_RUBBER_TITLE
AdiposeTissue_Sun
$#     mid        ro        pr         n        nv         g      sigf       ref
      8001     920.0    0.4995         0         6       0.0       0.0       0.0
$#     mu1       mu2       mu3       mu4       mu5       mu6       mu7       mu8
   1463000     7.009   -188900       0.0       0.0       0.0       0.0       0.0
$#  alpha1    alpha2    alpha3    alpha4    alpha5    alpha6    alpha7    alpha8
   0.03363     16.38    0.2578       0.0       0.0       0.0       0.0       0.0
$#      gi     betai      vflag
   0.04966       0.1          1
$#      gi     betai      vflag
 2.442e-07       1.0          0
$#      gi     betai      vflag
     0.585      10.0          0
$#      gi     betai      vflag
    0.2983     100.0          0
$#      gi     betai      vflag
 1.094e-07    1000.0          0
```

Figure 35. Adipose tissue material card and parameters.

Muscle Material Updates

The updated muscle material card is shown in Figure 36. Using the skin and adipose tissue models described above, the muscle material parameters were calibrated to experimental data from stress relaxation testing of cadaveric flesh, consisting of skin, adipose tissue, and muscle. Details regarding these experiments and the calibration process are reported in Kong et al., 2020 [4]. Results from this calibration process are shown in Figure 37. Finally, using the calibrated skin, adipose tissue, and muscle materials, the flesh model response was verified under experimental blunt impacts, conducted using cadaveric specimens [13]. Results from this component-level verification are shown in Figure 38. Details regarding this final component-level verification are reported in Kong et al., 2020 [4].

```
*MAT_OGDEN_RUBBER_TITLE
passive muscle (JNLW drop tower @ 4.5m/s SR test, 2020)
$#     mid        ro        pr         n        nv         g      sigf       ref
      8000    1000.0   0.49999         0         0       0.0       0.0       0.0
$#     mu1       mu2       mu3       mu4       mu5       mu6       mu7       mu8
7.11000E-4  -1230000  132000.0       0.0       0.0       0.0       0.0       0.0
$#  alpha1    alpha2    alpha3    alpha4    alpha5    alpha6    alpha7    alpha8
     23.26    -0.001     0.047       0.0       0.0       0.0       0.0       0.0
$#      gi     betai     vflag
1.0000E-20       1.0         1
$#      gi     betai     vflag
1.0000E-20      10.0         0
$#      gi     betai     vflag
1.0000E-20     100.0         0
$#      gi     betai     vflag
    0.9289    1000.0         0
$#      gi     betai     vflag
1.0000E-20   10000.0         0
```

Figure 36. Muscle material card in Skin Penetration Model 1.0.

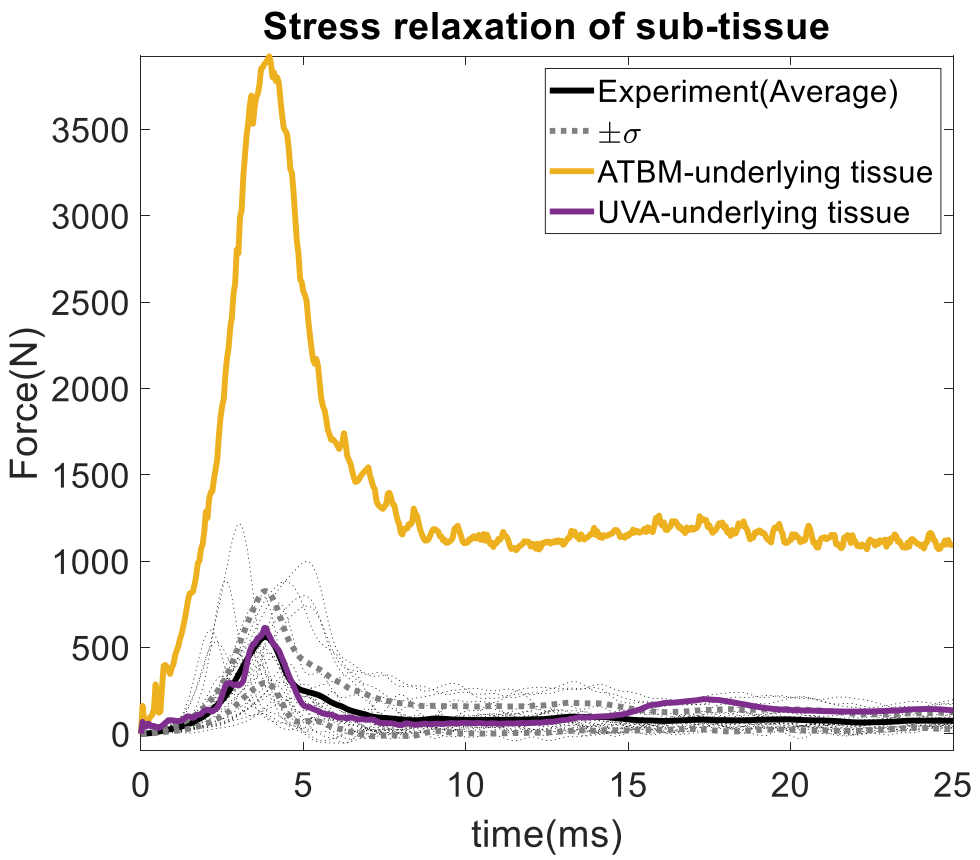


Figure 37. Stress relaxation results from underlying tissue (muscle) calibration.
σ represents experimental standard deviation.

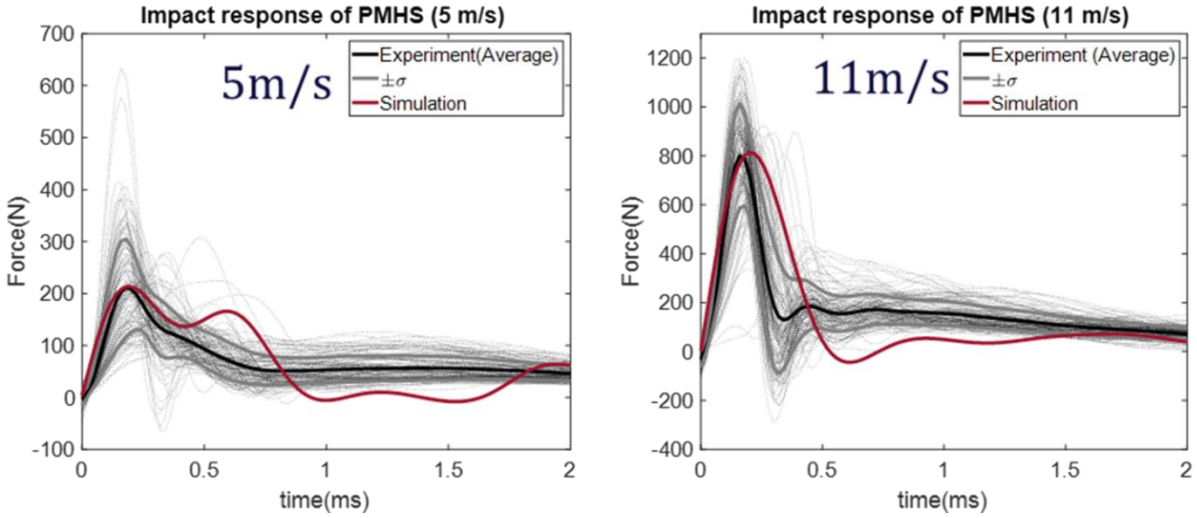


Figure 38. Flesh model verification.
Verification of flesh component-level model under blunt impact at 5 m/s (left) and 11 m/s (right). σ represents experimental standard deviation.

A comparison between the original ATBM and the modified flesh parts (skin, adipose, and muscle) response is shown in Figure 39. These data represent the material response in tension for skin and compression for adipose and muscle tissues. These results show that the previous materials implemented in the ATBM v0.86 torso flesh model were overly stiff.

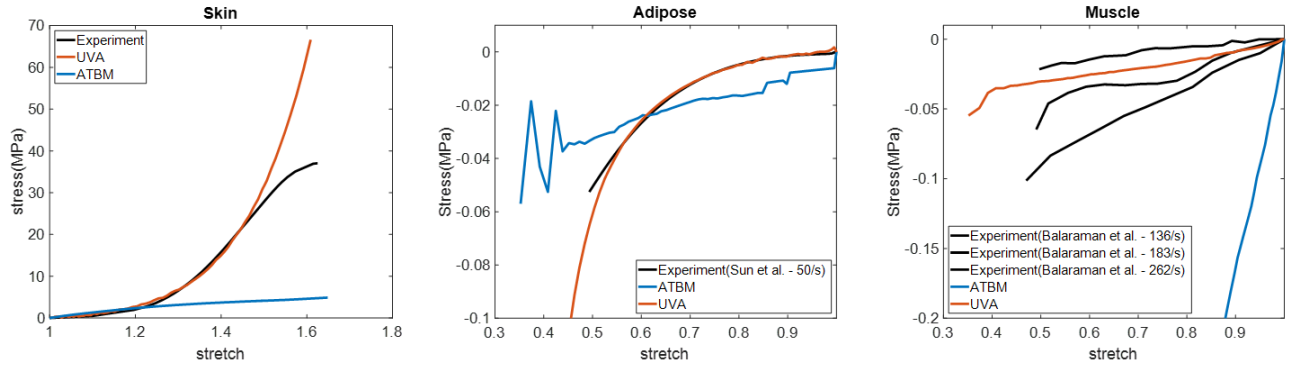


Figure 39. Comparison of flesh part responses between the ATBM and modified torso model. Note that stretch is unitless.

Mesh Refinement

An algorithm was developed to locally refine the flesh mesh at the site of impact. This approach was chosen, as opposed to remeshing the entire flesh, to minimize the computational cost required to run the simulations. This mesh refinement algorithm used a parametric mapping approach to map an idealized refined patch of flesh to the unrefined mesh topology at the site of impact (Figure 40). First, an unrefined patch of flesh, located at the impact location, was removed from the baseline, unrefined model. A parametric mapping function ($\phi(x, y, z)$) was defined between the nodes of the extracted patch and of an idealized, unrefined patch. Using a predefined topology map between the idealized, unrefined mesh and the idealized, refined mesh, the refined mesh was parametrically mapped back to the location of the extracted flesh patch. The mesh density and topology were selected such that the elements directly located within the impact site were uniform and sub-millimeter in characteristic length.

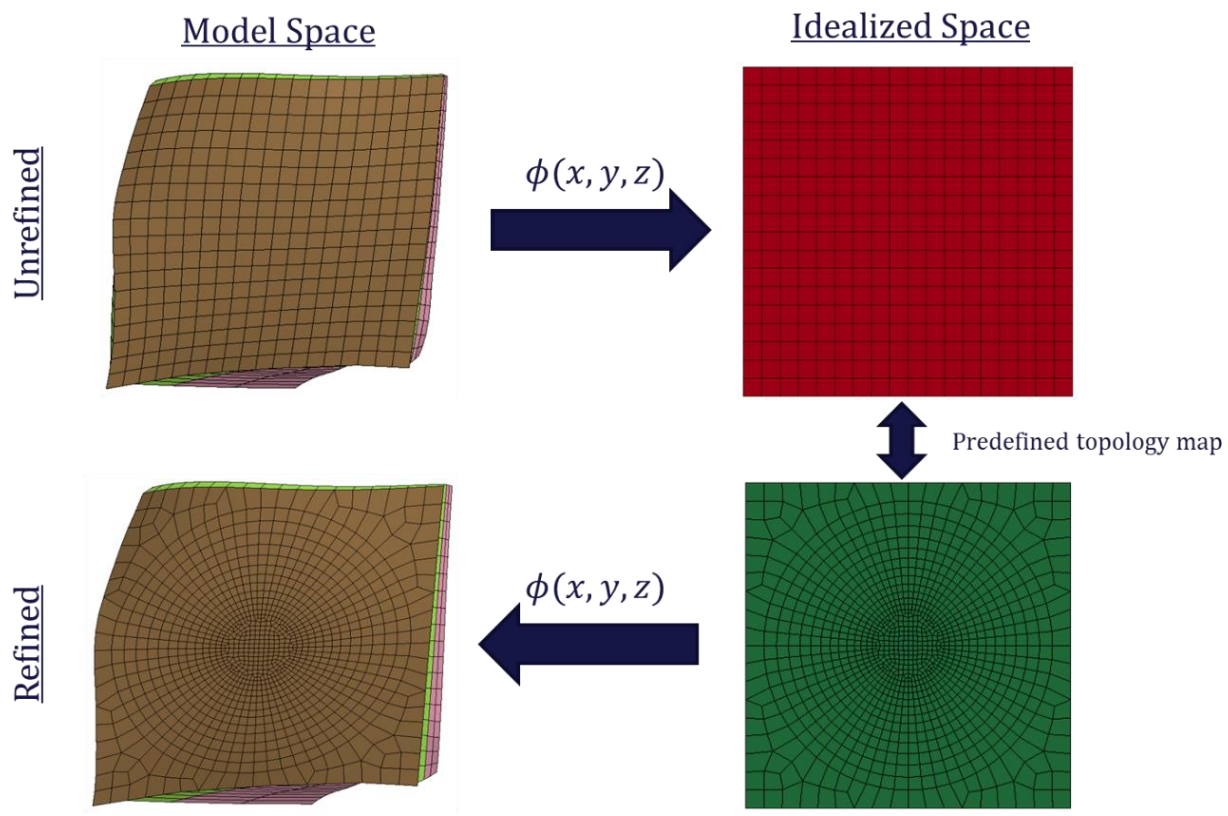


Figure 40. Overview of the parametric mesh refinement.

Boundary Conditions

Impactor Models

In this study, 6 impactor models, corresponding to the impactor geometries utilized in Aims 1 and 2, were developed (Figure 41). These included two impactor shapes (cylindrical and spherical) and three impactor diameters (0.50 in., 0.75 in., and 1.00 in.), with the cylindrical impactors having a 1/16 in. fillet to match those used in the experiments. All six impactors were developed to have consistent sectional densities (see Aim 1). All impactors, except the 1 in. sphere, were modeled as rigid aluminum parts, with a density of 2719 kg/m^3, Young's Modulus of 6.9x10^{10} Pa, and a Poisson's ratio of 0.39. The 1 in. sphere was manufactured from Delrin and modeled as a rigid Delrin part, with a density of 1370 kg/m^3, Young's Modulus of 3.2x10^9 Pa, and a Poisson's ratio of 0.35.

The static coefficient of friction defined in the contact between the aluminum impactors and skin parts was defined as 0.37. This was the average coefficient of friction between aluminum and skin (not including over the palm of the hand) measured and reported by Zhang and Mak (1999) [32].

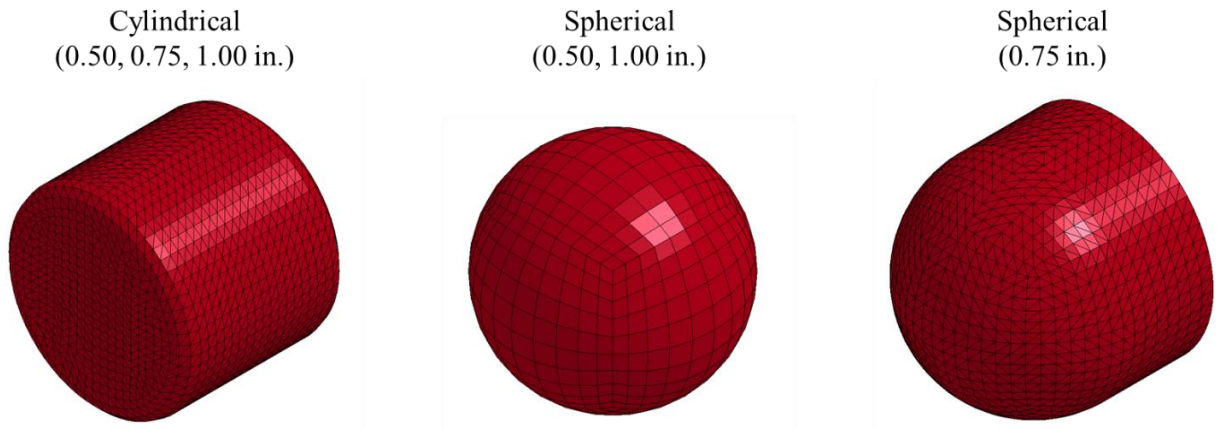


Figure 41. Impactor form factors.

Note the 0.75 in. spherical impactor had a different geometry than the 0.50 in. and 1.00 in. spherical impactors to preserve the required sectional density.

Impact Conditions

Simulations were conducted at the anatomical impact locations used and described in Aim 1. Due to model symmetry, only the right-sided impact locations were included in the simulations. For each of the PMHS tested in Aim 1, the impact locations were defined relative to the anatomical coordinate system and averaged across all six subjects. The same anatomical coordinate system was then defined in the ATBM v0.86 model and the nodes corresponding to the average impact locations were selected (Table LXIII). The locally refined meshes for each of these impact sites are shown in Figure 42.

Table LXIII. Impact locations, corresponding node ID in the unrefined ATBM v0.86 model, and the locations abbreviations.

Impact Location	Nodal ID	Location
Upper Chest	112626	UC-R
Abdomen	112951	AB-R
Upper Back	126042	UB-R
Lower Back	126023	LB-R

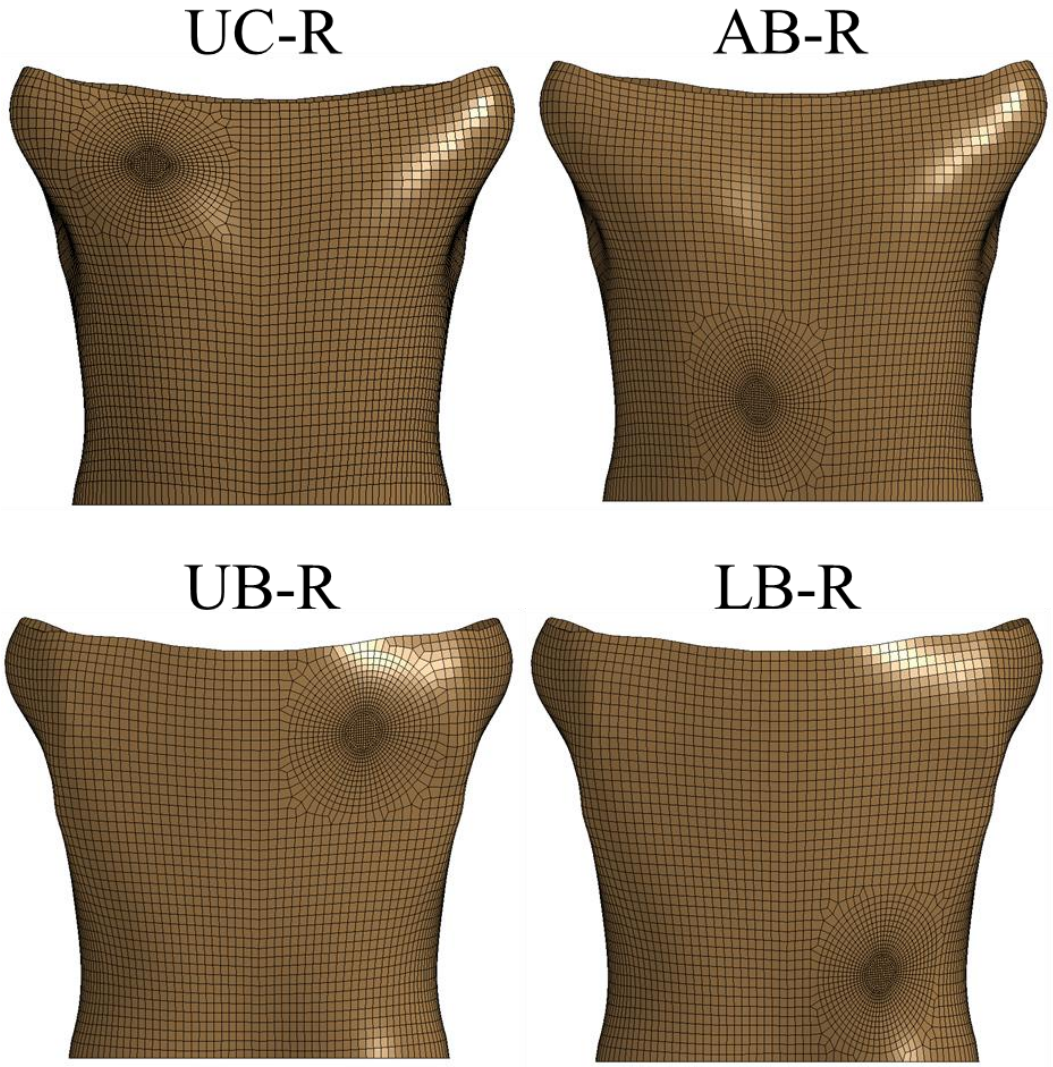


Figure 42. Locally refined flesh meshes for impact locations defined in Table LXIII.

Impact Velocities

For the UC-R, AB-R, UB-R, and LB-R impact locations, impact velocities corresponding to the 5, 25, 50, 75, and 95 percent risk of injury (determined from PMHS Model 1 developed in Aim 1) were simulated. These corresponded to 74.5, 102.1, 119.9, 136.0, and 156.6 m/s. Additional simulations were run at 50 and 200 m/s.

Parametric Study and Simulation Matrix

Parametric Study of Skin and Adipose Tissue Stiffness

In addition to the baseline material properties, which were fit to represent mean tissue responses, simulations were run with skin and adipose tissue material properties that were fit to represent material variation present in the population. For both the skin and adipose tissues, additional constitutive models

were implemented to represent the mean ± 1 standard deviation (SD). The upper bound (UB) and lower bound (LB) material models were derived from Kong et al., 2020 for the skin (Figure 43) and Sun et al., 2020 for the adipose tissue (Figure 44) [4, 25].

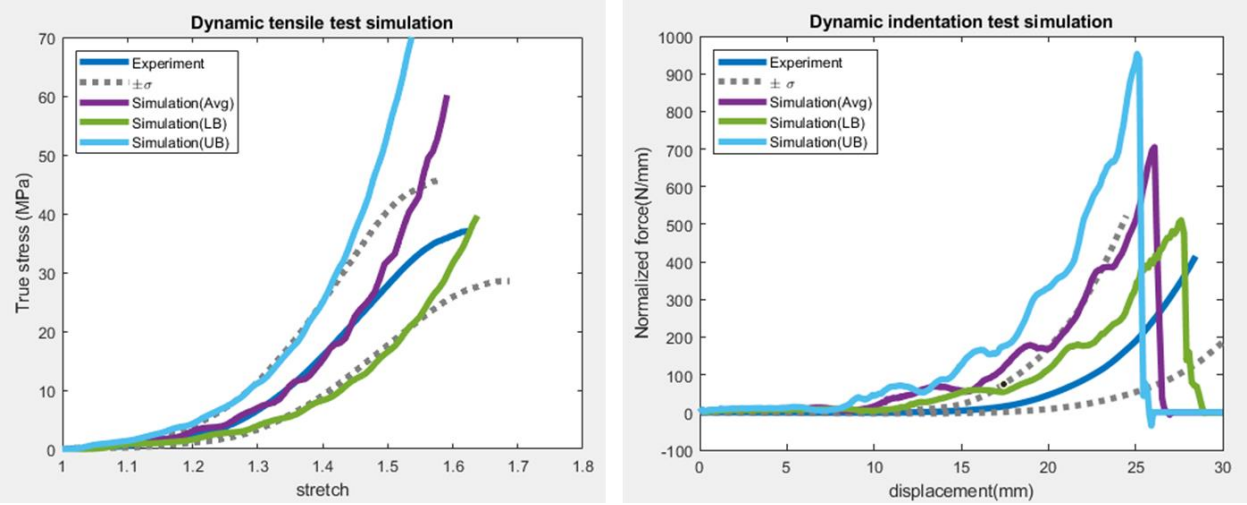


Figure 43. Material variation for the skin constitutive model.

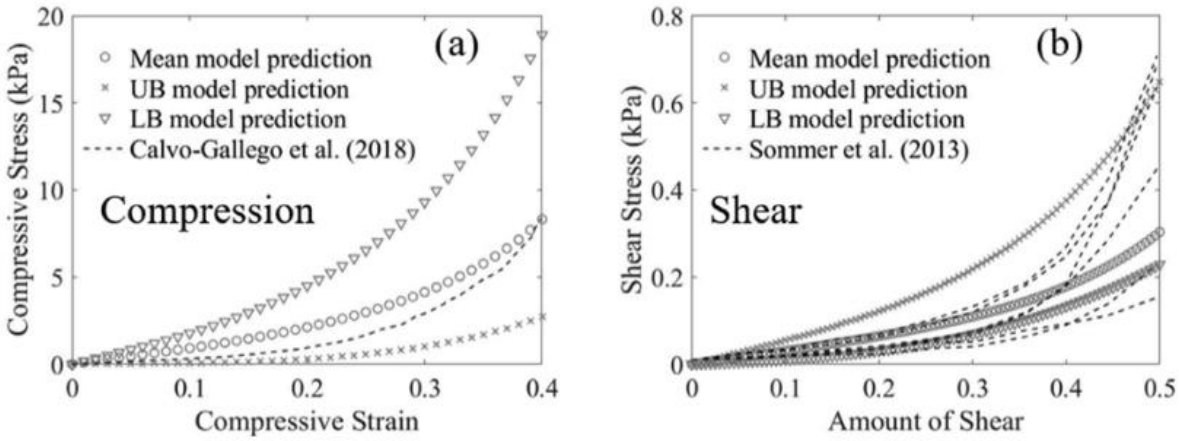


Figure 44. Material variation for the adipose tissue constitutive model (from Sun et al., 2020) [25].

Baseline (or Mean) Material Properties

A full-factorial design of experiments was used to explore the effects of the following factors on the skin deformation prediction:

- Impactor shape (N = 2)
  - Cylindrical or spherical
- Impactor diameter (N = 3)
  - 0.50 in., 0.75 in., or 1.00 in.
- Impact Location (N = 4)
  - Upper Chest (UC-R), Abdomen (AB-R), Upper Back (UB-R), or Lower Back (LB-R)

- Impact Velocities (N = 7)
    - 50.0, 74.5, 102.1, 119.9, 136.0, 156.6, and 200 m/s
- Skin material properties (N = 3)
    - Lower bound (mean – 1 SD), mean, and upper bound (mean + 1 SD)
- Adipose tissue material properties (N = 3)
    - Lower bound (mean – 1 SD), mean, and upper bound (mean + 1 SD)

A full-factorial design of experiment using these factors resulted in 1,512 (2x3x4x7x3x3) impact simulations. All simulations were run for 2 ms.

Simulation Post-Processing

In this work, skin deformation was quantified using maximum principal strain within a pre-defined "impact area". Specifically, the impact area was the central, circular, region of the refined mesh (Figure 45). As a metric for injury, the 95th percentile MPS (MPS-95; across elements and time) was used. To calculate MPS-95, the maximum MPS of each element across time was first determined. From the distribution of maximum MPS values across elements within the impact area, the 95th percentile value was determined (Figure 46).

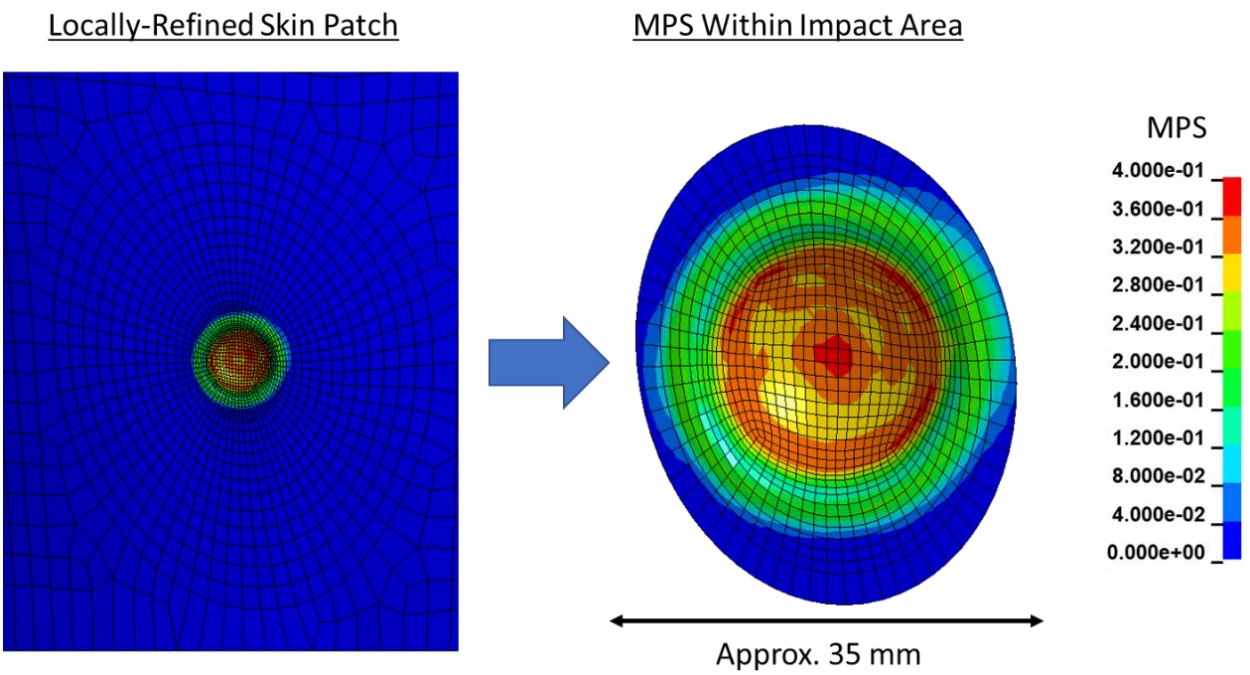


Figure 45. Impact area for computing the MPS for an impact simulation.

Note: the MPS fringe plot was nodally-averaged. This figure shows results from the 119.9 m/s impact to the AB-R impact site with the 0.75 in. sphere (t = 1.4e-4 s).

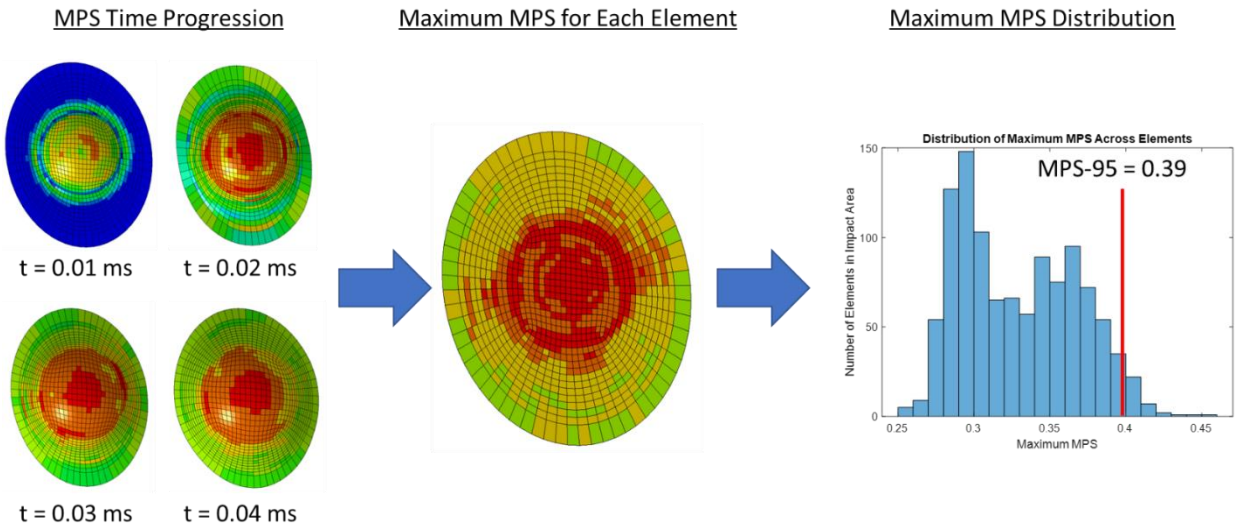


Figure 46: Process of calculating MPS-95 for an impact simulation.

For this simulation (AB-R, 119.9 m/s, 0.75 in. cylinder), the MPS-95 value was 0.39 and was indicated by the red line in the distribution shown on the right.

Statistical Meta-Modeling

Using the results from the large-scale parametric study, a statistical meta-model was developed to predict MPS-95 based on the following predictors: impact velocity (v_0), impactor diameter (d), skin stiffness (μ_{skin}; -1 to +1 SD, where 0 is mean), adipose tissue stiffness (μ_{adi}; -1 to +1 SD, where 0 is mean), the impactor shape (p, 0 for cylindrical, 1 for sphere), and impact location (loc, 0 for UC-R, 1 for AB-R, 2 for UB-R, and 3 for LB-R). The form of the meta-model is shown in Equation 9.

$$MPS_{95} = f(v_0, d, \mu_{skin}, \mu_{adi}, p, loc)$$

Equation 9: Form of the meta-model used to predict MPS-95.

For this aim, a quadratic response surface was fit (using the *fitlm* function in MATLAB) based on the predictors from each simulation case and the resulting MPS-95 values. This quadratic fit contained an intercept term, linear and squared terms for each predictor, and all products-of-pairs of distinct predictors. Simulations that error-terminated, and other outlier data points, were excluded from the meta-model fit.

Injury Risk Function Development

One objective of this aim was to develop an injury risk function that accounted for the variance in the predictors used to fit the meta-model, including population variance in flesh material properties. This was accomplished by using the meta-model to generate MPS-95 values and using the injury risk functions developed in Aim 1 to relate the meta-model predicted MPS-95 to penetration risk. Injury risk functions were developed for each of the four impact locations. The methods described below were used to develop each location-specific injury risk function.

The meta-model was used to determine MPS-95 for 100,000 cases. For each case, each of the predictors were sampled from a predefined distribution. For the skin and adipose tissue stiffnesses, normal

distributions ($\bar{x}$ = 0, σ = 0.33) were used to sample their material stiffnesses. For the impact velocity, impactor diameter, and impactor shape, uniform distributions were used to sample predictor values within the bounds used to construct the meta model. Since the impactor shape was either spherical or cylindrical, values sampled greater than 0.5 were classified as spherical and values lower than 0.5 were classified as cylindrical. The distributions used to sample the predictor variables are shown in Figure 47.

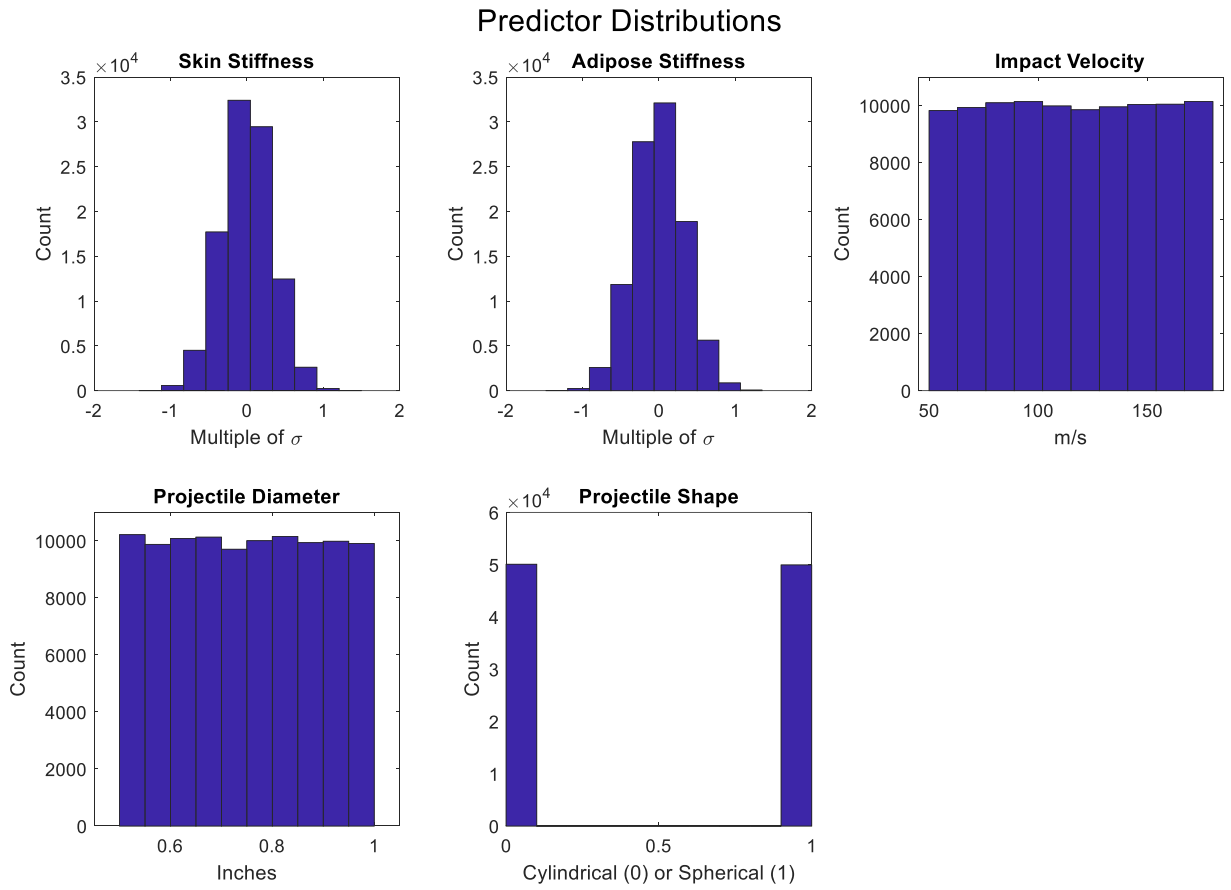


Figure 47: Predictor distributions (N = 100,000) for generation of injury risk function.

For each case, the injury risk was computed from the PMHS Model 1, which was developed in Aim 1. This model determined injury risk using impact velocity with skin thickness, impactor diameter, and impactor shape as covariates. Since skin was uniform in the torso model, the skin thickness was defined as 2 mm. The form and parameters for this injury risk function are shown in Aim 1 (Table XIII). As a result, the MPS-95 and injury risk were computed for each of the 100,000 cases simulated using the meta-model.

Since each injury risk was associated with a distribution of impact velocities (given variance in predictor variables), the 5th, 50th, and 95th percentile MPS-95 associated with each risk of injury was computed (Figure 48). For each of these, a Weibull cumulative density function was fit using the *nlinfit* function in MATLAB and evaluated over the range of MPS-95 values (0.2 – 0.5). These Weibull cumulative density functions represented the lower bound, median, and upper bound injury risk functions as a function of MPS-95, accounting for the variation in tissue mechanical properties and impactor geometry. In other words, the 5th percent injury risk function represents the most conservative measure of injury risk and the

95th percent injury risk function represents the least conservative measure. The form of the Weibull cumulative density function is shown in Equation 10, where λ and k are the scale and shape parameters, respectively.

$$MPS_{95} = 1 - e^{-\left(\frac{x}{\lambda}\right)^{k}}$$

Equation 10: Weibull cumulative density function for MPS-95.

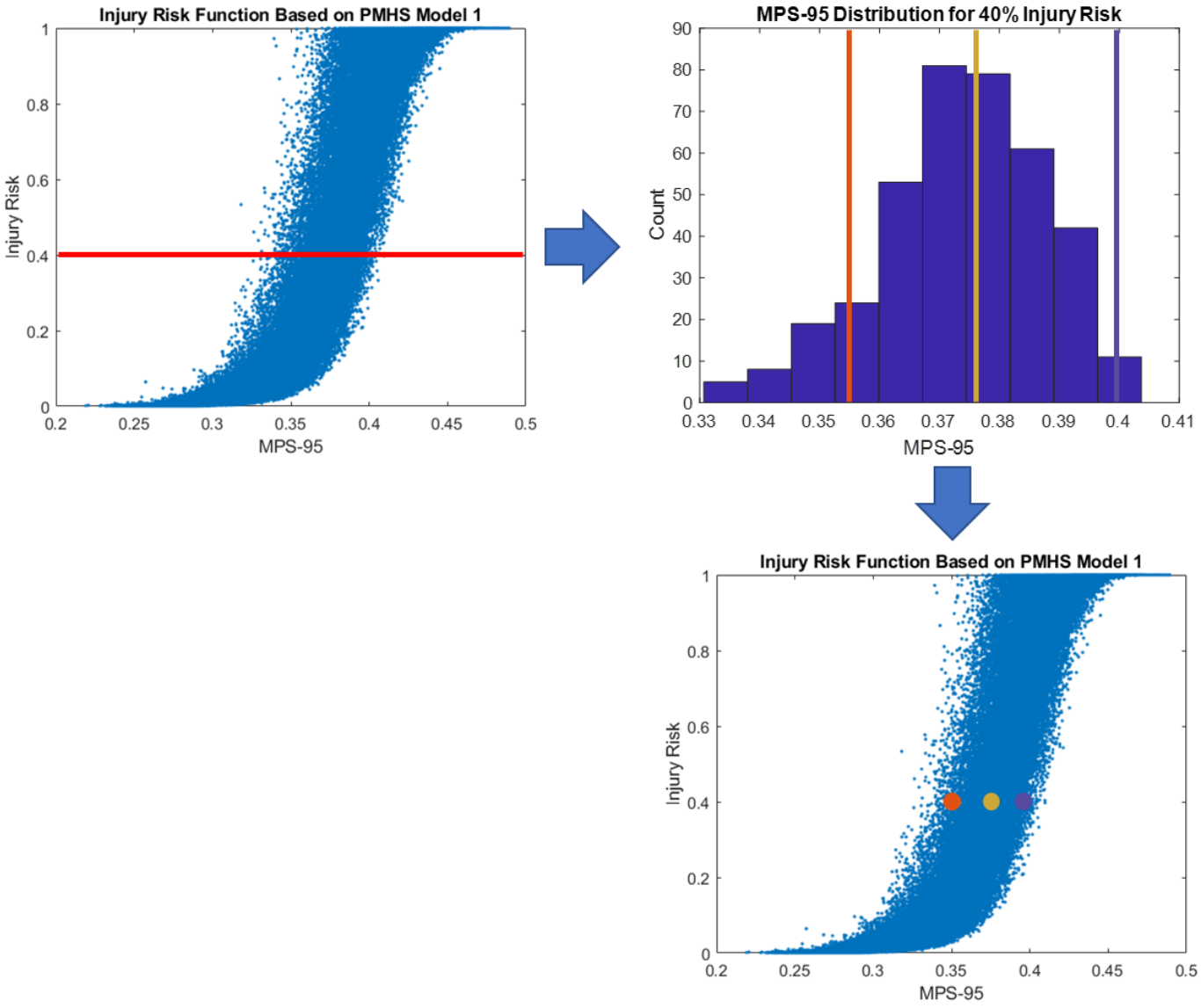


Figure 48: Calculation of 5th, 50th, and 95th percentile MPS-95 for each injury risk.

Results

Effect of Mesh Refinement

Local mesh refinement was implemented to improve the deformation response of the flesh parts, improve the spatial resolution in the simulated deformation fields, and decrease hourglass deformation modes in the adipose and muscle parts. The characteristic lengths of the elements in the locally refined mesh for the AB-R impact location are shown in Figure 49. At the impact area the characteristic lengths were approximately 0.4 – 1.0 mm, compared to 0.8 – 8.0 mm in the unrefined areas of the mesh. Figure 50 demonstrates the MPS distribution in a refined and unrefined model under a 119.9 m/s AB-R impact using the 0.75 in. spherical impactor. The difference in MPS-95 between coarse and locally refined models was 0.12 strain, with the unrefined model underpredicting MPS (0.39 in the refined model compared to 0.27 in the coarse model). In addition, the strain distributions were significantly different.

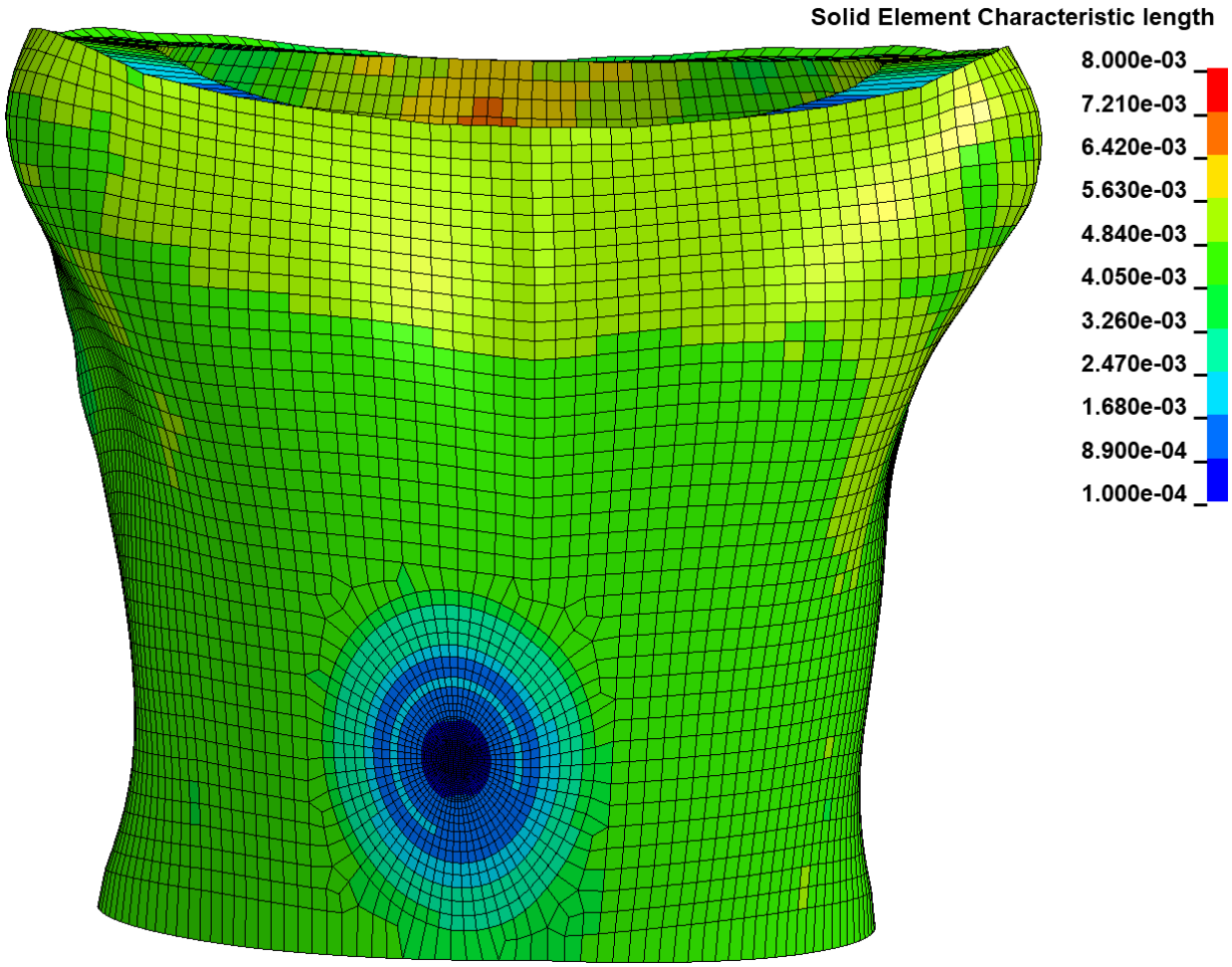


Figure 49: Characteristic length of the solid adipose layer elements in the locally-refined mesh for the AB-R impact location.

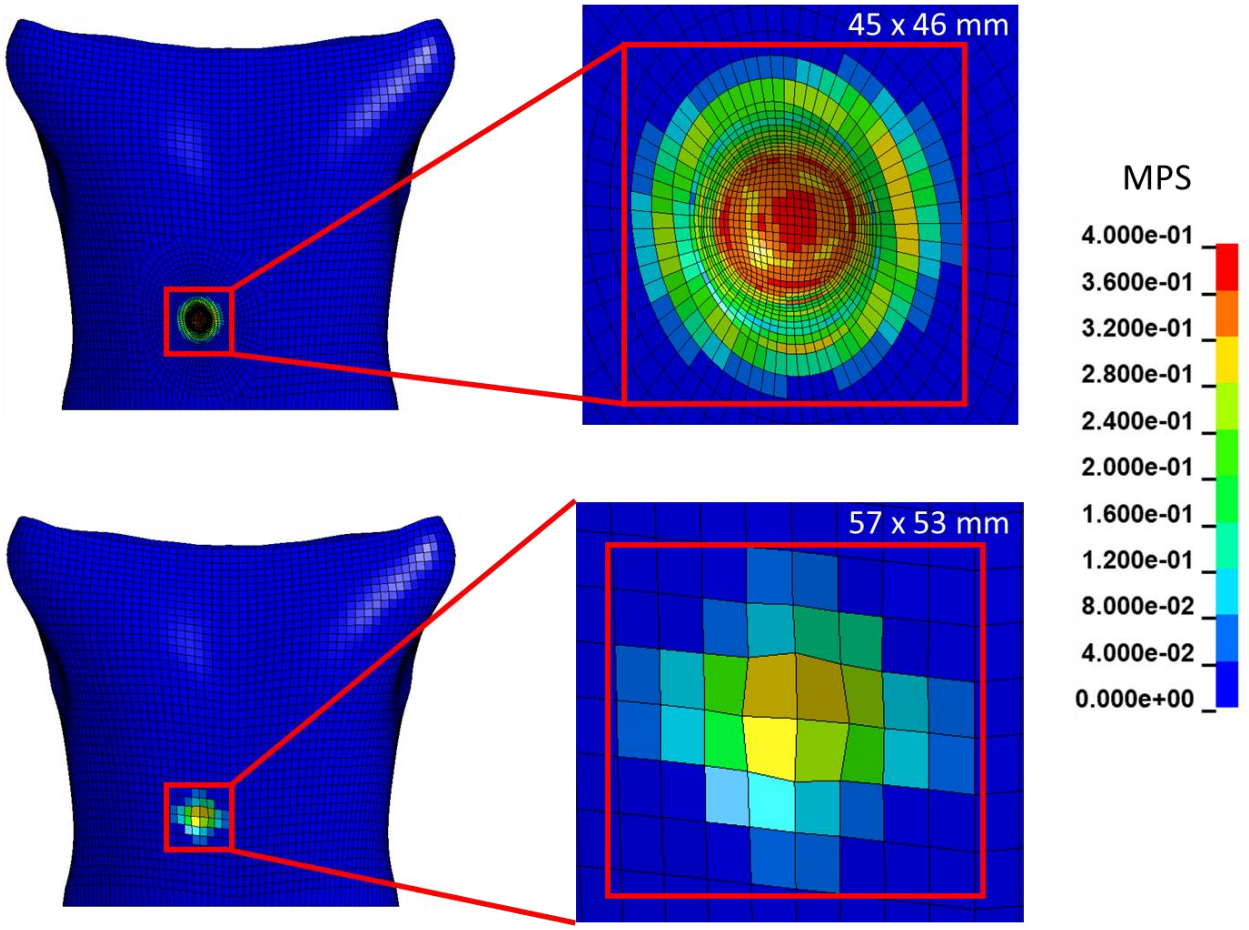


Figure 50: MPS prediction of the locally refined (top) and unrefined/coarse (bottom) models.

These simulations were run with the 0.75 in. spherical impactor at 119.9 m/s to the AB-R location. The MPS-95 in the refined and coarse models were 0.39 and 0.27, respectively.

Effect of Impactor and Impact Velocity

Figure 51 shows the relationship between the impact velocity and MPS-95 for the AB-R, UC-R, UB-R, and LB-R impact locations from simulations run with the mean skin and adipose tissue stiffnesses. In general, MPS-95 was consistent between the four impact locations. The only exception was for the 119.9, 136.0, and 156.6 m/s impacts with the 1.00 in. cylinder, where MPS-95 values at the UC-R impact location were greater than those in the other three impact locations. This was due to an interaction between the flesh and the underlying ribs caused by the large area of the 1.00 in. cylinder contact surface (Figure 53).

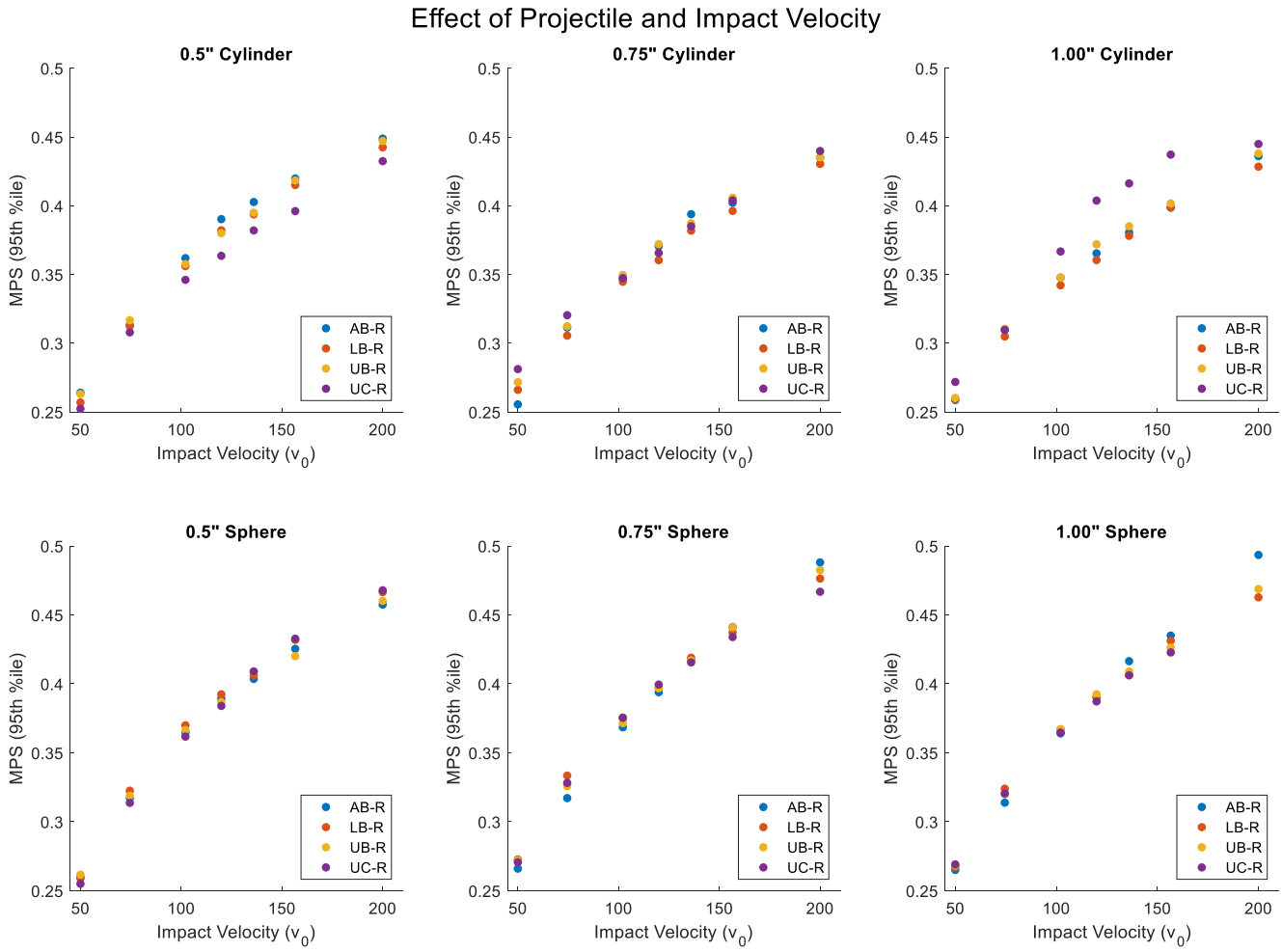


Figure 51: Effect of impact velocity and impactor geometry.
Impacts were conducted at the AB-R, UC-R, UB-R, and LB-R impact locations.

While MPS-95 values were generally consistent across the four impact locations (Table LXIV), there were some differences in the MPS distributions (Figure 52). For example, in the AB-R impact, the high strain region was located primarily at the center of the impact area, whereas in the UC-R impact, the high strain region was located inferior to the center of the impact area. In the AB-R impact location, the surface of the abdomen was approximately perpendicular to the line-of-flight of the impactor, whereas in the UC-R impact, the curvature of the surface resulted in an oblique impact between the impactor and skin. This obliqueness resulted in the impactor contacting the lower portion of the impact area first, resulting in the observed strain pattern. A similar effect was observed in the LB-R and UB-R impact locations.

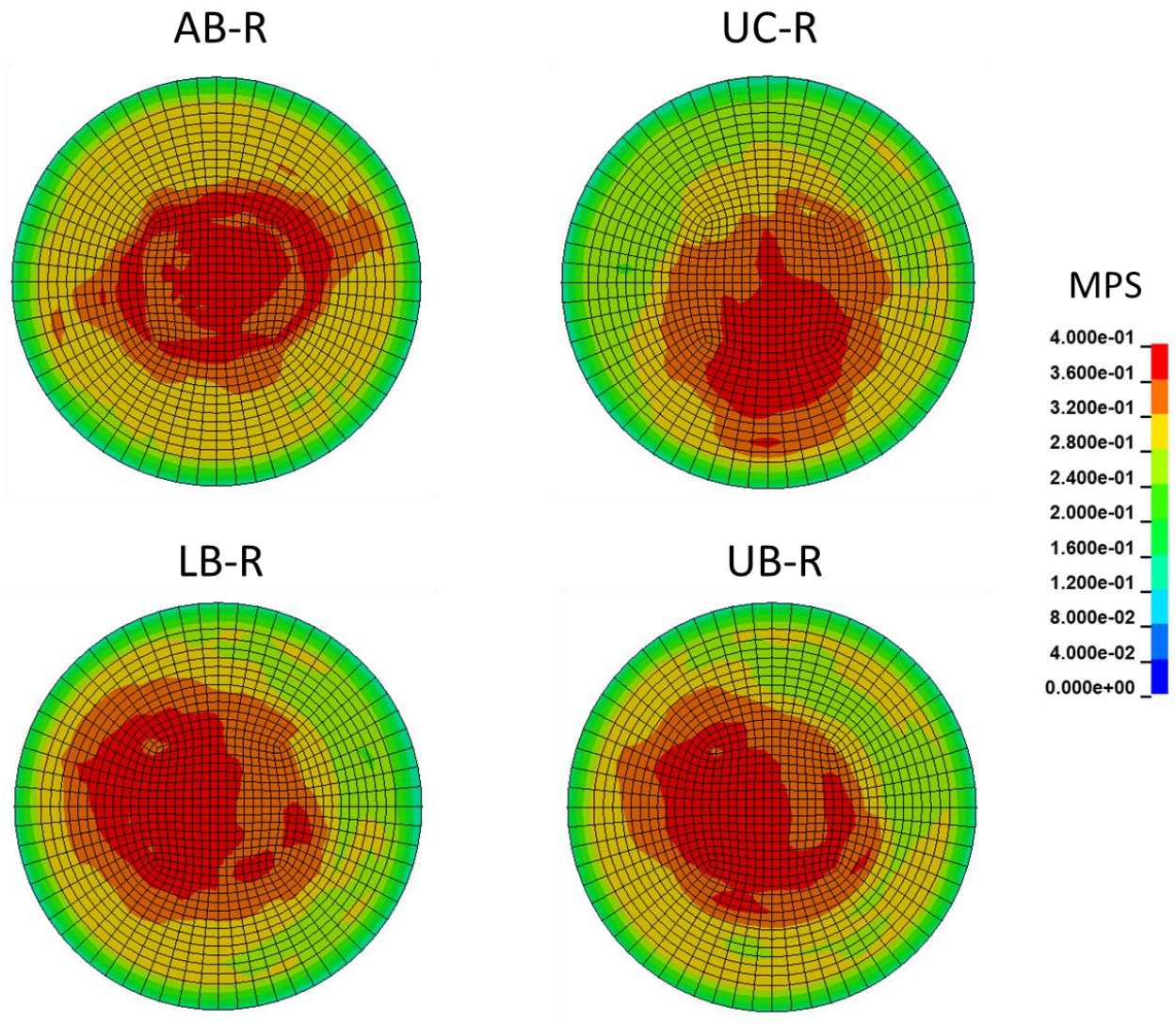


Figure 52: MPS distributions at each impact site.

Impacts were conducted at the AB-R, UC-R, LB-R, and UB-R impact locations using the 0.75 in. sphere at 119.9 m/s.

Table LXIV: MPS-95 results from the four impact locations using the 0.75 in. spherical impactor.

Impact Location	Impact Velocity (m/s)	Impactor	MPS-95
Abdomen (Right, AB-R)	119.9	0.75 in. Sphere	0.39
Upper Chest (UC-R)			0.40
Lower Back (LB-R)			0.40
Upper Back (UB-R)			0.40

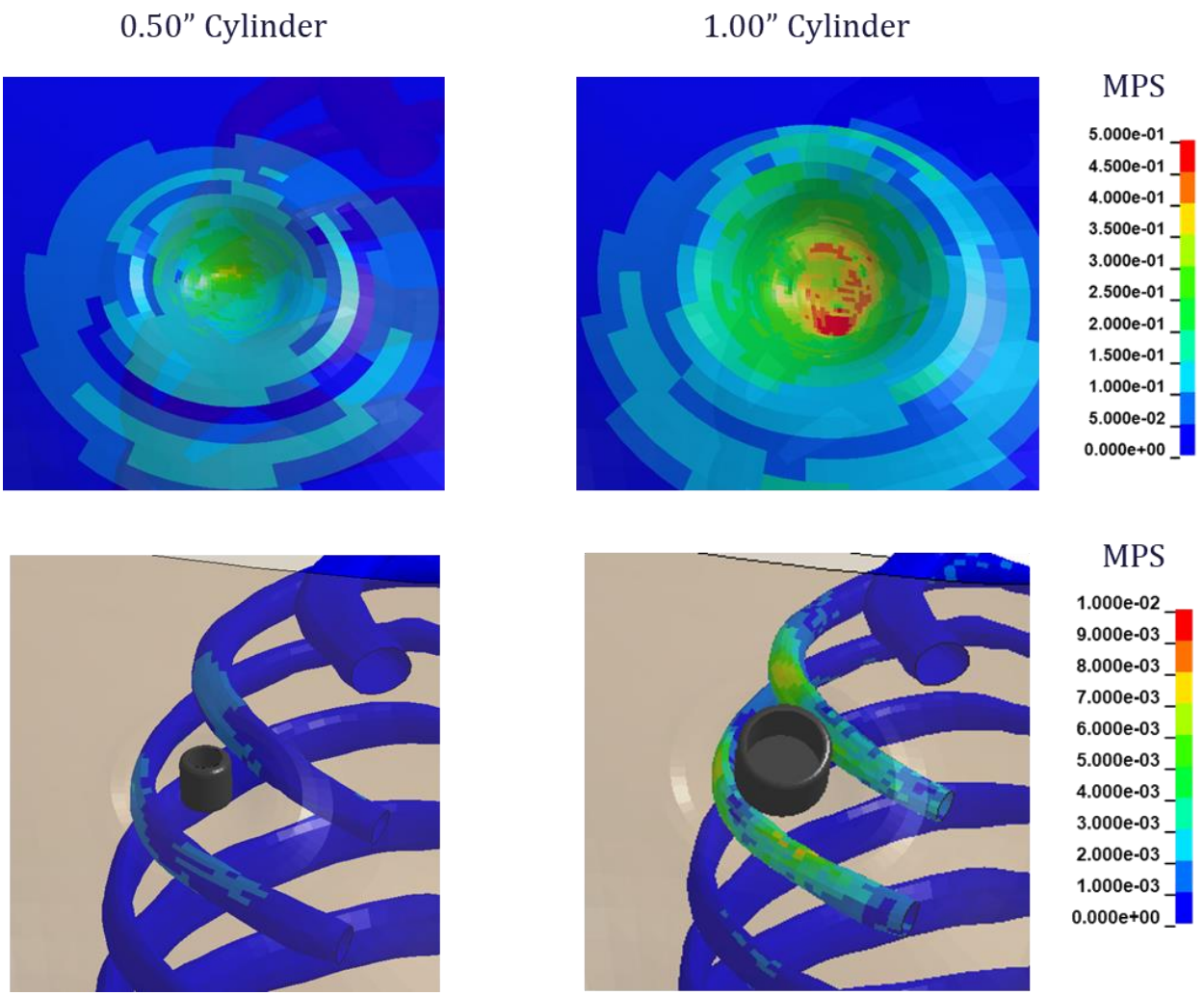


Figure 53: MPS of skin and rib using different impactor diameters.

Skin (top) and rib (bottom) MPS for the 119.9 m/s UC-R impact using the 0.50 in. (left) and 1.00 in. (right) impacts.

For all impact locations and impactor geometries, MPS-95 increased with impact velocity (Figure 54, Table LXV). The effect of impact velocity on the predicted MPS distribution is shown in Figure 54 for the AB-R impact using the 0.75 in. spherical impactor. For each of the impact velocities, the largest MPS values were located at the location of impact. As the impact velocity increased, the high strain region located at the impact site increased in MPS magnitude and in radius. For example, the 200 m/s impact had a very large high-strain region, occupying nearly the entire impact area, whereas in the 102 m/s, the high strain region was concentrated at the center of the impact area.

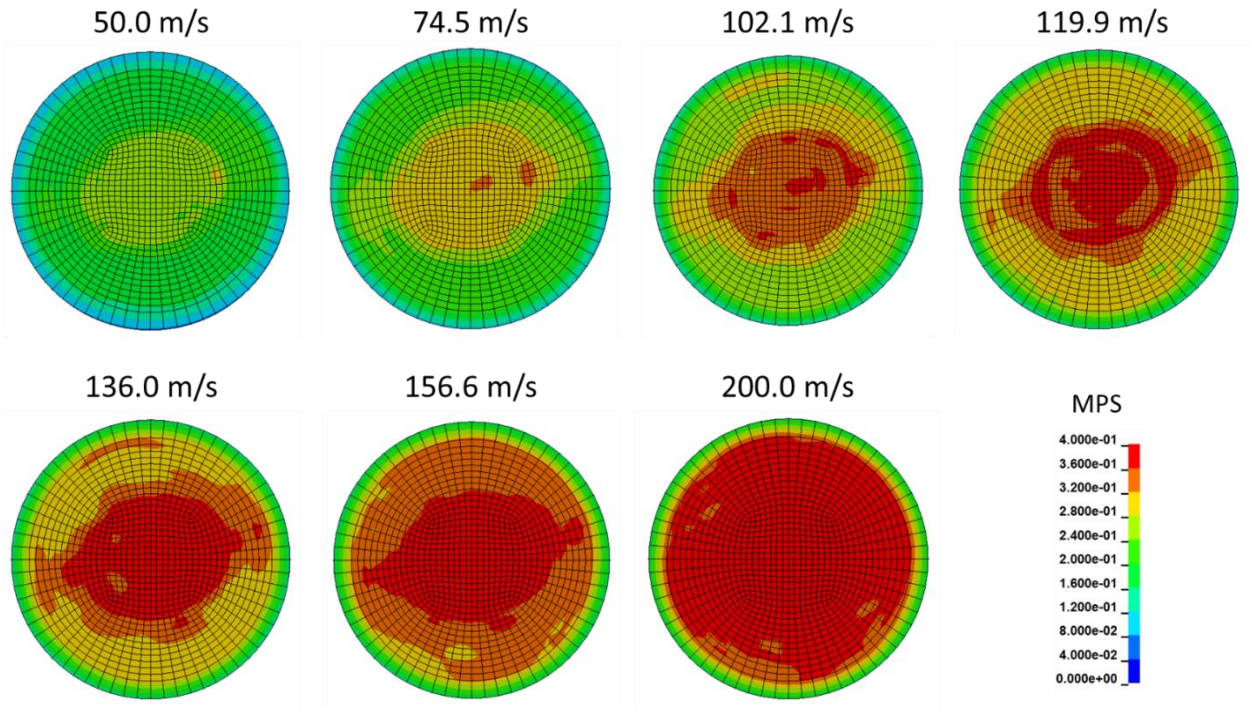


Figure 54: Effect of impact velocity on MPS distributions.
Impacts were conducted at the AB-R impacts using the 0.75 in. sphere impactor.

Table LXV: MPS-95 for the seven impact velocities simulated at the AB-R impact location.
Results are shown for the 0.75 in. sphere.

Impact Location	Impact Velocity (m/s)	Impactor	MPS-95
Abdomen (Right, AB-R)	50.0	0.75 in. Sphere	0.27
	74.5		0.32
	102.1		0.37
	119.9		0.39
	136.0		0.42
	156.6		0.44
	200.0		0.49

While MPS-95 values were similar for the six impactors (Table LXVI), the MPS distributions were impactor-dependent (Figure 55). For the spherical impactors, the largest strains were concentrated at the location of first contact. For the AB-R impact at 119 m/s shown in Figure 55, the location of first contact was near the center of the impact area. As the radius of the spherical impactor increased, the radius of the high strain region increased due to the larger contact surface of the impactor. Furthermore, a secondary strain concentration developed in the form of a ring, surrounding the primary central strain region. The cylindrical impactors resulted in strain concentrations primarily located around the perimeter of the

impactor. This was most evident for the 1.00 in. cylindrical impactor, where the MPS was large around the perimeter of the impact surface, but relatively low over the flat contact surface. This was also evident for the smaller (0.50 in. and 0.75 in.) impactors, however, these also resulted in some large MPS regions over the flat contact surface.

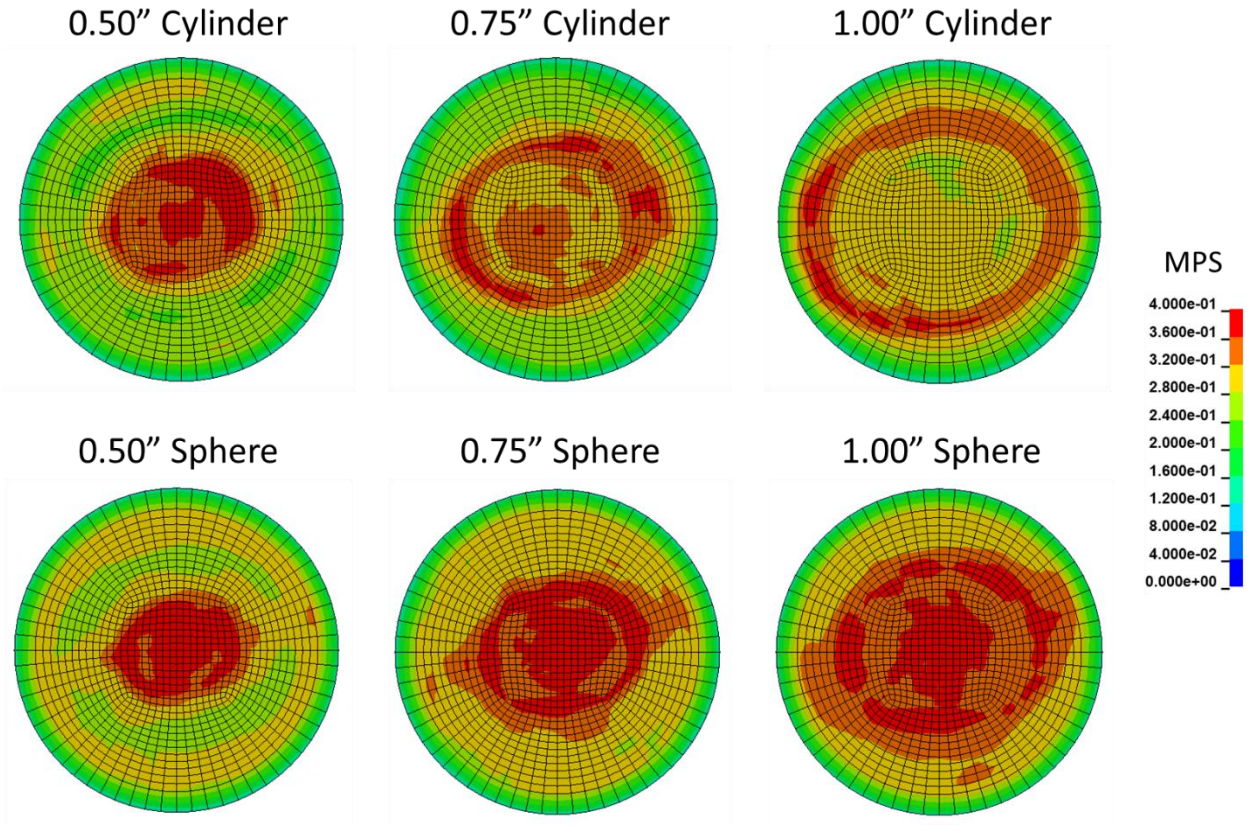


Figure 55: MPS distributions for the six impactor form factors.
Impacts were conducted at the AB-R impact location at 119.9 m/s.

Table LXVI: MPS-95 results for the six impactor form factors striking.
Impacts were conducted at the AB-R impact location at 119.9 m/s.

Impact Location	Impact Velocity (m/s)	Impactor	MPS-95
Abdomen (Right, AB-R)	119.9	0.50 in. Cylinder	0.39
		0.75 in. Cylinder	0.37
		1.00 in. Cylinder	0.37
		0.50 in. Sphere	0.39
		0.75 in. Sphere	0.39
		1.00 in. Sphere	0.39

These cylindrical projectile strain patterns were influenced by the friction between the impactor and skin surface. In general, as the contact friction increased, the MPS over the flat contact surface of the impactor decreased. While the contact friction influenced the resulting MPS distribution, changes in MPS-95 were negligible. Figure 56 shows the effect of the static coefficient of friction (varied between 0.1 – 0.9) on the MPS distributions and MPS-95 values for the 119.9 m/s AB-R impact using the 1.00 in. cylindrical impactor. Note that the baseline static coefficient of friction for the projectile-to-skin contact was defined as 0.37, which was obtained from experimental values reported in the literature by Zhang and Mak (1999) [32].

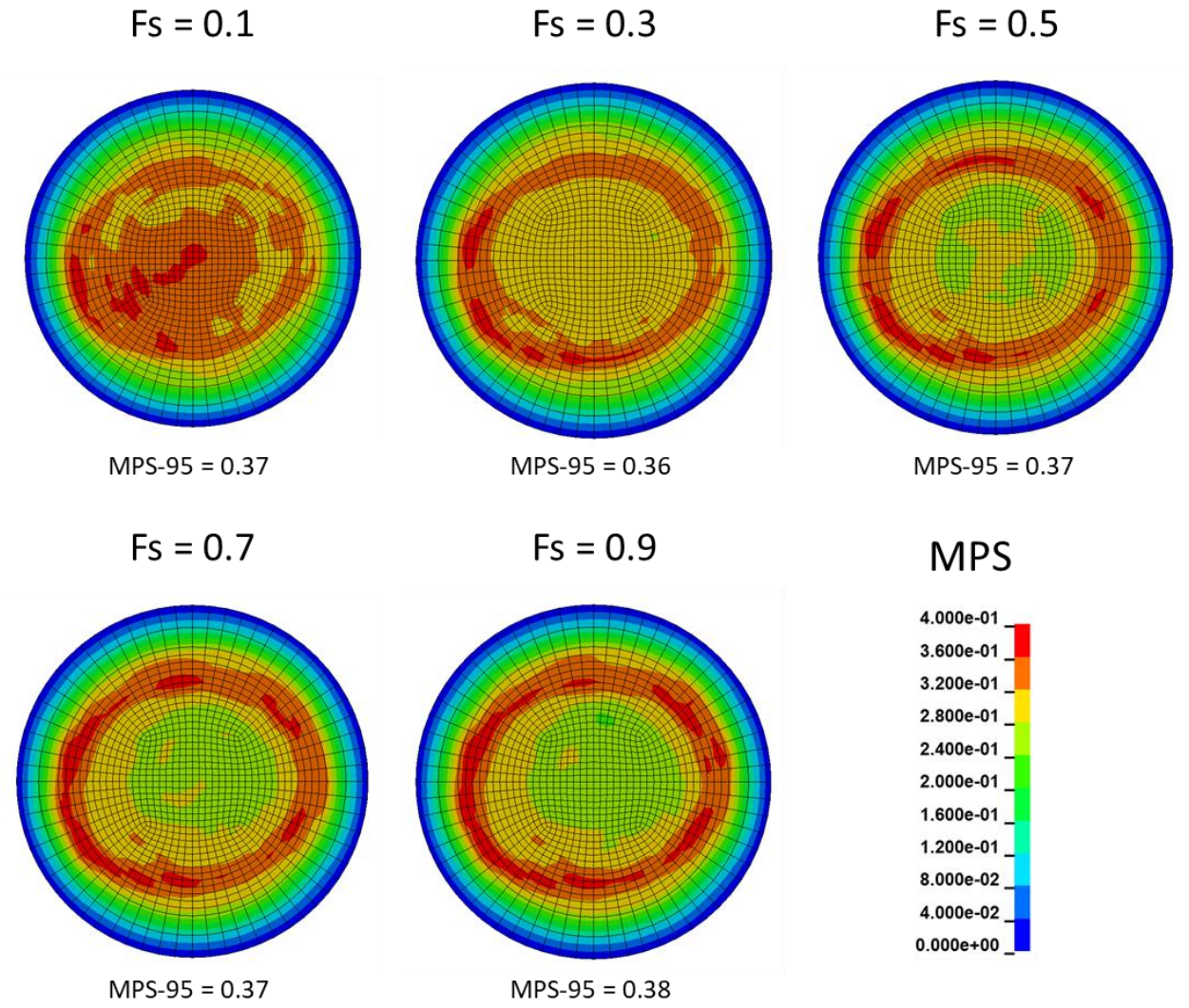


Figure 56: Effect of static coefficient of friction on MPS distribution and MPS-95.

Static coefficient of friction was defined between the aluminum impactor and skin. Results are shown for the 119.9 m/s impact to the AB-R impact location using the 1.00 in. cylindrical impactor.

Effect of Skin and Adipose Material Properties

While most (1475/1512 = 98%) simulations terminated normally, there were some cases that error-terminated (37/1512 = 2%). These were generally simulations that included the soft adipose tissue material, a large impactor (e.g., 1.00 in. sphere), and high impact velocity (v_0 > 119.9 m/s).

The effect of skin and adipose material properties for simulations that used the 1.00 in. cylinder at 156.6 m/s and for simulations that used the 0.75 in. sphere at 119.9 m/s are shown in Figure 57 and Figure 58, respectively. In general, MPS-95 was more sensitive to variations in skin stiffness than it was to adipose tissue stiffness. For example, in the 156.6 m/s impacts, using the 1.00 in. cylinder at the AB-R location, MPS-95 varied from 0.41 – 0.40 as adipose stiffness was varied from soft to stiff (keeping skin stiffness at the mean value) while MPS-95 varied from 0.42 – 0.35 as skin stiffness was varied from soft to stiff (keeping adipose stiffness at the mean value). While MPS-95 values varied slightly across impact locations, this trend was observed in all cases.

MPS distributions for these cases are shown in Figure 59 and Figure 60, respectively. Like the MPS-95 values, MPS distributions were sensitive to changes in skin material properties but not adipose material properties.

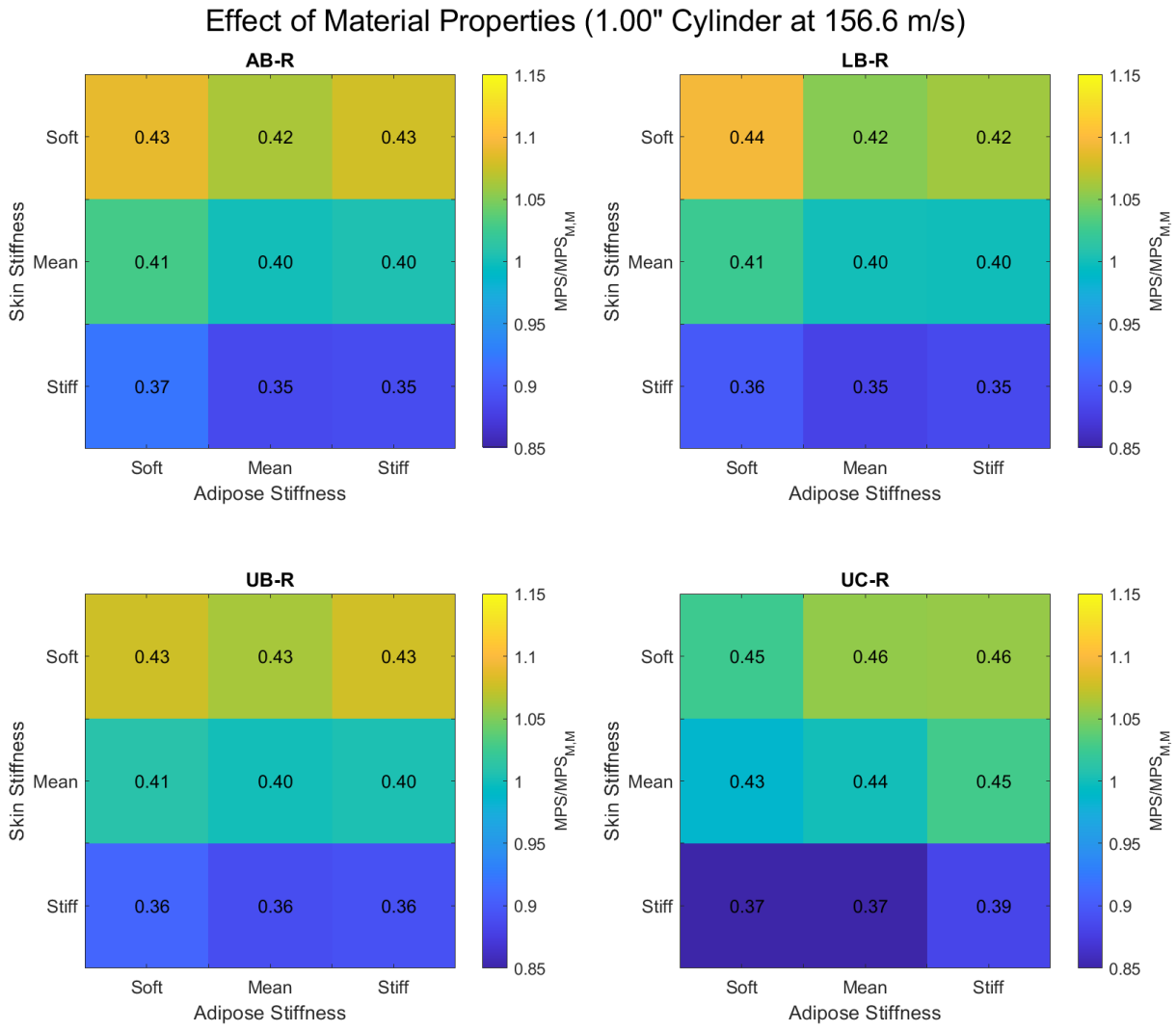


Figure 57: Effect of skin and adipose tissue stiffness for 156.6 m/s impacts using the 1.00 in. cylinder. The color plot indicates the relative MPS-95 of each condition (MPS-95 normalized by MPS-95 of the mean material properties simulation), and the overlaid values indicate MPS-95 for each condition.

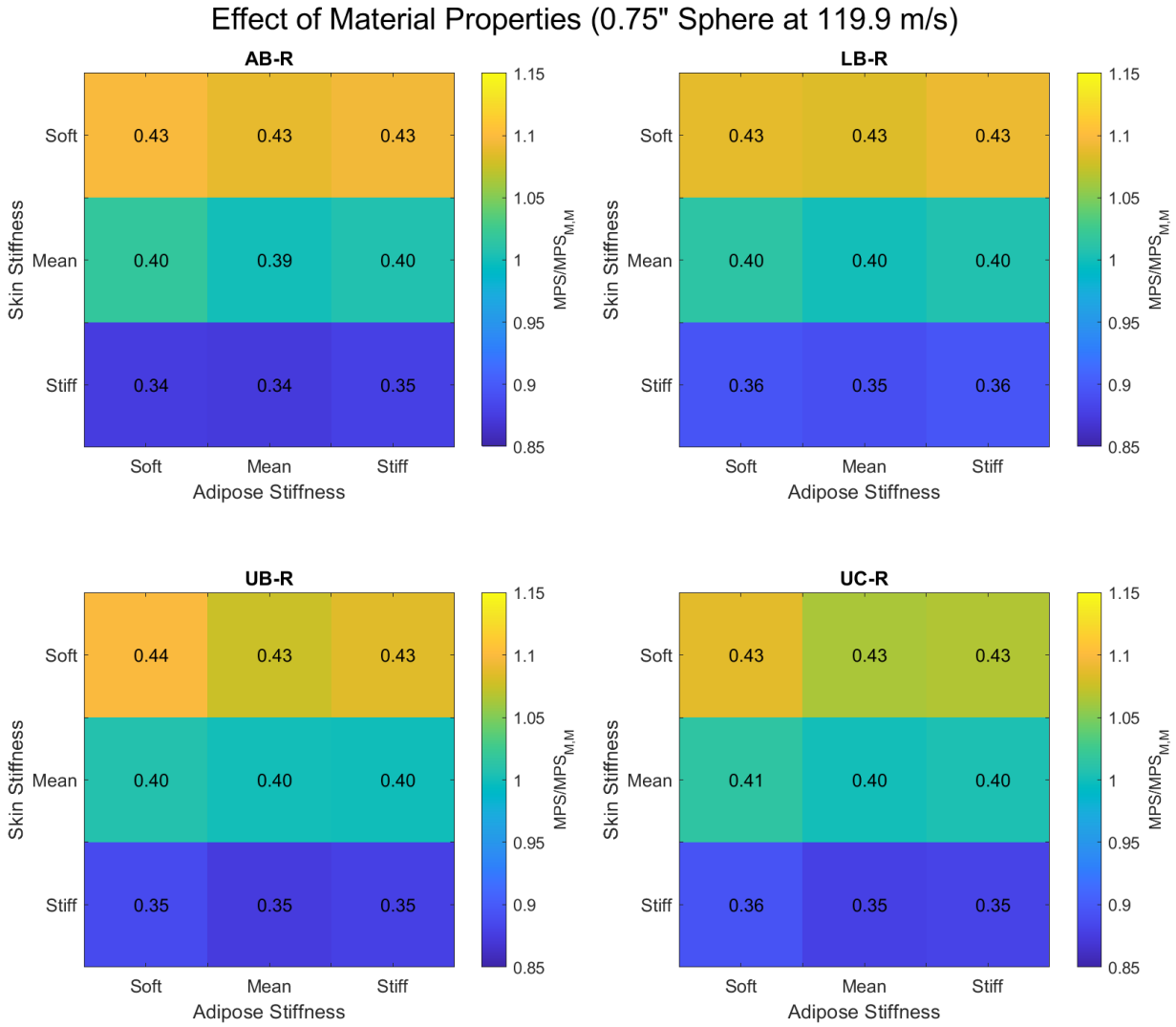


Figure 58: Effect of skin and adipose tissue stiffness for the 119.9 m/s impacts using the 0.75 in. sphere. The color plot indicates the relative MPS-95 of each condition (MPS-95 normalized by MPS-95 of the mean material properties simulation), and the overlaid values indicate MPS-95 for each condition.

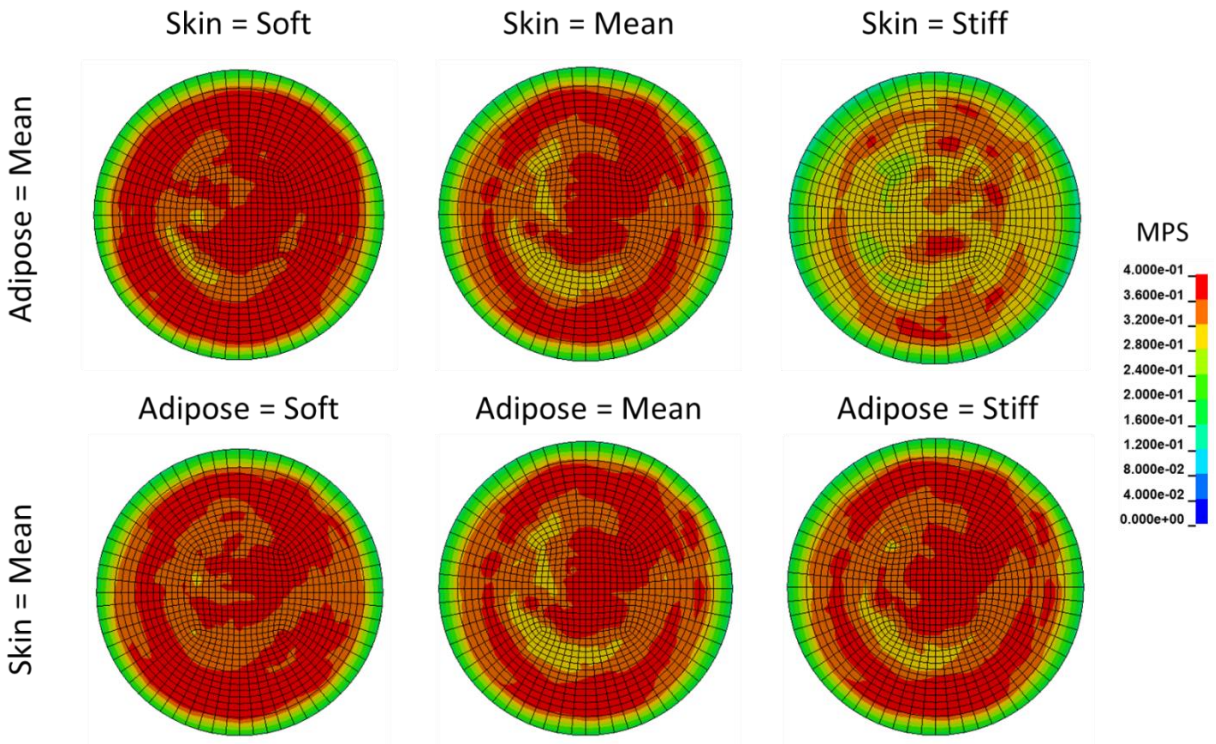


Figure 59: Effect of skin and adipose tissue stiffness on MPS distribution for the 156.6 m/s impacts using the 1.00 in. cylinder.

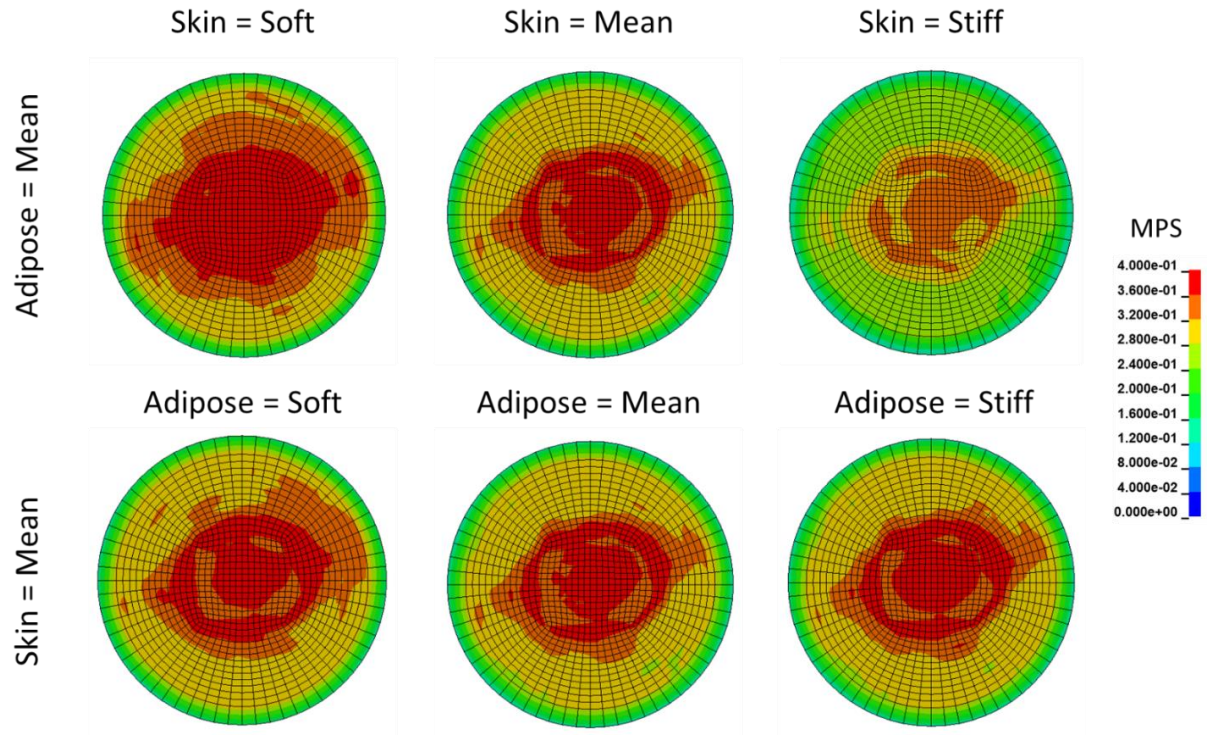


Figure 60: Effect of skin and adipose tissue stiffness on MPS distribution for the 119.9 m/s impacts using the 0.75 in. sphere.

Statistical Meta-Modeling

Excluding cases that error-terminated or were determined to be outliers, the meta-model was fit using the results from 1,433 simulations. Overall, the meta-model was capable of accurately predicting MPS-95. Comparing the meta-model predicted MPS-95 and the ground-truth data using linear regression, the R^2 value was 0.99, and the linear regression function had a slope of 0.99 and intercept of 0.003, indicating a near one-to-one linear relationship (Figure 61).

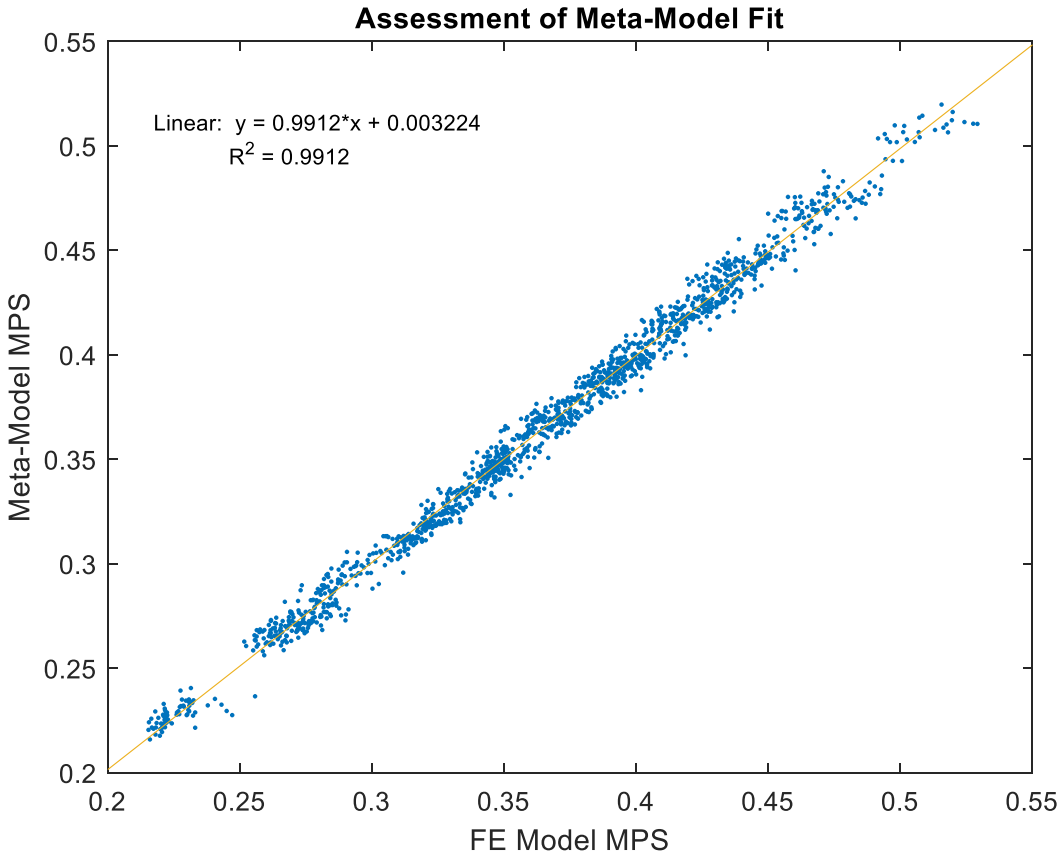


Figure 61: Assessment of meta-model fit.

Many of the relationships between the predictor variables and MPS-95 previously discussed were confirmed by the meta-model. Figure 62 shows a slice plot of the quadratic response surface. The two strongest predictors of MPS-95 were impact velocity and skin stiffness, with MPS-95 increasing nonlinearly with impact velocity and decreasing with increasing skin stiffness. Both impactor diameter and adipose tissue stiffness had minimal effect on MPS-95, whereas the shape of the impactor had a small effect, with spherical impactors resulting in slightly greater MPS-95 than cylindrical impactors (0.38 vs. 0.40).

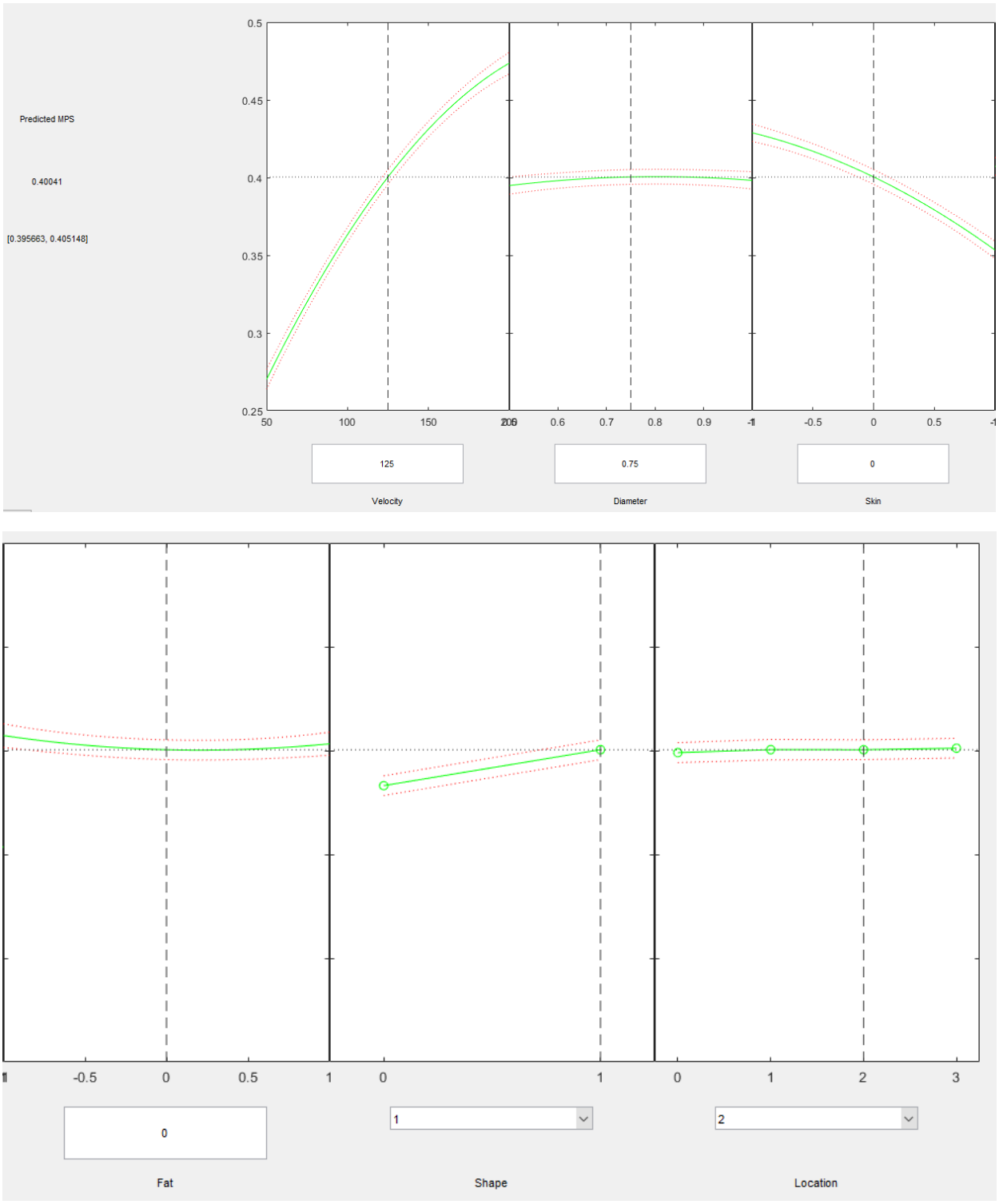


Figure 62: Slice plot of the fit meta-model.

The green lines indicate the predicted response, and the red lines indicate the 95% confidence intervals. Top) From left-to-right, the panels show the relationship between MPS-95 (on y-axis) and impact velocity, impactor diameter, and skin stiffness. Bottom) From left-to-right the panels show similar relationships for adipose tissue (fat) stiffness, and impactor shape (0 for cylindrical, 1 for spherical).

Injury Risk Function

The developed injury risk functions, representing lower bound, mean, and upper bound injury risk for each impact location are shown in Figure 63 - Figure 66. The variance in injury risk (i.e., between lower bound and upper bound) is attributed to the variance in tissue mechanical properties, which accounted for most of the response variance and variance in impactor design, which was relatively small. The lower bound curve represents the most conservative injury risk assessment, in which the MPS-95 was sustained under the most adverse conditions (e.g., soft skin and adipose tissue). Likewise, the upper bound curve represents the least conservative injury risk assessment, in which the MPS-95 was sustained under the least adverse conditions. For example, for a 50% chance of injury at the UC-R impact location, the lower bound, mean, and upper bound MPS-95 values are 0.371, 0.374, and 0.380, respectively (Table LXVIII). The parameters for each of the Weibull injury risk functions and associated injury risks are listed in Table LXVII - Table LXXIV.

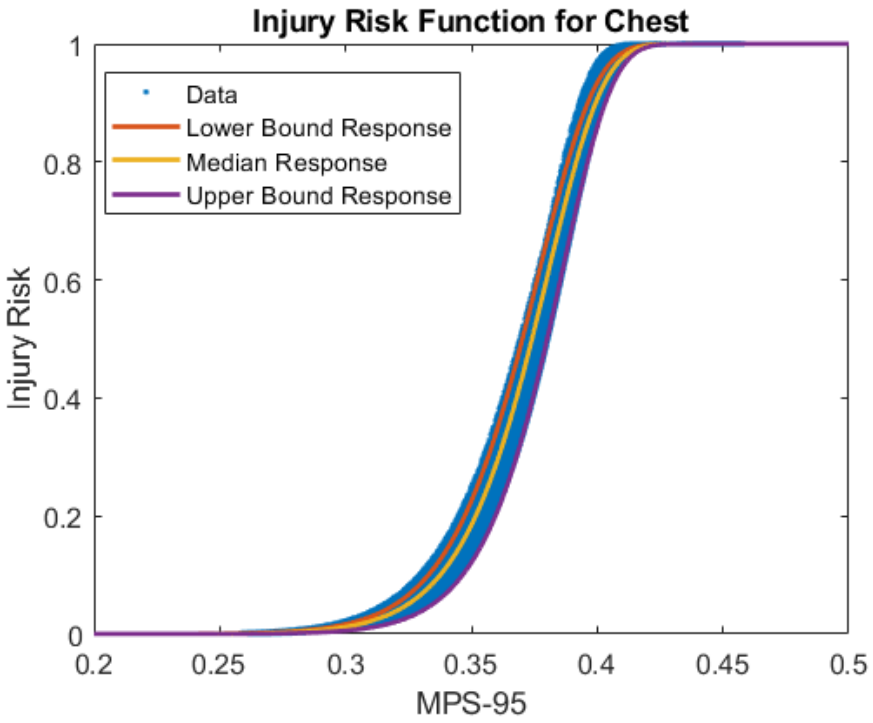


Figure 63: Lower bound, median, and upper bound injury risk function for the UC-R impact location. The bounds represent the variance in the predictor variables used to construct the meta-model.

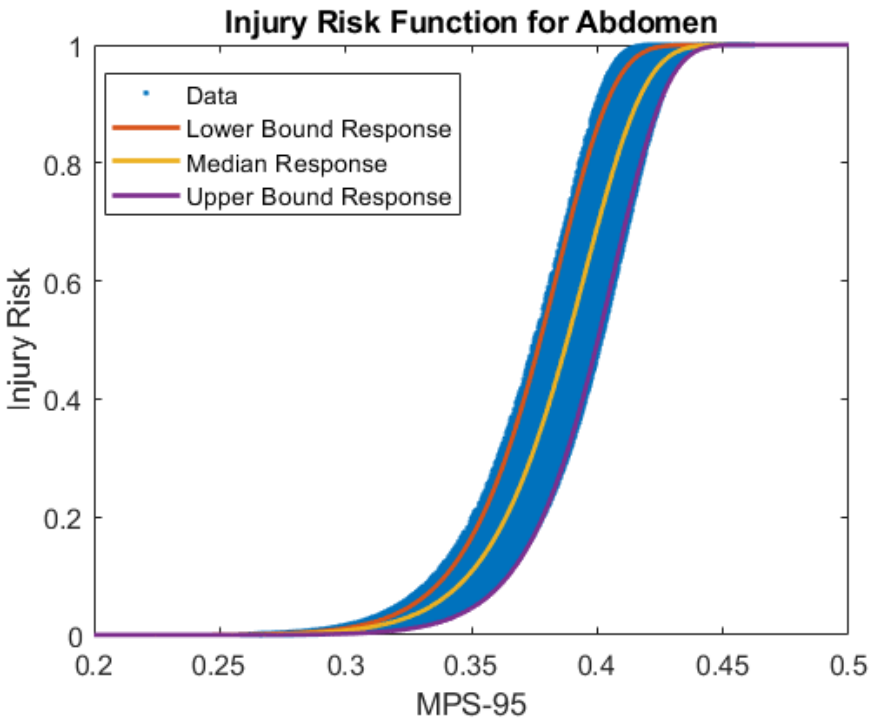


Figure 64: Lower bound, median, and upper bound injury risk function for the AB-R impact location. The bounds represent the variance in the predictor variables used to construct the meta-model.

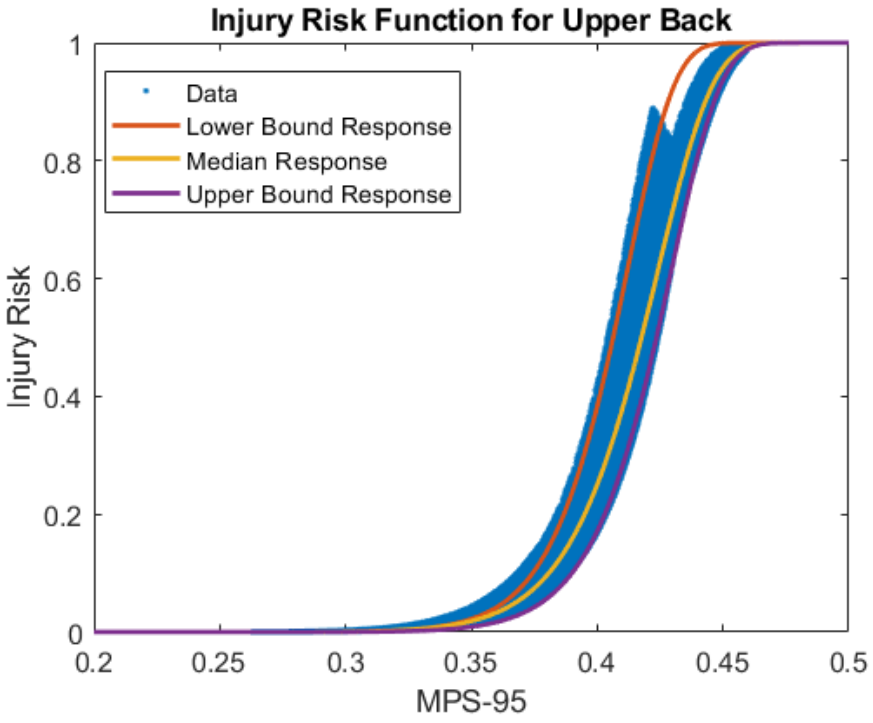


Figure 65: Lower bound, median, and upper bound injury risk function for the UB-R impact location. The bounds represent the variance in the predictor variables used to construct the meta-model.

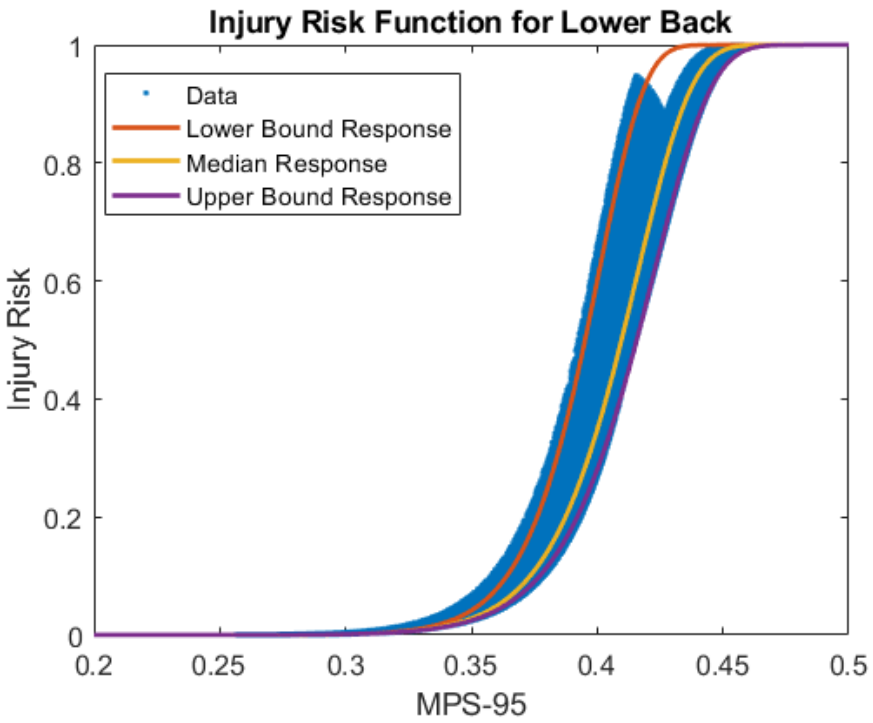


Figure 66: Lower bound, median, and upper bound injury risk function for the LB-R impact location. The bounds represent the variance in the predictor variables used to construct the meta-model.

Table LXVII: Weibull injury risk function parameters for UC-R location

Injury Risk Function	λ	k
Lower Bound (5th percentile)	0.378	17.678
Median (50th percentile)	0.382	18.287
Upper Bound (95th percentile)	0.387	20.338

Table LXVIII: Injury risk values for UC-R location

Injury Risk (%)	Lower Bound (MPS-95)	Median (MPS-95)	Upper Bound (MPS-95)
5	0.317	0.327	0.333
10	0.331	0.338	0.345
15	0.340	0.347	0.353
25	0.352	0.358	0.364
50	0.371	0.374	0.380
75	0.385	0.389	0.393

Table LXIX: Weibull injury risk function parameters for AB-R location

Injury Risk Function	λ	k
Lower Bound (5th percentile)	0.385	17.953
Median (50th percentile)	0.396	17.462
Upper Bound (95th percentile)	0.408	20.174

Table LXX: Injury risk values for AB-R location

Injury Risk (%)	Lower Bound (MPS-95)	Median (MPS-95)	Upper Bound (MPS-95)
5	0.324	0.332	0.348
10	0.338	0.347	0.363
15	0.347	0.356	0.371
25	0.359	0.369	0.383
50	0.377	0.389	0.401
75	0.392	0.404	0.414

Table LXXI: Weibull injury risk function parameters for UB-R location

Injury Risk Function	λ	k
Lower Bound (5th percentile)	0.413	22.782
Median (50th percentile)	0.425	20.273
Upper Bound (95th percentile)	0.430	22.836

Table LXXII: Injury risk values for UB-R location

Injury Risk (%)	Lower Bound (MPS-95)	Median (MPS-95)	Upper Bound (MPS-95)
5	0.355	0.362	0.375
10	0.370	0.378	0.389
15	0.379	0.387	0.397
25	0.390	0.400	0.408
50	0.407	0.419	0.424
75	0.418	0.431	0.436

Table LXXIII: Weibull injury risk function parameters for LB-R location

Injury Risk Function	λ	k
Lower Bound (5th percentile)	0.402	22.921
Median (50th percentile)	0.417	20.485
Upper Bound (95th percentile)	0.424	19.340

Table LXXIV: Injury risk values for LB-R location

Injury Risk (%)	Lower Bound (MPS-95)	Median (MPS-95)	Upper Bound (MPS-95)
5	0.347	0.355	0.364
10	0.361	0.371	0.378
15	0.369	0.380	0.387
25	0.379	0.392	0.398
50	0.396	0.410	0.415
75	0.407	0.423	0.431

To demonstrate the relative contribution of tissue properties and impactor design on MPS-95 variance, the meta-model was reevaluated (N = 100,000) without considering variation in tissue mechanical properties, predicting the MPS-95 responses using the mean skin and adipose tissue stiffnesses. Therefore, this second set of MPS-95 values represented the variation in impactor design only, within the bounds of the predictor variables. Figure 67 shows the injury risk for 100,000 meta-model simulations when accounting for both variation in tissue mechanical properties and impactor design (blue) and when accounting for only variation in impactor design (orange). It is clear from this analysis that most of the variation in the MPS-95 response is attributed to variation in tissue mechanical properties.

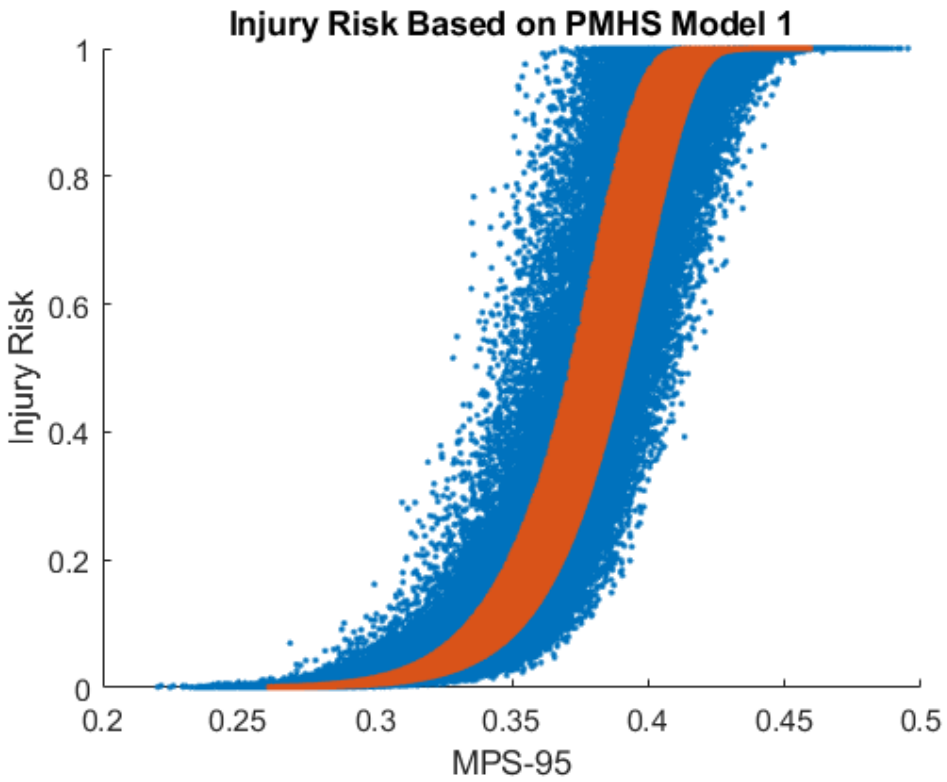


Figure 67: Injury risk variation when considering variation in both tissue mechanical properties and impactor design (blue) and considering variation in only impactor design (orange).

Conclusions

In this aim, the ATBM v0.86 torso model was updated to improve the flesh response performance under high-rate, blunt impact. These improvements included updating the skin, adipose, and muscle responses and were necessary since the baseline ATBM v0.86 was not suitable for penetration risk assessment from blunt impact. In the updated model, these materials were modeled using an Ogden quasi-linear viscoelastic constitutive model. For each of the tissue parts, the parameters were tuned to match experimental material and component-level experimental data. For all three parts, the original materials implemented in the ATBM v0.86 model were overly stiff, and the updated materials provided more biofidelic tissue responses (Figure 39).

In addition to the material updates, an automated algorithm for locally refining the mesh at the site of impact was implemented. This improved mesh quality and reduced element size at the site of impact (Figure 49), improved the spatial resolution of the simulated deformation response (Figure 50) and reduced hourglass deformation modes. Mesh refinement was performed only at the impact site to minimize the computational cost associated with running the impact simulations. Overall, the local mesh refinement increased computational cost by approximately 30% (30 vs. 22 minutes simulation time) and had a significant effect on the predicted MPS-95 values. Compared to the unrefined simulation (AB-R at 119.9 m/s with 0.75 in. sphere), the refined mesh predicted an MPS-95 value that was greater by 0.12 strain (0.39 vs. 0.27). The difference in deformation patterns between the refined and unrefined meshes was also noteworthy. In the unrefined simulation, the deformation pattern resembled a cross, with the

largest strains occurring at the impact location. While the largest strains also occurred at the impact location in the refined mesh simulation, the deformation pattern was circular and included high strain regions at the periphery of the impactor.

In this Aim, impacts were simulated to four different impact locations (AB-R, UC-R, UB-R, and LB-R) which were selected to correspond to the impact locations used to construct the injury risk functions in Aim 1. Since the torso model was symmetric, only the right-sided impacts were simulated, assuming that the left-sided deformation response would be identical. Impacts were simulated using the six impactor shapes used in Aim 1. These included spherical and cylindrical impactors with diameters of 0.5, 0.75, and 1.0 inches. All impactors were developed such that the sectional density was consistent for each impactor. Further details regarding these impactors are provided in Aim 1. Finally, simulations were run using 5 impact velocities, which corresponded to 5, 25, 50, 75, and 95% risk of skin penetration injury, determined from PMHS Model 1 developed in Aim 1 (74.5, 102.1, 119.9, 136.0, 156.6 m/s). Two additional impact velocities (50 and 200 m/s) were also included, for a total of seven impact velocities.

Overall, MPS-95 was consistent across the four impact locations, except for the 119.9, 136.0, and 156.6 m/s impacts at the UC-R impact location using the 1.00 in. cylinder (Figure 51). This was due to an interaction between the flesh and the underlying ribs caused by the large diameter of the 1.00 in. cylindrical impactor (Figure 53). This suggests that MPS may increase in areas where flesh-bone interactions are significant; however, more simulations are required to explore this phenomenon. Despite the similarity in MPS-95, there were some differences in MPS distributions related to the curvature of the flesh surface at the site of impact. In general, MPS was greatest in the areas that first contacted the impactor. For example, in the UC-R impact location the largest MPS occurred in the inferior portion of the impact area. This was a result of the flesh surface having an oblique angle with respect to the incident velocity vector of the impactor. In the torso model, skin was assumed to have uniform thickness throughout all body regions and was defined to be approximately the average skin thickness throughout the torso model. Since skin thickness is known to vary in different body regions and was shown to be a significant injury risk function covariate in Aim 1, it is possible that greater differences in MPS-95 and deformation patterns would be observed in a model that incorporated region-dependent skin thickness variation.

As impact velocity increased, the MPS-95 also increased. While the relationship between MPS-95 and initial velocity between 102.1 – 156.6 m/s was relatively linear, the simulations at 50.0, 74.5, and 200.0 m/s introduced some nonlinearity in this relationship. At lower velocities, MPS-95 increased at a higher rate, whereas at faster velocities, the MPS-95 response began to plateau (Figure 51). However, more simulations are required to explore the MPS-velocity relationship at slower and faster velocities. The MPS distributions were also affected by impact velocity, with faster impact velocities resulting in a larger high strain area. For example, in the AB-R impact location, the radius of the high strain region increased as impact velocity increased. However, given that deformation propagates through the tissue with time, it is likely that any skin failure associated with these impacts would be similar. For example, if skin failure occurred in the 119.9 m/s impact, it would be expected that the skin would also rupture in the 156.6 m/s with a similar failure pattern. However, skin failure was not assessed in these simulations and further simulations enabling element erosion would be required to investigate this hypothesis.

While MPS-95 values were similar for the six impactors (0.37 – 0.39 for the six impactors in the AB-R impact location at 119.9 m/s), the MPS distributions were dependent on the shape of the impactor (Figure

55). For the spherical impactors, MPS was generally concentrated at the location of first contact. For the 0.75 in. and 1.00 in. spherical impactors, additional strain concentrations were located at the periphery of the impactor. As the diameter of the impactor increased, the diameter of these high strain regions also increased, due to the larger contact surface of the impactor. While similar in magnitude, the cylindrical impactors resulted in MPS concentrations primarily located around the periphery of the impactor, where the impact surface joined the body of the impactor. For example, in the 1.00 in. cylindrical impactor, MPS was large at the periphery of the impactor's impact surface, but relatively low over the flat impact surface. In general, these strain distributions were consistent with, and resembled, the semicircular-outline skin rupture patterns observed in the experiments in Aims 1 and 2. The static coefficient of friction defined in the contact between the skin and impactor was also found to affect the MPS distribution, particularly for the rigid cylindrical impactors. While friction was defined based on experimental measurements of skin-to-aluminum friction coefficients, it is possible that other impactors using lower friction materials (e.g., Teflon, Nylon) may result in altered skin deformation patterns compared to the aluminum impactors investigated in this aim. The presence of clothes, which effectively reduce the friction between the impactor and skin, may also influence the deformation patterns and MPS-95.

Simulations were also run to investigate the effect of skin and adipose tissue stiffnesses. In addition to the baseline material properties implemented in the modified ATBM v0.86 torso model, additional constitutive models representing the upper bound (mean + 1 SD) and lower bound (mean – 1 SD) were implemented based on previous work by Kong et al., 2020 for the skin and Sun et al., 2020 for adipose tissue [4, 25]. A full factorial design of experiment was used, resulting in nine skin and adipose stiffness combinations. In general, MPS-95 was more sensitive to skin stiffness than it was to adipose tissue stiffness. While the MPS-95 values varied case-by-case, this trend was consistent. Like the MPS-95 values, MPS distributions were more sensitive to variations in skin stiffness than in adipose tissue stiffness. Given that the effective stiffness of the skin is related to its thickness, this also supports the notion that a model that resolves spatial differences in skin thickness could result in location-dependent deformation responses.

Using the results from the large-scale parametric study, a meta-model was constructed to predict MPS-95 based on the five predictor variables (impact velocity, skin stiffness, adipose stiffness, impactor diameter, and impactor shape). Excluding simulations that error-terminated and other outliers, the meta-model was able to predict the original MPS-95 data with an R^2 value of 0.99, slope of 0.99, and intercept of 0.004, indicating an excellent fit. The meta-model confirmed the relationships between the predictor variables and MPS-95 that were identified and discussed previously.

Using the meta-model, three injury risk functions, which represented the variance in MPS-95 due to population variance in the five predictor variables were constructed using a Weibull cumulative density function. These three injury risk functions represented lower bound (5th percentile), median (50th percentile), and upper bound (95th percentile) injury risk for a given MPS-95 value, where the lower bound injury risk function represented the worst-case scenario (e.g., soft tissue mechanical properties). The meta-model was also evaluated neglecting variance in tissue mechanical properties, with both skin and adipose tissue stiffness defined as the mean values. This analysis indicated that the spread between the lower and upper bound injury risk functions was primarily due to variance in tissue mechanical properties and not variance in impactor design. However, this analysis only investigated the impactors investigated in this study and the results may vary with different impactors.

There were several important limitations to the work conducted in this aim. First and foremost, the torso model was not validated for its system-level flesh deformation response. Since it was challenging to precisely measure the impactor kinematics and skin deformation in these tests, experimental data was not available to validate the torso model under these impact conditions. However, the individual flesh constitutive models were thoroughly validated for the relevant dynamic impacts. Additionally, the work conducted in this aim only considered specific, spherical and cylindrical, aluminum, rigid impactors. While the methods used in this aim could certainly be applied to investigate injury risk using other blunt impactors, additional simulation work is required to investigate how the results presented in this aim relate to other impactor designs. Furthermore, this work was performed using a torso model which modeled the skin as a uniform-thickness shell. The skin is known to vary in thickness throughout the torso and greater differences in regional skin deformations may be observed in a model that resolves regional skin thickness variation. Finally, the model represented a single anatomy, which corresponded to a 50th percentile male and may not be applicable to other demographic groups. In addition, the presence of clothes may influence the results and conclusions of this study. Finally, the constitutive models implemented in the modified ATBM v0.86 torso model were largely derived from experimental data conducted using tissue specimens harvested from cadaveric specimens and do not include any effects of active musculature. These may not be representative of live human tissue responses and future modeling studies should investigate the effect of active musculature, or bracing, on the skin deformation response and injury risk.

References

1. King AL, Finnin MS, Kramer CM (2019) Significance of Open Wounds Potentially Caused by Non-Lethal Weapons. Alexandria, VA

2. Olson KA, Haselden LE, Zaunbrecher RD, Weinfeld A, Brown LH, Bradley JA, Cardenas TCP, Trust MD, Coopwood B, Teixeira PG, Brown CVR, Aydelotte JD (2020) Penetrating Injuries from “Less Lethal” Beanbag Munitions. N Engl J Med 383:1081–1083 . https://doi.org/10.1056/NEJMc2025923

3. Kaske EA, Cramer SW, Pena Pino I, Do TH, Ladd BM, Sturtevant DT, Ahmadi A, Taha B, Freeman D, Wu JT, Cunningham BA, Hardeman RR, Satin DJ, Darrow DP (2021) Injuries from Less-Lethal Weapons during the George Floyd Protests in Minneapolis. N Engl J Med 384:774–775 . https://doi.org/10.1056/NEJMc2032052

4. Kong KSY (2020) Development of a Computational Model of Skin Damage under Blunt Impact to Investigate Skin Failure Threshold. University of Virginia

5. Sanders R (1973) Torsional Elasticity of Human Skin in vivo. Pflugers Arch 342:255–260

6. Diridollou S, Patat F, Gens F, Vaillant L, Black D, Lagarde JM, Gall Y, Berson M (2000) In vivo model of the mechanical properties of the human skin under suction

7. Joodaki H, Panzer MB (2018) Skin mechanical properties and modeling: A review. Proc. Inst. Mech. Eng. Part H J. Eng. Med. 232:323–343

8. Gallagher AJ, Anniadh AN, Bruyere K, Ottenio M, Xie H, Gilchrist MD (2012) Dynamic Tensile Properties of Human Skin. In: IRCOBI Conference2. pp 494–502

9. Escoffier C, de Rigal J, Rochefort A, Vasselet R, Léveˆque J-L, Agache PG (1989) Age-related mechanical properties of human skin: An in vivo study. J Invest Dermatol 93:353–357 . https://doi.org/10.1016/0022-202X(89)90058-4

10. Laurent A, Mistretta F, Bottigioli D, Dahel K, Goujon C, Nicolas JF, Hennino A, Laurent PE (2007) Echographic measurement of skin thickness in adults by high frequency ultrasound to assess the appropriate microneedle length for intradermal delivery of vaccines. Vaccine 25:6423–6430 . https://doi.org/10.1016/j.vaccine.2007.05.046

11. WHO (2021) Obestiy and overweight. In: World Heal. Organ. https://www.who.int/news-room/fact-sheets/detail/obesity-and-overweight

12. Gepner BD, Joodaki H, Sun Z, Jayathirtha M, Kim T, Forman JL, Kerrigan JR (2018) Performance of the Obese GHBMC Models in the Sled and Belt Pull Test Conditions. In: IRCOBI Conference. pp 355–368

13. Reynier KA, Shedd DF, Berthelson PR, Forman JL, Panzer MB (2021) Comparing passive and active

volunteer thoracic muscle stiffness to atonic muscle stiffness using shear wave elastography. Submitted

14. Kent RW, Funk JR (2004) Data censoring and parametric distribution assignment in the development of injury risk functions from biochemical data. SAE Tech Pap 1–12 . https://doi.org/10.4271/2004-01-0317

15. McMurry TL, Poplin GS (2015) Statistical Considerations in the Development of Injury Risk Functions. Traffic Inj Prev 16:618–626 . https://doi.org/10.1080/15389588.2014.991820

16. Bir C, Viano DC (2004) Design and injury assessment criteria for blunt ballistic impacts. J Trauma - Inj Infect Crit Care 57:1218–1224 . https://doi.org/10.1097/01.TA.0000114066.77967.DE

17. Bir CA, Stewart SJ, Wilhelm M (2005) Skin Penetration Assessment of Less Lethal Kinetic Energy Munitions. J Forensic Sci 50:1–4 . https://doi.org/10.1520/jfs2004551

18. James GR (2020) DEVELOPMENT OF MODELS TO ASSESS PENETRATING INJURY FROM BALLISTIC PROJECTILES. Cranfield University

19. Shedd D, Berthelson P, Rifkin J, McMahon J, Giudice J, Kopp K, Overby B, Forman J, Panzer M (2021) Injury Risk Assessment of Human Skin Penetration Under High-Rate Blunt Impact. Submitted

20. Meurs J (2016) The experimental design of postmortem studies: the effect size and statistical power. Forensic Sci Med Pathol 12:343–349 . https://doi.org/10.1007/s12024-016-9793-x

21. Hayashi S, Naito M, Kawata S, Qu N, Hatayama N, Hirai S, Itoh M (2016) History and future of human cadaver preservation for surgical training: from formalin to saturated salt solution method. Anat Sci Int 91:1–7 . https://doi.org/10.1007/s12565-015-0299-5

22. Kneubuehl B, Coupland R, Rothschild M, Thali M (2011) Wound Ballistics Basics and Applications. Springer

23. Summerfield A, Meurens F, Ricklin ME (2015) The immunology of the porcine skin and its value as a model for human skin. Mol Immunol 66:14–21 . https://doi.org/10.1016/j.molimm.2014.10.023

24. Sperrazza J, Kokinakis W (1968) BALLISTIC LIMITS OF TISSUE AND CLOTHING. Ann N Y Acad Sci 152:163–167 . https://doi.org/10.1111/j.1749-6632.1968.tb11973.x.

25. Breeze J, Carr DJ, Mabbott A, Beckett S, Clasper JC (2015) Refrigeration and freezing of porcine tissue does not affect the retardation of fragment simulating projectiles. J Forensic Leg Med 32:77–83 . https://doi.org/10.1016/j.jflm.2015.03.003

26. Sun Z (2021) Material Characterization and Computational Modeling of Human Subcutaneous Adipose Tissue. University of Virginia

27. Humphrey C, Henneberg M, Wachsberger C, Maiden N, Kumaratilake J (2017) Effects of Re-heating Tissue Samples to Core Body Temperature on High-Velocity Ballistic Projectile–tissue

Interactions. J Forensic Sci 62:1466–1471 . https://doi.org/10.1111/1556-4029.13473

28. (2017) Aixplorer Multiwave User's Guide Ref: SSIP01154, Revision 12A. In: SuperSonic imagine. https://www.supersonicimagine.com/content/download/4126/25649/version/1/file/PM.LAB.063+(Rev+A)-SSIP01154_Aixplorer_UserGuide_USA.pdf
29. Therneau TM, Lumley T, Atkinson E, Crowson C (2021) Package "survival"
30. Klein JP, Moeschberger ML (2003) SURVIVAL ANALYSIS Techniques for Censored and Truncated Data, 2nd Edition. Springer
31. Evermann J (2019) Q fever in Small Ruminants (Query fever; Coxiella burnetii; Coxiellosis)
32. Jackson C, Kerr K, Etu J, Panzer M, Forman J, Shedd D, Reynier K (2020) Mechanical Properties of Tissue in Living Humans
33. Zhang M, Mak AFT (1999) In vivo friction properties of human skin. Prosthet Orthot Int 23:135–141 . https://doi.org/10.3109/03093649909071625
34. (1999) Data Reference Guide Version 4.b Volume II: Biomechanical Tests

1. King AL, Finnin MS, Kramer CM (2019) Significance of Open Wounds Potentially Caused by Non-Lethal Weapons. Alexandria, VA
2. Olson KA, Haselden LE, Zaunbrecher RD, Weinfeld A, Brown LH, Bradley JA, Cardenas TCP, Trust MD, Coopwood B, Teixeira PG, Brown CVR, Aydelotte JD (2020) Penetrating Injuries from "Less Lethal" Beanbag Munitions. N Engl J Med 383:1081–1083 . https://doi.org/10.1056/NEJMc2025923
3. Kaske EA, Cramer SW, Pena Pino I, Do TH, Ladd BM, Sturtevant DT, Ahmadi A, Taha B, Freeman D, Wu JT, Cunningham BA, Hardeman RR, Satin DJ, Darrow DP (2021) Injuries from Less-Lethal Weapons during the George Floyd Protests in Minneapolis. N Engl J Med 384:774–775 . https://doi.org/10.1056/NEJMc2032052
4. Kong KSY (2020) Development of a Computational Model of Skin Damage under Blunt Impact to Investigate Skin Failure Threshold. University of Virginia
5. Sanders R (1973) Torsional Elasticity of Human Skin in vivo. Pflugers Arch 342:255–260
6. Diridollou S, Patat F, Gens F, Vaillant L, Black D, Lagarde JM, Gall Y, Berson M (2000) In vivo model of the mechanical properties of the human skin under suction
7. Joodaki H, Panzer MB (2018) Skin mechanical properties and modeling: A review. Proc. Inst. Mech. Eng. Part H J. Eng. Med. 232:323–343
8. Gallagher AJ, Anniadh AN, Bruyere K, Ottenio M, Xie H, Gilchrist MD (2012) Dynamic Tensile Properties of Human Skin. In: IRCOBI Conference2. pp 494–502

9. Escoffier C, de Rigal J, Rochefort A, Vasselet R, Léveˆque J-L, Agache PG (1989) Age-related mechanical properties of human skin: An in vivo study. J Invest Dermatol 93:353–357 . https://doi.org/10.1016/0022-202X(89)90058-4

10. Laurent A, Mistretta F, Bottigioli D, Dahel K, Goujon C, Nicolas JF, Hennino A, Laurent PE (2007) Echographic measurement of skin thickness in adults by high frequency ultrasound to assess the appropriate microneedle length for intradermal delivery of vaccines. Vaccine 25:6423–6430 . https://doi.org/10.1016/j.vaccine.2007.05.046

11. WHO (2021) Obestiy and overweight. In: World Heal. Organ. https://www.who.int/news-room/fact-sheets/detail/obesity-and-overweight

12. Gepner BD, Joodaki H, Sun Z, Jayathirtha M, Kim T, Forman JL, Kerrigan JR (2018) Performance of the Obese GHBMC Models in the Sled and Belt Pull Test Conditions. In: IRCOBI Conference. pp 355–368

13. Jackson C, Kerr K, Etu J, Panzer M, Forman J, Shedd D, Reynier K (2020) Mechanical Properties of Tissue in Living Humans

14. Kent RW, Funk JR (2004) Data censoring and parametric distribution assignment in the development of injury risk functions from biochemical data. SAE Tech Pap 1–12 . https://doi.org/10.4271/2004-01-0317

15. McMurry TL, Poplin GS (2015) Statistical Considerations in the Development of Injury Risk Functions. Traffic Inj Prev 16:618–626 . https://doi.org/10.1080/15389588.2014.991820

16. Bir C, Viano DC (2004) Design and injury assessment criteria for blunt ballistic impacts. J Trauma - Inj Infect Crit Care 57:1218–1224 . https://doi.org/10.1097/01.TA.0000114066.77967.DE

17. Bir CA, Stewart SJ, Wilhelm M (2005) Skin Penetration Assessment of Less Lethal Kinetic Energy Munitions. J Forensic Sci 50:1–4 . https://doi.org/10.1520/jfs2004551

18. James GR (2020) DEVELOPMENT OF MODELS TO ASSESS PENETRATING INJURY FROM BALLISTIC PROJECTILES. Cranfield University

19. Meurs J (2016) The experimental design of postmortem studies: the effect size and statistical power. Forensic Sci Med Pathol 12:343–349 . https://doi.org/10.1007/s12024-016-9793-x

20. Hayashi S, Naito M, Kawata S, Qu N, Hatayama N, Hirai S, Itoh M (2016) History and future of human cadaver preservation for surgical training: from formalin to saturated salt solution method. Anat Sci Int 91:1–7 . https://doi.org/10.1007/s12565-015-0299-5

21. Kneubuehl B, Coupland R, Rothschild M, Thali M (2011) Wound Ballistics Basics and

Applications. Springer

22. Summerfield A, Meurens F, Ricklin ME (2015) The immunology of the porcine skin and its value as a model for human skin. Mol Immunol 66:14–21 . https://doi.org/10.1016/j.molimm.2014.10.023

23. Sperrazza J, Kokinakis W (1968) BALLISTIC LIMITS OF TISSUE AND CLOTHING. Ann N Y Acad Sci 152:163–167 . https://doi.org/10.1111/j.1749-6632.1968.tb11973.x.

24. Breeze J, Carr DJ, Mabbott A, Beckett S, Clasper JC (2015) Refrigeration and freezing of porcine tissue does not affect the retardation of fragment simulating projectiles. J Forensic Leg Med 32:77–83 . https://doi.org/10.1016/j.jflm.2015.03.003

25. Sun Z (2021) Material Characterization and Computational Modeling of Human Subcutaneous Adipose Tissue. University of Virginia

26. Humphrey C, Henneberg M, Wachsberger C, Maiden N, Kumaratilake J (2017) Effects of Re-heating Tissue Samples to Core Body Temperature on High-Velocity Ballistic Projectile–tissue Interactions. J Forensic Sci 62:1466–1471 . https://doi.org/10.1111/1556-4029.13473

27. Crandall JR, Bose D, Forman J, Untaroiu CD, Arregui-Dalmases C, Shaw CG, Kerrigan JR (2011) Human surrogates for injury biomechanics research. Clin Anat 24:362–71 . https://doi.org/10.1002/ca.21152

28. (2017) Aixplorer Multiwave User's Guide Ref: SSIP01154, Revision 12A. In: SuperSonic imagine. https://www.supersonicimagine.com/content/download/4126/25649/version/1/file/PM.LAB.063+(Rev+A)-SSIP01154_Aixplorer_UserGuide_USA.pdf

29. Therneau TM, Lumley T, Atkinson E, Crowson C (2021) Package "survival"

30. Klein JP, Moeschberger ML (2003) SURVIVAL ANALYSIS Techniques for Censored and Truncated Data, 2nd Edition. Springer

31. Evermann J (2019) Q fever in Small Ruminants (Query fever; Coxiella burnetii; Coxiellosis)

32. Zhang M, Mak AFT (1999) In vivo friction properties of human skin. Prosthet Orthot Int 23:135–141 . https://doi.org/10.3109/03093649909071625

33. (1999) Data Reference Guide Version 4.b Volume II: Biomechanical Tests

Appendices

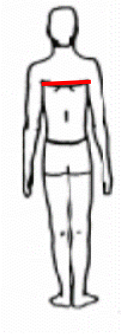
Appendix 1: PMHS Anthropometry Instructions

Anthropometry measurements were collected in accordance with the National Highway Traffic Safety Administration's (NHTSA) Data Reference Guide Version 4.b, Volume II: Biomechanical Tests [33]. All measurements were taken while the PMHS was in a supine position. All measurements used *cm* as the standard unit of measure.

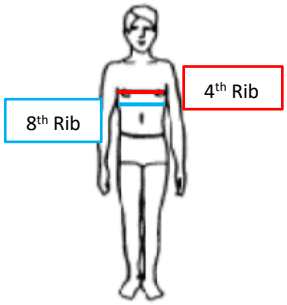
Shoulder (Biacromial) Breadth:
The breadth of the subject's shoulders, as measured between the lateral edges of the left and right acromions. Measured with calipers.



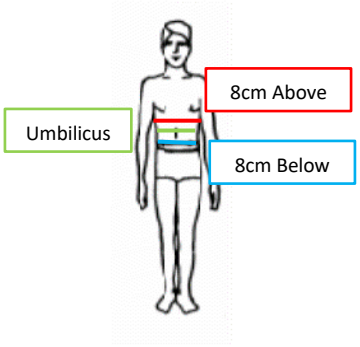
Interscye Distance:
The horizontal distance between the posterior scye point landmarks. Measured from armpit to armpit. Measured with calipers.



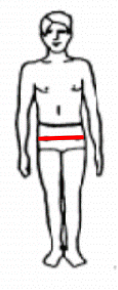
Chest Breadth:
The breadth of the subject's chest. For additional specificity, these measures were taken at the 4th and 8th rib of each subject. Measured with calipers.



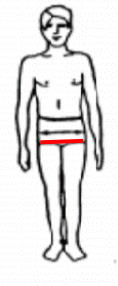
Waist Breadth:
The breadth of the subject's waist. For additional specificity, these measures were taken at the umbilicus, 8cm superior/above the umbilicus, and 8cm inferior/below the umbilicus. Measured with calipers.



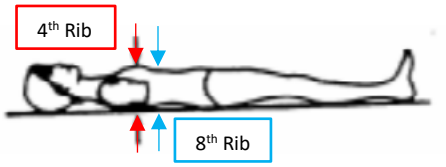
Hip Breadth:
The breadth of the subject's hip, measured between the right and left illocristale landmarks perpendicular to the mid-sagittal plane. Measured with calipers.



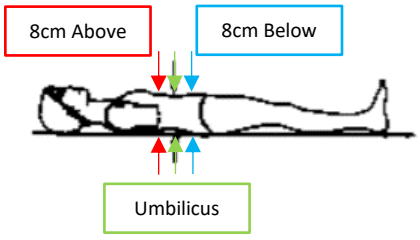
Buttock Breadth:
The breadth of the subject's buttock, measured at the level of the trochanterion surface landmarks. Measured with calipers.



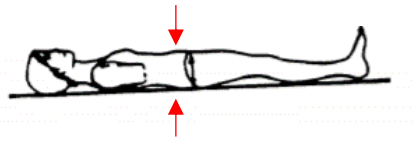
Chest Depth:
The depth of the subject's chest, measured at two locations: the 4th rib and the 8th rib. Measured using a ruler.



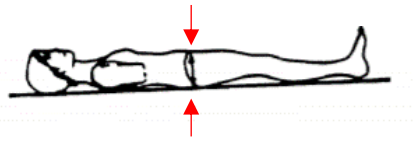
Waist Depth:
The depth of the subject's waist, measured at three locations: the umbilicus, 8cm superior/above the umbilicus, and 8cm inferior/below the umbilicus. Measured using a ruler.



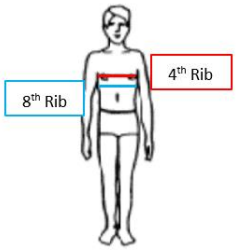
Hip Depth:
The breadth of the subject's hip, measured at the level of the illocristale landmarks. Measured with a ruler.



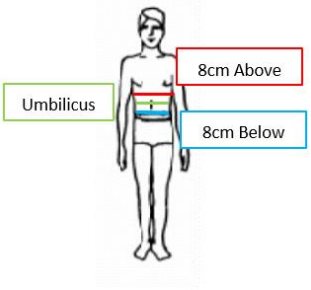
Buttock Depth:
The breadth of the subject's buttock, measured as the anterior-posterior distance on the medial plane projection at the level of the maximum posterior protrusion of the buttocks. Measured with a ruler.



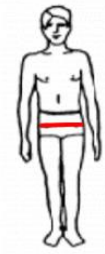
Chest Circumference:
The circumference of the subject's chest, measured at the 4th and 8th ribs. Measurements were made perpendicular to the long axis of the trunk using measuring tape.



Waist Circumference:
The circumference of the subject's waist, measured at three locations: the umbilicus, 8cm superior/above the umbilicus, and 8cm inferior/below the umbilicus. Measurements were made perpendicular to the long axis of the trunk using measuring tape.



Hip Circumference:
The circumference of the subject's hip, measured at the level of the illocristale landmarks. Measurements were made perpendicular to the long axis of the trunk using measuring tape.



Buttock Circumference:
The circumference of the subject's buttock, measured at the level of the trochanterion surface landmarks. Measurements were made perpendicular to the long axis of the trunk using measuring tape.



Appendix 2: PMHS Impact Descriptions

The following tables provide details of each PMHS impact test, such as the impacted body region, side of the body, impactor shape, impactor diameter, velocity, and binary injury result. Further details on the injury severity from each test are provided in Appendix 3, with corresponding impact numbers.

Table A2-LXXV: PMHS 1 Impact Descriptions

Impact	Body Region	Side	Impactor Shape	Impactor Diameter (in.)	Impactor Velocity (m/s)	Skin Penetration (> 5mm)
1	Upper Chest	Right	Sphere	0.50	117.90	Yes
2					100.63	Yes
3					76.56	No
4					91.63	Yes
5					76.52	Yes
6	Upper Chest	Left	Cylinder	0.50	102.36	Yes
7					79.16	Yes
8					59.97	No
9					76.56	No
10					96.33	Yes
11	Abdomen	Right	Sphere	0.75	122.35	Yes
12					102.97	No
13					120.58	Yes
14					113.15	Yes
15					102.42	No
16	Abdomen	Left	Cylinder	0.75	121.65	Yes
17					100.39	No
18					115.65	No
19					124.17	Yes

20	Upper Back	Right	Sphere	0.75	115.93	No
21					134.13	Yes
22					115.92	No
23					121.05	Yes
24					128.53	Yes
25	Upper Back	Left	Cylinder	0.75	117.03	No
26					133.73	No
27					118.38	No
28					124.39	No
29					133.66	No
30	Lower Back	Right	Sphere	0.50	91.41	No
31					108.29	Yes
32					93.41	No
33					111.51	Yes
34					110.83	No
35	Lower Back	Left	Cylinder	0.50	95.24	No
36					117.86	No
37					117.00	No
38					124.61	Yes
39					127.87	Yes

Table A2-LXXVI: PMHS 2 Impact Descriptions

Impact	Body Region	Side	Impactor Shape	Impactor Diameter (in.)	Impactor Velocity (m/s)	Skin Penetration (> 5mm)
1	Upper Chest	Right	Sphere	1.00	119.27	Yes
2					103.05	No
3					120.57	Yes
4					103.69	No
5	Upper Chest	Left	Cylinder	1.00	125.51	Yes
6					114.49	Yes
7					98.94	No
8					114.54	No
9	Abdomen	Right	Sphere	0.50	122.06	No
10					135.80	Yes
11					123.36	Yes
12					113.78	No
13					121.23	No
14	Abdomen	Left	Cylinder	0.50	124.10	No
15					137.74	No
16					156.53	No
17					166.56	No
18					161.21	No
19	Upper Back	Right	Sphere	0.50	121.53	No
20					149.29	No
21					160.40	No
22					160.93	No
23					165.34	No

24	Upper Back	Left	Cylinder	0.50	117.03	No
25					133.73	No
26					118.38	No
27					124.39	No
28					133.66	No
29	Lower Back	Right	Sphere	1.00	119.50	No
30					143.91	Yes
31					133.50	No
32					147.32	No
33	Lower Back	Left	Cylinder	1.00	114.82	No
34					126.46	No
35					136.65	No
36					122.77	No

Table A2-LXXVII: PMHS 3 Impact Descriptions

Impact	Body Region	Side	Impactor Shape	Impactor Diameter (in.)	Impactor Velocity (m/s)	Skin Penetration (> 5mm)
1	Upper Chest	Right	Sphere	0.50	100.92	No
2					114.57	No
3					125.06	Yes
4					117.08	Yes
5					104.07	Yes
6	Upper Chest	Left	Cylinder	0.50	100.02	No
7					116.16	No
8					128.58	Yes
9					117.29	No
10					130.84	Yes
11	Abdomen	Right	Sphere	1.00	138.50	Yes
12					124.56	Yes
13					93.82	No
14					111.96	No
15	Abdomen	Left	Cylinder	1.00	120.23	No
16					130.53	No
17					140.70	Yes
18					137.65	Yes
19	Upper Back	Right	Sphere	1.00	142.02	No
20					152.07	Yes
21					141.90	No
22					149.15	No

23	Upper Back	Left	Cylinder	1.00	128.67	No
24					151.80	Yes
25					145.42	No
26					152.58	No
27	Lower Back	Right	Sphere	0.75	130.17	Yes
28					114.51	No
29					129.51	Yes
30					115.33	Yes
31					104.47	No
32	Lower Back	Left	Cylinder	0.75	131.46	No
33					145.58	Yes
34					135.71	Yes
35					129.81	No
36					136.08	Yes

Table A2-LXXVIII: PMHS 4 Impact Descriptions

Impact	Body Region	Side	Impactor Shape	Impactor Diameter (in.)	Impactor Velocity (m/s)	Skin Penetration (> 5mm)
1	Upper Chest	Right	Cylinder	0.50	88.97	No
2					117.45	No
3					129.45	Yes
4					115.01	No
5					141.97	Yes
6	Upper Chest	Left	Sphere	0.50	105.91	Yes
7					90.63	No
8					102.53	No
9					115.38	Yes
10					118.69	Yes
11	Abdomen	Right	Cylinder	0.75	129.43	Yes
12					117.67	No
13					129.94	No
14					144.38	Yes
15	Abdomen	Left	Sphere	0.75	130.12	Yes
16					116.21	Yes
17					103.01	No
18					112.92	Yes
19	Upper Back	Right	Cylinder	0.75	142.59	Yes
20					126.58	No
21					140.74	No
22					149.19	Yes
23					139.20	No

24	Upper Back	Left	Sphere	0.75	136.87	No
25					128.85	Yes
26					119.51	No
27					134.22	No
28					138.12	Yes
29	Lower Back	Right	Cylinder	0.50	120.76	No
30					128.94	No
31					134.40	No
32					151.09	No
33					154.17	No
34	Lower Back	Left	Sphere	0.50	114.80	Yes
35					111.70	No
36					119.23	No
37					131.61	No
38					156.08	Yes

Table A2-LXXIX: PMHS 5 Impact Descriptions

Impact	Body Region	Side	Impactor Shape	Impactor Diameter (in.)	Impactor Velocity (m/s)	Skin Penetration (> 5mm)
1	Upper Chest	Right	Cylinder	1.00	101.37	No
2					118.56	Yes
3					87.01	No
4					93.35	No
5	Upper Chest	Left	Sphere	1.00	108.74	Yes
6					87.86	No
7					100.79	Yes
8					98.08	No
9	Abdomen	Right	Cylinder	0.50	105.48	No
10					109.80	No
11					127.63	No
12					134.67	No
13					123.10	No
14	Abdomen	Left	Sphere	0.50	94.07	No
15					116.04	No
16					112.09	No
17					114.32	No
18					124.22	Yes
19	Upper Back	Right	Cylinder	0.50	109.34	No
20					131.25	No
21					116.64	No
22					128.19	No
23					96.17	No

24	Upper Back	Left	Sphere	0.50	106.39	No
25					113.26	No
26					124.51	No
27					151.30	Yes
28					127.12	Yes
29	Lower Back	Right	Cylinder	1.00	127.13	Yes
30					105.22	No
31					118.75	No
32					89.30	No
33	Lower Back	Left	Sphere	1.00	122.73	Yes
34					110.71	Yes
35					91.31	No
36					99.85	No

Table A2-LXXX: PMHS 6 Impact Descriptions

Impact	Body Region	Side	Impactor Shape	Impactor Diameter (in.)	Impactor Velocity (m/s)	Skin Penetration (> 5mm)
1	Upper Chest	Right	Cylinder	0.75	106.70	Yes
2					91.89	No
3					108.85	No
4					120.55	Yes
5					109.08	No
6	Upper Chest	Left	Sphere	0.75	110.35	Yes
7					89.56	Yes
8					71.89	No
9					88.80	No
10					111.47	Yes
11	Abdomen	Right	Sphere	1.00	122.35	Yes
12					120.58	Yes
13					113.15	Yes
14					102.42	No
15	Abdomen	Left	Cylinder	1.00	99.94	No
16					106.78	Yes
17					85.35	No
18					95.31	Yes
19	Upper Back	Right	Cylinder	1.00	143.10	No
20					143.30	No
21					127.13	No
22					116.86	No

23	Upper Back	Left	Sphere	1.00	139.63	Yes
24					134.63	Yes
25					108.85	No
26					113.66	No
27	Lower Back	Right	Cylinder	0.75	119.02	No
28					124.41	Yes
29					117.40	No
30					113.21	Yes
31					120.62	Yes
32	Lower Back	Left	Sphere	0.75	113.41	No
33					133.86	Yes
34					120.49	No
35					100.48	No
36					90.12	No

Appendix 3: PMHS Autopsy Results

The following tables present autopsy results for each of the PMHS. Results are based on “yes” or “no” binary designations at the levels of injury described in

Table VI. Impact numbers correlate with the impact tests described in Appendix 2.

Table A3-LXXXI: PMHS 1 Autopsy Results

Impact	Minor	Skin Failure	Penetration (> 5mm)	Full Fat Disruption	Partial Muscle Disruption	Full Muscle Disruption	Full Penetration	Presence of Bone	Bone Fracture
1	Yes	Yes	Yes	Yes	Yes	Yes	No	Yes	No
2	Yes	Yes	Yes	Yes	Yes	No	No	Yes	No
3	Yes	No	No	No	No	No	No	No	
4	Yes	Yes	Yes	Yes	Yes	Yes	No	Yes	No
5	Yes	Yes	Yes	Yes	Yes	No	No	No	
6	Yes	Yes	Yes	Yes	Yes	No	No	No	
7	Yes	Yes	Yes	No	No	No	No	No	
8	Yes	No	No	No	No	No	No	No	
9	Yes	No	No	No	No	No	No	No	
10	Yes	Yes	Yes	No	No	No	No	No	
11	Yes	Yes	Yes	Yes	Yes	Yes	Yes	No	
12	Yes	No	No	No	No	No	No	No	
13	Yes	Yes	Yes	Yes	Yes	Yes	No	No	
14	Yes	Yes	Yes	Yes	Yes	No	No	No	
15	No	No	No	No	No	No	No	Yes	No
16	Yes	Yes	Yes	No	No	No	No	No	
17	Yes	No	No	No	No	No	No	No	
18	Yes	No	No	No	No	No	No	No	
19	Yes	Yes	Yes	Yes	Yes	No	No	Yes	No
20	Yes	No	No	No	No	No	No	No	
21	Yes	Yes	Yes	Yes	Yes	No	No	No	
22	Yes	No	No	No	No	No	No	No	
23	Yes	Yes	Yes	Yes	Yes	No	No	Yes	No
24	Yes	Yes	Yes	Yes	No	No	No	Yes	No
25	Yes	No	No	No	No	No	No	Yes	No

26	Yes	Yes	No	No	No	No	No	No	
27	Yes	No	No	No	No	No	No	Yes	No
28	Yes	No	No	No	No	No	No	Yes	No
29	Yes	Yes	No	No	No	No	No	Yes	No
30	Yes	No	No	No	No	No	No	Yes	No
31	Yes	Yes	Yes	Yes	Yes	No	No	No	
32	Yes	No	No	No	No	No	No	No	
33	Yes	Yes	Yes	Yes	Yes	No	No	Yes	No
34	No	No	No	No	No	No	No	No	
35	No	No	No	No	No	No	No	Yes	No
36	Yes	No	No	No	No	No	No	No	
37	Yes	Yes	No	No	No	No	No	No	
38	Yes	Yes	Yes	Yes	Yes	No	No	No	
39	Yes	Yes	Yes	Yes	Yes	Yes	No	No	

Table ALXXXII: PMHS 2 Autopsy Results

Impact	Minor	Skin Failure	Penetration (> 5mm)	Full Fat Disruption	Partial Muscle Disruption	Full Muscle Disruption	Full Penetration	Presence of Bone	Bone Fracture
1	Yes	Yes	Yes	Yes	Yes	No	No	No	
2	Yes	No	No	No	No	No	No	No	
3	Yes	Yes	Yes	Yes	Yes	No	No	No	
4	Yes	No	No	No	No	No	No	No	
5	Yes	Yes	Yes	No	No	No	No	No	
6	Yes	Yes	Yes	No	No	No	No	No	
7	Yes	No	No	No	No	No	No	Yes	No
8	Yes	No	No	No	No	No	No	No	
9	Yes	No	No	No	No	No	No	No	
10	Yes	Yes	Yes	Yes	No	No	No	No	
11	Yes	Yes	Yes	Yes	No	No	No	No	
12	Yes	No	No	No	No	No	No	No	
13	Yes	No	No	No	No	No	No	No	
14	No	No	No	No	No	No	No	No	
15	Yes	No	No	No	No	No	No	No	
16	Yes	Yes	No	No	No	No	No	No	
17	Yes	Yes	No	No	No	No	No	No	
18	Yes	Yes	Yes	Yes	No	No	No	No	
19	Yes	No	No	No	No	No	No	Yes	No
20	Yes	No	No	No	No	No	No	No	
21	Yes	No	No	No	No	No	No	No	
22	Yes	Yes	No	No	No	No	No	No	
23	Yes	Yes	No	No	No	No	No	Yes	No
24	Yes	No	No	No	No	No	No	Yes	No
25	Yes	No	No	No	No	No	No	Yes	No
26	Yes	No	No	No	No	No	No	No	

27	Yes	Yes	No	No	No	No	No	No	
28	Yes	Yes	No	No	No	No	No	No	
29	Yes	No	No	No	No	No	No	No	
30	Yes	Yes	Yes	Yes	No	No	No	No	
31	Yes	No	No	No	No	No	No	No	
32	Yes	No	No	No	No	No	No	No	
33	Yes	No	No	No	No	No	No	No	
34	Yes	No	No	No	No	No	No	No	
35	Yes	No	No	No	No	No	No	No	
36	Yes	No	No	No	No	No	No	No	

Table A3-LXXXIII: PMHS 3 Autopsy Results

Impact	Minor	Skin Failure	Penetration (> 5mm)	Full Fat Disruption	Partial Muscle Disruption	Full Muscle Disruption	Full Penetration	Presence of Bone	Bone Fracture
1	Yes	No	No	No	No	No	No	No	
2	Yes	Yes	No	No	No	No	No	No	
3	Yes	Yes	Yes	Yes	Yes	No	No	Yes	No
4	Yes	Yes	Yes	No	No	No	No	Yes	No
5	Yes	Yes	Yes	No	No	No	No	Yes	No
6	Yes	No	No	No	No	No	No	No	
7	Yes	Yes	No	No	No	No	No	Yes	No
8	Yes	Yes	Yes	Yes	Yes	No	No	No	
9	Yes	No	No	No	No	No	No	Yes	No
10	Yes	Yes	Yes	Yes	No	No	No	Yes	No
11	Yes	Yes	Yes	Yes	Yes	No	No	No	
12	Yes	Yes	Yes	Yes	Yes	Yes	No	No	
13	No	No	No	No	No	No	No	No	
14	No	No	No	No	No	No	No	No	
15	No	No	No	No	No	No	No	No	
16	Yes	No	No	No	No	No	No	No	
17	Yes	Yes	Yes	Yes	Yes	Yes	Yes	No	
18	Yes	Yes	Yes	Yes	Yes	Yes	Yes	No	
19	No	No	No	No	No	No	No	Yes	No
20	Yes	Yes	Yes	Yes	Yes	No	No	No	
21	Yes	No	No	No	No	No	No	No	
22	No	No	No	No	No	No	No	No	
23	Yes	No	No	No	No	No	No	No	
24	Yes	Yes	Yes	Yes	Yes	No	No	No	
25	Yes	No	No	No	No	No	No	No	
26	Yes	No	No	No	No	No	No	No	

27	Yes	Yes	Yes	Yes	Yes	No	No	No	
28	No	No	No	No	No	No	No	No	
29	Yes	Yes	Yes	No	No	No	No	No	
30	Yes	Yes	Yes	Yes	Yes	No	No	Yes	No
31	Yes	No	No	No	No	No	No	Yes	No
32	Yes	No	No	No	No	No	No	Yes	No
33	Yes	Yes	Yes	Yes	Yes	No	No	Yes	No
34	Yes	Yes	Yes	No	No	No	No	Yes	No
35	Yes	No	No	No	No	No	No	Yes	No
36	Yes	Yes	Yes	Yes	No	No	No	Yes	No

Table A3-LXXXIV: PMHS 4 Autopsy Results

Impact	Minor	Skin Failure	Penetration (> 5mm)	Full Fat Disruption	Partial Muscle Disruption	Full Muscle Disruption	Full Penetration	Presence of Bone	Bone Fracture
1	Yes	No	No	No	No	No	No	No	
2	Yes	Yes	No	No	No	No	No	No	
3	Yes	Yes	Yes	Yes	No	No	No	Yes	No
4	Yes	No	No	No	No	No	No	Yes	No
5	Yes	Yes	Yes	No	No	No	No	Yes	No
6	Yes	Yes	Yes	Yes	Yes	No	No	Yes	No
7	No	No	No	No	No	No	No	No	
8	Yes	No	No	No	No	No	No	No	
9	Yes	Yes	Yes	No	No	No	No	No	
10	Yes	Yes	Yes	Yes	Yes	Yes	No	Yes	No
11	Yes	Yes	Yes	No	No	No	No	No	
12	Yes	No	No	No	No	No	No	No	
13	Yes	No	No	No	No	No	No	No	
14	Yes	Yes	Yes	Yes	No	No	No	No	
15	Yes	Yes	Yes	Yes	Yes	Yes	Yes	No	
16	Yes	Yes	Yes	Yes	No	No	No	No	
17	Yes	No	No	No	No	No	No	No	
18	Yes	Yes	Yes	No	No	No	No	No	
19	Yes	Yes	Yes	No	No	No	No	Yes	No
20	Yes	No	No	No	No	No	No	No	
21	Yes	No	No	No	No	No	No	Yes	No
22	Yes	Yes	Yes	No	No	No	No	Yes	No
23	Yes	Yes	No	No	No	No	No	No	
24	Yes	Yes	No	No	No	No	No	Yes	No
25	Yes	Yes	Yes	No	No	No	No	Yes	No
26	Yes	No	No	No	No	No	No	Yes	No

27	Yes	No	No	No	No	No	No	No	
28	Yes	Yes	Yes	Yes	No	No	No	Yes	No
29	Yes	Yes	No	No	No	No	No	No	
30	Yes	Yes	No	No	No	No	No	No	
31	Yes	No	No	No	No	No	No	No	
32	Yes	No	No	No	No	No	No	No	
33	Yes	No	No	No	No	No	No	No	
34	Yes	Yes	Yes	No	No	No	No	No	
35	Yes	No	No	No	No	No	No	No	
36	Yes	No	No	No	No	No	No	No	
37	Yes	No	No	No	No	No	No	Yes	No
38	Yes	Yes	Yes	Yes	Yes	No	No	No	

Table A3-LXXXV: PMHS 5 Autopsy Results

Impact	Minor	Skin Failure	Penetration (> 5mm)	Full Fat Disruption	Partial Muscle Disruption	Full Muscle Disruption	Full Penetration	Presence of Bone	Bone Fracture
1	Yes	Yes	No	No	No	No	No	No	
2	Yes	Yes	Yes	Yes	No	No	No	Yes	No
3	Yes	No	No	No	No	No	No	Yes	Yes
4	No	No	No	No	No	No	No	No	
5	Yes	Yes	Yes	Yes	No	No	No	No	
6	Yes	No	No	No	No	No	No	Yes	No
7	Yes	Yes	Yes	Yes	No	No	No	Yes	No
8	Yes	No	No	No	No	No	No	Yes	Yes
9	Yes	No	No	No	No	No	No	No	
10	Yes	No	No	No	No	No	No	No	
11	Yes	No	No	No	No	No	No	No	
12	Yes	Yes	No	No	No	No	No	No	
13	Yes	Yes	No	No	No	No	No	No	
14	No	No	No	No	No	No	No	No	
15	Yes	No	No	No	No	No	No	No	
16	Yes	No	No	No	No	No	No	No	
17	Yes	Yes	No	No	No	No	No	No	
18	Yes	Yes	Yes	Yes	Yes	No	No	No	
19	Yes	No	No	No	No	No	No	Yes	No
20	Yes	No	No	No	No	No	No	No	
21	Yes	No	No	No	No	No	No	Yes	No
22	Yes	No	No	No	No	No	No	Yes	No
23	No	No	No	No	No	No	No	No	
24	Yes	No	No	No	No	No	No	No	
25	Yes	No	No	No	No	No	No	Yes	No
26	Yes	Yes	No	No	No	No	No	Yes	No

27	Yes	Yes	Yes	Yes	Yes	No	No	No	
28	Yes	Yes	Yes	Yes	Yes	No	No	Yes	No
29	Yes	Yes	Yes	Yes	Yes	No	No	No	
30	Yes	No	No	No	No	No	No	Yes	No
31	Yes	Yes	No	No	No	No	No	No	
32	No	No	No	No	No	No	No	Yes	No
33	Yes	Yes	Yes	Yes	Yes	No	No	Yes	No
34	Yes	Yes	Yes	Yes	Yes	No	No	No	
35	Yes	Yes	No	No	No	No	No	No	
36	Yes	No	No	No	No	No	No	No	

Table A3-LXXXVI: PMHS 6 Autopsy Results

Impact	Minor	Skin Failure	Penetration (> 5mm)	Full Fat Disruption	Partial Muscle Disruption	Full Muscle Disruption	Full Penetration	Presence of Bone	Bone Fracture
1	Yes	Yes	Yes	Yes	No	No	No	No	
2	Yes	No	No	No	No	No	No	No	
3	Yes	No	No	No	No	No	No	No	
4	Yes	Yes	Yes	Yes	Yes	Yes	No	Yes	No
5	Yes	No	No	No	No	No	No	No	
6	Yes	Yes	Yes	Yes	Yes	Yes	Yes	Yes	Yes
7	Yes	Yes	Yes	Yes	Yes	No	No	No	
8	No	No	No	No	No	No	No	Yes	No
9	No	No	No	No	No	No	No	Yes	No
10	Yes	Yes	Yes	Yes	No	No	No	Yes	Yes
11	Yes	Yes	No	No	No	No	No	No	
12	Yes	Yes	Yes	No	No	No	No	No	
13	Yes	No	No	No	No	No	No	No	
14	Yes	Yes	Yes	Yes	No	No	No	No	
15	Yes	Yes	Yes	Yes	No	No	No	No	
16	Yes	Yes	No	No	No	No	No	No	
17	Yes	Yes	No	No	No	No	No	No	
18	Yes	Yes	Yes	No	No	No	No	No	
19	Yes	No	No	No	No	No	No	Yes	No
20	Yes	No	No	No	No	No	No	Yes	No
21	Yes	Yes	No	No	No	No	No	Yes	No
22	Yes	No	No	No	No	No	No	Yes	No
23	Yes	Yes	Yes	Yes	Yes	No	No	No	
24	Yes	Yes	Yes	Yes	No	No	No	Yes	No
25	Yes	No	No	No	No	No	No	Yes	No
26	Yes	No	No	No	No	No	No	Yes	Yes

27	No	No	No	No	No	No	No	No	
28	Yes	Yes	Yes	No	No	No	No	No	
29	Yes	No	No	No	No	No	No	No	
30	Yes	Yes	Yes	Yes	No	No	No	No	
31	Yes	Yes	Yes	No	No	No	No	No	
32	Yes	No	No	No	No	No	No	No	
33	Yes	Yes	Yes	Yes	Yes	Yes	No	Yes	Yes
34	Yes	Yes	No	No	No	No	No	No	
35	Yes	No	No	No	No	No	No	No	
36	Yes	Yes	No	No	No	No	No	No	

Appendix 4: PMHS Injury Risk Function Covariate Assessment

As described in Aim 1, the validity of every possible variable was assessed by independently implementing the covariate into the PMHS IRF. The log-likelihood p-value for each single-covariate IRF is provided in Table A4-LXXXVII. Additionally, the "Missing Data" column describes the number of datapoints that did not include the relevant covariate information and, therefore, would be excluded from the model fit. This was primarily a result of ultrasound and SWE limitations, such as the depth of imaging.

Table A4-LXXXVII: Full PMHS Covariate Assessment (In Increasing Order of p-Value)

Covariate	p-Value	Missing Data
Skin Thickness (mm)	4.0e-07	PMHS 1
Body Region	2.0e-06	0
Impactor Shape	4.6e-03	0
Specimen ID	1.3e-02	0
Fascia Stiffness/SWE Velocity (m/s)	1.4e-02	PMHS 1 + 47 Datapoints
Muscle Thickness (mm)	5.8e-02	PMHS 1 + 26 Datapoints
Fat Stiffness/SWE Velocity (m/s)	1.5e-01	PMHS 1
Muscle Stiffness/SWE Velocity (m/s)	2.6e-01	PMHS 1 + 74 Datapoints
Impactor Diameter	3.1e-01	0
Fascia Thickness (mm)	4.6e-01	PMHS 1 + 17 Datapoints
Fat Thickness (mm)	5.7e-01	PMHS 1 + 12 Datapoints
Presence of Bone	6.7e-01	0
Side	6.9e-01	0
Skin Stiffness/SWE Velocity (m/s)	7.4e-01	PMHS 1
Surface Temperature (°F)	8.6e-01	0

The following figures represent the variability resulting from all possible model covariates shown in Table A4-LXXXVII. For categorical covariates, the model prediction for each category is plotted. For continuous covariates, the mean value ± 1 SD is plotted.

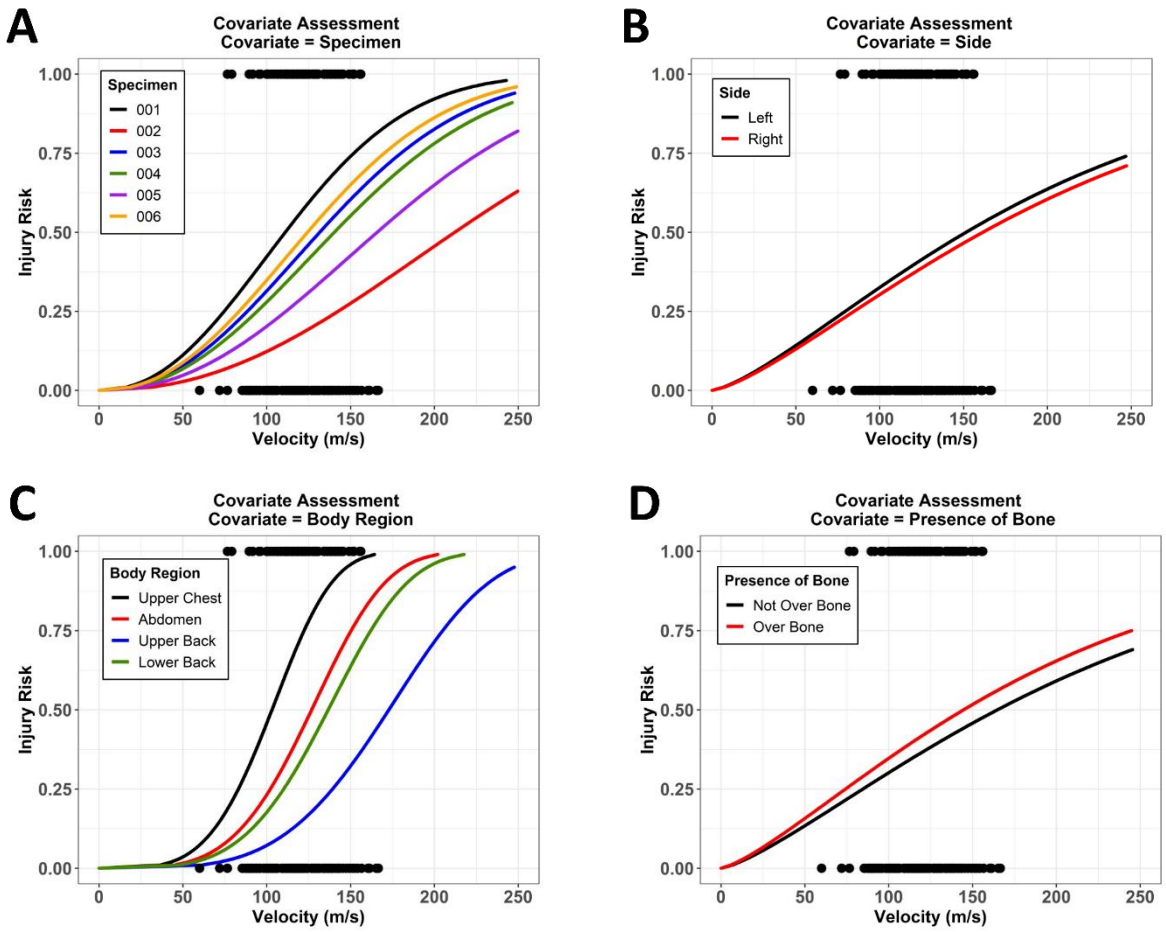


Figure A4-68: PMHS covariate assessment for the impact location variables.

Variability of the following covariates is presented: (a) Specimen is the categorical specimen ID (1, 2, …, 6), (b) Side is the categorical side of the body (Left and Right), (c) Body Region is the categorical body region (Upper Chest, Abdomen, Upper Back, and Lower Back), and (d) Presence of Bone is the categorical variable that describes whether the impact occurred over bone.

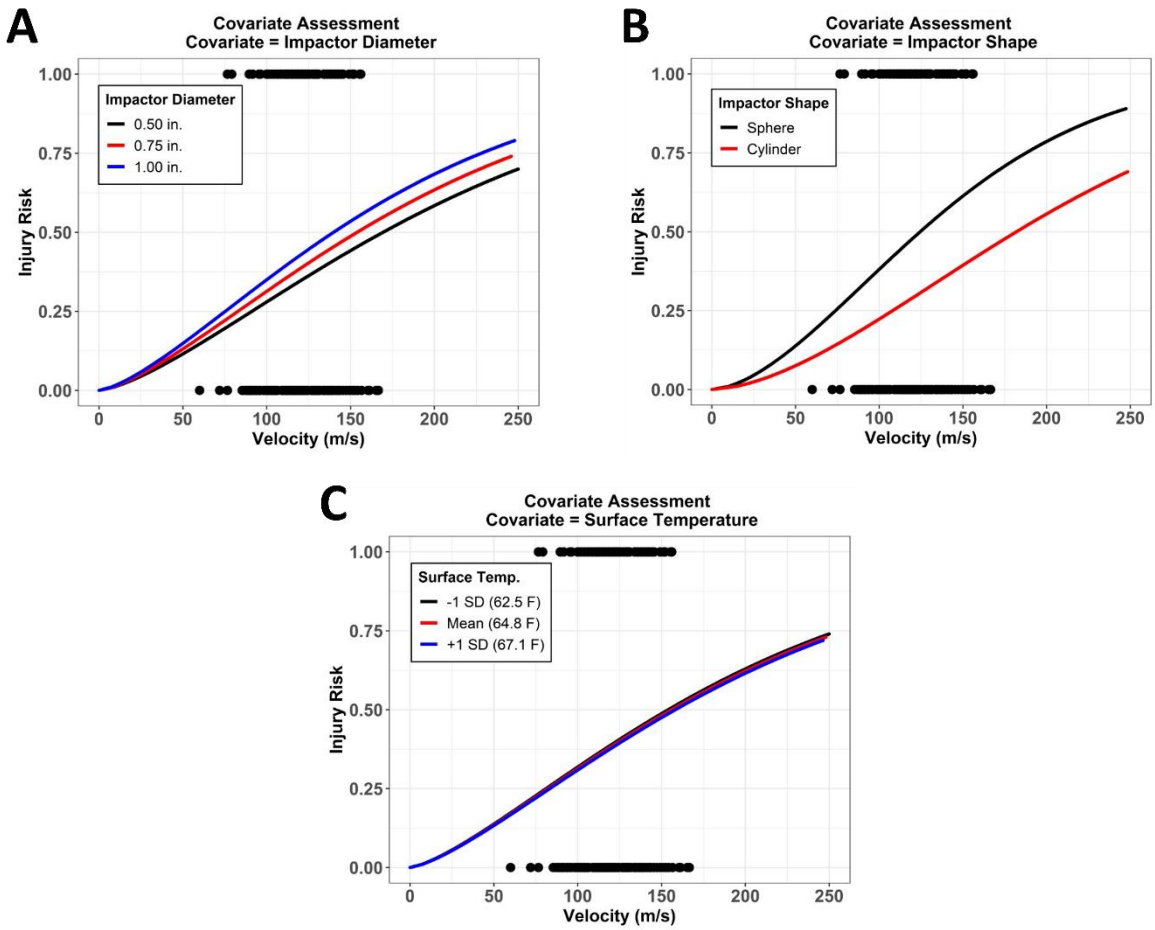


Figure A4-69: PMHS covariate assessment for the impact condition variables.

Variability of the following covariates is presented: (a) Diameter is the continuous impactor diameter from 0.50 in. to 1.00 in., (b) Shape is the categorical impactor shape (Sphere and Cylinder), and (c) Surface Temp is the continuous surface tissue temperature.

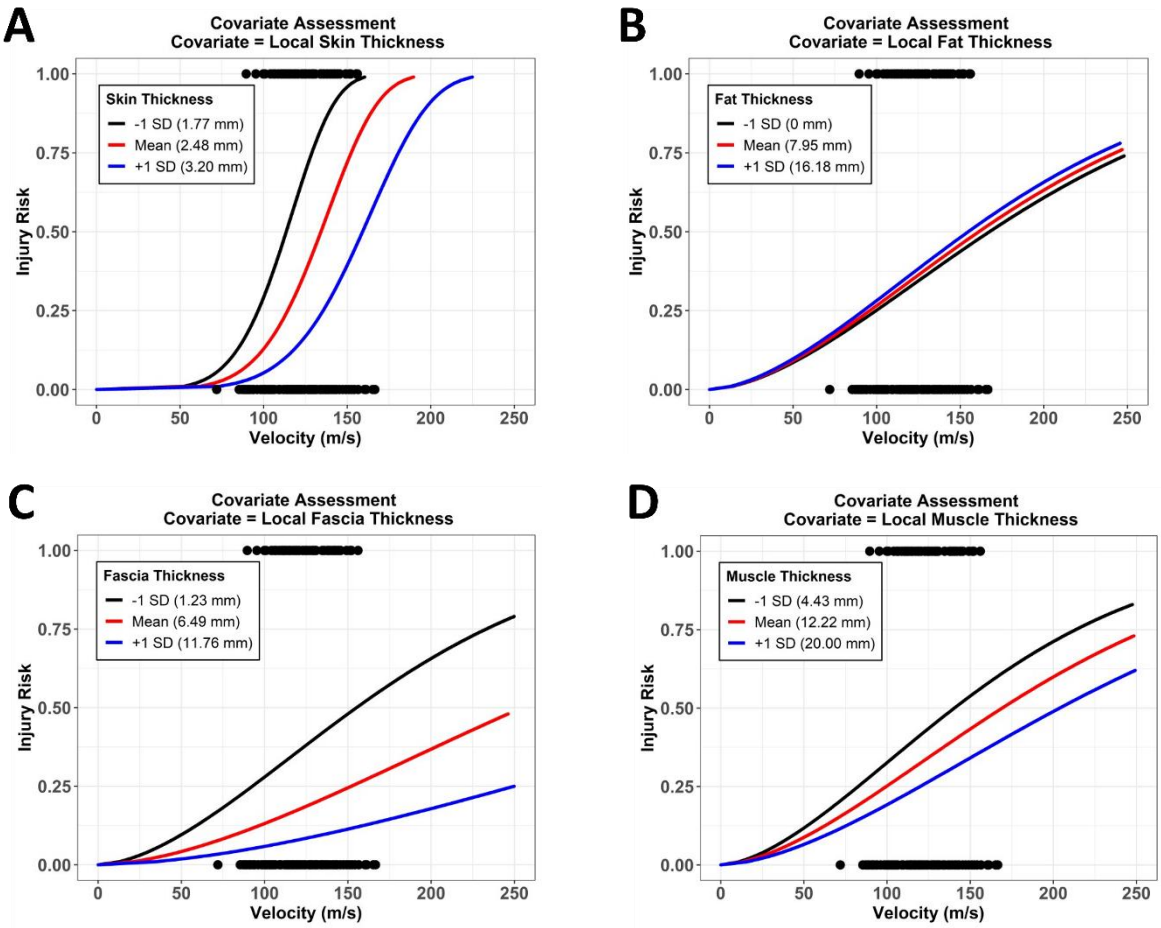


Figure A4-70: PMHS covariate assessment for the tissue thickness variables.

Variability of the following covariates is presented: (a) Local Skin Thickness is the continuous thickness of the skin layer, (b) Local Fat Thickness is the continuous thickness of the fat layer, (c) Local Fascia Thickness is the continuous thickness of the fascia layer, and (d) Local Muscle Thickness is the continuous thickness of the muscle layer.

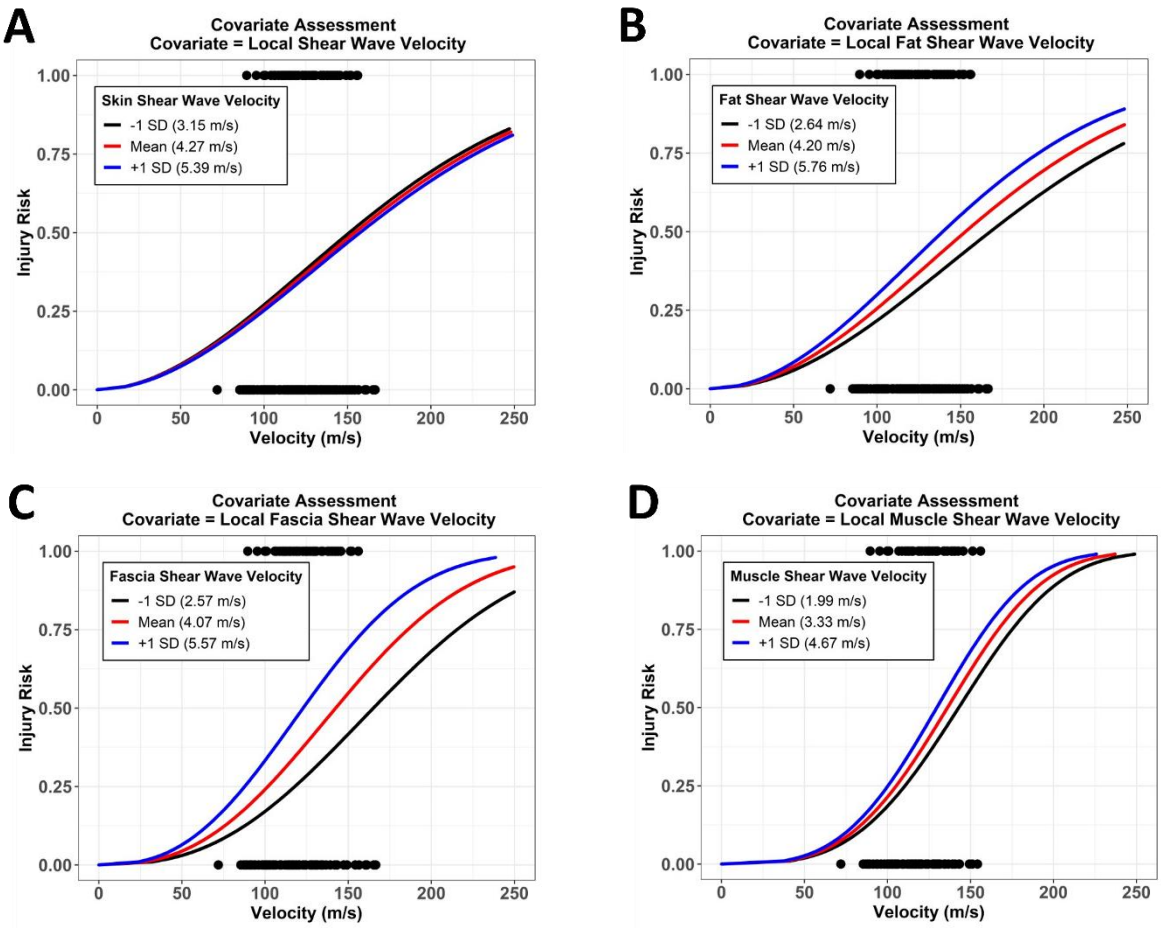
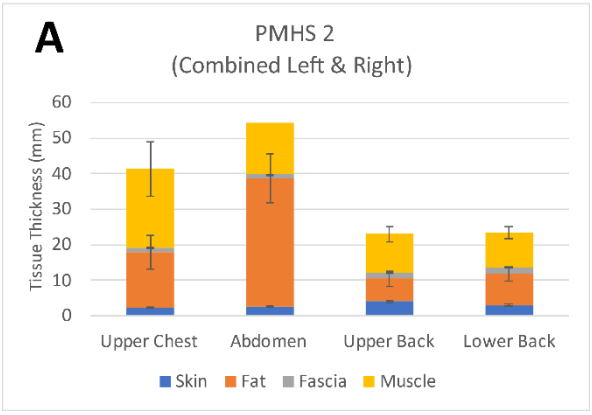


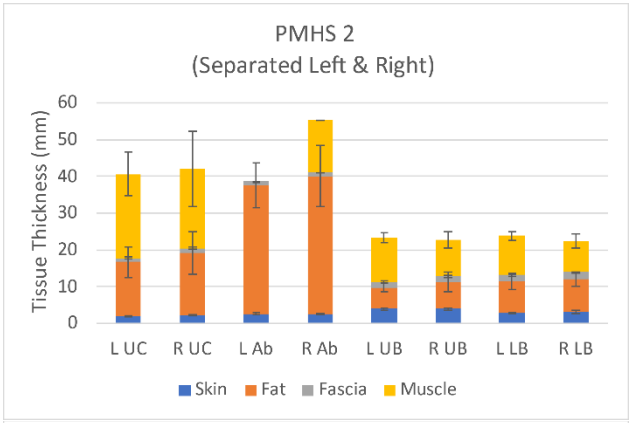
Figure A4-71: PMHS covariate assessment for the tissue shear wave velocity variables.

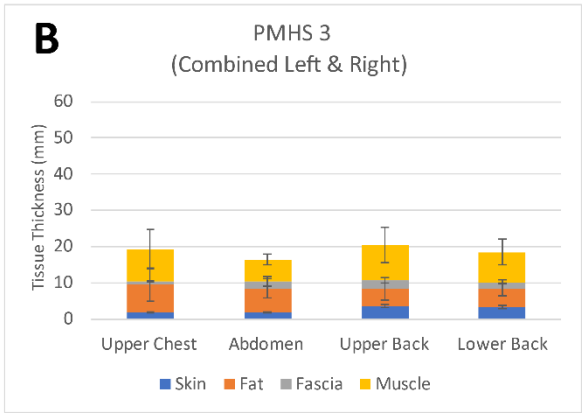
Variability of the following covariates is presented: (a) Local Skin Shear Wave Velocity is the continuous shear wave velocity of the skin layer, (b) Local Fat Shear Wave Velocity is the continuous shear wave velocity of the fat layer, (c) Local Fascia Shear Wave Velocity is the continuous shear wave velocity of the fascia layer, and (d) Local Muscle Shear Wave Velocity is the continuous shear wave velocity of the muscle layer.

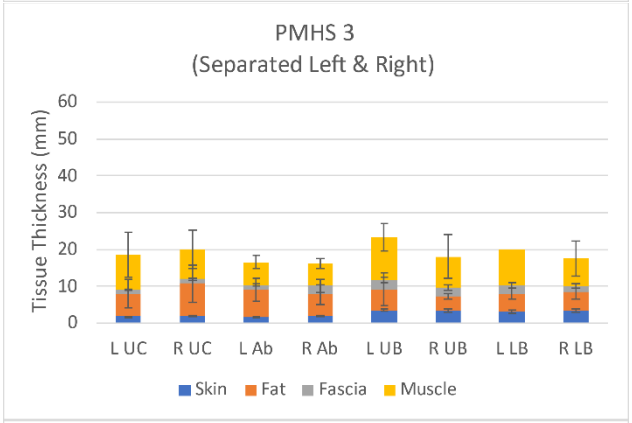
Appendix 5: PMHS Tissue Thickness

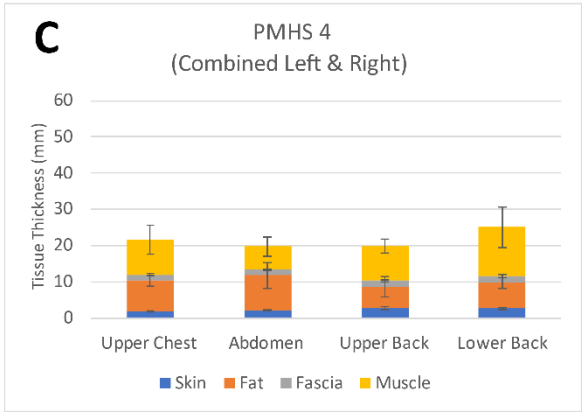
Stacked bar charts of mean tissue thickness are presented to show intra-subject and inter-subject variations between the body regions.











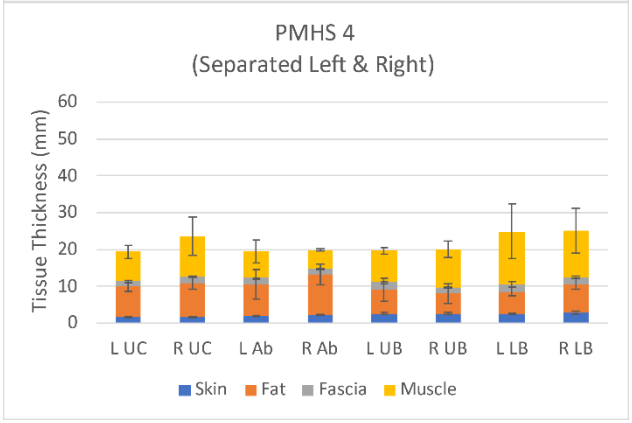




Figure A5-72: Intra-subject comparison of mean tissue thickness per PMHS body region.

Bar charts represent the mean thickness of each tissue layer at each body region for both combined and separated left & right regions for (a) PMHS 2, (b) PMHS 3, (c) PMHS 4, (d) PMHS 5, and (e) PMHS 6. Error bars represent 1 SD. UC = Upper Chest, Ab = Abdomen, UB = Upper Back, and LB = Lower Back. L = Left and R = Right.

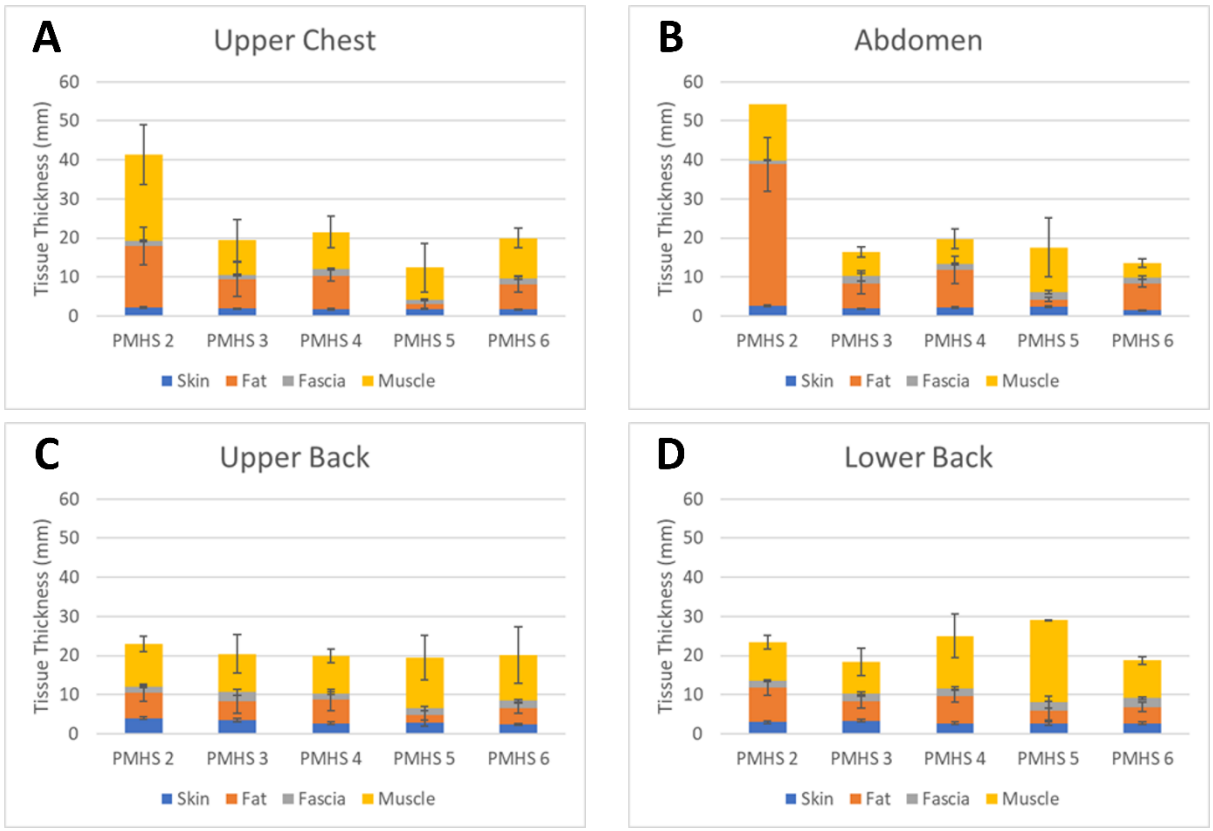
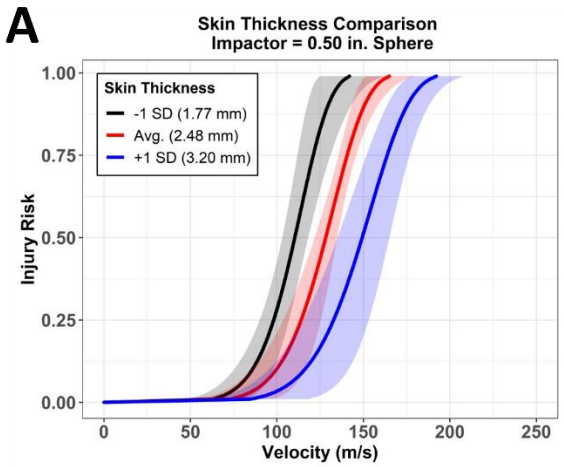


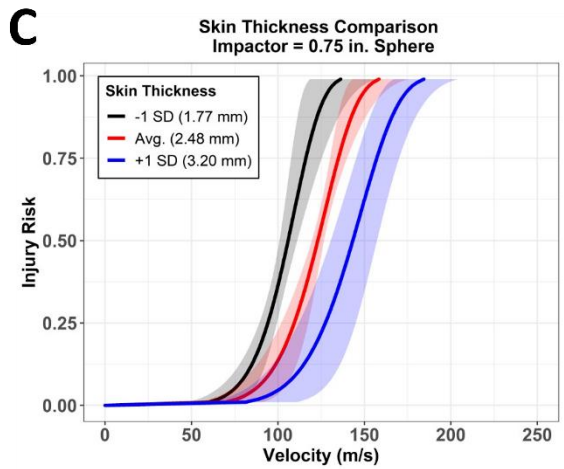
Figure A5-73: Comparison of variations in subject-level tissue thickness at each PMHS body region. Bar charts represent the mean tissue layer thickness with error bars of 1 SD for the (a) Upper Chest, (b) Abdomen, (c) Upper Back, and (d) Lower Back.

Appendix 6: PMHS Model 1 Covariate Comparisons

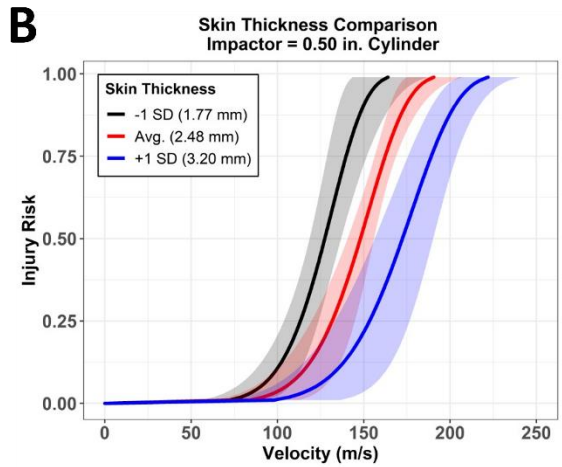
The following figures present comparisons of model covariates for PMHS Model 1. These covariates include Local Skin Thickness, Impactor Shape, and Impactor Diameter. Additionally, Body Region is compared as a factor of Local Skin Thickness by comparing the average skin thickness at each PMHS body region.

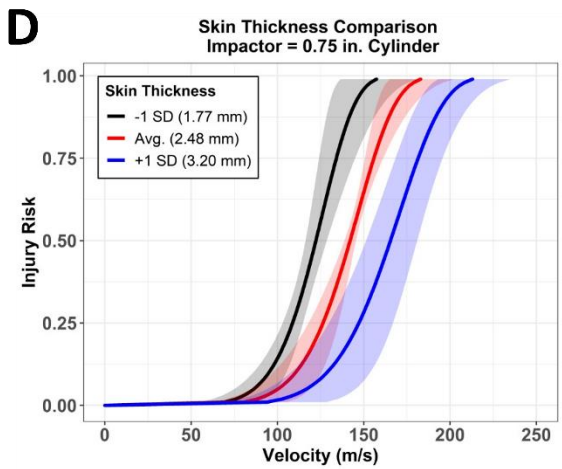
Impactor Shape = Sphere





Impactor Shape = Cylinder





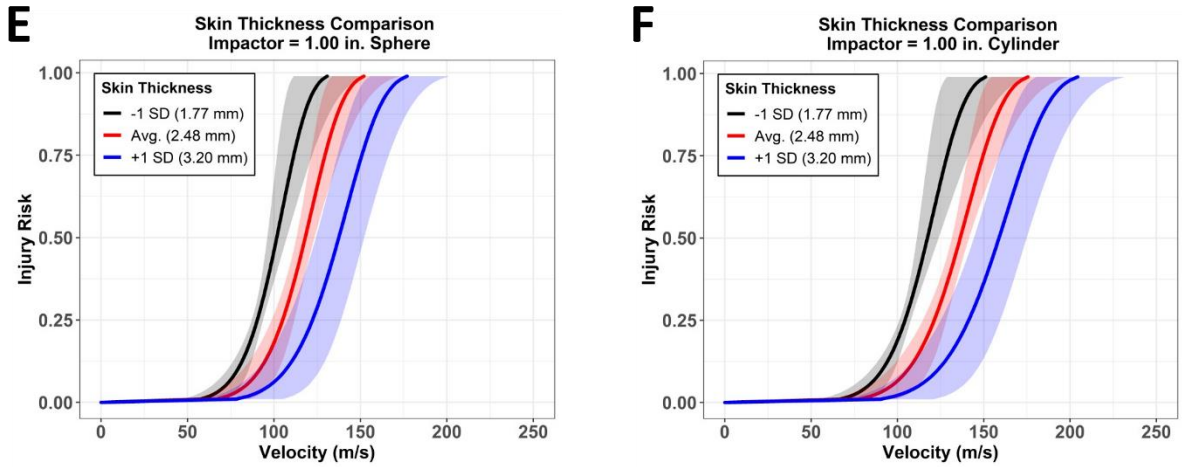
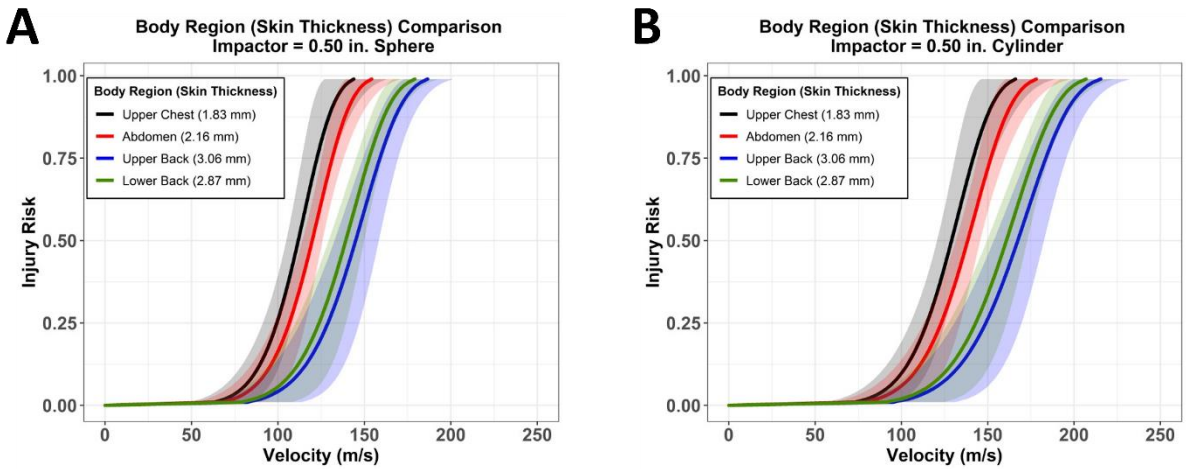


Figure A6-74: Comparison of Local Skin Thickness effects (PMHS Model 1).

The model fit was predicted at three skin thickness levels (1.77 mm, 2.48 mm, and 3.20 mm) representing the average thickness ± 1 SD of the six PMHS. Corridors represent the 95% confidence interval for each predicted IRF. Every tested combination of Impactor Shape and Diameter was assessed: (a) 0.50 in. Sphere, (b) 0.50 in. Cylinder, (c) 0.75 in. Sphere, (d) 0.75 in. Cylinder, (e) 1.00 in. Sphere, and (f) 1.00 in. Cylinder.

Impactor Shape = Sphere **Impactor Shape = Cylinder**



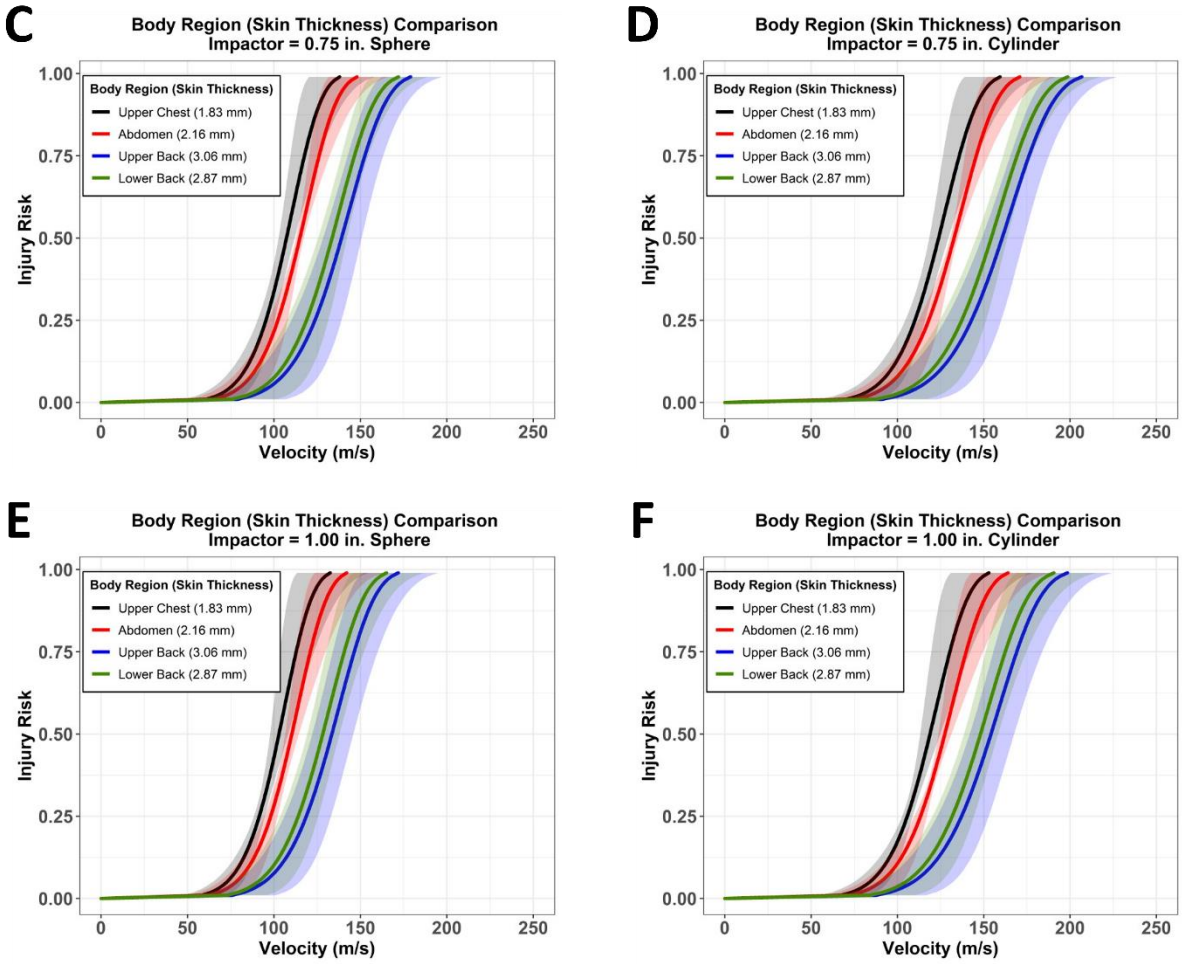


Figure A6-75: Comparison of Body Region effects (PMHS Model 1).

The model fit was predicted at four skin thickness levels (1.83 mm, 2.16 mm, 3.06 mm, and 2.87 mm) representing the average thickness of each body region (Upper Chest, Abdomen, Upper Back, and Lower Back, respectively) for the six PMHS. Corridors represent the 95% confidence interval for each predicted IRF. Every tested combination of Impactor Shape and Diameter was assessed: (a) 0.50 in. Sphere, (b) 0.50 in. Cylinder, (c) 0.75 in. Sphere, (d) 0.75 in. Cylinder, (e) 1.00 in. Sphere, and (f) 1.00 in. Cylinder.

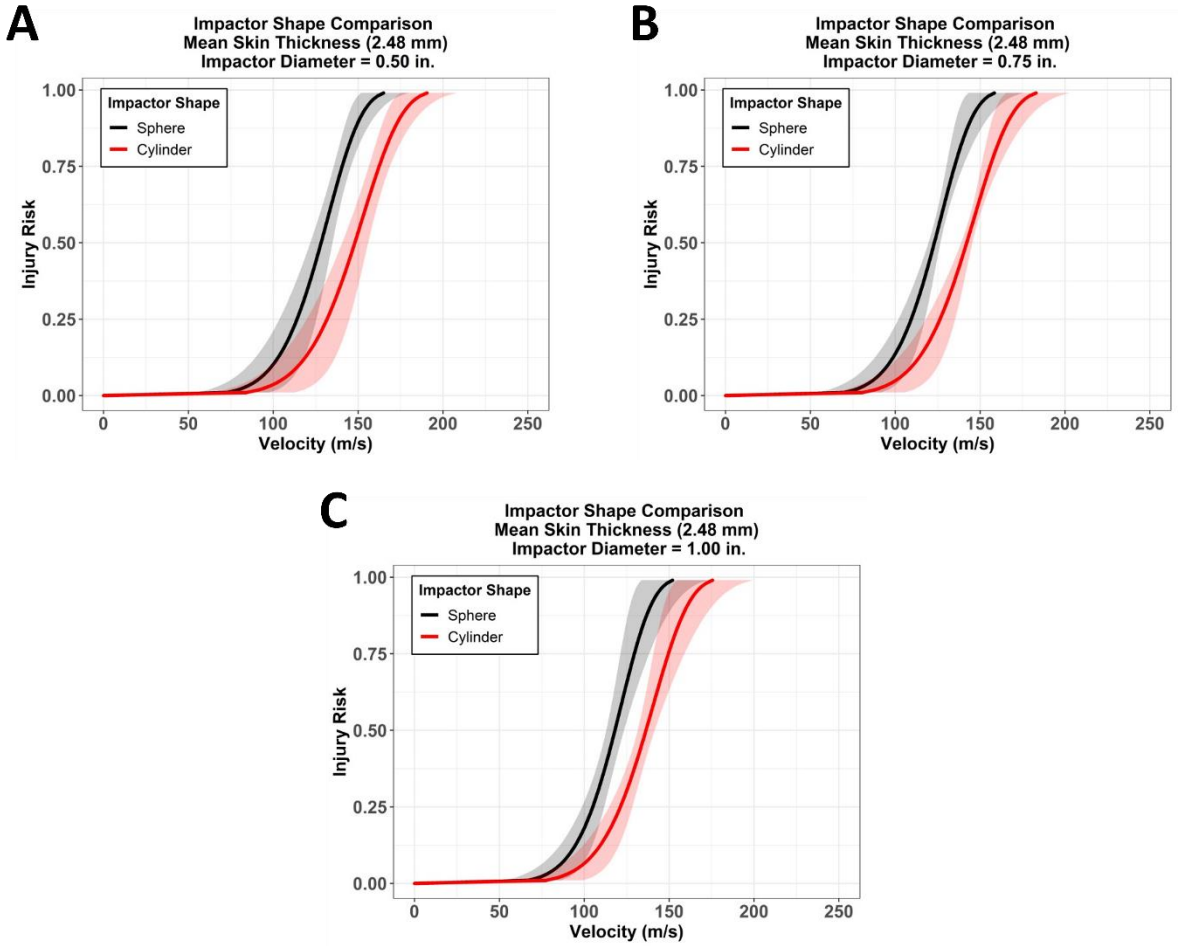


Figure A6-76: Comparison of Impactor Shape effects (PMHS Model 1, mean skin thickness).

The model fit was predicted for both impactor shapes (Sphere and Cylinder) at the mean PMHS skin thickness (2.48 mm). Corridors represent the 95% confidence interval for each predicted IRF. The comparison was assessed for each tested impactor diameter: (a) 0.50 in., (b) 0.75 in., and (c) 1.00 in.

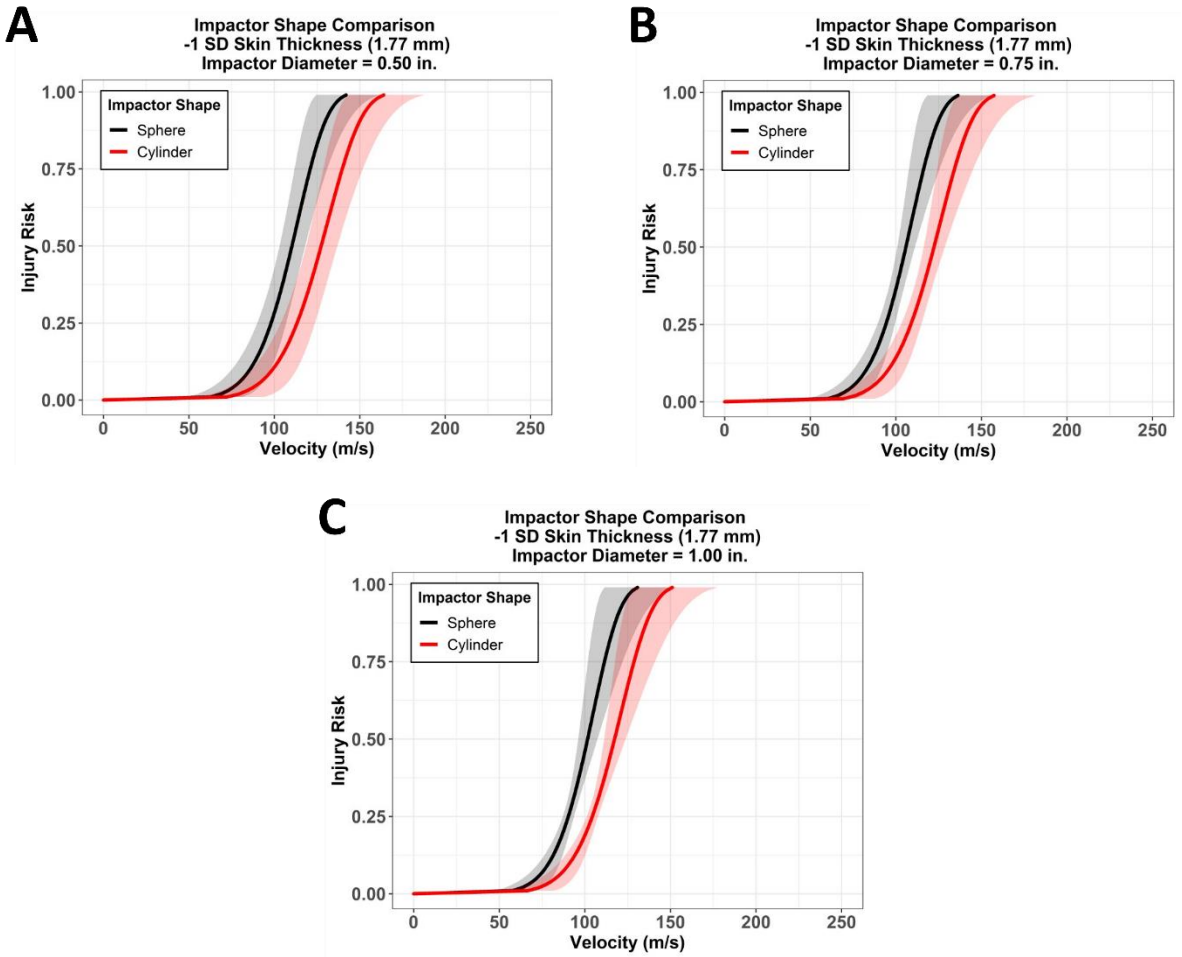


Figure A6-77: Comparison of Impactor Shape effects (PMHS Model 1, -1 SD skin thickness).

The model fit was predicted for both shapes (Sphere and Cylinder) at the -1 SD PMHS skin thickness (1.77 mm). Corridors represent the 95% confidence interval for each predicted IRF. The comparison was assessed for each tested impactor diameter: (a) 0.50 in., (b) 0.75 in., and (c) 1.00 in.

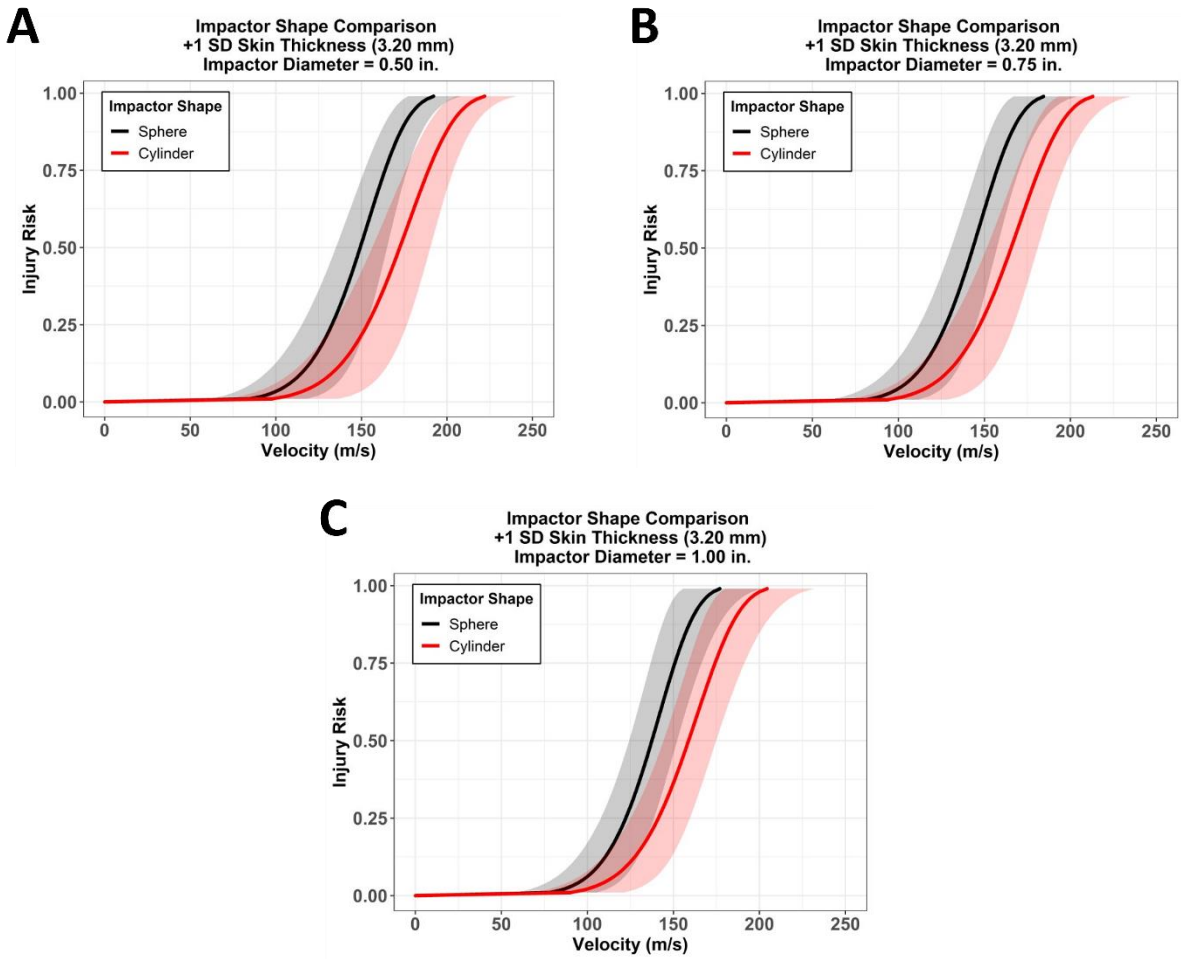


Figure A6-78: Comparison of Impactor Shape effects (PMHS Model 1, +1 SD skin thickness).

The model fit was predicted for both shapes (Sphere and Cylinder) at the +1 SD PMHS skin thickness (3.20 mm). Corridors represent the 95% confidence interval for each predicted IRF. The comparison was assessed for each tested impactor diameter: (a) 0.50 in., (b) 0.75 in., and (c) 1.00 in.

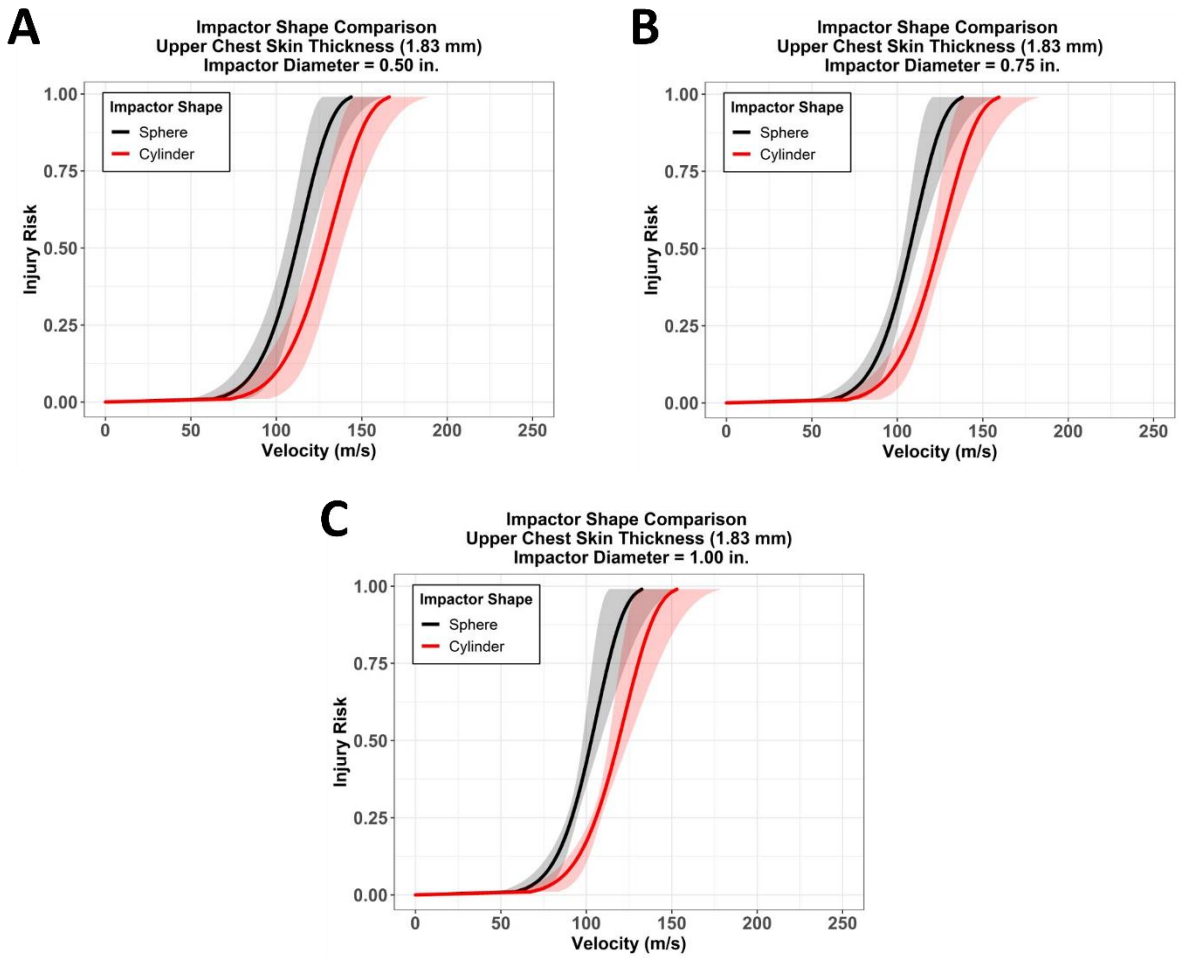


Figure A6-79: Comparison of Impactor Shape effects (PMHS Model 1, Upper Chest skin thickness).

The model fit was predicted for both shapes (Sphere and Cylinder) at the mean Upper Chest skin thickness (1.83 mm). Corridors represent the 95% confidence interval for each predicted IRF. The comparison was assessed for each tested impactor diameter: (a) 0.50 in., (b) 0.75 in., and (c) 1.00 in.

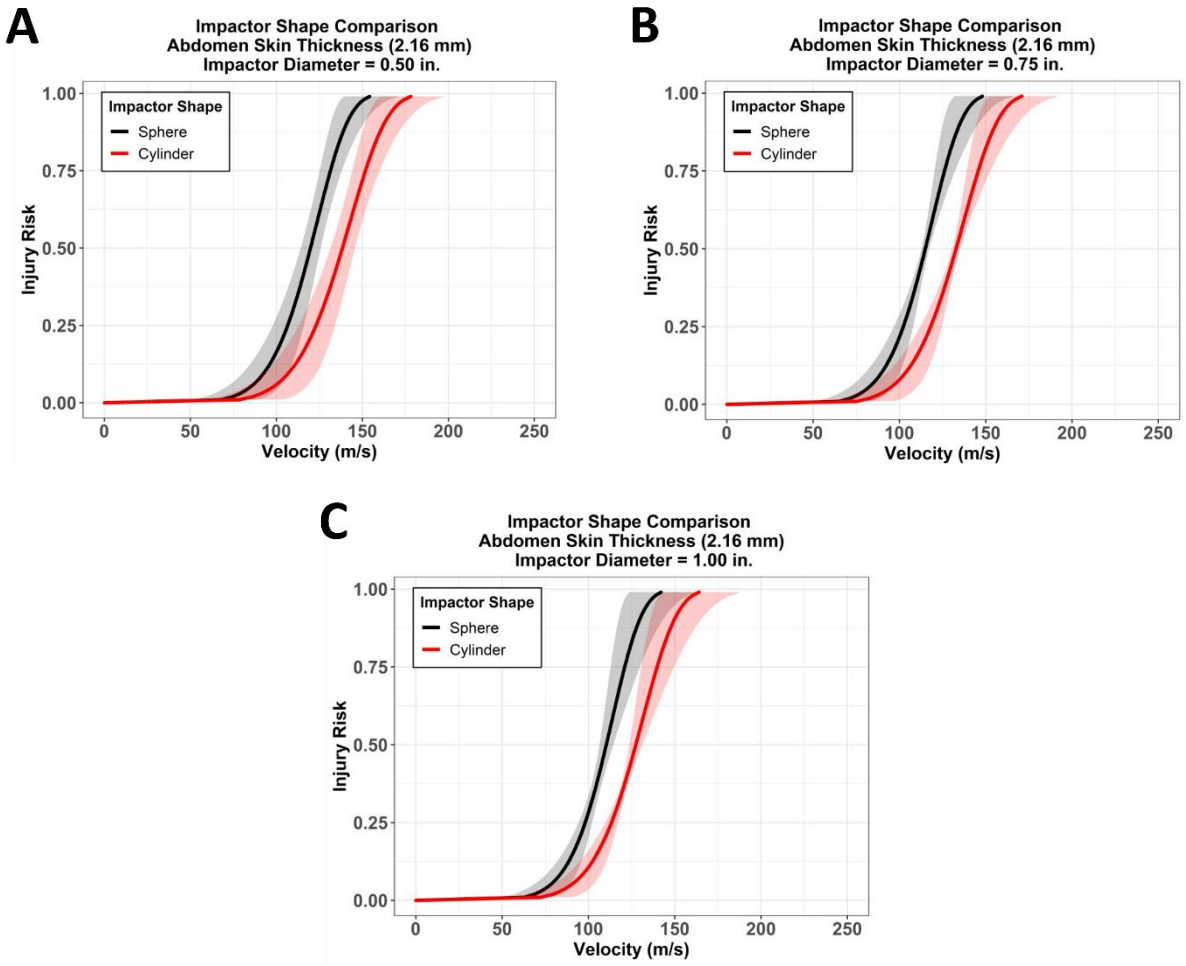


Figure A6-80: Comparison of Impactor Shape effects (PMHS Model 1, Abdomen skin thickness).

The model fit was predicted for both shapes (Sphere and Cylinder) at the mean Abdomen skin thickness (2.16 mm). Corridors represent the 95% confidence interval for each predicted IRF. The comparison was assessed for each tested impactor diameter: (a) 0.50 in., (b) 0.75 in., and (c) 1.00 in.

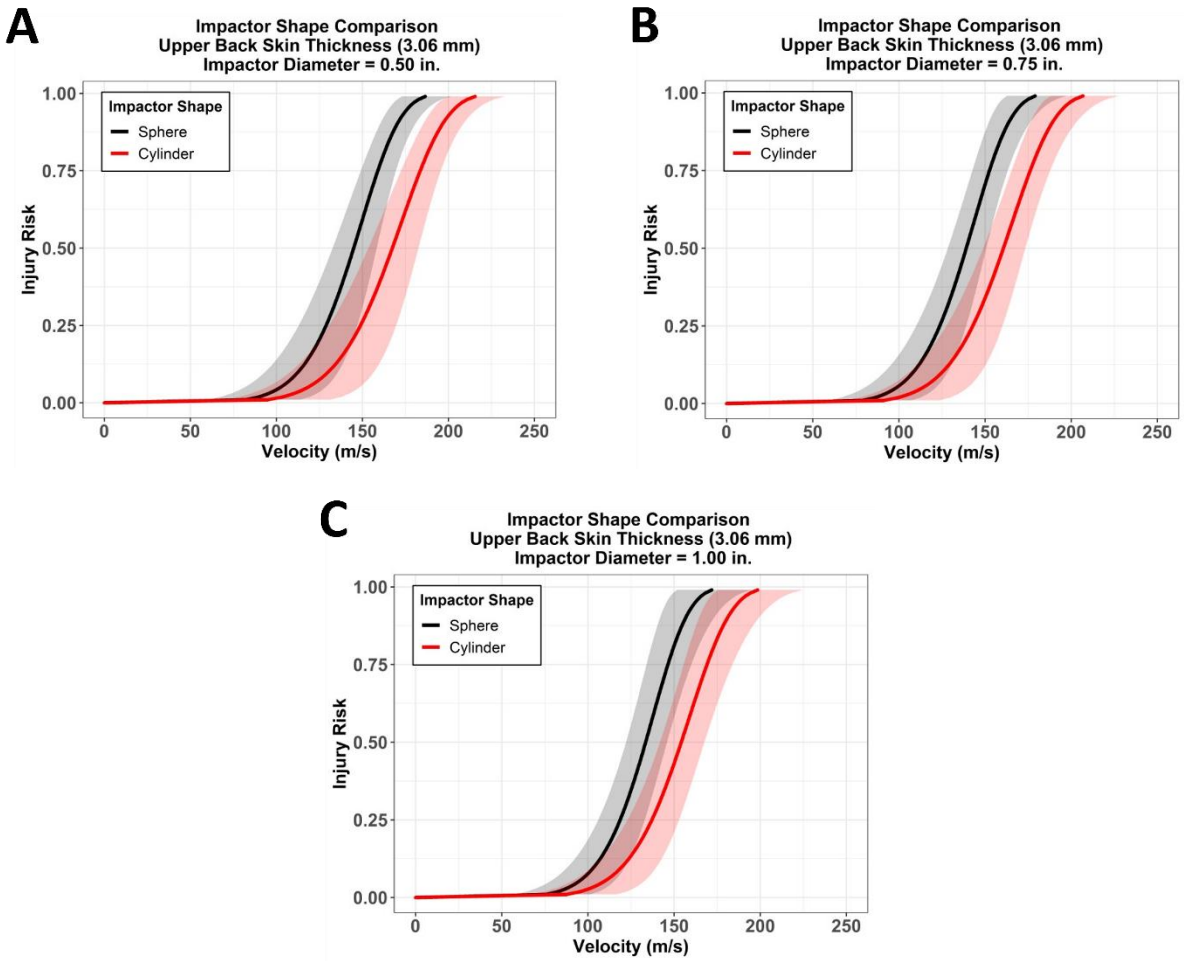


Figure A6-81: Comparison of Impactor Shape effects (PMHS Model 1, Upper Back skin thickness).

The model fit was predicted for both shapes (Sphere and Cylinder) at the mean Upper Back skin thickness (3.06 mm). Corridors represent the 95% confidence interval for each predicted IRF. The comparison was assessed for each tested impactor diameter: (a) 0.50 in., (b) 0.75 in., and (c) 1.00 in.

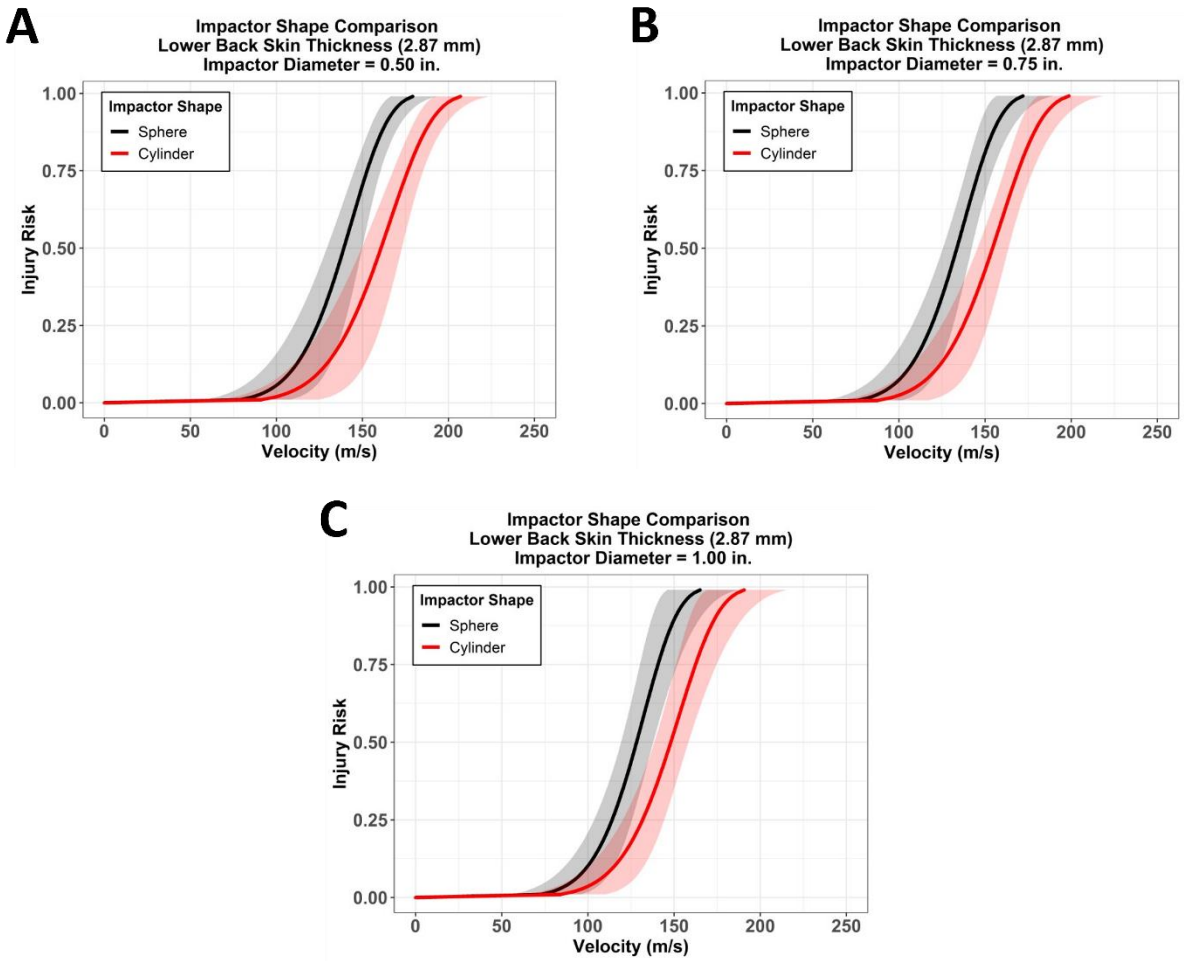


Figure A6-82: Comparison of Impactor Shape effects (PMHS Model 1, Lower Back skin thickness).

The model fit was predicted for both shapes (Sphere and Cylinder) at the mean Lower Back skin thickness (2.87 mm). Corridors represent the 95% confidence interval for each predicted IRF. The comparison was assessed for each tested impactor diameter: (a) 0.50 in., (b) 0.75 in., and (c) 1.00 in.

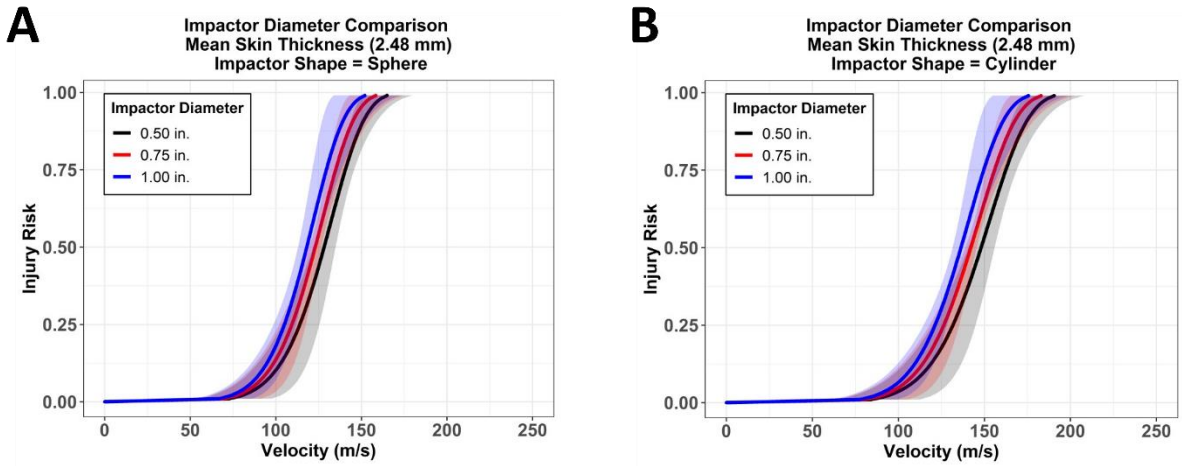


Figure A6-83: Comparison of Impactor Diameter effects (PMHS Model 1, mean skin thickness).

The model fit was predicted for three diameters (0.50 in., 0.75 in., and 1.00 in.) at the mean PMHS skin thickness (2.48 mm). Corridors represent the 95% confidence interval for each predicted IRF. The comparison was assessed for both tested impactor shapes: (a) Sphere and (b) Cylinder.

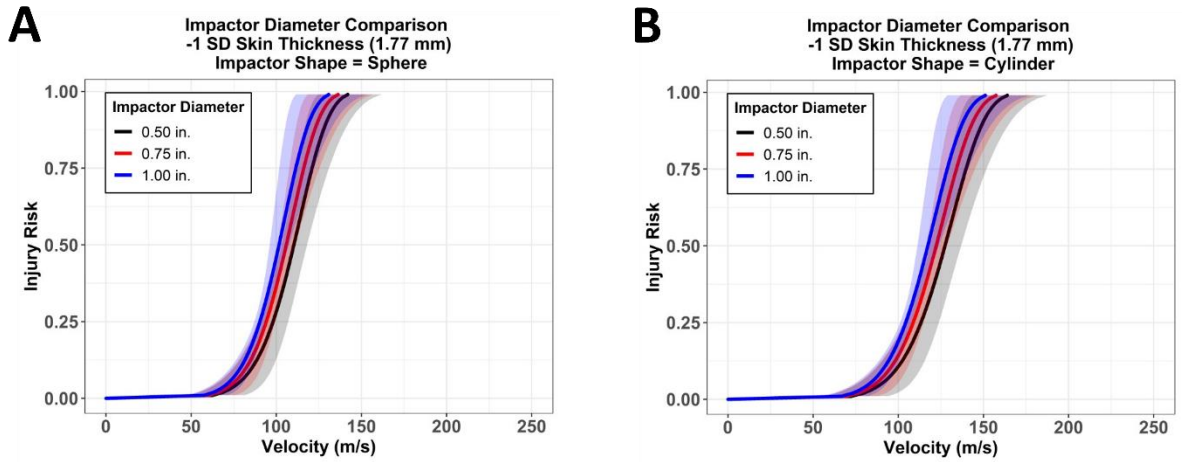


Figure A6-84: Comparison of Impactor Diameter effects (PMHS Model 1, -1 SD skin thickness).

The model fit was predicted for three diameters (0.50 in., 0.75 in., and 1.00 in.) at the -1 SD PMHS skin thickness (1.77 mm). Corridors represent the 95% confidence interval for each predicted IRF. The comparison was assessed for both tested impactor shapes: (a) Sphere and (b) Cylinder.

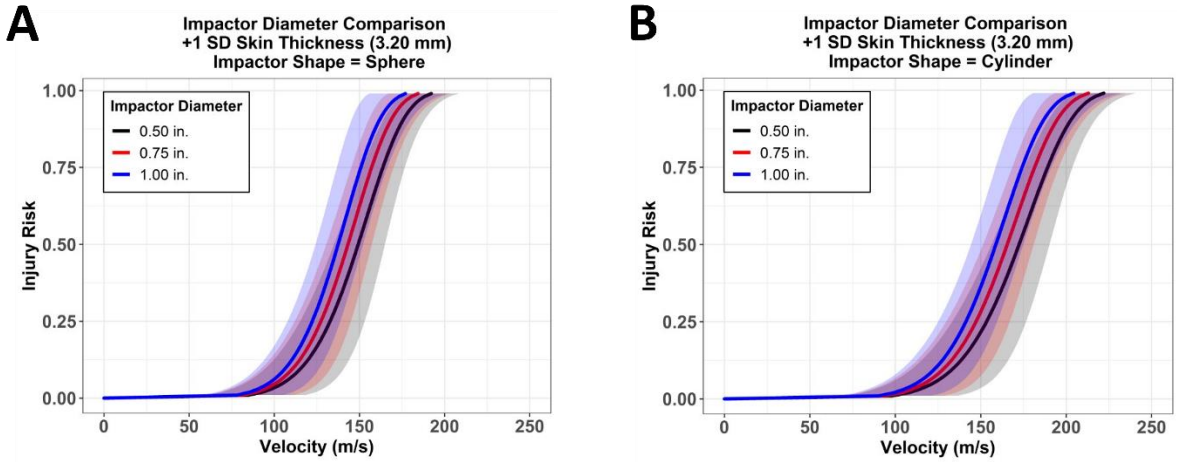


Figure A6-85: Comparison of Impactor Diameter effects (PMHS Model 1, +1 SD skin thickness).

The model fit was predicted for three diameters (0.50 in., 0.75 in., and 1.00 in.) at the +1 SD PMHS skin thickness (3.20 mm). Corridors represent the 95% confidence interval for each predicted IRF. The comparison was assessed for both tested impactor shapes: (a) Sphere and (b) Cylinder.

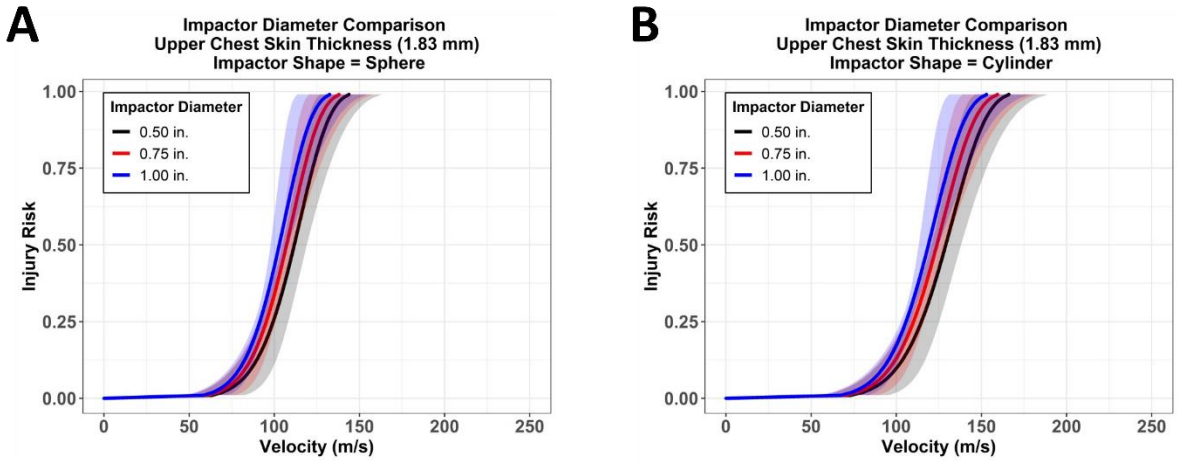


Figure A6-86: Comparison of Impactor Diameter effects (PMHS Model 1, Upper Chest skin thickness).

The model fit was predicted for three diameters (0.50 in., 0.75 in., and 1.00 in.) at the mean Upper Chest skin thickness (1.83 mm). Corridors represent the 95% confidence interval for each predicted IRF. The comparison was assessed for both tested impactor shapes: (a) Sphere and (b) Cylinder.

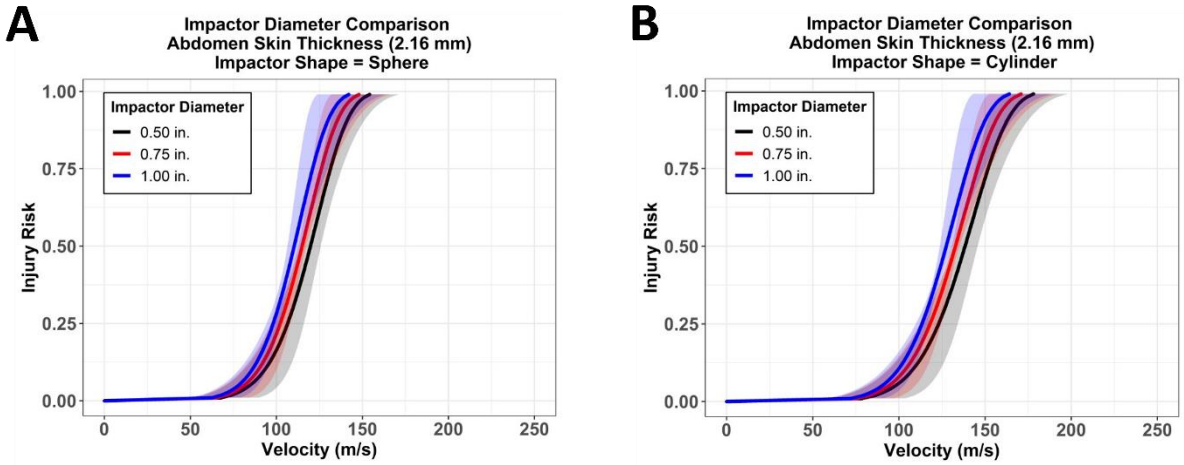


Figure A6-87: Comparison of Impactor Diameter effects (PMHS Model 1, Abdomen skin thickness). The model fit was predicted for three diameters (0.50 in., 0.75 in., and 1.00 in.) at the mean Abdomen skin thickness (2.16 mm). Corridors represent the 95% confidence interval for each predicted IRF. The comparison was assessed for both tested impactor shapes: (a) Sphere and (b) Cylinder.

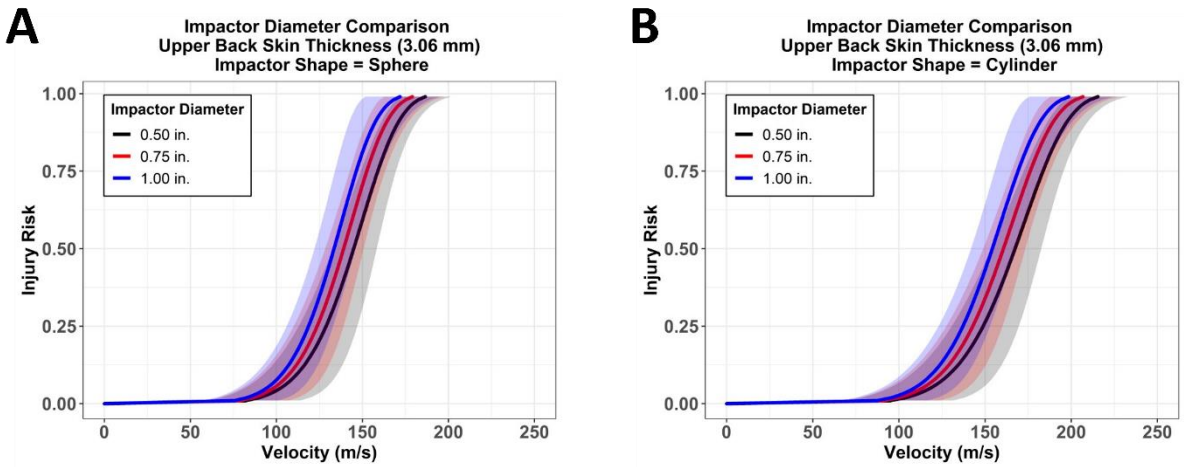


Figure A6-88: Comparison of Impactor Diameter effects (PMHS Model 1, Upper Back skin thickness). The model fit was predicted for three diameters (0.50 in., 0.75 in., and 1.00 in.) at the mean Upper Back skin thickness (3.06 mm). Corridors represent the 95% confidence interval for each predicted IRF. The comparison was assessed for both tested impactor shapes: (a) Sphere and (b) Cylinder.

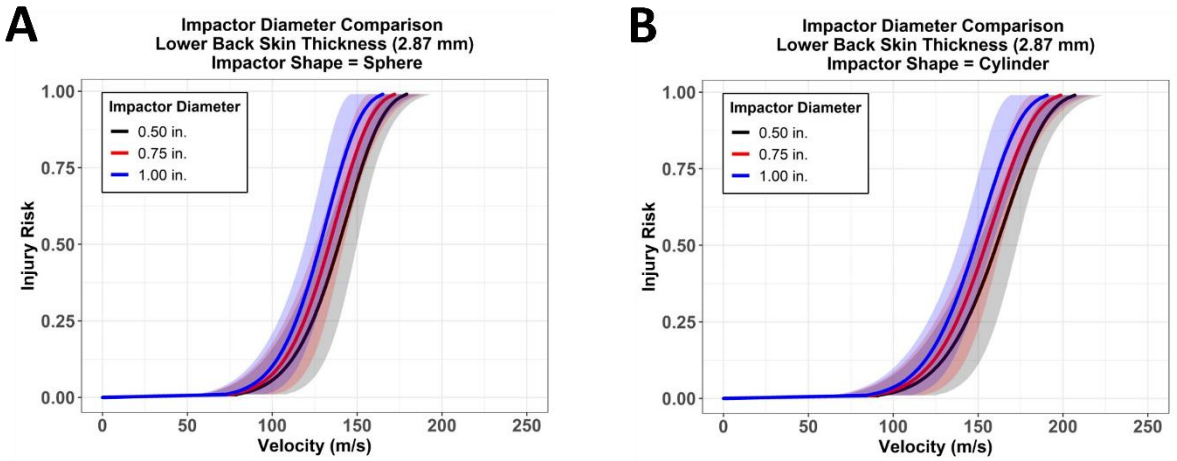


Figure A6-89: Comparison of Impactor Diameter effects (PMHS Model 1, Lower Back skin thickness). The model fit was predicted for three diameters (0.50 in., 0.75 in., and 1.00 in.) at the mean Lower Back skin thickness (2.87 mm). Corridors represent the 95% confidence interval for each predicted IRF. The comparison was assessed for both tested impactor shapes: (a) Sphere and (b) Cylinder.

Appendix 7: PMHS Model 2 Covariate Comparisons

The following figures present comparisons of model covariates for PMHS Model 2. These covariates include Local Skin Thickness and Impactor Shape. Additionally, Body Region is compared as a factor of Local Skin Thickness by comparing the average skin thickness at each PMHS body region.

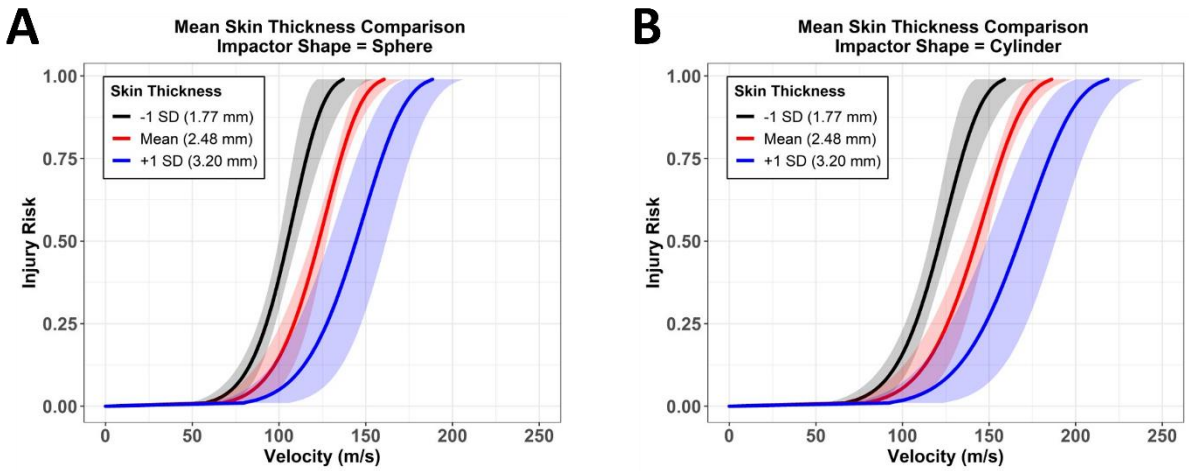


Figure A7-90: Comparison of Skin Thickness effects (PMHS Model 2).

The model fit was predicted for three skin thicknesses (1.77 mm, 2.48 mm, and 3.20 mm) representing the mean ± 1 SD PMHS skin thickness. Corridors represent the 95% confidence interval for each predicted IRF. The comparison was assessed for both tested impactor shapes: (a) Sphere and (b) Cylinder.

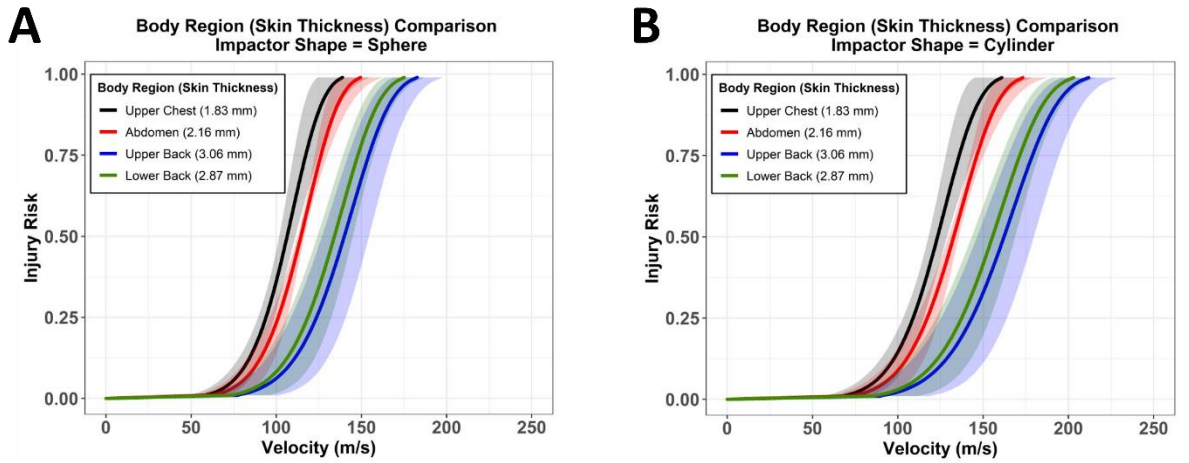


Figure A7-91: Comparison of Body Region effects (PMHS Model 2).

The model fit was predicted for four skin thicknesses (1.83 mm, 2.16 mm, 3.06 mm, and 2.87 mm) representing the mean skin thickness for each body region (Upper Chest, Abdomen, Upper Back, and Lower Back, respectively). Corridors represent the 95% confidence interval for each predicted IRF. The comparison was assessed for both tested impactor shapes: (a) Sphere and (b) Cylinder.

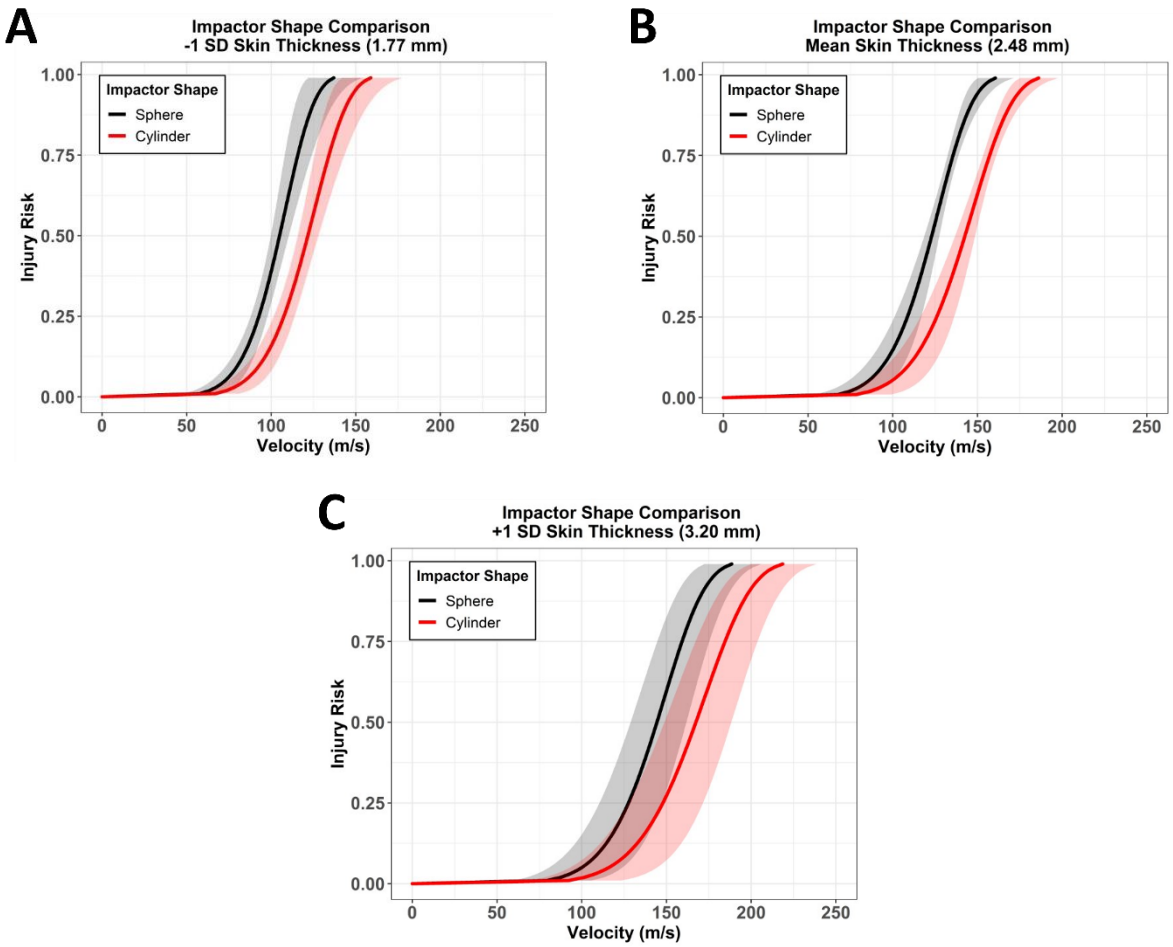


Figure A7-92: Comparison of Impactor Shape effects (PMHS Model 2, mean skin thickness).

The model fit was predicted for both impactor shapes (Sphere and Cylinder). Corridors represent the 95% confidence interval for each predicted IRF. The comparison was assessed at three skin thicknesses: (a) -1 SD (1.77 mm), (b) mean (2.48 mm), and (c) +1 SD (3.20 mm).

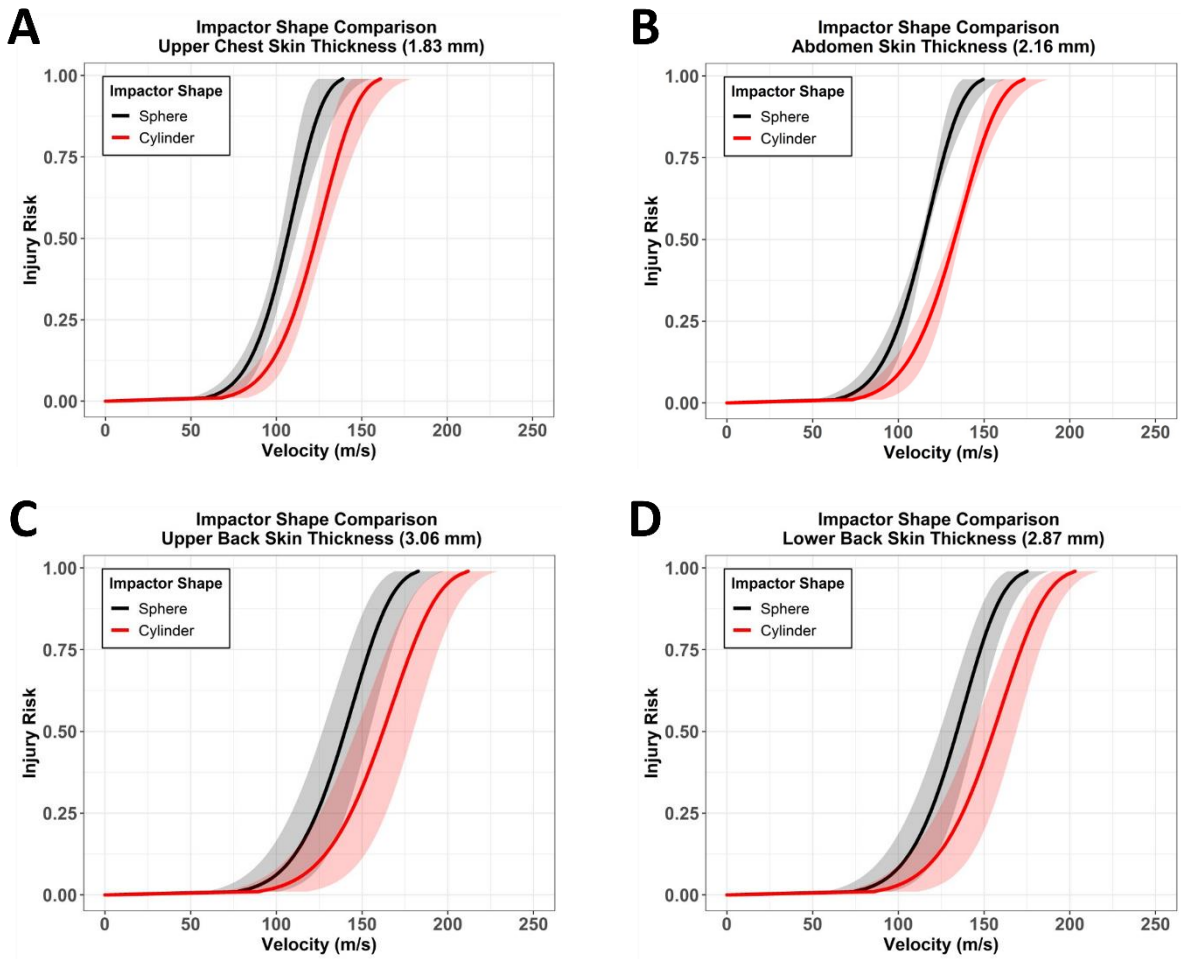


Figure A7-93: Comparison of Impactor Shape effects (PMHS Model 2, regional skin thickness).

The model fit was predicted for both impactor shapes (Sphere and Cylinder). Corridors represent the 95% confidence interval for each predicted IRF. The comparison was assessed at four skin thicknesses based on each body region: (a) Upper Chest (1.83 mm), (b) Abdomen (2.16 mm), (c) Upper Back (3.06 mm), and (d) Lower back (2.87 mm).

Appendix 8: PMHS Model 3 Covariate Comparisons

The following figures present comparisons of the sole model covariate for PMHS Model 3, Local Skin Thickness. Additionally, Body Region is compared as a factor of Local Skin Thickness by comparing the average skin thickness at each PMHS body region.

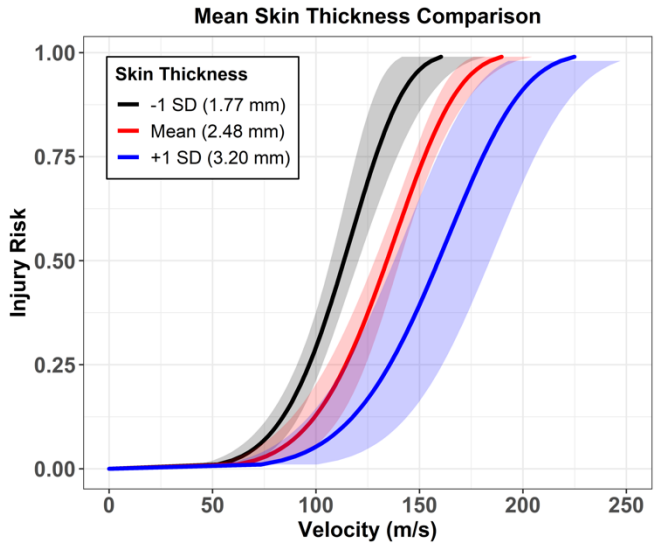


Figure A8-94: Comparison of Skin Thickness effects (PMHS Model 3).

The model fit was predicted for three skin thickness levels (1.77 mm, 2.48 mm, and 3.20 mm) representing the mean PMHS skin thickness ± 1 SD. Corridors represent the 95% confidence interval for each predicted IRF.

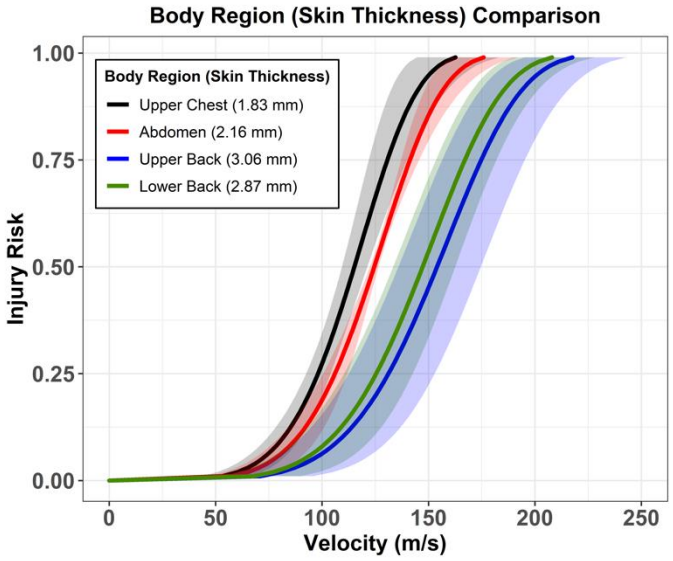


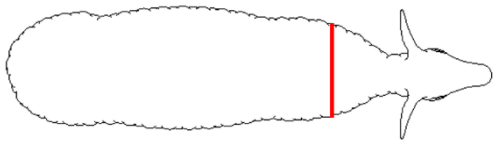
Figure A8-95: Comparison of Body Region effects (PMHS Model 3).

The model fit was predicted for four skin thickness levels (1.83 mm, 2.16 mm, 3.06 mm, and 2.87 mm) representing the mean thickness of each body region (Upper Chest, Abdomen, Upper Back, and Lower Back, respectively) for the six PMHS. Corridors represent the 95% confidence interval for each predicted IRF.

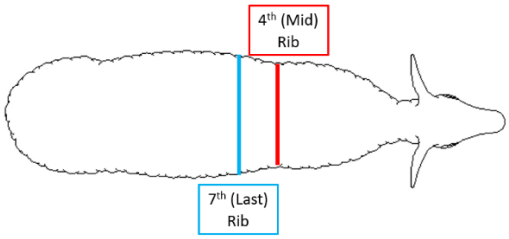
Appendix 9: Ovine Anthropometry Instructions

The following anthropometry measurements were collected for each of the ovine specimen.

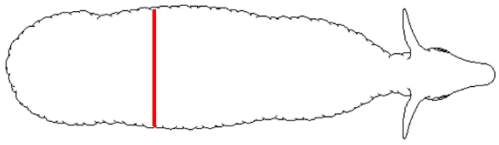
Shoulder Breadth:
The breadth of the specimen's shoulders, as measured near the center of the Shoulder body region. Measured with calipers.



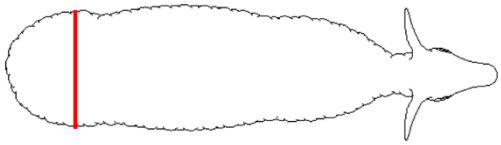
Chest Breadth:
The breadth of the specimen's chest, measured at the 4th (mid) rib and 7th (last) rib. Measured with calipers.



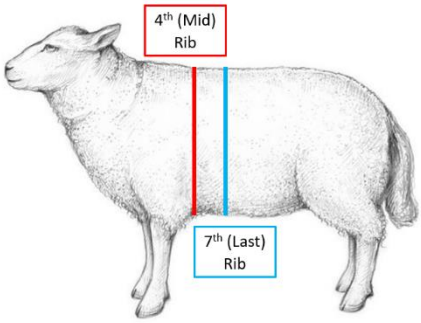
Stomach Breadth:
The breadth of the specimen's stomach, as measured near the center of the Stomach body region. This region was defined as posterior to the ribcage and anterior to the pelvis. Measured with calipers.



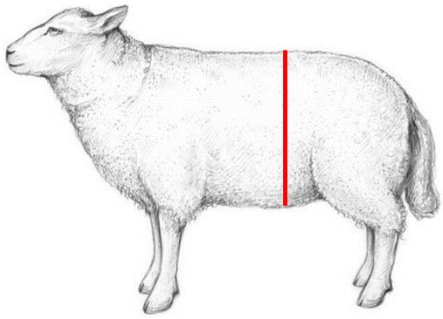
Rump Breadth:
The breadth of the specimen's rump, as measured near the center of the Rump body region. Measured with calipers.



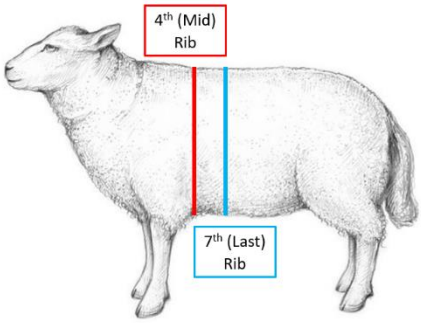
Chest Depth:
The depth of the specimen's chest, measured at the 4th (mid) rib and 7th (last) rib. Measured with calipers.



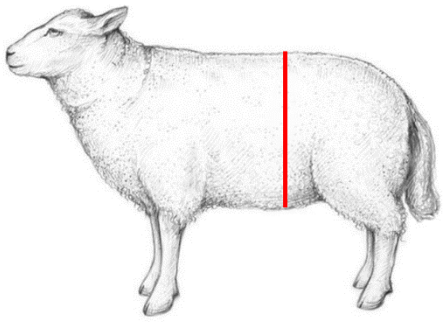
Stomach Depth:
The depth of the specimen's stomach, as measured near the center of the Stomach body region. Measured with calipers.



Chest Circumference:
The circumference of the specimen's chest, measured at the 4th (mid) rib and 7th (last) rib. Measurements were made perpendicular to the long axis of the trunk using measuring tape.



Stomach Circumference:
The circumference of the specimen's stomach, as measured near the center of the Stomach impact body region. Measurements were made perpendicular to the long axis of the trunk using measuring tape.



Appendix 10: Ovine Impact Descriptions

The following tables provide details of each Ovine impact test, such as the impacted body region, surface temperature, internal temperature, velocity, and binary injury result. Further details on the injury severity from each test are provided in Appendix 11, with corresponding impact numbers.

Table A10-LXXXVIII: Ovine 1 (Fresh/Lab Temp Flank) Impact Descriptions

Impact	Body Region	Surface Temp. (°F)	Internal Temp. (°F)	Impactor Velocity (m/s)	Skin Penetration (> 5mm)
1	Shoulder	73		120.10	No
2		69.9		136.43	No
3		73.8		143.03	Yes
4		75.5		133.25	Yes
5		76		121.50	No
6	Ribs	77.4		123.06	Yes
7		78.5		105.72	No
8		76.9		120.84	Yes
9		76.2		107.50	No
10		77.9		87.94	No
11	Stomach	74.6		119.94	No
12		75.5		132.62	Yes
13		75.8		122.08	No
14		76.6		129.47	Yes
15		76.8		107.75	No
16	Rump	75.8		119.30	No
17		74.9		106.69	No
18		74.6		85.82	No
19		74.6		106.81	No
20		74.4		119.57	No

Table A10-LXXXIX: Ovine 1 (Thawed/Lab Temp Flank) Impact Descriptions

Impact	Body Region	Surface Temp. (°F)	Internal Temp. (°F)	Impactor Velocity (m/s)	Skin Penetration (> 5mm)
1	Shoulder	66.5	65	121.35	No
2		66.8	65	134.33	Yes
3		65.9	65	107.81	No
4		66.8	65	135.42	Yes
5	Ribs	68.9	65	106.93	No
6		69.5	65	119.79	Yes
7		68.7	65	136.16	Yes
8		67.1	65	87.24	No
9		66.5	65	121.60	Yes
10	Stomach	71.2	66	123.70	Yes
11		71.8	66	108.42	No
12		70.4	66	89.68	No
13		69.4	66	122.46	No
14		71.6	66	134.12	No
15	Rump	68.9	66	107.55	No
16		68.8	66	123.17	No
17		69.1	66	136.18	Yes
18		67.2	66	121.28	Yes
19		68.9	66	88.41	No

Table A10-XC: Ovine 2 (Fresh/Lab Temp Flank) Impact Descriptions

Impact	Body Region	Surface Temp. (°F)	Internal Temp. (°F)	Impactor Velocity (m/s)	Skin Penetration (> 5mm)
1	Shoulder	71.1	72	120.66	Yes
2		71.6	71	107.42	Yes
3		71	71	89.53	Yes
4		70.3	71	63.43	No
5		70.9	71	65.93	No
6	Ribs	67	71	105.82	Yes
7		67.4	71	88.36	No
8		67.5	71	63.56	No
9		68.5	71	78.87	No
10		68.2	71	73.39	No
11	Stomach	69.3	70	87.41	No
12		68.5	70	107.75	No
13		68.8	70	63.68	No
14		68.9	70	97.23	No
15		68.7	70	120.64	Yes
16	Rump	69	71	86.18	No
17		68	71	106.40	Yes
18		68.2	71	62.44	No
19		67.8	71	95.86	No
20		67	71	95.06	No

Table A10-XCI: Ovine 2 (Thawed/Lab Temp Flank) Impact Descriptions

Impact	Body Region	Surface Temp. (°F)	Internal Temp. (°F)	Impactor Velocity (m/s)	Skin Penetration (> 5mm)
1	Shoulder	62.5	61	87.12	Yes
2		65.3	61	104.84	Yes
3		63.7	61	63.08	No
4		63.5	61	87.93	Yes
5		64.3	61	63.46	No
6	Ribs	64.9	61	89.00	No
7		68.2	61	105.89	No
8		68.8	61	121.12	No
9		65.1	61	61.34	No
10		69.7	61	131.88	Yes
11	Stomach	71	61	89.23	No
12		72	61	107.32	Yes
13		70.4	61	63.92	No
14		66.5	61	87.66	No
15		70.7	61	101.07	No
16	Rump	64.5	61	88.09	No
17		67.5	61	105.26	Yes
18		66.6	61	122.65	Yes
19		66.2	61	62.84	No
20		68.9	61	107.58	No

Table A10-XCII: Ovine 3 (Fresh/Lab Temp Flank) Impact Descriptions

Impact	Body Region	Surface Temp. (°F)	Internal Temp. (°F)	Impactor Velocity (m/s)	Skin Penetration (> 5mm)
1	Shoulder	55.1	51	106.94	No
2		55.5	51	85.96	No
3		57.2	51	61.58	No
4		56.4	52	86.16	No
5		58	52	100.71	No
6	Ribs	61.6	52	108.21	Yes
7		59.5	53	86.85	No
8		60.5	54	60.67	No
9		60	54	87.27	No
10		60.3	54	77.36	No
11	Stomach	64.7	56	103.44	No
12		63.4	56	85.48	No
13		63.6	56	103.04	No
14		60.9	56	117.96	No
15		63.3	56	129.20	No
16	Rump	60	54	104.46	No
17		60.8	54	86.73	No
18		58.3	54	60.42	No
19		60.4	55	119.52	No
20		60.6	55	130.97	Yes

Table A10-XCIII: Ovine 3 (Thawed/Lab Temp Flank) Impact Descriptions

Impact	Body Region	Surface Temp. (°F)	Internal Temp. (°F)	Impactor Velocity (m/s)	Skin Penetration (> 5mm)
1	Shoulder	59.8	61	86.61	No
2		61.9	61	103.12	No
3		61.0	61	117.81	Yes
4		61.5	61	131.01	Yes
5		61.1	61	60.62	No
6	Ribs	63.1	61	85.47	No
7		66.1	61	106.51	No
8		64.7	61	118.53	No
9		61.8	61	132.15	No
10		62.9	61	144.60	Yes
11	Stomach	69	62	118.20	No
12		68.1	62	130.52	No
13		68.8	62	141.20	Yes
14		68.3	62	104.04	No
15		66.8	63	130.10	No
16	Rump	61.8	61	118.75	No
17		65.9	61	131.91	No
18		63.5	61	142.90	No
19		62.4	62	155.64	Yes
20		63.7	62	141.57	No

Table A10-XCIV: Ovine 4 (Fresh/Lab Temp Flank) Impact Descriptions

Impact	Body Region	Surface Temp. (°F)	Internal Temp. (°F)	Impactor Velocity (m/s)	Skin Penetration (> 5mm)
1	Shoulder	65.2	60	104.34	No
2		67.3	60	123.24	Yes
3		66.9	60	88.70	No
4		63.9	60	133.36	No
5		67.9	60	121.52	No
6	Ribs	69.4	61	105.82	Yes
7		68.7	61	89.12	No
8		68.9	61	109.26	Yes
9		66.8	61	62.04	No
10		68	61	119.80	No
11	Stomach	69.9	63	108.35	No
12		69.9	63	121.33	No
13		70.3	63	130.66	Yes
14		70	63	85.62	No
15		69.8	63	61.21	No
16	Rump	66.1	62	121.92	No
17		66.9	62	108.13	No
18		67	62	88.01	No
19		64.9	62	62.34	No
20		65.4	62	134.67	Yes

Table A10-XCV: Ovine 4 (Fresh/Warmed Flank) Impact Descriptions

Impact	Body Region	Surface Temp. (°F)	Internal Temp. (°F)	Impactor Velocity (m/s)	Skin Penetration (> 5mm)
1	Shoulder	96.5	83	105.79	No
2		100.3	83	118.65	No
3		96.5	83	133.20	No
4		94.2	83	88.05	No
5		96.5	82	147.12	Yes
6	Ribs	90.9	82	103.98	No
7		90.4	82	87.81	No
8		91.9	82	62.33	No
9		92.5	82	105.86	No
10		93.2	82	121.69	No
11	Stomach	86.6	81	120.79	No
12		85.4	81	131.51	Yes
13		86.2	81	105.21	Yes
14		86.5	81	87.48	No
15		85.3	81	62.02	No
16	Rump	81.6	82	119.00	No
17		83.1	82	132.63	No
18		83.1	82	144.96	No
19		83.5	82	154.39	Yes
20		83.6	81	106.11	No

Table A10-XCVI: Ovine 5 (Fresh/Lab Temp Flank) Impact Descriptions

Impact	Body Region	Surface Temp. (°F)	Internal Temp. (°F)	Impactor Velocity (m/s)	Skin Penetration (> 5mm)
1	Shoulder	65.6	67	104.87	No
2		66.6	67	87.76	No
3		65.9	67	120.92	Yes
4		65.6	67	63.47	No
5		66.3	67	105.42	No
6	Ribs	68.9	67	104.24	No
7		67.9	67	120.24	Yes
8		68.7	67	88.52	No
9		68	67	62.66	No
10		68.8	67	105.89	No
11	Stomach	71.6	68	105.35	No
12		72.7	68	121.33	Yes
13		72.8	68	86.69	No
14		72.3	68	62.16	No
15		73.7	68	107.43	No
16	Rump	67.3	68	106.78	No
17		68.5	68	120.12	Yes
18		68.7	68	86.63	No
19		68.7	68	62.11	No
20		68.9	68	105.17	No

Table A10-XCVII: Ovine 5 (Fresh/Warmed Flank) Impact Descriptions

Impact	Body Region	Surface Temp. (°F)	Internal Temp. (°F)	Impactor Velocity (m/s)	Skin Penetration (> 5mm)
1	Shoulder	99.3	90	104.93	No
2		106.7	90	120.73	Yes
3		99.8	90	87.97	No
4		91.4	90	64.02	No
5		98.5	90	107.78	Yes
6	Ribs	96.9	90	106.81	Yes
7		99.6	90	87.50	No
8		96.4	90	63.53	No
9		98.3	90	105.78	Yes
10*	Stomach	95.4*	89*	104.29*	Yes*
11*		94.2*	89*	87.62*	No*
12*		93.1*	89*	62.41*	No*
13*		92.6*	89*	62.10*	Yes*
14*		90.5*	89*	49.02*	Yes*
15	Rump	90.4	90	106.55	No
16		83.6	90	121.27	No
17		89.3	90	132.62	No
18		91	89	146.63	Yes
19		86.5	89	130.50	Yes

*Datapoint is excluded from analysis due to overheating of the tissue.

Table A10-XCVIII: Ovine 6 (Fresh/Lab Temp Flank) Impact Descriptions

Impact	Body Region	Surface Temp. (°F)	Internal Temp. (°F)	Impactor Velocity (m/s)	Skin Penetration (> 5mm)
1	Shoulder	64.8	65	108.35	Yes
2		66.2	65	89.14	No
3		66.1	65	63.42	No
4		64.6	65	88.68	No
5		66	65	106.70	No
6	Ribs	69.2	66	106.56	No
7		67.2	66	124.91	Yes
8		68.9	66	88.63	No
9		68.3	66	62.15	No
10		67.6	66	107.78	No
11	Stomach	71.4	67	107.45	No
12		72.1	67	89.71	No
13		72.1	67	63.43	No
14		69.9	67	122.41	No
15		71.7	67	136.28	Yes
16	Rump	68.8	66	105.90	No
17		71.1	66	123.18	Yes
18		68.6	66	89.98	No
19		68.4	67	64.32	No
20		68.3	66	106.22	No

Table A10-XCIX: Ovine 6 (Fresh/Warmed Flank) Impact Descriptions

Impact	Body Region	Surface Temp. (°F)	Internal Temp. (°F)	Impactor Velocity (m/s)	Skin Penetration (> 5mm)
1	Shoulder	78.4	89	108.37	Yes
2		79.3	89	90.78	No
3		79.4	89	65.35	No
4		78.8	89	108.88	Yes
5		83.6	89	124.90	Yes
6	Ribs	86.3	89	109.31	Yes
7		87.8	89	90.47	No
8		87.4	89	65.89	No
9		86.8	89	125.41	Yes
10		88.6	89	110.28	Yes
11	Stomach	86.40	88	107.78	Yes
12		85.70	88	89.95	No
13		84.40	88	64.42	No
14		83.10	88	89.99	No
15		83.90	88	106.77	No
16	Rump	81.7	89	109.47	No
17		78.8	89	126.81	No
18		81.3	89	90.56	No
19		83.7	88	132.93	Yes
20		80.5	88	109.17	No

Table A10-C: Ovine 7 (Fresh/Lab Temp Flank) Impact Descriptions

Impact	Body Region	Surface Temp. (°F)	Internal Temp. (°F)	Impactor Velocity (m/s)	Skin Penetration (> 5mm)
1	Shoulder	67.4	67	79.89	No
2		69.6	67	76.39	No
3		69.2	67	78.57	No
4		68.5	67	79.69	No
5		70.4	67	157.26	Yes
6	Ribs	70.4	68	79.38	No
7		69.8	67	78.67	No
8		70.1	67	78.69	No
9		70.2	67	77.46	No
10		69.6	67	157.51	Yes
11	Stomach	71.5	67	79.12	No
12		70.7	67	80.59	No
13		71.5	67	78.44	No
14		70.8	67	79.56	No
15		70.9	67	161.51	No
16	Rump	68.9	67	80.43	No
17		70.0	67	78.12	No
18		69.7	67	80.42	No
19		67.8	67	82.90	No
20		68.5	67	151.45	Yes

Table A10-CI: Ovine 7 (Thawed/Lab Temp Flank) Impact Descriptions

Impact	Body Region	Surface Temp. (°F)	Internal Temp. (°F)	Impactor Velocity (m/s)	Skin Penetration (> 5mm)
1	Shoulder	64.6	62	79.99	No
2		64.4	62	78.46	No
3		65.6	62	79.40	No
4		65.7	62	80.96	No
5		64.9	62	155.38	Yes
6	Ribs	66.5	62	77.58	No
7		67.1	62	79.95	No
8		67.0	62	80.49	No
9		66.2	62	79.92	No
10		66.9	62	158.98	Yes
11	Stomach	72.0	63	79.76	No
12		70.2	63	79.76	No
13		71.3	63	77.73	No
14		71.2	63	77.90	No
15		69.2	63	155.51	Yes
16	Rump	65.0	63	81.47	No
17		68.1	63	80.32	No
18		66.5	63	80.28	No
19		66.1	63	80.77	No
20		67.3	63	150.83	Yes

Table A10-CII: Ovine 8 (Thawed/Lab Temp, Left Flank) Impact Descriptions

Impact	Body Region	Surface Temp. (°F)	Internal Temp. (°F)	Impactor Velocity (m/s)	Skin Penetration (> 5mm)
1	Shoulder	66.2	65	78.67	No
2		66.2	65	78.96	No
3		66.3	66	81.54	No
4		66.6	66	79.54	No
5		66.7	66	157.05	Yes
6	Ribs	68.1	66	80.34	No
7		69.1	66	78.97	No
8		69.2	66	79.54	No
9		68.8	66	80.24	Yes
10		69.2	66	155.35	Yes
11	Stomach	71.8	66	79.29	No
12		72.4	66	79.85	No
13		72.1	66	78.61	No
14		70.3	66	78.67	No
15		71.0	66	162.18	Yes
16	Rump	70.0	66	79.24	No
17		69.8	66	79.93	No
18		69.9	66	80.32	No
19		68.3	66	82.41	No
20		69.8	66	155.25	Yes

Table A10-CIII: Ovine 8 (Thawed/Lab Temp, Right Flank) Impact Descriptions

Impact	Body Region	Surface Temp. (°F)	Internal Temp. (°F)	Impactor Velocity (m/s)	Skin Penetration (> 5mm)
1	Shoulder	66.2	65	81.45	No
2		66.7	65	79.95	No
3		66.3	65	81.16	No
4		66.7	65	81.24	No
5		66.7	65	157.70	Yes
6	Ribs	66.2	65	79.90	No
7		68.1	65	80.69	No
8		67.4	65	81.17	No
9		67.7	65	80.34	No
10		67.6	65	160.22	Yes
11	Stomach	70.4	65	80.74	No
12		70.1	65	79.33	No
13		70.1	65	79.16	No
14		68.7	65	81.91	No
15		69.0	65	158.10	Yes
16	Rump	66.2	65	81.27	No
17		66.4	65	81.12	No
18		66.4	65	81.17	No
19		67.1	65	80.20	No
20		65.6	65	158.88	Yes

Appendix 11: Ovine Autopsy Results

The following tables present autopsy results for each of the ovine specimen. Results are based on “yes” or “no” binary designations at the levels of injury described in

Table VI. Impact numbers correlate with the impact tests described in Appendix 10.

Table A11-CIV: Ovine 1 (Fresh/Lab Temp Flank) Autopsy Results

Impact	Minor	Skin Failure	Penetration (> 5mm)	Full Fat Disruption	Partial Muscle Disruption	Full Muscle Disruption	Full Penetration	Presence of Bone	Fracture
1	Yes	No	No	No	No	No	No	No	
2	Yes	No	No	No	No	No	No	Yes	No
3	Yes	Yes	Yes	Yes	Yes	No	No	No	
4	Yes	Yes	Yes	Yes	No	No	No	No	
5	Yes	No	No	No	No	No	No	Yes	No
6	Yes	Yes	Yes	No	No	No	No	No	
7	Yes	No	No	No	No	No	No	No	
8	Yes	Yes	Yes	Yes	No	No	No	No	
9	Yes	No	No	No	No	No	No	Yes	No
10	Yes	No	No	No	No	No	No	Yes	No
11	Yes	No	No	No	No	No	No	No	
12	Yes	Yes	Yes	Yes	Yes	Yes	Yes	No	
13	Yes	No	No	No	No	No	No	No	
14	Yes	Yes	Yes	Yes	Yes	Yes	Yes	No	
15	Yes	No	No	No	No	No	No	No	
16	Yes	Yes	No	No	No	No	No	No	
17	Yes	No	No	No	No	No	No	No	
18	No	No	No	No	No	No	No	No	
19	Yes	No	No	No	No	No	No	No	
20	Yes	No	No	No	No	No	No	Yes	No

Table A11-CV: Ovine 1 (Thawed/Lab Temp Flank) Autopsy Results

Impact	Minor	Skin Failure	Penetration (> 5mm)	Full Fat Disruption	Partial Muscle Disruption	Full Muscle Disruption	Full Penetration	Presence of Bone	Fracture
1	Yes	No	No	No	No	No	No	Yes	No
2	Yes	Yes	Yes	Yes	No	No	No	Yes	No
3	Yes	No	No	No	No	No	No	Yes	No
4	Yes	Yes	Yes	Yes	Yes	Yes	No	Yes	Yes
5	Yes	Yes	No	No	No	No	No	No	
6	Yes	Yes	Yes	No	No	No	No	Yes	No
7	Yes	Yes	Yes	Yes	Yes	No	No	No	
8	Yes	No	No	No	No	No	No	Yes	No
9	Yes	Yes	Yes	No	No	No	No	No	
10	Yes	Yes	Yes	Yes	Yes	No	No	No	
11	Yes	No	No	No	No	No	No	No	
12	Yes	No	No	No	No	No	No	No	
13	Yes	No	No	No	No	No	No	No	
14	Yes	No	No	No	No	No	No	No	
15	Yes	No	No	No	No	No	No	Yes	No
16	Yes	No	No	No	No	No	No	Yes	No
17	Yes	Yes	Yes	Yes	No	No	No	Yes	No
18	Yes	Yes	Yes	Yes	Yes	No	No	Yes	No
19	Yes	No	No	No	No	No	No	Yes	No

Table A11-CVI: Ovine 2 (Fresh/Lab Temp Flank) Autopsy Results

Impact	Minor	Skin Failure	Penetration (> 5mm)	Full Fat Disruption	Partial Muscle Disruption	Full Muscle Disruption	Full Penetration	Presence of Bone	Fracture
1	Yes	Yes	Yes	Yes	Yes	No	No	Yes	No
2	Yes	Yes	Yes	Yes	No	No	No	No	
3	Yes	Yes	Yes	Yes	Yes	No	No	No	
4	Yes	No	No	No	No	No	No	Yes	No
5	Yes	No	No	No	No	No	No	Yes	No
6	Yes	Yes	Yes	No	No	No	No	Yes	No
7	Yes	No	No	No	No	No	No	Yes	No
8	No	No	No	No	No	No	No	Yes	No
9	Yes	No	No	No	No	No	No	Yes	No
10	Yes	No	No	No	No	No	No	No	
11	Yes	No	No	No	No	No	No	No	
12	Yes	No	No	No	No	No	No	No	
13	No	No	No	No	No	No	No	No	
14	Yes	No	No	No	No	No	No	No	
15	Yes	Yes	Yes	Yes	Yes	Yes	No	No	
16	Yes	No	No	No	No	No	No	Yes	No
17	Yes	Yes	Yes	No	No	No	No	No	
18	Yes	No	No	No	No	No	No	Yes	No
19	Yes	No	No	No	No	No	No	Yes	No
20	Yes	No	No	No	No	No	No	Yes	No

Table A11-CVII: Ovine 2 (Thawed/Lab Temp Flank) Autopsy Results

Impact	Minor	Skin Failure	Penetration (> 5mm)	Full Fat Disruption	Partial Muscle Disruption	Full Muscle Disruption	Full Penetration	Presence of Bone	Fracture
1	Yes	Yes	Yes	Yes	No	No	No	Yes	No
2	Yes	Yes	Yes	Yes	Yes	No	No	Yes	No
3	Yes	No	No	No	No	No	No	No	
4	Yes	Yes	Yes	No	No	No	No	No	
5	Yes	No	No	No	No	No	No	Yes	No
6	Yes	No	No	No	No	No	No	No	
7	Yes	No	No	No	No	No	No	Yes	No
8	Yes	No	No	No	No	No	No	No	
9	No	No	No	No	No	No	No	Yes	No
10	Yes	Yes	Yes	Yes	Yes	Yes	No	Yes	No
11	Yes	No	No	No	No	No	No	No	
12	Yes	Yes	Yes	Yes	Yes	Yes	Yes	No	
13	Yes	No	No	No	No	No	No	No	
14	Yes	No	No	No	No	No	No	No	
15	Yes	No	No	No	No	No	No	No	
16	Yes	No	No	No	No	No	No	Yes	No
17	Yes	Yes	Yes	Yes	No	No	No	No	
18	Yes	Yes	Yes	Yes	Yes	No	No	No	
19	Yes	No	No	No	No	No	No	Yes	No
20	Yes	Yes	No	No	No	No	No	No	

Table A11-CVIII: Ovine 3 (Fresh/Lab Temp Flank) Autopsy Results

Impact	Minor	Skin Failure	Penetration (> 5mm)	Full Fat Disruption	Partial Muscle Disruption	Full Muscle Disruption	Full Penetration	Presence of Bone	Fracture
1	Yes	No	No	No	No	No	No	Yes	No
2	No	No	No	No	No	No	No	Yes	No
3	Yes	No	No	No	No	No	No	No	
4	Yes	No	No	No	No	No	No	Yes	No
5	Yes	No	No	No	No	No	No	Yes	No
6	Yes	Yes	Yes	Yes	Yes	No	No	Yes	No
7	No	No	No	No	No	No	No	Yes	No
8	No	No	No	No	No	No	No	Yes	No
9	Yes	No	No	No	No	No	No	Yes	No
10	Yes	No	No	No	No	No	No	Yes	No
11	Yes	No	No	No	No	No	No	No	
12	Yes	No	No	No	No	No	No	No	
13	Yes	No	No	No	No	No	No	No	
14	Yes	No	No	No	No	No	No	No	
15	Yes	No	No	No	No	No	No	No	
16	Yes	No	No	No	No	No	No	Yes	No
17	Yes	No	No	No	No	No	No	Yes	No
18	Yes	No	No	No	No	No	No	Yes	No
19	Yes	No	No	No	No	No	No	Yes	No
20	Yes	Yes	Yes	Yes	Yes	No	No	No	

Table A11-CIX: Ovine 3 (Thawed/Lab Temp Flank) Autopsy Results

Impact	Minor	Skin Failure	Penetration (> 5mm)	Full Fat Disruption	Partial Muscle Disruption	Full Muscle Disruption	Full Penetration	Presence of Bone	Fracture
1	Yes	No	No	No	No	No	No	Yes	No
2	Yes	No	No	No	No	No	No	Yes	No
3	Yes	Yes	Yes	No	No	No	No	Yes	No
4	Yes	Yes	Yes	Yes	Yes	No	No	Yes	No
5	Yes	No	No	No	No	No	No	Yes	No
6	Yes	No	No	No	No	No	No	Yes	No
7	Yes	No	No	No	No	No	No	Yes	No
8	Yes	No	No	No	No	No	No	Yes	No
9	Yes	No	No	No	No	No	No	No	
10	Yes	Yes	Yes	No	No	No	No	No	
11	Yes	No	No	No	No	No	No	No	
12	Yes	No	No	No	No	No	No	Yes	No
13	Yes	Yes	Yes	Yes	Yes	Yes	No	No	
14	Yes	No	No	No	No	No	No	No	
15	Yes	No	No	No	No	No	No	No	
16	No	No	No	No	No	No	No	Yes	No
17	Yes	No	No	No	No	No	No	Yes	No
18	Yes	No	No	No	No	No	No	No	
19	Yes	Yes	Yes	Yes	Yes	Yes	No	No	
20	Yes	No	No	No	No	No	No	Yes	No

Table A11-CX: Ovine 4 (Fresh/Lab Temp Flank) Autopsy Results

Impact	Minor	Skin Failure	Penetration (> 5mm)	Full Fat Disruption	Partial Muscle Disruption	Full Muscle Disruption	Full Penetration	Presence of Bone	Fracture
1	Yes	No	No	No	No	No	No	Yes	No
2	Yes	Yes	Yes	No	No	No	No	Yes	No
3	Yes	No	No	No	No	No	No	Yes	No
4	Yes	No	No	No	No	No	No	Yes	No
5	Yes	No	No	No	No	No	No	No	
6	Yes	Yes	Yes	No	No	No	No	Yes	No
7	Yes	No	No	No	No	No	No	Yes	No
8	Yes	Yes	Yes	No	No	No	No	Yes	No
9	Yes	No	No	No	No	No	No	Yes	No
10	Yes	No	No	No	No	No	No	Yes	No
11	Yes	No	No	No	No	No	No	No	
12	Yes	No	No	No	No	No	No	No	
13	Yes	Yes	Yes	No	No	No	No	No	
14	Yes	No	No	No	No	No	No	No	
15	No	No	No	No	No	No	No	No	
16	Yes	No	No	No	No	No	No	Yes	No
17	Yes	No	No	No	No	No	No	Yes	No
18	Yes	No	No	No	No	No	No	Yes	No
19	Yes	No	No	No	No	No	No	Yes	No
20	Yes	Yes	Yes	Yes	Yes	No	No	No	

Table A11-CXI: Ovine 4 (Fresh/Warmed) Autopsy Results

Impact	Minor	Skin Failure	Penetration (> 5mm)	Full Fat Disruption	Partial Muscle Disruption	Full Muscle Disruption	Full Penetration	Presence of Bone	Fracture
1	Yes	No	No	No	No	No	No	Yes	No
2	Yes	No	No	No	No	No	No	Yes	No
3	Yes	No	No	No	No	No	No	Yes	No
4	Yes	No	No	No	No	No	No	Yes	No
5	Yes	Yes	Yes	Yes	Yes	Yes	Yes	No	
6	Yes	No	No	No	No	No	No	Yes	No
7	Yes	No	No	No	No	No	No	Yes	No
8	Yes	No	No	No	No	No	No	No	
9	Yes	No	No	No	No	No	No	No	
10	Yes	Yes	No	No	No	No	No	No	
11	Yes	No	No	No	No	No	No	No	
12	Yes	Yes	Yes	Yes	Yes	Yes	No	No	
13	Yes	Yes	Yes	Yes	No	No	No	No	
14	Yes	No	No	No	No	No	No	No	
15	No	No	No	No	No	No	No	No	
16	Yes	No	No	No	No	No	No	Yes	No
17	Yes	No	No	No	No	No	No	Yes	No
18	Yes	No	No	No	No	No	No	Yes	No
19	Yes	Yes	Yes	Yes	Yes	Yes	Yes	Yes	No
20	Yes	No	No	No	No	No	No	No	

Table A11-CXII: Ovine 5 (Fresh/Lab Temp Flank) Autopsy Results

Impact	Minor	Skin Failure	Penetration (> 5mm)	Full Fat Disruption	Partial Muscle Disruption	Full Muscle Disruption	Full Penetration	Presence of Bone	Fracture
1	Yes	No	No	No	No	No	No	No	
2	Yes	No	No	No	No	No	No	No	
3	Yes	Yes	Yes	Yes	Yes	No	No	Yes	No
4	Yes	No	No	No	No	No	No	No	
5	Yes	No	No	No	No	No	No	No	
6	Yes	No	No	No	No	No	No	Yes	No
7	Yes	Yes	Yes	Yes	Yes	Yes	No	Yes	No
8	Yes	No	No	No	No	No	No	No	
9	Yes	No	No	No	No	No	No	No	
10	Yes	No	No	No	No	No	No	No	
11	Yes	No	No	No	No	No	No	No	
12	Yes	Yes	Yes	Yes	Yes	Yes	No	No	
13	Yes	No	No	No	No	No	No	No	
14	No	No	No	No	No	No	No	No	
15	Yes	No	No	No	No	No	No	No	
16	Yes	Yes	No	No	No	No	No	Yes	No
17	Yes	Yes	Yes	Yes	Yes	No	No	Yes	No
18	Yes	No	No	No	No	No	No	Yes	No
19	Yes	No	No	No	No	No	No	Yes	No
20	Yes	No	No	No	No	No	No	Yes	No

Table A11-CXIII: Ovine 5 (Fresh/Warmed) Autopsy Results

Impact	Minor	Skin Failure	Penetration (> 5mm)	Full Fat Disruption	Partial Muscle Disruption	Full Muscle Disruption	Full Penetration	Presence of Bone	Fracture
1	Yes	Yes	No	No	No	No	No	No	
2	Yes	Yes	Yes	No	No	No	No	No	
3	Yes	No	No	No	No	No	No	No	
4	No	No	No	No	No	No	No	No	
5	Yes	Yes	Yes	Yes	Yes	No	No	No	
6	Yes	Yes	Yes	Yes	Yes	No	No	No	
7	Yes	No	No	No	No	No	No	No	
8	Yes	No	No	No	No	No	No	No	
9	Yes	Yes	Yes	No	No	No	No	Yes	No
10*	Yes	Yes	Yes	Yes	Yes	Yes	Yes	No	
11*	Yes	No	No	No	No	No	No	No	
12*	Yes	Yes	No	No	No	No	No	No	
13*	Yes	Yes	Yes	No	No	No	No	No	
14*	Yes	Yes	Yes	No	No	No	No	No	
15	Yes	No	No	No	No	No	No	Yes	No
16	Yes	No	No	No	No	No	No	Yes	No
17	Yes	No	No	No	No	No	No	Yes	No
18	Yes	Yes	Yes	Yes	Yes	No	No	No	
19	Yes	Yes	Yes	Yes	Yes	Yes	No	Yes	No

*Datapoint is excluded from analysis due to overheating of the tissue.

Table A11-CXIV: Ovine 6 (Fresh/Lab Temp Flank) Autopsy Results

Impact	Minor	Skin Failure	Penetration (> 5mm)	Full Fat Disruption	Partial Muscle Disruption	Full Muscle Disruption	Full Penetration	Presence of Bone	Fracture
1	Yes	Yes	Yes	No	No	No	No	Yes	No
2	Yes	No	No	No	No	No	No	Yes	No
3	Yes	No	No	No	No	No	No	Yes	No
4	Yes	Yes	No	No	No	No	No	Yes	No
5	Yes	No	No	No	No	No	No	No	
6	Yes	No	No	No	No	No	No	No	
7	Yes	Yes	Yes	No	No	No	No	Yes	No
8	Yes	No	No	No	No	No	No	Yes	No
9	Yes	No	No	No	No	No	No	Yes	No
10	Yes	No	No	No	No	No	No	No	
11	Yes	No	No	No	No	No	No	No	
12	Yes	No	No	No	No	No	No	No	
13	Yes	No	No	No	No	No	No	No	
14	Yes	No	No	No	No	No	No	No	
15	Yes	Yes	Yes	Yes	Yes	Yes	Yes	No	
16	Yes	No	No	No	No	No	No	No	
17	Yes	Yes	Yes	Yes	Yes	No	No	Yes	No
18	Yes	No	No	No	No	No	No	No	
19	Yes	No	No	No	No	No	No	Yes	No
20	Yes	Yes	No	No	No	No	No	Yes	No

Table A11-CXV: Ovine 6 (Fresh/Warmed) Autopsy Results

Impact	Minor	Skin Failure	Penetration (> 5mm)	Full Fat Disruption	Partial Muscle Disruption	Full Muscle Disruption	Full Penetration	Presence of Bone	Fracture
1	Yes	Yes	Yes	No	No	No	No	Yes	No
2	Yes	No	No	No	No	No	No	Yes	No
3	Yes	No	No	No	No	No	No	Yes	No
4	Yes	Yes	Yes	Yes	No	No	No	Yes	No
5	Yes	Yes	Yes	Yes	Yes	No	No	No	
6	Yes	Yes	No	No	No	No	No	No	
7	Yes	No	No	No	No	No	No	Yes	No
8	Yes	No	No	No	No	No	No	Yes	No
9	Yes	Yes	Yes	Yes	Yes	Yes	Yes	Yes	No
10	Yes	Yes	Yes	No	No	No	No	No	
11	Yes	Yes	Yes	Yes	Yes	Yes	Yes	No	
12	Yes	No	No	No	No	No	No	No	
13	Yes	No	No	No	No	No	No	No	
14	Yes	No	No	No	No	No	No	No	
15	Yes	No	No	No	No	No	No	No	
16	Yes	No	No	No	No	No	No	Yes	No
17	Yes	Yes	No	No	No	No	No	Yes	No
18	Yes	No	No	No	No	No	No	Yes	No
19	Yes	Yes	Yes	Yes	Yes	Yes	Yes	No	
20	Yes	No	No	No	No	No	No	Yes	No

Table A11-CXVI: Ovine 7 (Fresh/Lab Temperature) Autopsy Results

Impact	Minor	Skin Failure	Penetration (> 5mm)	Full Fat Disruption	Partial Muscle Disruption	Full Muscle Disruption	Full Penetration	Presence of Bone	Fracture
1	Yes	No	No	No	No	No	No	Yes	No
2	Yes	No	No	No	No	No	No	Yes	No
3	Yes	No	No	No	No	No	No	No	
4	Yes	No	No	No	No	No	No	Yes	No
5	Yes	Yes	Yes	Yes	Yes	No	No	No	
6	Yes	No	No	No	No	No	No	Yes	No
7	Yes	No	No	No	No	No	No	Yes	No
8	Yes	No	No	No	No	No	No	Yes	No
9	Yes	No	No	No	No	No	No	Yes	No
10	Yes	Yes	Yes	Yes	Yes	Yes	No	No	
11	Yes	No	No	No	No	No	No	No	
12	Yes	No	No	No	No	No	No	No	
13	Yes	No	No	No	No	No	No	No	
14	Yes	No	No	No	No	No	No	No	
15	Yes	No	No	No	No	No	No	No	
16	Yes	No	No	No	No	No	No	No	
17	Yes	No	No	No	No	No	No	Yes	No
18	Yes	No	No	No	No	No	No	No	
19	Yes	No	No	No	No	No	No	Yes	No
20	Yes	Yes	Yes	Yes	Yes	No	No	No	

Table A11-CXVII: Ovine 7 (Thawed/Lab Temperature) Autopsy Results

Impact	Minor	Skin Failure	Penetration (> 5mm)	Full Fat Disruption	Partial Muscle Disruption	Full Muscle Disruption	Full Penetration	Presence of Bone	Fracture
1	Yes	No	No	No	No	No	No	Yes	No
2	Yes	No	No	No	No	No	No	Yes	No
3	Yes	No	No	No	No	No	No	No	
4	Yes	No	No	No	No	No	No	Yes	No
5	Yes	Yes	Yes	Yes	Yes	No	No	No	
6	Yes	No	No	No	No	No	No	No	
7	Yes	No	No	No	No	No	No	Yes	No
8	Yes	No	No	No	No	No	No	No	
9	Yes	No	No	No	No	No	No	Yes	No
10	Yes	Yes	Yes	Yes	Yes	Yes	Yes	Yes	No
11	Yes	No	No	No	No	No	No	No	
12	Yes	No	No	No	No	No	No	No	
13	Yes	No	No	No	No	No	No	No	
14	Yes	No	No	No	No	No	No	No	
15	Yes	Yes	Yes	Yes	Yes	Yes	Yes	No	
16	Yes	No	No	No	No	No	No	Yes	No
17	Yes	No	No	No	No	No	No	Yes	No
18	Yes	No	No	No	No	No	No	Yes	No
19	Yes	No	No	No	No	No	No	Yes	No
20	Yes	Yes	Yes	Yes	Yes	Yes	Yes	No	

Table A11-CXVIII: Ovine 8 (Thawed/Lab Temperature, Left Flank) Autopsy Results

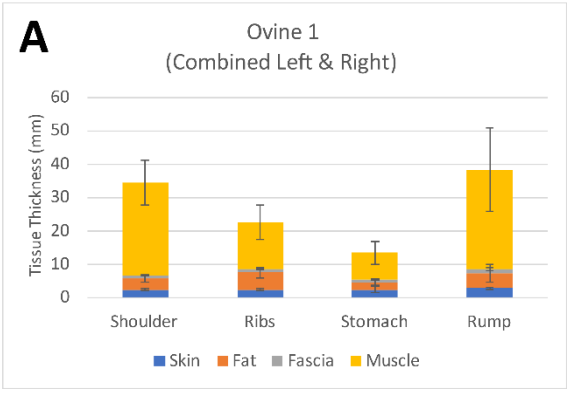
Impact	Minor	Skin Failure	Penetration (> 5mm)	Full Fat Disruption	Partial Muscle Disruption	Full Muscle Disruption	Full Penetration	Presence of Bone	Fracture
1	Yes	No	No	No	No	No	No	Yes	No
2	Yes	No	No	No	No	No	No	Yes	No
3	Yes	No	No	No	No	No	No	Yes	No
4	Yes	No	No	No	No	No	No	Yes	No
5	Yes	Yes	Yes	Yes	Yes	Yes	Yes	No	
6	Yes	No	No	No	No	No	No	No	
7	Yes	Yes	No	No	No	No	No	Yes	No
8	Yes	No	No	No	No	No	No	No	
9	Yes	Yes	Yes	No	No	No	No	No	
10	Yes	Yes	Yes	Yes	Yes	Yes	Yes	Yes	Yes
11	Yes	No	No	No	No	No	No	No	
12	Yes	No	No	No	No	No	No	No	
13	Yes	No	No	No	No	No	No	No	
14	Yes	No	No	No	No	No	No	No	
15	Yes	Yes	Yes	Yes	Yes	Yes	Yes	No	
16	Yes	Yes	No	No	No	No	No	No	
17	Yes	Yes	No	No	No	No	No	Yes	No
18	Yes	No	No	No	No	No	No	Yes	No
19	Yes	No	No	No	No	No	No	No	
20	Yes	Yes	Yes	Yes	Yes	Yes	Yes	Yes	No

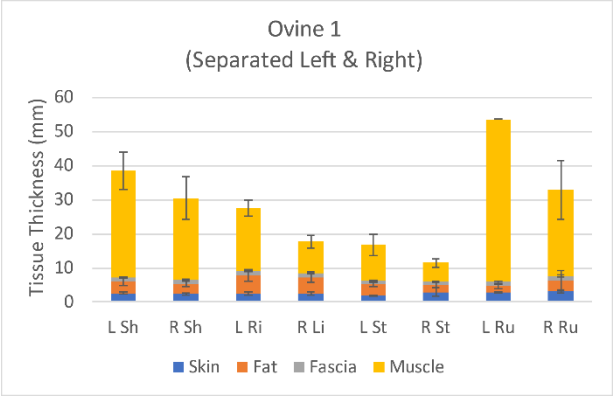
Table A11-CXIX: Ovine 8 (Thawed/Lab Temperature, Right Flank) Autopsy Results

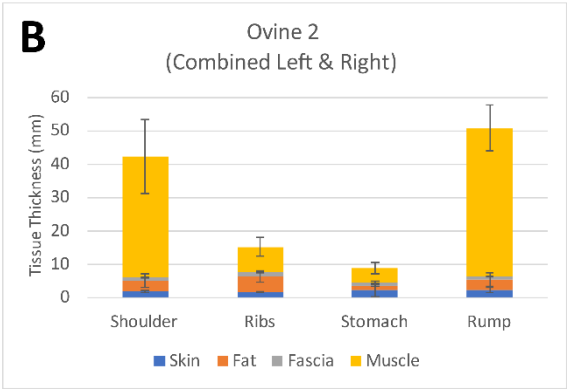
Impact	Minor	Skin Failure	Penetration (> 5mm)	Full Fat Disruption	Partial Muscle Disruption	Full Muscle Disruption	Full Penetration	Presence of Bone	Fracture
1	Yes	No	No	No	No	No	No	Yes	No
2	Yes	No	No	No	No	No	No	Yes	No
3	Yes	No	No	No	No	No	No	Yes	No
4	Yes	No	No	No	No	No	No	Yes	No
5	Yes	Yes	Yes	Yes	Yes	Yes	No	No	
6	Yes	No	No	No	No	No	No	No	
7	Yes	No	No	No	No	No	No	Yes	No
8	Yes	No	No	No	No	No	No	Yes	No
9	Yes	No	No	No	No	No	No	No	
10	Yes	Yes	Yes	Yes	Yes	Yes	Yes	No	
11	Yes	No	No	No	No	No	No	No	
12	Yes	No	No	No	No	No	No	No	
13	Yes	No	No	No	No	No	No	No	
14	Yes	No	No	No	No	No	No	No	
15	Yes	Yes	Yes	Yes	Yes	Yes	Yes	No	
16	Yes	No	No	No	No	No	No	Yes	No
17	Yes	No	No	No	No	No	No	Yes	No
18	Yes	No	No	No	No	No	No	No	
19	Yes	No	No	No	No	No	No	Yes	No
20	Yes	Yes	Yes	Yes	Yes	Yes	Yes	Yes	No

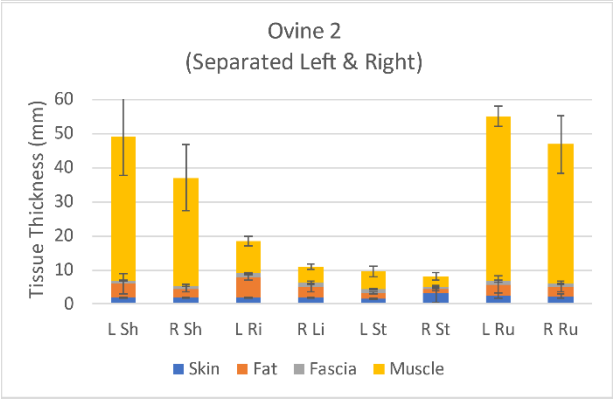
Appendix 12: Ovine Tissue Thickness

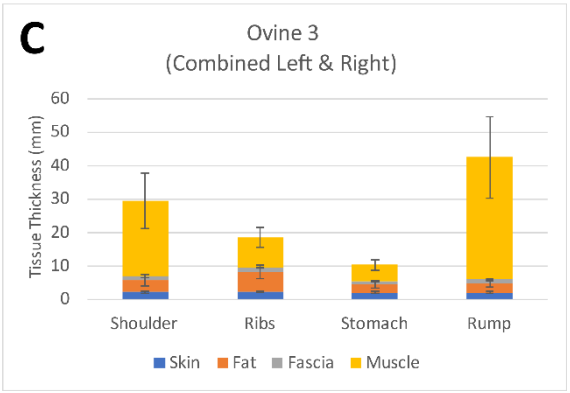
Stacked bar charts of mean tissue thickness are presented to show intra-subject and inter-subject variations between the body regions.

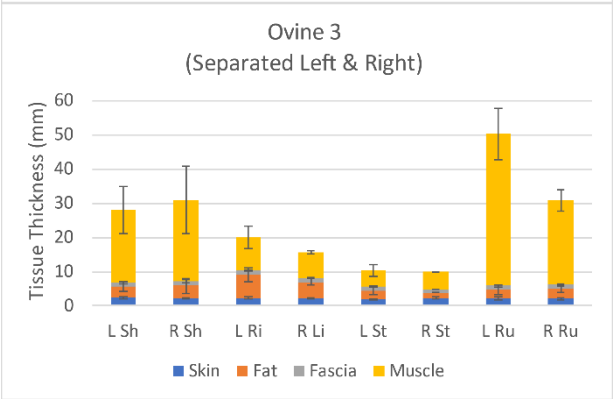


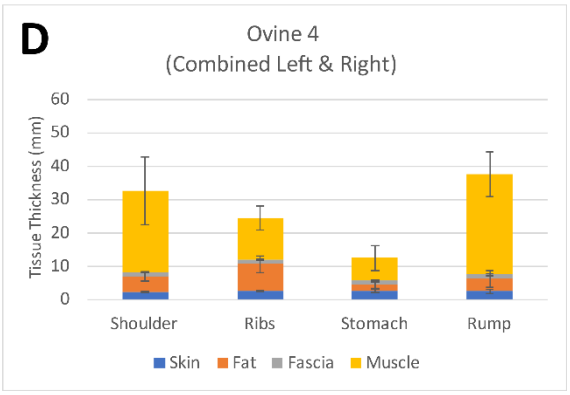


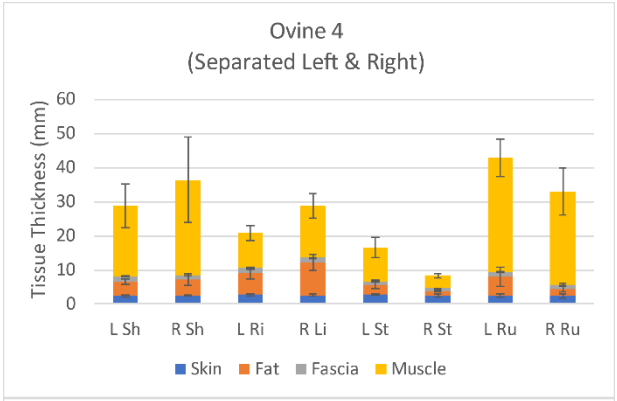


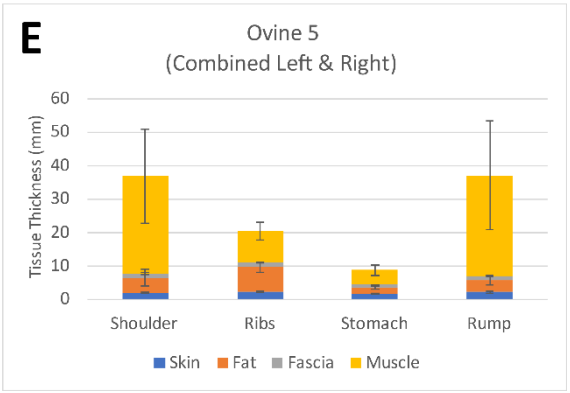


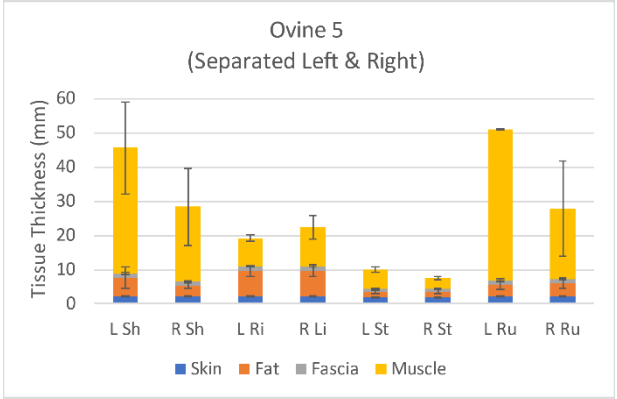


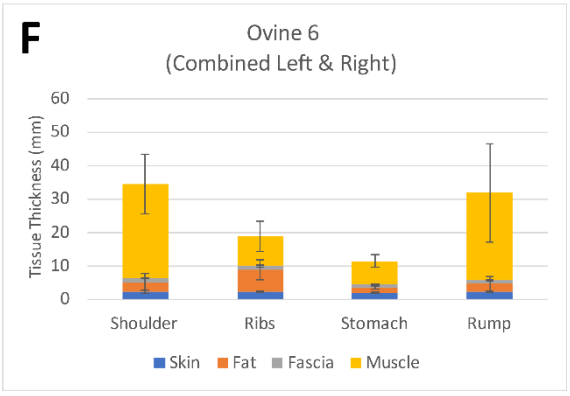


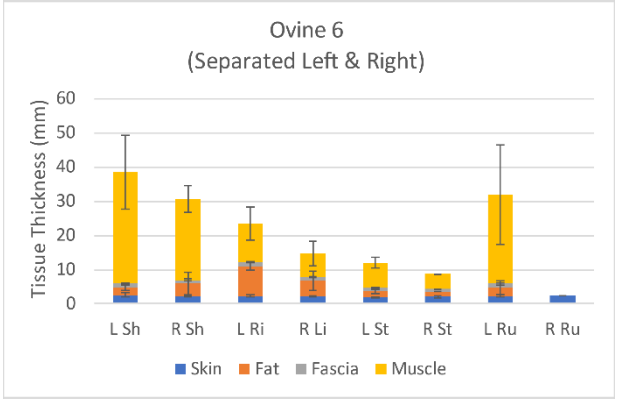

D
Ovine 4
(Combined Left & Right)
Tissue Thickness (mm)
60
50
40
30
20
10
0
Shoulder
Ribs
Stomach
Rump
Skin
Fat
Fascia
Muscle

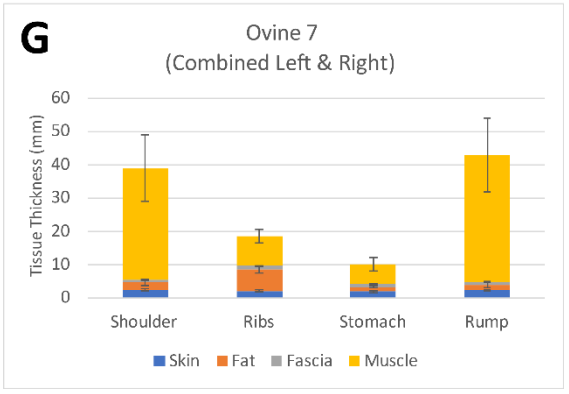

Ovine 4
(Separated Left & Right)
Tissue Thickness (mm)
60
50
40
30
20
10
0
L Sh
R Sh
L Ri
R Li
L St
R St
L Ru
R Ru
Skin
Fat
Fascia
Muscle

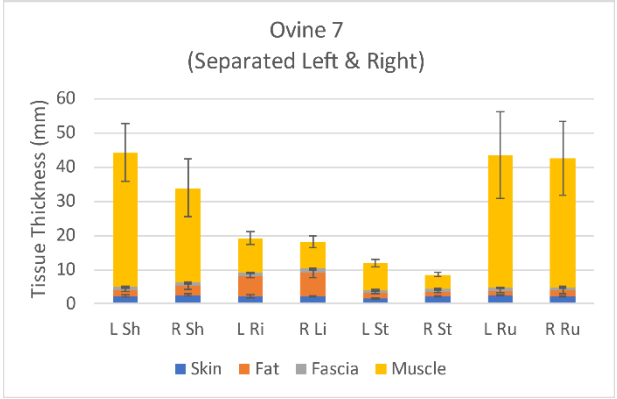

E
Ovine 5
(Combined Left & Right)
Tissue Thickness (mm)
60
50
40
30
20
10
0
Shoulder
Ribs
Stomach
Rump
Skin
Fat
Fascia
Muscle


Ovine 5
(Separated Left & Right)
Tissue Thickness (mm)
60
50
40
30
20
10
0
L Sh
R Sh
L Ri
R Li
L St
R St
L Ru
R Ru
Skin
Fat
Fascia
Muscle


F
Ovine 6
(Combined Left & Right)
Tissue Thickness (mm)
60
50
40
30
20
10
0
Shoulder
Ribs
Stomach
Rump
Skin
Fat
Fascia
Muscle


Ovine 6
(Separated Left & Right)
Tissue Thickness (mm)
60
50
40
30
20
10
0
L Sh
R Sh
L Ri
R Li
L St
R St
L Ru
R Ru
Skin
Fat
Fascia
Muscle


G
Ovine 7
(Combined Left & Right)
Tissue Thickness (mm)
60
50
40
30
20
10
0
Shoulder
Ribs
Stomach
Rump
Skin
Fat
Fascia
Muscle


Ovine 7
(Separated Left & Right)
Tissue Thickness (mm)
60
50
40
30
20
10
0
L Sh
R Sh
L Ri
R Li
L St
R St
L Ru
R Ru
Skin
Fat
Fascia
Muscle

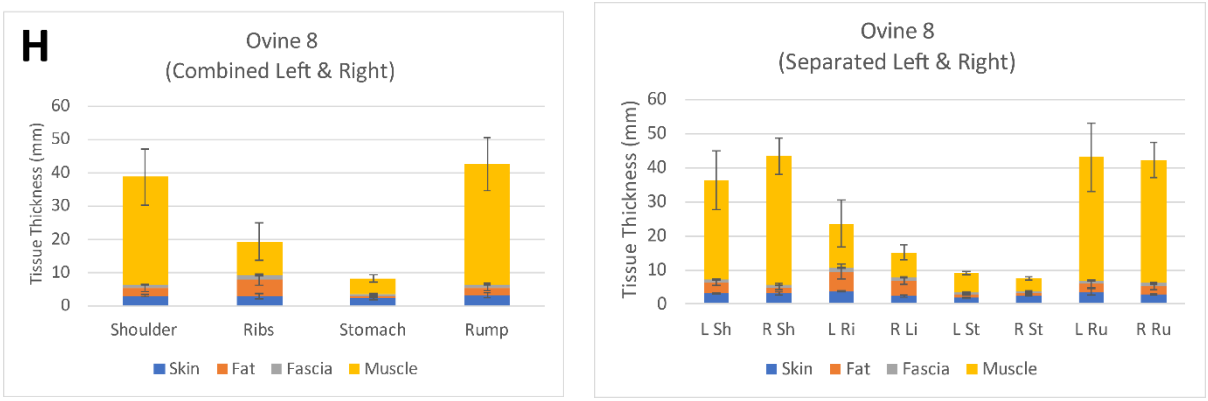


Figure A12-96: Intra-subject comparison of mean tissue thickness per Ovine body region.

Bar charts represent the mean thickness of each tissue layer at each body region for both combined and separated left & right regions for (a) Ovine 1, (b) Ovine 2, (c) Ovine 3, (d) Ovine 4, (e) Ovine 5, (f) Ovine 6, (g) Ovine 7, and (h) Ovine 8. Sh = Shoulder, Ri = Ribs, St = Stomach, and Ru = Rump. L = Left and R = Right.

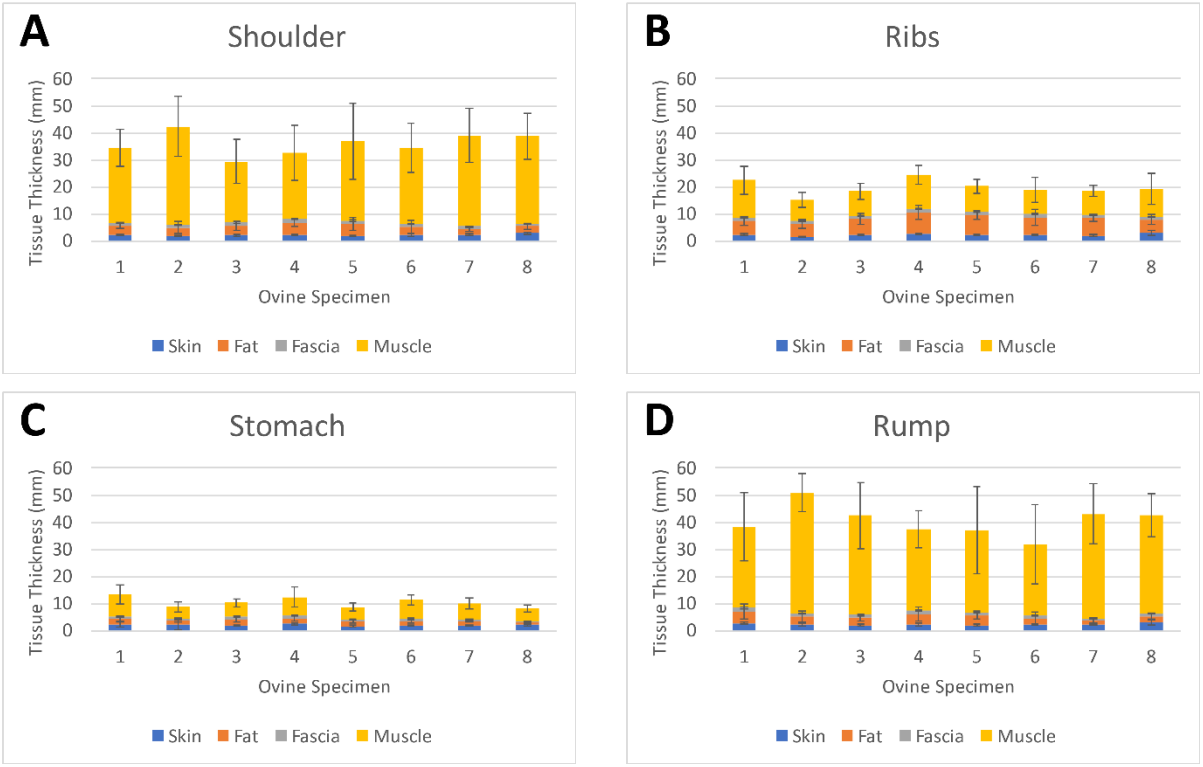


Figure A12-97: Comparison of variations in subject-level tissue thickness at each ovine body region.

Bar charts represent the mean tissue layer thickness with error bars of 1 SD for the (a) Shoulder, (b) Ribs, (c) Stomach, and (d) Rump.

Appendix 13: Ovine Injury Risk Function Covariate Assessment

As described in Aim 2, the significance of every possible variable was assessed by independently implementing the covariate into the Ovine IRF. The log-likelihood p-value for each single-covariate IRF is provided in Table A13-CXX. Additionally, the "Missing Data" column describes the number of datapoints that did not include the relevant covariate information and, therefore, would be excluded from the model fit. This was primarily a result of ultrasound and SWE limitations, such as the depth of imaging.

Table A13-CXX: All Possible Ovine Covariates (In Increasing Order of p-Value)

Covariate	p-Value	Missing Datapoints
Specimen ID	1.1e-04	0
Body Region	5.2-03	0
Fascia Stiffness/Shear Wave Velocity (m/s)	1.3e-01	28
Fat Stiffness/Shear Wave Velocity (m/s)	1.4e-01	16
Internal Temperature (°F)	2.9e-01	Ovine 1's Fresh/Lab Temp Flank
Fat Thickness (mm)	3.5e-01	17
Presence of Bone	4.2e-01	0
Surface Temperature (°F)	4.9e-01	0
Fascia Thickness (mm)	6.3e-01	17
Skin Thickness (mm)	6.8e-01	9
Muscle Stiffness/Shear Wave Velocity (m/s)	8.0e-01	43
Side	8.9e-01	0
Storage	9.1e-01	0
Muscle Thickness (mm)	9.6e-01	51
Skin Stiffness/Shear Wave Velocity (m/s)	9.8e-01	4

The following figures represent the variability resulting from all possible model covariates shown in Table A13-CXX. For categorical covariates, the model prediction for each category is plotted. For continuous covariates, the mean value ± 1 SD is plotted.

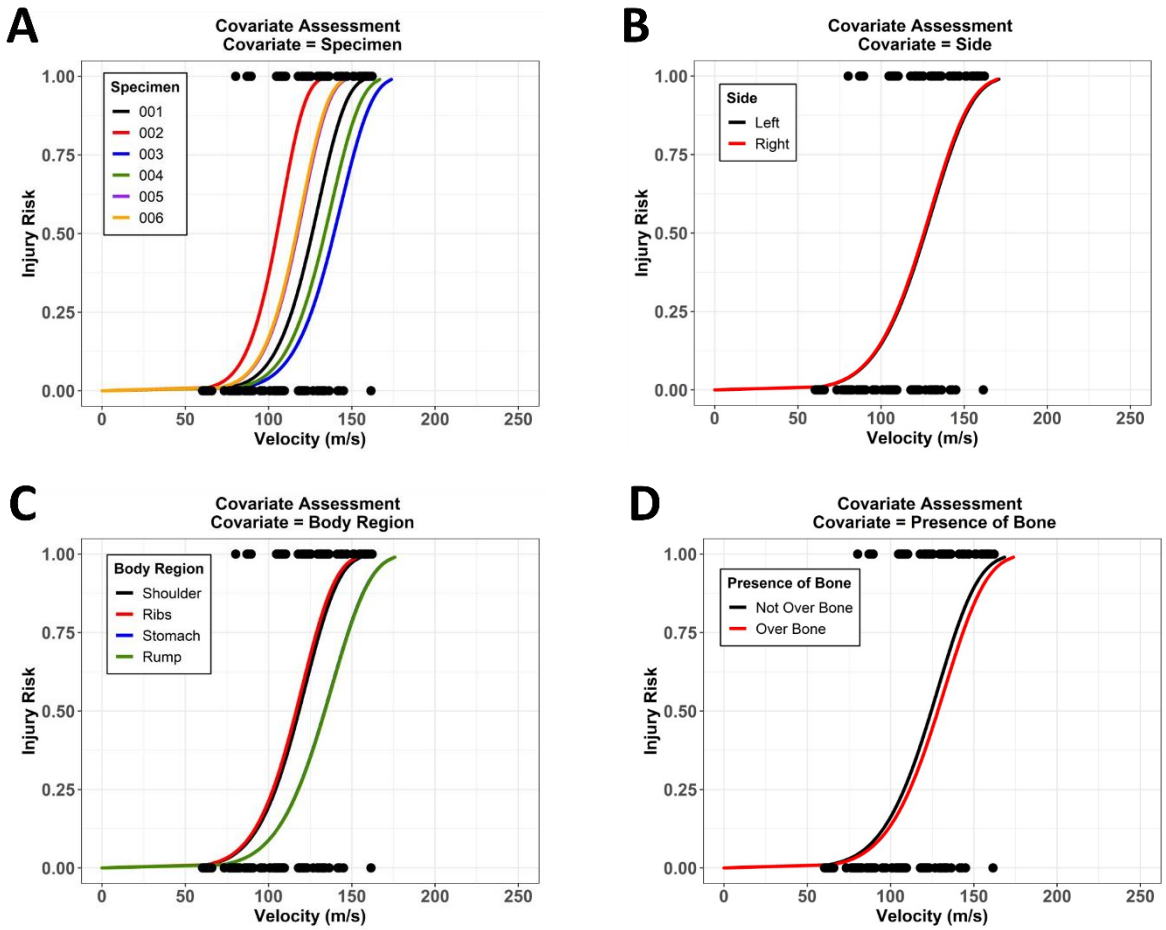


Figure A13-98: Ovine covariate assessment for the impact location variables.

Variability of the following covariates is presented: (a) Specimen is the categorical specimen ID (1, 2, …, 8), (b) Side is the categorical side of the body (Left and Right), (c) Body Region is the categorical body region (Shoulder, Ribs, Stomach, and Rump), and (d) Presence of Bone is the categorical body region that describes whether an impact occurred over bone (No Bone and Bone).

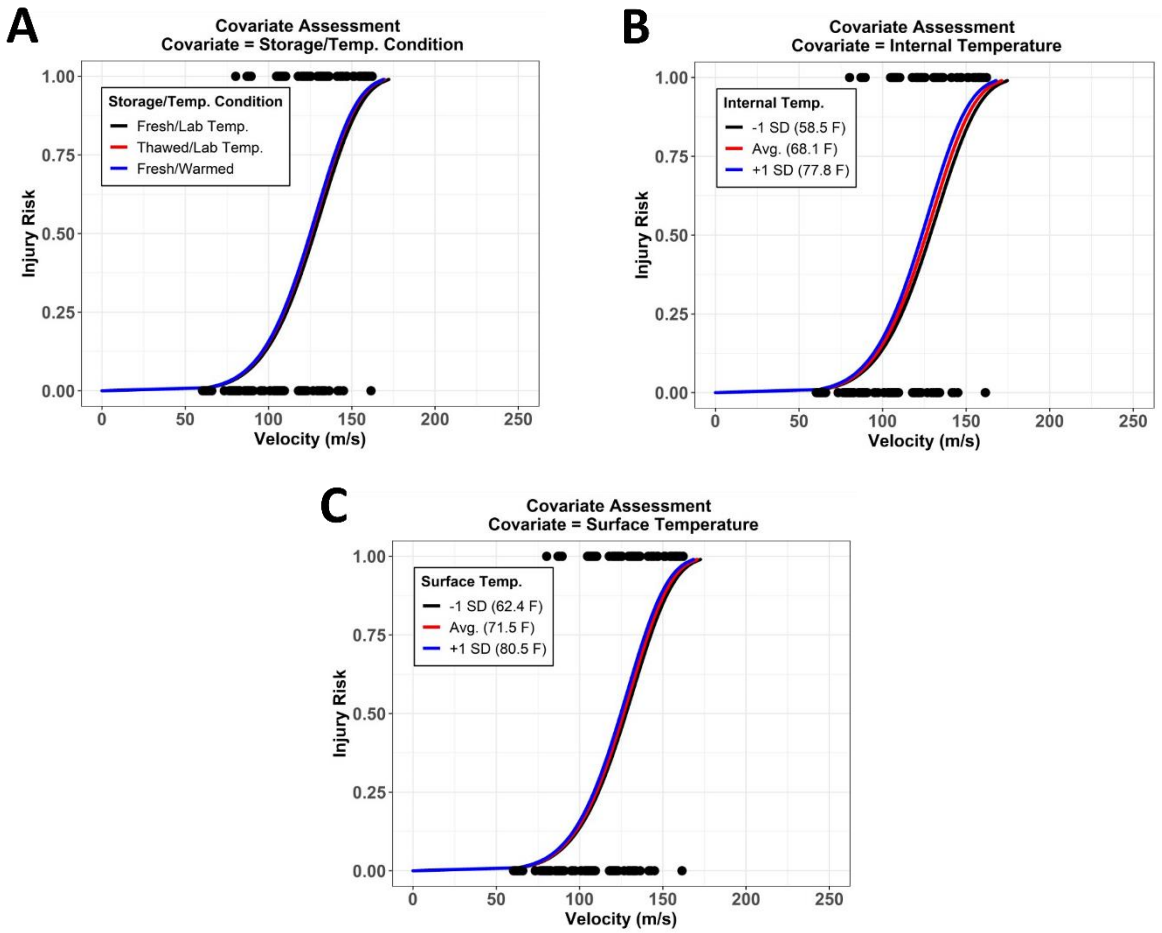


Figure A13-99: Ovine covariate assessment for the tissue temperature variables.

Variability of the following covariates is presented: (a) Storage/Temp. Condition is the categorical variable which describes the tissue preparation for each impact (Fresh/Lab Temp., Thawed/Lab Temp., and Fresh/Warmed), (b) Internal Temperature is the continuous variable that describes the internal temperature of the tissue, and (c) Surface Temperature is the continuous variable that describes the surface temperature of the tissue.

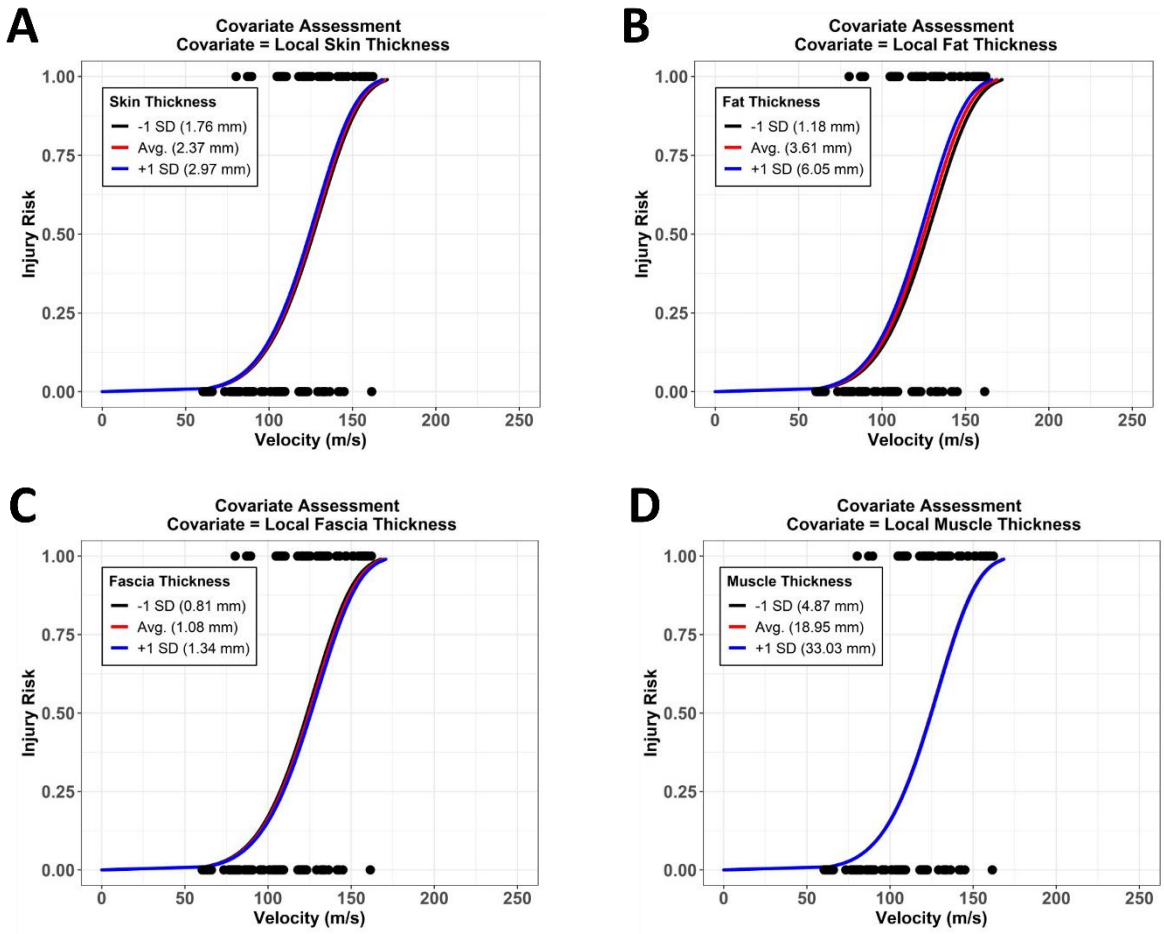


Figure A13-100: Ovine covariate assessment for the tissue thickness variables.

Variability of the tissue thickness covariates for the following tissue layers: (a) Skin, (b) Fat, (c) Fascia, and (d) Muscle.

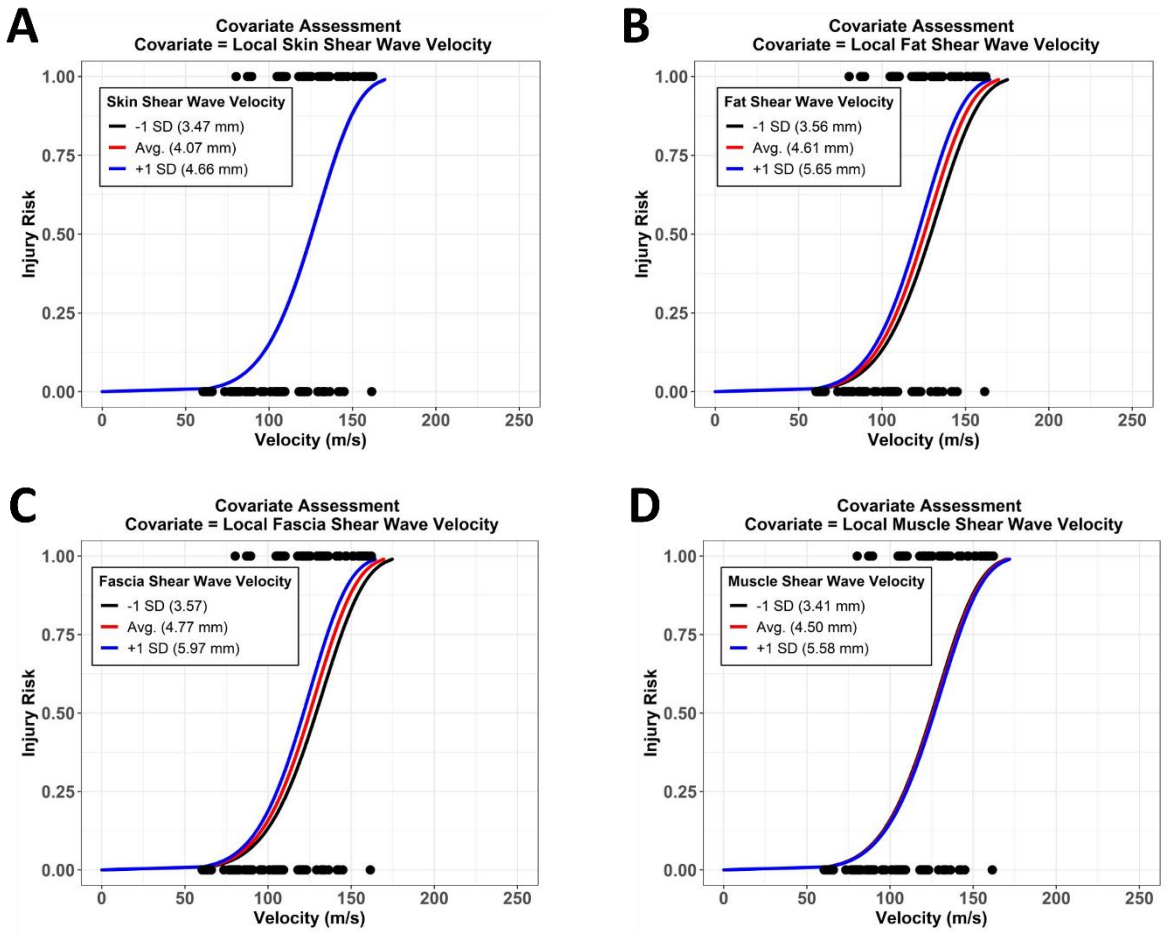


Figure A13-101: Ovine covariate assessment for the tissue shear wave velocity variables.

Variability of the tissue shear wave velocity covariates for the following tissue layers: (a) Skin, (b) Fat, (c) Fascia, and (d) Muscle.

Appendix 14: Ovine Model 2 Plotting

In addition to Ovine Model 1, the univariate IRF provided a significant fit to the test data. A few key injury risk values are provided in Table A14-CXXI, and the IRF is plotted in Figure A14-102.

Table A14-CXXI: Predicted Injury Risk for Ovine Model 2

Injury Risk (%)	Impactor Velocity (m/s)
5	83.56
10	93.64
15	100.3
25	109.8
50	126.2
75	140.8

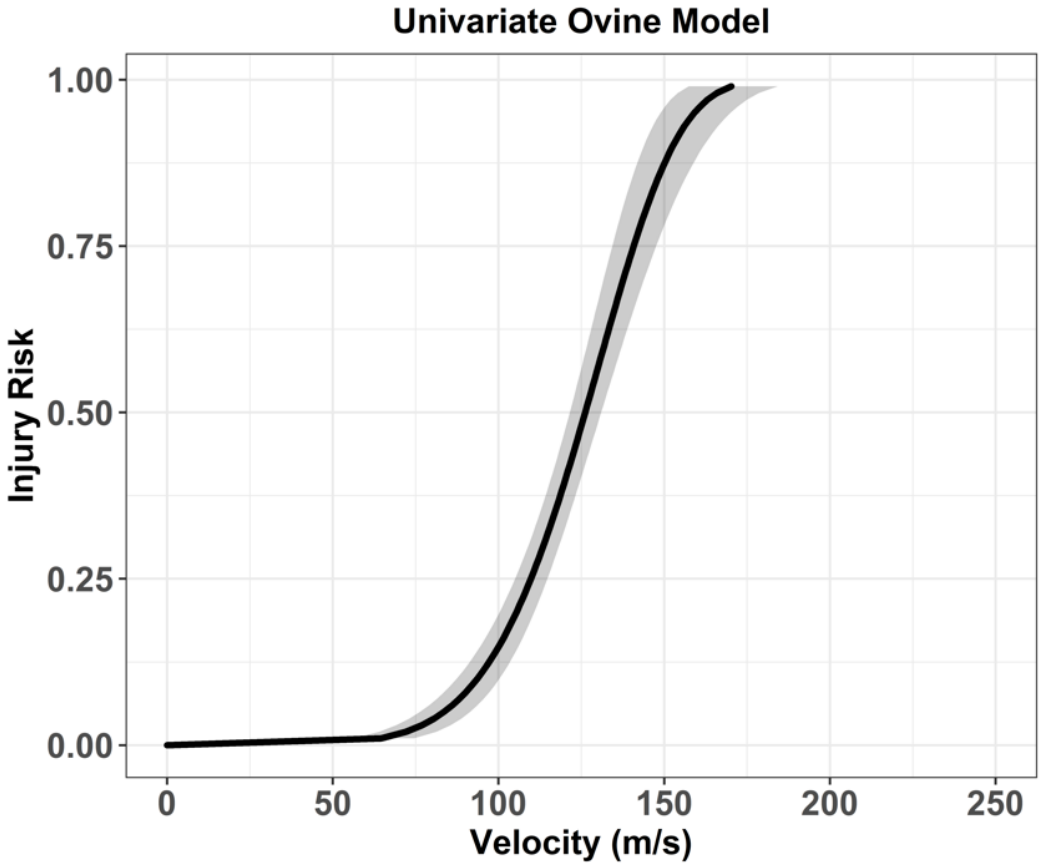


Figure A14-102: Univariate ovine model with 95% confidence interval.